nagra
National Cooperative for the
Disposal of Radioactive Waste

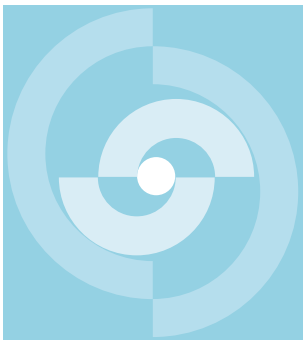

TECHNICAL REPORT 00-09

Grimsel Test Site
Investigation Phase IV (1994-1996)

The Nagra-JNC in situ study of safety relevant radionuclide retardation in fractured crystalline rock I: Radionuclide Migration Experiment – Overview 1990-1996

December 2001

P.A. Smith, W.R. Alexander, W. Heer, T. Fierz,
P.M. Meier, B. Baeyens, M.H. Bradbury,
M. Mazurek, I.G. McKinley

Hardstrasse 73, CH-5430 Wettingen/Switzerland, Telephone +41-56-437 11 11

nagra
National Cooperative for the
Disposal of Radioactive Waste

TECHNICAL REPORT 00-09

Grimsel Test Site
Investigation Phase IV (1994-1996)

The Nagra-JNC in situ study of safety relevant radionuclide retardation in fractured crystalline rock I: Radionuclide Migration Experiment – Overview 1990-1996

December 2001

P.A. Smith[1)], W.R. Alexander[2)], W. Heer[3)], T. Fierz[4)], P.M. Meier[5)], B. Baeyens[3)], M.H. Bradbury[3)], M. Mazurek[6)], I.G. McKinley[2)]

[1)] SAM, United Kingdom

[2)] Nagra, Switzerland

[3)] PSI, Switzerland

[4)] Solexperts, Switzerland

[5)] Polytechnical University of Catalonia, Spain (now NOK, Switzerland)

[6)] GGWW, University of Berne, Switzerland

Hardstrasse 73, CH-5430 Wettingen/Switzerland, Telephone +41-56-437 11 11

This report was prepared on behalf of Nagra. The viewpoints presented and conclusions reached are those of the author(s) and do not necessarily represent those of Nagra.

ISSN 1015-2636

FOREWORD

Concepts for the disposal of radioactive waste in geological formations depend crucially on a thorough knowledge of relevant processes in the host rock and on an understanding of the whole repository system, comprising both engineered and geological barriers. The Grimsel Test Site (GTS) is an underground rock laboratory which is used to investigate many of these processes in hard, fractured rocks. It has been operated since 1984 by the Swiss National Cooperative for the Disposal of Radioactive Waste (NAGRA).

The laboratory is located in the crystalline rock of the Central Aar Massif, 450 m below the eastern flank of the Juchlistock at an altitude of 1730 m. It is reached via a 1200 m long horizontal access tunnel, operated by the hydropowerplant company KWO. The layout of the tunnels that comprise the GTS allowed the establishment of a radiation controlled zone (IAEA type B/C) in 1990 in which experiments with radioactive tracers are carried out. With increasing experience in the implementation of in-situ experiments, improved process understanding and more advanced repository concepts, the experimental programmes at the GTS have gradually become more complex and more directly related to open questions defined by performance assessors or by regulatory bodies. Demonstration of disposal concepts by performing large- or full-scale, long-term experiments has also become a key aspect of investigations in the rock laboratory. The GTS Phase IV, 1994 – 1996, was initiated in close co-operation with a number of international partner organisations. The performed programmes focused on the characterisation and conceptualisation of the tunnel nearfield of geophysical investigations and experiments related on radionuclide retardation.

Within the current investigation phase (Phase V; 1997 – 2002) seven experimental programmes and projects are included (see www.grimsel.com for details).

Within GTS Phase IV, the Nagra-JNC Radionuclide Migration Programme (RMP) examined the behaviour of a large suite of radionuclides in the geosphere. The Radionuclide Migration Experiment (MI) is an integral part of RMP, beginning in 1985 and continuing until 1996, and this report summarises the results for the period 1990 – 1996 (for 1985 – 1990, see FRICK et al. 1992a, NTB 91-04). The main aim of MI was testing radionuclide transport models and this was supported by a suite of supporting projects including: site characterisation methodology development, the study of the hydrogeology, hydrochemistry and geochemistry of a rock-water system, detailed structural and mineralogical characterisation of the experimental site (a complex shear zone) and an integrated programme of supporting laboratory and modelling studies.

This report is one of a series of four Nagra Technical Reports (NTBs) on RMP, including NTB 00-06 (*Excavation Project EP-Phase II, Radionuclide Retardation Project* RRP methodology), NTB 00-07 (*EP-Phase III,* RRP final report) and NTB 00-08 (*Connected Porosity* CP report) which will be synthesised in ALEXANDER et al. (2001a).

The MI raw data are now available free-of-charge on www.grimsel.com.

VORWORT

Bei Lagerkonzepten für die Entsorgung radioaktiver Abfälle in geologischen Formationen sind eine vertiefte Kenntnis der relevanten Prozesse im Wirtgestein sowie ein Verständnis des gesamten Lagersystems mit den technischen und geologischen Barrieren von entscheidender Bedeutung. Das Felslabor Grimsel (FLG) ist ein standortunabhängiges Felslabor, in welchem zahlreiche dieser Prozesse in geklüftetem Festgestein untersucht werden. Es wird seit 1984 von der Nagra (Nationale Genossenschaft für die Lagerung radioaktiver Abfälle) betrieben.

Das FLG befindet sich im Kristallingestein des Zentralen Aarmassives 450 m unterhalb der Ostflanke des Juchlistocks auf einer Höhe von 1730 m ü.M. und kann durch einen 1200 m langen horizontalen Zugangsstollen der Kraftwerke Oberhasli AG (KWO) erreicht werden. 1990 wurde in einem Stollenabschnitt des FLG eine kontrollierte Zone (IAEA Typ B/C) für Versuche mit radioaktiven Tracern eingerichtet. Mit zunehmender Erfahrung bei der Durchführung von Feldversuchen und verbessertem Systemverständnis der weiter entwickelten Lagerkonzepte, verlagerten sich die experimentellen Programmschwerpunkte hin zu komplexen, direkt auf die Anforderungen der Sicherheitsanalyse und Behörden ausgerichteten Versuche. Langzeit-Demonstrationsversuche in grösserem oder Originalmassstab gewannen im Felslabor zunehmend an Bedeutung. Die FLG Untersuchungsphase IV (1994 – 1996) wurde in enger Zusammenarbeit mit einer Anzahl internationaler Partnerorganisationen geplant. Die durchgeführten Versuchsprogramme konzentrierten sich auf die Charakterisierung und Konzeptualisierung des Tunnelnahfeldbereichs mit geophysikalischen Methoden und Versuchen zur Radionuklidrückhaltung.

Die jetzige Untersuchungsphase (Phase V, 1997 – 2002) umfasst sieben Versuchsprogramme und -projekte (siehe auch www.grimsel.com für Einzelheiten).

Innerhalb der FLG Phase IV wurde mit dem Nagra-JNC Radionuklid-Migrationsprojekt (Radionuclide Migration Programme, RMP) das Verhalten einer Reihe von Radionukliden in der Geosphäre untersucht. Der Migrationsversuch (MI) ist ein eigenständiges Teilprojekt von RMP, das 1985 begonnen und bis 1996 fortgeführt wurde. Der vorliegende Bericht fasst die im Zeitraum 1990 – 1996 erhobenen Daten zusammen (Ergebnisse 1985 – 1990, siehe FRICK et al. 1992a, NTB 91-04). Die Hauptzielsetzung von MI war der Test von Radionuklid-Transportmodellen, dies erfolgte anhand einer Reihe von unterstützenden Projekten, wie die Entwicklung einer Methodik zur Standortcharakterisierung, die hydrogeologische, hydrochemische und geochemische Untersuchung eines Gestein-Wasser-Systems, die detaillierte strukturelle und mineralogische Charakterisierung des Versuchsstandorts (komplexe Scherzone) und ein umfassendes Programm unterstützender Labor- und Modellierungsstudien.

Der vorliegende Bericht ist Teil einer Reihe von vier Nagra Technischen Berichten (NTB) zum Thema RMP, zusammen mit NTB 00-06 (Methodik RRP, *Radionuclide Retardation Project, Excavation Project EP-Phase II*), NTB 00-07 (Schlussbericht RRP, *EP-Phase III*) und NTB 00-08 (Bericht CP, *Connected Porosity*), deren Synthese in ALEXANDER et al. (2001a) dargelegt ist.

Die Rohdaten des Migrationsversuchs sind gratis unter www.grimsel.com erhältlich.

PRÉFACE

Les concepts développés pour le dépôt de déchets radioactifs dans des formations géologiques dépendent étroitement d'une connaissance approfondie des processus significatifs qui se déroulent dans la roche d'accueil et de la compréhension globale de tout le système de dépôt, comprenant les barrières techniques et les barrières géologiques. Le laboratoire souterrain du Grimsel (LSG) est un laboratoire souterrain destiné à l'investigation de nombre de ces processus se déroulant en roche cohérente fissurée. En fonction depuis 1984, il est exploité par la Société coopérative nationale pour l'entreposage de déchets radioactifs (NAGRA).

Le laboratoire est situé à une altitude de 1730 m dans les roches granitiques du Massif Central de l'Aar, à 450 m de profondeur sous le flanc est du Juchlistock. On l'atteint par un tunnel d'accès horizontal à un longueur de 1200 m exploité par la centrale électrique de Oberhasli de la société KWO. La disposition des galeries qui accueillent le LSG a permis l'aménagement en 1990 d'une zone de radiation contrôlée (type B/C de l'AIEA) dans laquelle sont effectués des essais utilisant des traceurs radioactifs. Au fil des expériences acquises dans la réalisation des essais in-situ, d'une connaissance améliorée des processus et de l'évolution des concepts de dépôts, les programmes expérimentaux au LSG ont gagné en complexité et ont été mieux reliés aux questions en suspens posées par les analystes de la sûreté ou par les autorités de surveillance. La démonstration de faisabilité de concepts de dépôt sur la base d'expériences à grande échelle ou à l'échelle réelle et à long terme est devenue un élément clé des recherches au laboratoire souterrain. La phase IV du LSG, conduite de 1994 à 1996, a été mise sur pied en collaboration étroite avec plusieurs organisations partenaires au niveau international. Les programmes réalisés ont mis l'accent sur la caractérisation et la conceptualisation du champ proche de la galerie, déjà ausculté par les investigations géophysiques et les essais du retardement des radioéléments.

La phase V des investigations, actuellement en cours (1997 – 2002), comprend sept projets et programmes expérimentaux (cf. www.grimsel.com, pour détails).

Au cours de la phase IV du LSG, le programme RMP (Radionuclide Migration Programme) de la Nagra et du JNC sur l'étude de la migration des radioéléments a examiné le comportement d'une vaste gamme de radioéléments dans la géosphère. Le volet d'expériences sur la migration des radioéléments (MI), partie intégrante du RMP, a débuté en 1985 et s'est poursuivi jusqu'en 1996. Le présent rapport rend compte des résultats acquis durant la période 1990 – 1996 (pour la période 1985 – 1990, voir FRICK et al. 1992a, NTB 91-04). L'objectif principal du MI, le test de modèles de transport de radioéléments, a été appuyé par une série de projets comprenant: le développement d'une méthodologie de caractérisation de site, l'étude des contextes hydrogéologique, hydrochimique et géochimique du système eau-roche, une caractérisation structurale et minéralogique détaillée du site expérimental (une zone de cisaillement complexe), ainsi que par un programme d'accompagnement constitué d'études de laboratoire et de modélisation.

Le présent rapport est l'un des quatre rapports techniques de la Nagra (NTB) sur le programme RMP, les autres étant le NTB 00-06 (méthodologie RRP, *Radionuclide Retardation Project, Excavation Project EP-Phase II*), le NTB 00-07 (rapport final RRP, *EP-Phase III*) et le NTB 00-08 (rapport CP, *Connected Porosity*), qui seront résumés dans ALEXANDER (2001a). Les donnés sources sont dès maintenant disponibles gratuitement à l'adresse www.grimsel.com.

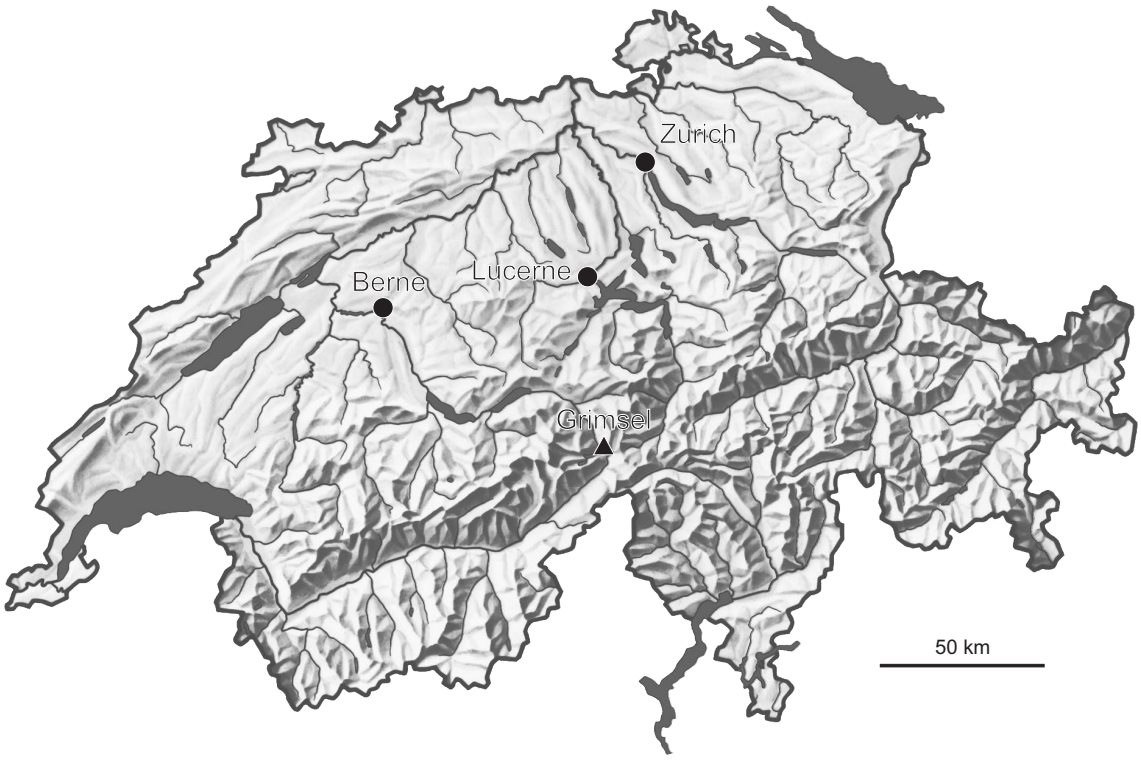

Location of Nagra's underground test facility at the Grimsel Pass in the Central Alps (Bernese Alps) of Switzerland

Grimsel area (view to the west)

1 Grimsel Test Site 2 Lake Raeterichsboden 3 Lake Grimsel 4 Juchlistock

Grimsel Test Site (GTS)

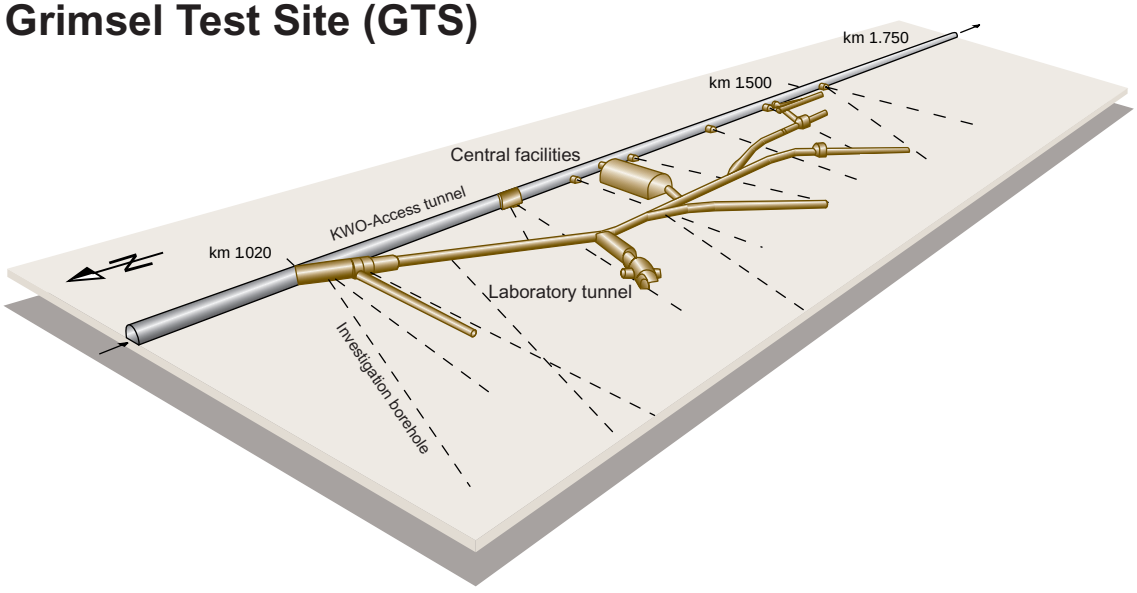

Grimsel Test Site
GTS

KWO-Access tunnel

Laboratory tunnel

Central Aaregranite (CAGR)
High biotite content CAGR

Grimsel-Granodiorite

Shear zone

Lamprophyre

SB — Investigation borehole

ZB Central facilities

BK Fracture system flow

GS Rock stresses

MI Migration

VE Ventilation test

WT Heater test

GTS Phase IV 1994-1996

BOS Borehole Sealing

TOM Further Development of Seismic Tomography

EDZ Excavation Disturbed Zone

TPF Two-Phase Flow

RRP Radionuclide Retardation Project

ZPK Two-Phase Flow in Fracture Networks of the Tunnel Near-field

ZPM Two-Phase Flow in the Unsaturated Matrix of Crystalline Rocks

FEBEX 1:1 EBS – Demonstration (HLW)

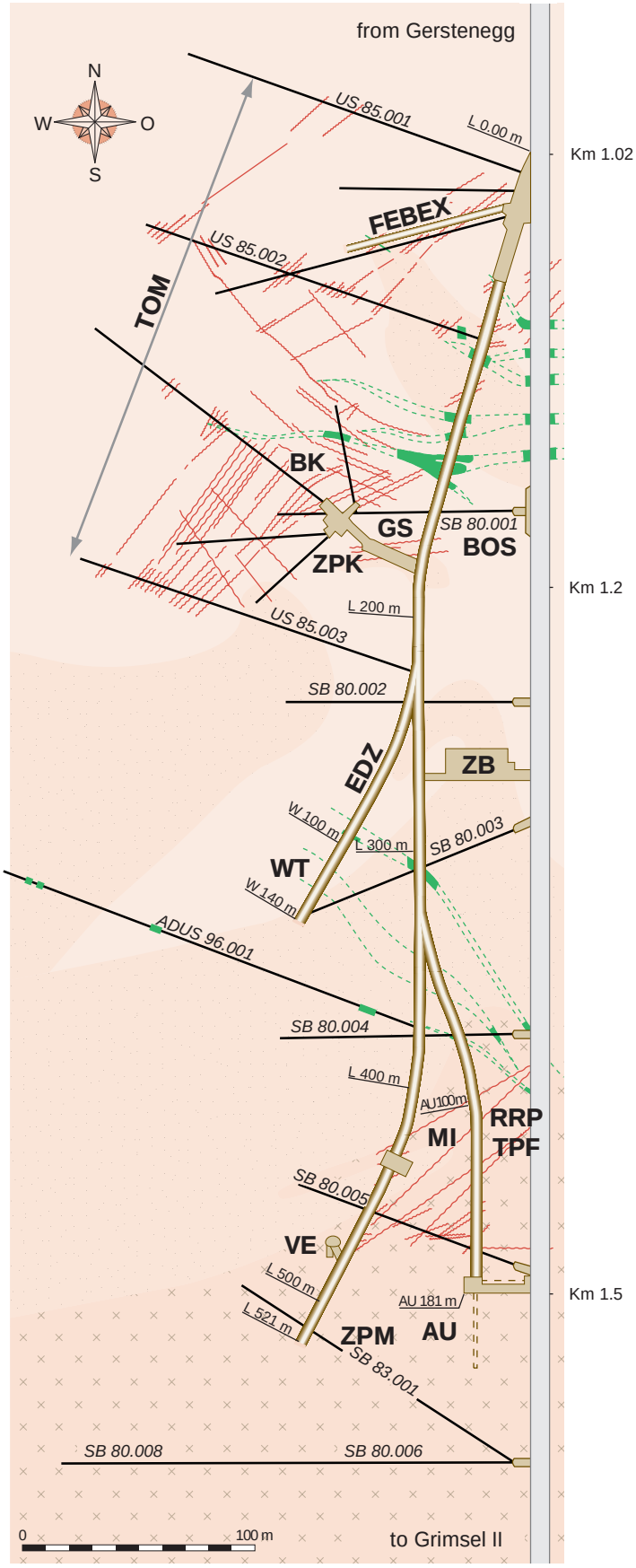

ABSTRACT

The Nagra-JNC[1] Radionuclide Migration Experiment (MI) is one of several investigations into the behaviour of radionuclides in the geosphere carried out at the Grimsel Test Site. The aims of MI were the development of methodologies for site characterisation, the study of the hydrology and geochemistry of fractured rock, the focussing of laboratory, field and modelling studies on the detailed characterisation of a single water-conducting feature, and the testing of models of radionuclide transport. The present report summarises the results of MI, updating an earlier overview report, provides a guide to detailed technical reports describing specific aspects of MI, and discusses the contribution of MI to building confidence in radionuclide transport models, including the applicability of these models to the performance assessment of radioactive waste repositories.

The central component of MI is a series of radionuclide transport tests performed in a single, approximately planar shear zone, in which well-defined dipole flow fields could be generated by injecting water at one location and extracting it at another. Tests were performed in flow fields of various sizes, strengths and locations and with a range of sorbing and non-sorbing radionuclides. In the course of carrying out the tests, a number of improvements were made to the test equipment, enhancing its reliability and minimising experimental artefacts that might affect tracer breakthrough curves. Accuracy of the measured breakthrough curves is particularly important since the effects of various retardation processes are apparent in the form of the curves only if they are measured for time periods that are several orders of magnitude longer, and for concentrations that are orders of magnitude lower, than the breakthrough peak.

In order to support the development and parameterisation of transport models, a detailed geological, geochemical and hydrogeological characterisation of the MI shear zone was carried out. The geological characterisation included an evaluation of the small- to micro-scale structure of the shear zone and the distribution of both flow and rock matrix porosity, which provide direct input to the development of transport models, as does the hydrogeological characterisation. Furthermore, natural decay-series isotope profiles perpendicular to the MI shear zone provide unambiguous evidence of connected, diffusion-accessible porosity extending for some centimetres into the rock matrix.

A series of laboratory and field experiments was performed to support the selection of sorbing tracers for the radionuclide transport tests, to determine the sorption properties of these tracers in laboratory conditions and to predict the *in situ* sorption properties of these tracers in the MI shear zone. The laboratory experiments centred on rock-water interaction tests and batch-sorption measurements on material from the shear zone (crushed mylonite). They included the evaluation of sorption kinetics, reversibility and concentration-dependence ("non-linearity"). A field hydrogeochemical equilibration experiment was also carried out and yielded further information on sorption properties. Three sorbing radionuclides were identified for transport tests: weakly-sorbing sodium and moderately-sorbing strontium, both of which sorb linearly, and more strongly-sorbing caesium, which displays non-linear sorption. A mechanistic sorption model was used to predict the *in situ* sorption behaviour of caesium, in order to take account of competition with potassium, which is present at lower concentrations in natural Grimsel groundwater than in the laboratory experiments.

Three different models were developed, and applied to MI breakthrough curves, by the Paul Scherrer Institute (PSI) and by the Federal Institute of Technology (ETH) in Switzerland, and by JNC in Japan. All of the models assume the dominant mechanisms for radionuclide transport

[1] The Japan Nuclear Cycle Development Institute (previously PNC, Power Reactor and Nuclear Fuel Development Corporation).

to be advection and dispersion in the MI shear zone, with retardation due to matrix diffusion into stagnant pore water (largely within the fault gouge) and, for sorbing tracers, sorption on mineral surfaces. The conceptual differences between the models were relatively minor. The JNC model, unlike the PSI and ETH models, took into account transmissivity heterogeneity in the shear zone, as derived from pumping tests. The ETH model, unlike the other two, incorporated transverse, as well as longitudinal dispersion. The models also differed in the manner in which the dipole flow field was discretised in order to solve the governing equations for transport.

All of the models were tested in terms of their ability to fit break-through curves and the consistency of the fitted parameters with what is known about the system. Furthermore, in order to maximise the contribution of MI to confidence building, emphasis was, where possible, placed on *predictive* model testing. Model parameters were derived from independent observations (e.g. sorption parameters inferred from laboratory experiments) and by inverse modelling (fitting) of the breakthrough curve for a non-sorbing tracer. Predictions were then made of the break-through curves for sorbing tracers (in advance of each test).

The PSI model was applied to a particularly wide range of tracer tests, in both inverse and predictive modelling exercises, including those with a shorter dipole flow field, where the different transport mechanisms are weighted differently. The success of these exercises for the majority of tests not only supports concepts underlying the model, indicating that no relevant processes have been overlooked, but also indicates that, for tracers that sorb rapidly and exhibit reversible cation exchange, the results of laboratory experiments can be extrapolated reasonably well to *in situ* conditions. Adequate care must, however, be taken in selecting and preparing rock samples, so as to ensure that they properly reflect the geological character of the site. There are indications that sorption kinetics may influence the breakthrough curve of caesium, which has slower sorption kinetics, in the case of the shorter dipole flow field. Such effects are not, however, relevant to the much longer spatial and temporal scales of performance assessment.

There are limitations to the degree to which the success of modelling breakthrough curves may be said to "validate" the models, in the sense of building confidence in their applicability in performance assessment. No information is provided, for example, on processes that, though irrelevant on the spatial and temporal scales of the transport tests, may be important over the scales relevant to performance assessment. Thus, the success of the predictions of the PSI, JNC and ETH models does not necessarily mean that the differences between the models are insignificant if applied in performance assessment and these differences may require further consideration.

Overall, MI has demonstrated that the methodology adopted for the characterisation of water-conducting features, the simplification of this characterisation for modelling purposes, the adaptation of laboratory data (particularly sorption data) to field conditions, the selection of transport-relevant processes and the numerical solution of the governing equations, is applicable to the modelling of solute transport through a fractured crystalline rock. Apart from the technical achievements (and limitations) noted above, the participation in MI has resulted in the development of a culture of rigorous model testing and, arguably more importantly, of predictive model testing in the organisations involved. Furthermore, experience of working in a multi-disciplinary team on a long-term, challenging project has been considered to be of value to all participants, establishing successful communications between geoscientists, laboratory and field experimenters and modellers.

ZUSAMMENFASSUNG

Der Nagra-JNC[2] Migrationsversuch MI (Radionuclide Migration Experiment) ist Teil einer Reihe von Untersuchungen zum Verhalten von Radionukliden in der Geosphäre, die im Felslabor Grimsel durchgeführt wurden. Die Zielsetzung von MI umfasste die Entwicklung von Methoden zur Standortcharakterisierung, die Untersuchung der Hydrologie und Geochemie von geklüftetem Gestein, die Ausrichtung von Labor-, Feld- und Modellierungsstudien auf die detaillierte Charakterisierung einer einzelnen wasserführenden Kluft und den Test von Radionuklid-Transportmodellen. Der vorliegende Bericht fasst die Resultate des MI zusammen, wobei ein früherer Übersichtsbericht aktualisiert wird, und verweist auf weitere detaillierte Technische Berichte, die spezifische Aspekte des MI beschreiben. Ausserdem wird diskutiert, inwieweit MI zum Aufbau von Vertrauen in Radionuklid-Transportmodelle beiträgt, und ob solche Modelle in der Sicherheitsanalyse für die Lagerung radioaktiver Abfälle anwendbar sind.

Der zentrale Teil des MI besteht aus einer Reihe von Radionuklidtransport-Tests, die in einer einzelnen, ungefähr planaren Scherzone durchgeführt wurden, in der gut definierte Dipol-Fliessfelder erzeugt werden konnten durch Injektion von Wasser an einer bestimmten Stelle und Extrahieren dieses Wassers an einer anderen. Es wurden Tests in Fliessfeldern unterschiedlicher Grösse, Stärke und Lokalität durchgeführt mit einer Reihe von sorbierenden und nicht-sorbierenden Radionukliden. Im Verlauf dieser Tests wurde das Testequipment mehrfach verbessert, damit deren Zuverlässigkeit optimiert und experimentelle Artefakte verringert, welche die Tracer-Durchbruchskurven hätten beeinflussen können. Die Genauigkeit der gemessenen Durchbruchskurven ist besonders wichtig, da sich die Auswirkungen der verschiedenen Retardierungsprozesse nur in der Kurvenform manifestieren, sofern die dafür gemessenen Zeiträume einige Grössenordnungen länger und die Konzentrationen einige Grössenordnungen kleiner sind als der Durchbruchspeak.

Zur Unterstützung der Entwicklung und Parametrisierung von Transportmodellen wurde eine detaillierte geologische, geochemische und hydrogeologische Charakterisierung der MI-Scherzone durchgeführt. Die geologische Charakterisierung umfasste eine Evaluation der kleinräumlichen Strukturen und Mikrostrukturen der Scherzone und die Verteilung sowohl der Fliessporosität als auch der Matrixporosität, die – wie die hydrogeologische Charakterisierung – einen direkten Input für die Entwicklung von Transportmodellen liefert. Zudem zeigen Profile von Isotopen der natürlichen Zerfallsreihen senkrecht zur MI Scherzone klare Anzeichen einer verbundenen, für die Diffusion zugänglichen Porosität, die sich einige Zentimeter weit in die Gesteinsmatrix erstreckt.

Es wurde eine Anzahl von Labor- und Feldexperimenten durchgeführt, die die Auswahl von sorbierenden Tracern für die Radionuklidtransport-Tests, die Bestimmung der Sorptionseigenschaften dieser Tracer unter Laborbedingungen sowie die Vorhersage der In-situ-Sorptionseigenschaften der Tracer in der MI-Scherzone unterstützen sollten. Die Laborexperimente konzentrierten sich auf Tests zur Gestein-Wasser-Wechselwirkung und Batch-Sorptionsversuche mit Material aus der Scherzone (zermahlener Mylonit). Sie schlossen die Evaluation der Sorptionskinetik, Reversibilität und Konzentrationsabhängigkeit ein ("Nicht-Linearität"). Im Feld wurde ebenfalls ein hydrogeochemisches Gleichgewichtsexperiment durchgeführt, das weitere Informationen zu den Sorptionseigenschaften lieferte. Drei sorbierende Radionuklide konnten für die Transport-Tests identifiziert werden: schwach-sorbierendes Natrium, mässig-sorbierendes Strontium, wobei beide linear sorbieren, sowie stärker-sorbierendes Cäsium, das ein nicht-lineares Sorptionsverhalten aufweist. Ein mechanistisches Sorptionsmodell wurde verwendet, um das In-situ-Sorptionsverhalten von Cäsium vorauszusagen und damit einer

[2] The Japan Nuclear Cycle Development Institute (früher PNC, Power Reactor and Nuclear Fuel Development Corporation).

Konkurrenzierung durch Kalium Rechnung zu tragen, das im natürlich vorhandenen Grimsel-Grundwasser in niedrigeren Konzentrationen als in den Laborexperimenten vorhanden ist.

Vom Paul Scherrer Institut (PSI) und der Eidgenössischen Technischen Hochschule (ETH) in der Schweiz sowie JNC in Japan wurden drei verschiedene Modelle entwickelt und für die MI-Durchbruchskurven angewendet. Alle Modelle nehmen an, dass Advektion und Dispersion die vorherrschenden Mechanismen für den Radionuklidtransport in der MI-Scherzone sind, wobei die Retardierung aufgrund von Matrixdiffusion in stagnierendes Porenwasser (weitgehend innerhalb der Kluftfüllung) erfolgt und bei den sorbierenden Tracern aufgrund der Sorption auf Mineraloberflächen. Die konzeptuellen Unterschiede zwischen den verschiedenen Modellen waren dabei eher unwesentlich. Das JNC-Modell berücksichtigte, im Gegensatz zu den PSI- und ETH-Modellen, Transmissivitätsheterogenitäten innerhalb der Scherzone, die aus Pumpversuchen abgeleitet wurden. Das ETH-Modell implementierte, im Gegensatz zu den anderen beiden Modellen, sowohl transversale als auch longitudinale Dispersion. Die Modelle unterscheiden sich ebenfalls in der Art der Diskretisierung des Dipol-Fliessfelds zur Lösung der bestimmenden Transportgleichungen.

Sämtliche Modelle wurden bezüglich ihrer Reproduzierbarkeit der gemessenen Durchbruchskurven getestet und der Konsistenz der gefitteten Parameter mit den bekannten Systemeigenschaften. Zudem wurde nach Möglichkeit das Testen von Vorhersagemodellen in den Vordergrund gestellt, um den Beitrag des MI zur Evaluierung der Belastbarkeit der Modelle zu erhöhen. Die Modellparameter wurden von unabhängigen Beobachtungen (z. B. Sorptionsparametern anhand von Laborexperimenten) abgeleitet sowie durch inverse Modellierung (Fitting) der Durchbruchskurve für einen nicht-sorbierenden Tracer. Für die Durchbruchskurven der sorbierenden Tracer wurden dann Vorhersagen getroffen (vor jedem Test).

Das PSI-Modell wurde auf eine grosse Anzahl von Tracertests angewendet mit zwei verschiedenen Modellansätzen – inverser Modellierung und Vorhersagemodell – einschliesslich solcher mit kürzerem Dipol-Fliessfeld, wobei die jeweiligen Transportmechanismen unterschiedlich gewichtet wurden. Die erfolgreichen Ergebnisse dieses Aufwands unterstützen bei der Mehrzahl der Tests nicht nur die Modellkonzepte, indem dargelegt werden kann, dass keine relevanten Prozesse übersehen wurden, sondern zeigen auch, dass die Resultate der Laborexperimente für schnell sorbierende Tracer, die reversiblen Kationenaustausch aufweisen, relativ gut auf die In-situ-Bedingungen übertragen werden können. Allerdings müssen die Gesteinsproben sorgfältig ausgewählt und vorbereitet werden, um sicherzustellen, dass sie repräsentativ für die geologischen Eigenschaften des Standorts sind. Es gibt Hinweise, dass beim kürzeren Dipolfeld die Durchbruchskurve von Cäsium, das eine langsamere Sorptionskinetik aufweist, durch die Sorptionskinetik beeinflusst werden kann. Solche Effekte sind jedoch nicht relevant für die weitaus längeren räumlichen und zeitlichen Massstäbe der Sicherheitsanalyse.

Es gibt Grenzen, inwieweit die erfolgreiche Modellierung der Durchbruchskurven zur Validierung der Modelle herangezogen werden kann, im Sinne des Aufbaus von Vertrauen bzw. der Belastbarkeit bei deren Anwendung in der Sicherheitsanalyse. Beispielsweise wird keine Information zu Prozessen geliefert, die zwar bezüglich des räumlichen und zeitlichen Massstabs der Transport-Tests unerheblich sind, aber dennoch im Rahmen der für die Sicherheitsanalyse betrachteten Massstäbe wichtig sein könnten. Somit bedeuten die mit den PSI-, JNC- und ETH-Modellen erfolgreich getroffenen Voraussagen nicht unbedingt, dass die Unterschiede zwischen den Modellen unbedeutend sind, wenn sie in der Sicherheitsanalyse angewendet werden. Diese Unterschiede müssten näher untersucht werden.

Insgesamt hat MI gezeigt, dass die angewandte Methodik für die Charakterisierung der wasserführenden Strukturen, die Vereinfachung dieser Charakterisierung für Modellierungszwecke, die Übertragung der Labordaten (insbesondere der Sorptionsdaten) auf Feldbedingungen, die Auswahl der transportrelevanten Prozesse sowie für die numerische Lösung der modellbestimmenden Gleichungen zur Modellierung des Lösungstransports durch das geklüftete kristalline Gestein geeignet ist. Abgesehen von den oben erwähnten technischen Leistungen (und Grenzen), hat die Teilnahme am MI bei den involvierten Organisationen zur Entwicklung eines strikten Modelltestverfahrens geführt und vielleicht noch wichtiger, eines Verfahrens zum Test von Vorhersagemodellen. Zudem wurden die Erfahrungen bei der Zusammenarbeit innerhalb eines multidisziplinären Teams in einem herausfordernden Langzeitprojekt von allen Teilnehmern als wertvoll erachtet und resultierte in einer erfolgreichen Kommunikation zwischen Geowissenschaftlern, Labor- und Feldexperimentatoren und Modellierern.

RÉSUMÉ

L'expérience de migration de radioéléments (MI) de la Nagra et du JNC[3] est l'une des multiples investigations sur le comportement des radioéléments dans la géosphère menées au laboratoire souterrain du Grimsel. Le projet MI avait pour objectifs le développement de méthodologies pour la caractérisation d'un site, l'étude de l'hydraulique et de la géochimie des roches fissurées, la synergie d'études en laboratoire, sur le terrain et par modèles sur la caractérisation détaillée d'une structure aquifère isolée, ainsi que le test de modèles de transport de radioéléments. Le présent rapport résume les résultats de ce projet tout en actualisant un rapport précédent, fournit un guide des rapports techniques sur les aspects spécifiques de la MI, et évalue son apport à la fiabilité des modèles de transport de radioéléments, ainsi qu'à leur applicabilité à l'analyse de sûreté de dépôts de déchets radioactifs.

La partie principale de la MI consiste en une série d'essais de traçage effectués dans une zone cisaillement bien distincte et à peu près plane, dans laquelle on a pu générer des champs d'écoulement dipolaire bien définis en injectant de l'eau à un endroit et en la soutirant à un autre. Les essais ont été effectués à différents endroits, échelles et intensités. Un certain nombre d'améliorations ont été apportées à l'équipement au cours des essais, avec pour résultat de renforcer sa fiabilité et de minimiser les artefacts expérimentaux pouvant affecter les courbes de restitution des traceurs. La précision des courbes de restitution est particulièrement importante, puisque le processus de retardement dû à la diffusion dans la matrice n'apparaît sous forme de courbe que si les mesures sont faites sur des périodes plus longues de plusieurs ordres de grandeur que celles du pic d'apparition, et à des concentrations de plusieurs ordres de grandeur plus faibles.

Pour faciliter le développement et la paramétrisation des modèles de transport, on a entrepris une caractérisation détaillée de la zone de cisaillement de la MI sur les plans géologique, géochimique et hydrogéologique. La caractérisation géologique a permis d'évaluer la structure de la zone de cisaillement à petite et micro-échelle, ainsi que la distribution spatiale des porosités totale et efficace. Elle a ainsi fourni des données directement utilisables pour le développement des modèles de transport, comme l'a aussi fait la caractérisation hydrogéologique. De plus, des profils de désintégration d'isotopes naturels, perpendiculaires à la zone de cisaillement, ont montré la présence univoque d'une porosité interconnectée accessible à la diffusion sur quelques centimètres à partir des régions d'écoulement d'eau souterraine.

Une série d'essais en laboratoire et sur le terrain a été effectuée pour faciliter la sélection de traceurs adsorbants à utiliser pour les essais. Ces tests étaient destinés à évaluer les propriétés d'adsorption des traceurs dans des conditions de laboratoire, et d'en tirer une prévision sur leurs propriétés d'adsorption in situ dans la zone de cisaillement. Les essais en laboratoire ont été focalisés sur des tests d'interaction eau-roche et sur des mesures d'adsorption globale sur des échantillons de la zone de cisaillement (mylonite broyée). Ils ont permis d'évaluer les cinétiques d'adsorption, la réversibilité et le rôle de la concentration ("non-linéarité"). Le retour à l'équilibre géochimique a également été testé in situ, ce qui a fourni des informations supplémentaires sur les propriétés d'adsorption. Trois traceurs adsorbant ont été sélectionnés pour les essais de traçage : du sodium faiblement adsorbant et du strontium modérément adsorbant, tous deux adsorbant de manière linéaire, et du césium plus fortement adsorbant, adsorbant de manière non linéaire. Un modèle d'adsorption mécaniste a été utilisé pour prédire le comportement adsorbant in situ du césium, afin de tenir compte de la compétition avec le potassium, présent en plus faible concentration dans l'eau souterraine naturelle du Grimsel que dans les essais en laboratoire.

[3] Japan Nuclear Cycle Development Institute (autrefois PNC, Power Reactor and Nuclear Fuel Development Corporation).

Trois modèles différents ont été développés et appliqués aux courbes de restitution de la MI, en Suisse par l'Institut Paul Scherrer (PSI) et par l'Ecole polytechnique fédérale (EPF), et au Japon par le JNC. Tous ces modèles supposent que les mécanismes dominants de transport des traceurs sont la convection et la dispersion dans la zone de cisaillement, avec un effet retardateur dû à la diffusion à travers la matrice rocheuse, dans l'eau stagnante des pores (en grande partie à l'intérieur des matériaux de colmatage) et, pour les traceurs adsorbants, à l'adsorption sur la surface des minéraux. Les différences de conception des modèles sont relativement mineures. Le modèle du JNC, à la différence de ceux du PSI et de l'EPF, prend en compte l'hétérogénéité de la transmissivité dans la zone de cisaillement, obtenue par l'analyse des essais de pompage. Le modèle de l'EPF, à l'encontre des deux autres, inclut les dispersions longitudinale et transversale. Les modèles se distinguent aussi dans la discrétisation du champ d'écoulement dipolaire effectuée pour résoudre les équations de transport.

Tous les modèles ont été testés sur leur capacité à reproduire les courbes de restitution et sur la cohérence des paramètres ajustés avec les connaissances déjà acquises du système. En outre l'accent a été mis, là où c'était possible, sur l'examen des capacités prédictives des modèles, afin de maximiser l'apport de l'expérience MI à la fiabilité des analyses de sûreté. Les paramètres des modèles ont été déduits d'observations indépendantes (par exemple les paramètres d'adsorption proviennent d'expériences en laboratoire) et de la modélisation inverse (ajustement) des courbes de restitution d'un traceur non adsorbant. Les prévisions des courbes de restitution ont ensuite été simulées pour des traceurs adsorbants (avant chaque essai).

Le modèle du PSI a été appliqué à une palette particulièrement large de tests, pour des simulations inverses et des simulations prédictives, en particulier celles portant sur un champ d'écoulement dipolaire court, où les différents mécanismes de transport sont pondérés de manière variée. Le succès de ces exercices, dans la majorité des cas, non seulement confirme les concepts sous-jacents au modèle, indiquant qu'aucun processus significatif n'a été omis, mais il indique aussi que pour les traceurs qui sont rapidement adsorbés et qui ont une capacité d'échange cationique réversible, les résultats acquis en laboratoire peuvent être extrapolés raisonnablement bien aux conditions in situ. Un soin particulier doit toutefois être apporté dans la sélection et la préparation des échantillons, afin d'assurer qu'ils représentent correctement les propriétés géologiques du site. Dans le cas du champ dipolaire court, il y a des éléments indiquant que les cinétiques d'adsorption peuvent influencer les courbes de restitution du césium, dont les cinétiques d'adsorption sont plus lentes. Des effets de ce genre ne sont toutefois pas significatifs pour les champs d'écoulement bien plus étendus, sur les plans spatial temporel, pris en compte dans les analyses de sûreté.

Modéliser avec succès des courbes de restitution ne doit pas toujours être considéré comme une validation des modèles, au sens de la confiance qu'on peut leur accorder pour les analyses de sûreté. Par exemple, on ne dispose pas d'information sur des processus insignifiants à l'échelle spatiale et temporelle des essais de traçage effectués mais qui pourraient devenir importants aux échelles considérées pour les analyses de sûreté. Ainsi, les prévisions correctes des modèles du PSI, de l'EPF et du JNC ne signifient pas nécessairement que les différences entre eux resteront insignifiantes lorsqu'on utilisera ces modèles pour les analyses de sûreté; ces différences devront peut-être faire l'objet d'une évaluation ultérieure.

Avant tout, le projet MI a démontré la faisabilité de la modélisation du transport de soluté en roche cristalline fracturée, avec la méthodologie adoptée pour la caractérisation des structures aquifères, leur simplification pour les besoins de la modélisation, l'adaptation des résultats de laboratoire (en particulier les valeurs d'adsorption) aux conditions de terrain, la sélection des processus significatifs pour le transport et la solution numérique des équations le gouvernant.

En dehors des réalisations techniques (et des limitations) mentionnés plus haut, la participation au projet MI a permis aux organisations concernées de développer un savoir-faire pour le test rigoureux de modèles et, mieux encore, pour le test de modèles prévisionnels. De plus, le fait de travailler dans une équipe pluridisciplinaire sur un projet de longue haleine représentant un défi a été considéré par tous les participants comme une expérience précieuse de communication réussie entre géologues, techniciens de laboratoire et de terrain et modélistes.

LIST OF CONTENTS

LIST OF TABLES

LIST OF FIGURES

1 INTRODUCTION

P.A. Smith and W.R. Alexander

1.1 Aims and Structure of the Report

Nagra (Swiss National Cooperative for the Disposal of Radioactive Waste) and JNC (Japan Nuclear Cycle Development Institute, previously PNC, Power Reactor and Nuclear Fuel Development Corporation) in collaboration with PSI (Paul Scherrer Institute, Switzerland) have worked together for over a decade on a Radionuclide Migration Programme at the Grimsel Test Site (GTS), the Nagra underground research laboratory situated in the Central Swiss Alps. This report provides a summary of part of the field, laboratory and modelling work carried out as part of the Nagra-JNC Radionuclide Migration Experiment (MI), one of several investigations of various aspects of radionuclide behaviour in the geosphere carried out at the GTS (see SMITH et al. 2001, for details). The many component studies within MI are presented in numerous Nagra Technical Reports (NTBs) and external publications in the open literature, with a detailed overview of investigations carried out in the period 1985 – 1990 provided by FRICK et al. (1992a). The present report emphasises work carried out from 1990 until the end of the MI project in 1996. Specific aims of the report are:

- to summarise the results of MI, including modelling work and supporting laboratory studies, updating the earlier overview report;
- to provide a guide to detailed technical reports describing specific components of MI;
- to discuss the contribution that the MI has made to the building of confidence in the methodologies, models and data that are available for the prediction of radionuclide transport through a host rock for a radioactive waste repository.

Chapter 1 describes the location of the GTS, and the objectives and scope of the research performed there. Also presented are the aims of MI, the broad characteristics of the shear zone in which the tracer tests are performed and the phase of radionuclide-migration studies at the GTS which followed MI, namely those within the RRP, the Radionuclide Retardation Project. Finally, the contribution that projects such as MI can make to repository performance assessment, through confidence building in methodologies, models and data, is discussed.

Chapter 2 describes, in more detail, the contribution made by MI to the testing ("validation") of models and data for geosphere transport. The approach to model testing is described whereby alternative models are formulated and tested independently to address conceptual model uncertainty. For each model, two levels of testing are distinguished: level 1 (the weaker) tests the degree to which a model can reproduce, or fit, experimental results and can be used to calibrate a model for level 2 (stronger) predictive (or 'blind') testing.

Chapter 3 presents a historical background to the MI experiment, an overview of how the field experiments were physically carried out, includes a list of all experimental runs (a total of 90) and, finally, gives brief information on apparatus development.

Chapter 4 describes the geological and geochemical and hydrogeological characterisation of the MI shear zone. The origin, mineralogy, porosity and pore-space distribution of mylonite and fault gouges in the MI shear zone, as well as of the parent rock, are presented. The pathways for advection, the existence of connected porosity for matrix diffusion, the key features of the groundwater composition and hydrogeological characteristics, including heterogeneity, are discussed.

Chapter 5 describes the laboratory and field tests that have been performed in support of MI. These include, in the laboratory, rock-water interaction tests, batch-sorption tests and a dynamic infiltration experiment (the latter found only limited use due to problems with the apparatus). In the field, a hydrogeochemical equilibration experiment was performed. The interpretation of the test results in order to select suitable tracers for MI and to understand and predict their sorption behaviour is discussed.

Chapter 6 describes the three alternative models that have been applied to data produced in MI. The concepts and physical and chemical processes that are common to all of the transport models are first discussed and the capabilities of the computer codes that are used to solve the equations for transport are listed, before presenting the differences between the models. Data for the transport models are evaluated using supporting models (described in detail) for (i), the large-scale distribution of flow within the shear zone plane, (ii) the small-scale structure of the shear zone and (iii), sorption processes.

Chapter 7 describes the form of the break-through curves that have been generated in MI in terms of the underlying transport processes and discusses the application of these results to the alternative transport models. Examples of both level 1 and level 2 testing are given. All the models are capable of generating curves that closely match most experimental break-through curves. An examination of the parameters required for these fits, as well as the predictive model exercises, were, however, more revealing in terms of the limitations of the models. Technical conclusions from the application of the alternative models to MI are drawn.

Chapter 8 summarises the achievements and limitations of MI and, finally, a number of general conclusions are drawn based on the experience gained over the twelve-year duration of the project.

1.2 Background to the Grimsel Test Site (GTS)

The GTS, a series of drifts located approximately 450 metres beneath the east flank of the Juchlistock mountain in the crystalline rocks of the Aare Massif in the central Swiss Alps, was opened in 1984. The tunnel system of the GTS is at an altitude of 1749 – 1789 metres above sea level and branches off a pre-existing access tunnel to a hydro-electric power scheme. It was mainly excavated using a full-face tunnel-boring machine with a diameter of 3.5 m. The environs of the GTS have been characterised by a variety of geological, geophysical, rock-mechanical, hydrological and hydrogeochemical techniques. A list of the major references describing this characterisation is presented in Table 1.1.

The objectives of research at the Grimsel Test Site are:

- the acquisition of practical experience in the development and application of investigation methodologies, measurement techniques and test equipment that will be of use during actual repository site investigation
- the investigation of physical and chemical processes that are relevant to the safety of a repository
- the accumulation of know-how in various scientific and technical disciplines necessary for planning, performing and interpreting field experiments.

The research programme to date has been subdivided into five phases, comprising the experiments shown in Table 1.2.

Tab. 1.1: Major references for the geological, geophysical, rock-mechanical, hydrological and hydrogeochemical characterisation of the environs of the GTS (update of Tab. 2-1 of FRICK et al. 1992a)

Geology: GEOTEST AG & INGENIEURUNTERNEHMUNG AG BERN (1981); STALDER (1981); NAGRA (1985); GEOTEST (1987); MÜLLER (1988); KEUSEN et al. (1989); MAJER et al. (1990c); MARTEL & PETERSON (1990)
Structural Geology, Tectonics: LABHART (1966); STECK (1968); CHOUKROUNE & GAPAIS (1983); MARQUER et al. (1985); BOSSART & MARTEL (1990); MAJER et al. (1990c); MARTEL & PETERSON (1990, 1991); BOSSART & MAZUREK (1991); MÖRI et al. (2001a, b)
Geophysics: FALK et al. (1988); WBK (1988); BLÜMLING & SATTEL (1988); NIVA et al. (1988); BRÄUER et al. (1989); FLACH & NOELL (1989); MAJER et al. (1990a, b); MARTEL & PETERSON (1990); NOELL & ZÜRN (1991); ALBERT et al. (1999)
Rock Mechanics, Neotectonics: EGGER (1986); PAHL et al. (1986); BRÄUER et al. (1989); PAHL et al. (1989); SCHNEEFUSS et al. (1989); FLACH & NOELL (1989); MAJER et al. (1990c); NOELL & ZÜRN (1991)
Hydrology: GEOTEST AG & INGENIEURUNTERNEHMUNG AG BERN (1981); GEOTEST (1987); BREWITZ et al. (1988); FALK et al. (1988); FRICK et al. (1988); LIEDTKE & ZUIDEMA (1988); NIVA et al. (1988); HERZOG (1989); WYSS (1989); HOEHN et al. (1990); KELLEY & FRIEG (1990); MAJER et al. (1990c); WATANABE (1991); BOSSART & MAZUREK (1991); PAHL et al. (1992); KULL et al. (1993); CORREA (1994); LIEDTKE et al. 1994; MARSCHALL & VOMVORIS (1995); MARSCHALL et al. (1999); MEIER (2002)
Hydrodynamic Modelling: HUFSCHMIED & ADANK (1988); HERZOG (1989); KUHLMANN (1989); STIESS (1990); WYSS (1990); DAVEY et al. (1990); FINSTERLE et al. (1990); LONG et al. (1990); HERZOG (1991); VOBORNY et al. (1991); KULL & MIEHE (1995)
Hydrochemistry: OHSE (1983); GEOTEST (1987); FRICK et al. (1988); BRADBURY (1989); EIKENBERG (1989); DEGUELDRE et al. (1989); DEGUELDRE et al. (1990); HOEHN et al. (1990); AKSOYOGLU et al. (1991); BAERTSCHI et al. (1991); EIKENBERG et al. (1991, 1994)
Isotope and Analogue Studies: WERNLI et al. (1984); ALEXANDER et al. (1990a, b); BAERTSCHI et al. (1991)

The experiments are carried out with extensive international co-operation. Participating organisations are listed in Table 1.3.

Progress and results in Phases I – III projects, and interim results of the Phase IV projects, are summarised in KICKMAIER & McKINLEY (1996) and final results of Phase IV along with interim results of Phase V are presented in KICKMAIER et al. (2001).

Tab. 1.2: Experiments at the Grimsel Test Site within Phases I – V

Experiment	Scope	Participating Organisations (*see Table 1.3*)
PHASES I – II (1984 – 1990)		
AU	Excavation disturbed zone	Nagra
BK	Fracture system flow test	BGR
EM	Electromagnetic high-frequency measurements	BGR
FRI	Fracture zone investigation	Nagra, USDoE
GS	Rock stress measurements	BGR
HPA	Hydraulic potential	Nagra
MI	Migration experiment	Nagra, JNC
MOD	Hydrodynamic modelling	Nagra
NFH	Nearfield hydraulics	Nagra
NM	Tilt metres	GRS
SVP	Prediction ahead of tunnel face	Nagra
US	Underground seismics	Nagra
UR	Underground radar	Nagra
VE	Ventilation test	GRS
WT	Heater test	GRS
PHASE III (1990 – 1993)		
BK	Fracture system flow test	BGR, Nagra
MI	Migration experiment	Nagra, JNC
MOD	Hydrodynamic modelling	Nagra
UZ	Unsaturated zone	Nagra
VE	Ventilation test	GRS, Nagra
-	Large-scale drilling test	ANDRA
PHASE IV (1994 – 1996)		
BOS	Borehole sealing	Nagra, ANDRA
CP	Connected porosity in the rock matrix	Nagra, JNC
EDZ	Excavation disturbed zone	Nagra
FEBEX	Full-scale engineered barriers experiment	ENRESA, Nagra, EC
MI	Migration experiment	Nagra, JNC
RRP	Radionuclide retardation project	Nagra, JNC
TOM	Further development of seismic tomography	Nagra
TPF	Two-phase flow	Nagra
ZPK	Two-phase flow in fracture networks	BGR
ZPM	Two-phase flow in rock matrix	GRS
PHASE V (1997 – 2002)		
HPF	Hyperalkaline plume in fractured rocks	Nagra, JNC, SKB, USDoE, SNL, ANDRA
CRR	Colloid and radionuclide retardation experiment	Nagra, BMWi, FZK/INE, ENRESA, JNC, USDoE, SNL, ANDRA
GAM	Gas migration in shear zones	Nagra, ENRESA, USDoE, SNL, ANDRA
CTN	Conclusion of the tunnel near field	Nagra, BMWi, GRS, BGR, ERL/ITRI
FEBEX	Full-scale engineered barrier experiment	ENRESA, EC, Nagra
GMT	Gas migration test in the EBS and geosphere	RWMC, Nagra, Obayashi
EFP	Effective parameters	BMWi, BGR, GRS, Nagra
GMB	Geophysical methods in boreholes	ANDRA, Nagra
FOM	Operational safety monitoring with fibre optic sensing systems	BMWi, DBE/T, ID-FOS, Nagra

Tab. 1.3: Funding organisations participating in research carried out at the GTS

Switzer-land:	Nagra	*National Cooperative for the Disposal of Radioactive Waste, Wettingen*
	GNW	*Genossenschaft für Nukleare Entsorgung, Wettingen*
	BBW	*Bundesamt für Bildung und Wissenschaft, Bern*
Czech Republic:	RAWRA	*Radioactive Waste Repository Authority, Praha*
Germany:	BGR	*Bundesanstalt für Geowissenschaften und Rohstoffe, Hannover*
	BMWi	*Bundesministerium für Wirtschaft und Technologie, Bonn*
	DBE/T	*Deutsche Gesellschaft zum Bau und Betrieb von Endlagern für Abfallstoffe mbH Technologie, Peine*
	FZK/INE	*Forschungszentrum Karlsruhe, Institut für Nukleare Entsorgungstechnik, Karlsruhe*
	GRS	*Gesellschaft für Anlagen- und Reaktorsicherheit GmbH, Köln*
France:	ANDRA	*Agence Nationale pour la Gestion des Déchets Radioactifs, Fontenay-aux-Roses*
Japan:	JNC	*Japan Nuclear Cycle Development Institute, Tokai*
	RWMC	*Radioactive Waste Management Funding and Research Centre, Tokyo*
	Obayashi	*Obayashi Corporation, Tokyo*
Spain:	ENRESA	*Empresa Nacional de Residuos Radioactivos SA, Madrid*
Sweden:	SKB	*Svensk Kärnbränslehantering AB, Stockholm*
Taiwan:	ERL/ITRI	*Energy and Resources Laboratories, Industrial Technology Research Institute, Chutung Hsinchu*
USA:	USDoE	*Department of Energy, Washington D.C.*
European Union:	EC	*European Commission, Brussels*

1.3 Background to the Migration Experiment

The Migration Experiment was initially conceived as a collaborative project between Nagra and the Paul Scherrer Institute (PSI, previously EIR, Swiss Federal Reactor Research Institute). The project was substantially extended following the signing in 1989 of a bilateral agreement with PNC, the Japanese Power Reactor and Nuclear Fuel Development Corporation (now JNC, Japanese Nuclear Cycle Development Institute). The original project proposal of McKINLEY & GROGAN (1984) gives the aims of MI as:

- the development of methodologies for site characterisation,
- the study of the hydrology and geochemistry of fractured rock,
- the focussing of laboratory, field and modelling studies on the detailed characterisation of a single water-conducting feature,
- the testing of models of radionuclide transport.

The central component of MI is a series of tracer transport tests performed in well-defined dipole flow fields within a single, approximately planar, shear zone (AU 96 in Figure 1.1). Water is injected at one location in the shear zone and extracted typically at a higher flow rate, at another location, giving rise to the dipole flow field. MI is supported by a range of field, natural analogue and laboratory investigations and modelling studies aimed at understanding and, ultimately, predicting the results of the tracer tests.

The shear zone was selected on the basis of the following site-selection criteria (Section 2.4 of FRICK et al. 1992a):

- steady-state hydrochemistry (i.e. little or no variation with time of the concentrations of major and trace elements in the groundwater),
- steady-state hydrology (i.e. little or no variation with time of hydrogeological characteristics – especially pressures and transmissivities – over the time scale of typical tracer tests),
- practicable experimental time scales (i.e. breakthrough of moderately retarded tracers over distances of a few metres should occur within a few weeks or less),
- minimal disturbance (i.e. uncontaminated setting and no interference with other activities at the GTS),
- saturated flow conditions.

In order to avoid possible hydrological and hydrochemical disturbances associated with the laboratory tunnel, the tracer tests were conducted in a portion of the shear zone at some distance from the tunnel wall, accessed by boreholes drilled from the tunnel. During 1986 and 1987, a total of eight boreholes, between 6 and 25 m long, were drilled to intersect the shear zone at distances of 3 to 16 m from the tunnel wall (Figure 1.1). Two of the eight boreholes intersected relatively impermeable parts of the migration shear zone, while subsequent hydrogeological testing of the six water-discharging boreholes revealed local heterogeneity in the transmissivity, with transmissivity values ranging from 5×10^{-6} to about 10^{-9} $m^2 s^{-1}$. On the scale of a few metres, however, part of the shear zone can be treated as relatively homogeneous with an average transmissivity of 2×10^{-6} $m^2 s^{-1}$, based on the results of a large number of cross-hole tests (HOEHN et al. 1990, Chapter 4 of FRICK et al. 1992a). However, as pointed out in Chapter 4 and Appendix 1 of this report, the shear zone transmissivity is heterogeneous at larger scales, in agreement with the structural data discussed in the same chapter. The groundwater in the shear zone is suboxic to anoxic, alkaline (pH ~ 9.6) and has a low ionic strength (0.0012 M, see Chapter 4 for details).

First pilot tracer tests were carried out in 1988, but a variety of experimental problems had to be solved before a suite of tracer experiments suitable for transport model testing, employing a range of conservative and sorbing tracers in an imposed dipole flow field (see Figure 1.1), commenced in 1990. The experimental procedures, with their emphasis on achieving precise, artefact-free results, are discussed in Chapter 3 of the present report and are also described in EIKENBERG et al. (1991) and FRICK et al. (1992a).

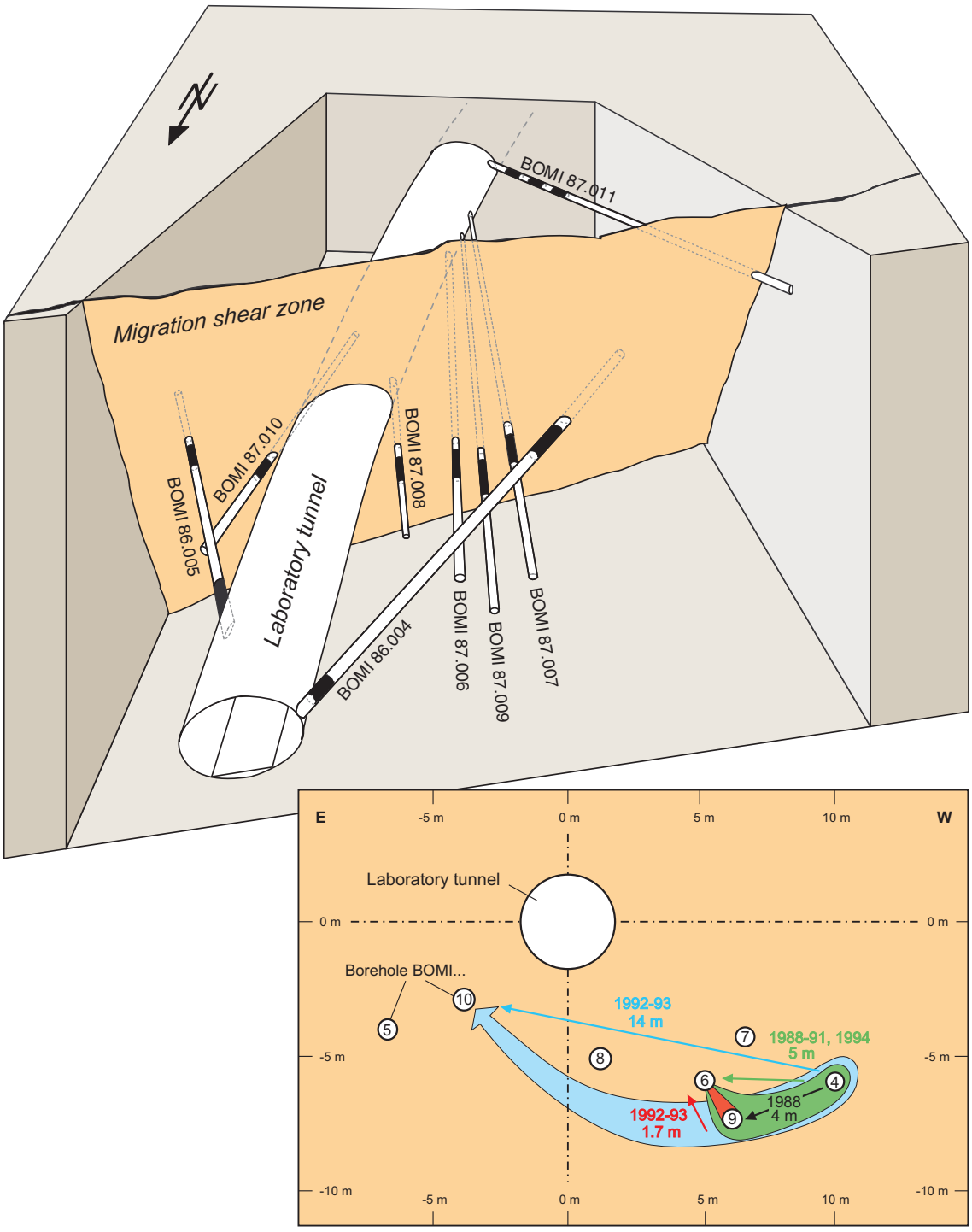

Fig. 1.1: Schematic diagram of the MI experimental shear zone indicating the borehole positions and approximate positions of the various dipole fields employed in the project

Laboratory rock-water interaction and batch radionuclide sorption studies have been carried out, under controlled atmospheric conditions, in support of MI. These are discussed in Chapter 5 of the present report and in BRADBURY (1989) and AKSOYOGLU et al. (1991).

MI was concluded in Phase IV of the GTS investigations with a long-term experiment using a relatively strongly sorbing tracer (caesium, in the form of ^{137}Cs). With joint funding by Nagra and JNC, however, studies of radionuclide migration at the GTS continued in the form of the Radionuclide Retardation Project (RRP). The RRP expands on the tracer techniques used in the earlier phases to include:

(i) The Excavation Project (EP): This focusses on the structure of the shear zone and on the behaviour of radionuclides that are relevant to repository post-closure safety, but are so strongly retarded by interaction with the shear zone rock that they are not expected to pass through the dipole flow field in experimentally reasonable times. A "post-mortem" analysis of the shear zone was conducted, in which the entire dipole flow field has been immobilised, excavated and taken back to the laboratory for analysis of its three-dimensional structure and of the distribution of injected radionuclides within the flow field (details in ALEXANDER et al. 1996, 2001a, EIKENBERG et al. 1998, FRIEG et al. 1998 and MÖRI et al. 2001a).

(ii) The Connected Porosity (CP) Project: This focusses on the form and distribution of porosity in the undisturbed rock matrix at depth (up to several metres) normal to the plane of a fracture. Although radionuclides would not be expected to penetrate this porosity significantly on experimental time scales, wall-rock porosity may be a key feature affecting radionuclide retardation over performance assessment time scales (see, for example, NAGRA 1994). In the CP Project, a specially developed resin was injected into the rock matrix, wall-rock samples were excavated and the pore structure of the impregnated material was compared in the laboratory with material excavated by conventional drilling techniques and then impregnated with resin (for details see ALEXANDER et al. 1996, OTA et al. 2001 and MÖRI et al. 2001b).

1.4 Modelling the Migration Experiment (MI): Relevance to Performance Assessment

Performance assessment of a radioactive-waste repository cannot rely solely on direct observations, because of the long time scales that the assessment must cover. The use of mathematical models to assess and bound the evolution of the repository system is therefore central to performance assessment. Swiss regulatory requirements for the disposal of radioactive waste (HSK & KSA 1993) require that the models used to assess the long term safety of a repository are "validated" (see also Chapter 2), in the sense that there are arguments that give confidence in their applicability to performance assessment. There may remain uncertainties in the models and their associated databases, but the effects of these uncertainties should be taken into account.

MI is relevant to performance assessment requirements, with respect to the quantification of radionuclide migration in the geosphere, in the contribution that it makes to:

- The building of confidence that relevant geological structures and key physical and chemical processes have been identified and incorporated in an appropriate transport model and that a satisfactory methodology exists by means of which the rates of processes and the spatial extent of structures can be determined from laboratory and field data.

  There are various ways to build confidence in a model and, in particular, to ensure, as far as possible, that relevant features and processes have been identified (i.e. that the conceptual model is adequate) and that the methodology (e.g. supporting models) for quantifying rates and spatial extents is satisfactory. A model and its output should be shown to be consistent with all available information about a system. Ideally, this information is wide ranging (e.g. general scientific understanding, observations of natural system, laboratory and field experiments), and may include experimental results of the type generated by MI. Furthermore,

confidence can be greatly enhanced if a model is able to predict results in advance of an experiment (see the discussion in PATE et al. 1994).

- The identification of uncertainties in the understanding of structures and processes (conceptual model uncertainty) and reduction of these uncertainties.

  Even if a model is successful in reproducing or predicting experimental results, uncertainties may still exist in the understanding of structures and processes, since there may be alternative models that perform equally well. These uncertainties must be recognised in performance assessment, particularly if they lead to divergent long-term predictions of radionuclide migration through the geosphere. Ideally, experiments should be designed to discriminate between alternative models; the failure of a particular alternative can serve to falsify hypotheses concerning structures and processes, and thus reduces the degree of uncertainty.

In order to address conceptual-model uncertainty, three alternative models were developed and applied by different research groups (Chapters 6 and 7). Model parameters were derived from independent observations and from experiments using a particular dipole flow field and used to predict the results of experiments using a different dipole flow field, where transport mechanisms were expected to be differently weighted (Chapter 7). In addition, the consistency of sorption parameters derived from MI and from independent laboratory experiments was assessed.

In situ field tracer tests have the advantages over laboratory experiments that they are less susceptible to experimental artefacts and can address migration over spatial scales that would otherwise be impractical. Nevertheless, practical considerations have limited MI to dipole flow fields with distances from injection to extraction of a few tens of metres. Large-scale structural heterogeneity (on a scale of hundreds of metres) is, however, a highly relevant phenomenon in geosphere performance assessment. The testing of models of radionuclide migration over such distances is beyond the scope of MI or, indeed, any presently conceived *in situ* radionuclide migration experiment.

The three models applied to the MI can be classified as "research models". They differ from performance assessment models in that they are based on a detailed description of single feature (the shear zone), rather than a simplified description of a larger rock mass[4]. Performance assessment models do not necessarily aim at realism, but rather at bounding (at least for less well-understood aspects) the limits of the behaviour of the repository system. More detailed research models, such as those applied to MI, aim at realism and, if successful, provide a theoretical framework within which some of the assumptions of the simplified assessment models can be justified. The capability of the three alternative models to reproduce and, more importantly, to predict tracer-test results within the MI is assessed in Chapter 7 and more detailed discussions of predictive model testing and *in situ* field tests in the GTS are provided in ALEXANDER et al. (1994 and 2001b), SMITH et al. (2001) and OTA et al. (2001).

[4] The governing equations for migration may, however, be similar or identical in both cases, since the same physico-chemical processes are incorporated (e.g. matrix diffusion), and may be solved using the same computer code. For example, the governing equations of the PSI model for MI are solved using the same computer code (RANCHMDNL) that has been used in several Nagra performance assessments (e.g. NAGRA 1994).

2 APPROACH TO TESTING AND VALIDATION OF TRANSPORT MODELS

P.A. Smith

2.1 The Migration Experiment and Model Validation

Validation is defined by the Swiss regulators (HSK & KSA 1993) as:

"Providing confidence that a computer code used in safety analysis is applicable for the specific repository system."

Applicability of a computer code implies applicability of both the underlying conceptual and mathematical models and the data used. A range of testing procedures, outlined below, has been adopted by Nagra to ensure the applicability of the models and data used in safety analyses (see, for example, Section 2.7 in NAGRA 1994). The present report describes the contribution made by the Grimsel migration experiment to the validation of radionuclide transport models for the geosphere. The testing procedures include[5]:

(i) *Systematic and transparent approaches to model development and consideration of alternative conceptual models*

The approach to radionuclide transport model development, based on (a), well established physical and chemical processes, (b) results from hydrogeological modelling and (c), information on structural geology, is discussed in the following chapters. For MI, alternative conceptual models (each following the same general approach to model development) have been formulated independently (Chapter 6). The present report focusses mainly on the model developed by PSI in Switzerland, which has been applied to the widest range of tracer tests within MI. Alternative models have, however, been developed by JNC in Japan and by the Swiss Federal Institute of Technology (ETH); these models are compared to the PSI model in order to address the issue of conceptual model uncertainty.

(ii) *Iteration between model development and collection of experimental data, both in the laboratory and in the field*

Laboratory and field data provide a basis for the formulation of the radionuclide transport models; for example, the models should be geometrically consistent with the observations of structural geology and the sorption processes incorporated in the model should be consistent with understanding derived from laboratory data (although simplifications may be made, depending on the intended application). Models are refined as further data become available. However, model predictions themselves provide as feedback an indication of the critical ranges of key parameters and of the accuracy required in data collection, although account must be taken here of conceptual model uncertainty.

(iii) *Testing of the models using data from laboratory and field*

MI includes not only field measurements of the transport behaviour of tracers, but also laboratory measurements aimed at providing an independent evaluation of key, transport-

[5] Other measures include the use of natural analogues (and palaeohydrogeological data) to test transport models and to evaluate uncertainties arising from the prolonged temporal scales that are of concern in safety analysis; these topics are discussed at length in PATE et al. (1994) and MILLER et al. (1994 and 2000), and recommendations for combined approach, using field, laboratory and natural analogue data are made in ALEXANDER et al. (1998 and 2001b).

relevant processes – in particular, the sorption properties of radionuclide tracers. Models are tested (a) by assessing their ability to reproduce ("fit") field measurements using parameter values that are consistent with independent field and laboratory measurements and (b) by assessing their ability to predict the outcome of field experiments using parameter values derived from independent measurements. These two "levels of model testing" are discussed further in Section 2.2, below. In order to provide a convincing test of transport models, it is also important to demonstrate the negligible impact of phenomena with the potential to perturb the experimental results. Thus, as described in Chapter 4, direct measurements have been made of colloidal and microbial populations and, as described in FRICK et al. (1992b) and Chapter 3, care has been taken to minimise potential testing artefacts (e.g. sorption of radionuclides on to the borehole equipment).

(iv) *Ongoing critical peer review through presentations, publications in open literature and participation in international projects and workshops*

Specific aspects of MI, as well as overviews, have been presented in numerous international conferences and workshops and published in the open literature and have therefore benefited from peer review (see e.g. McKINLEY et al. 1988, ALEXANDER et al. 1992, 1994 and 1997a and 1997b, FRICK 1994, FRICK et al. 1992b, HADERMANN & HEER 1996, OTA et al. 2001, SMITH et al. 2001). The present report, which has undergone both internal and external review, is also intended to contribute to this aspect of validation.

2.2 Aspects of Model Testing

2.2.1 Levels of Model Testing

Models of tracer transport through fractured rock have been applied to MI by PSI and ETH in Switzerland and by JNC in Japan. As described in Chapter 6, the models are based on identical (and widely accepted) concepts for the processes and structures that are relevant to transport, but differ in the way in which these processes and structures are simplified to allow quantitative evaluation of tracer transport. The models have been tested using data from the laboratory and from the field. Ideally, these models should:

- describe a large class of observations
- make definite predictions about the results of future observations
- contain only a few arbitrary elements.

Arbitrary elements may be interpreted as model parameters that are not obtained directly from observations or from experiments independent of those for which predictions are being made; i.e. free variables. Models of radionuclide transport in the geosphere inevitably contain some such parameters, principally due to:

- the complexity of the natural systems that they describe (e.g. heterogeneity on all spatial scales)
- the incomplete characterisation of this complexity
- uncertainty in the description of processes operating in natural systems (giving rise, for example, to uncertainty in the extrapolation of data from the laboratory to the field) and
- the need to simplify the description of the natural systems in order that governing equations can be formulated, and solved either analytically or numerically.

In the case of the models describing MI (see Chapters 6 and 7), a few parameters are fixed *a priori* from observations and independent experiments (examples are the thickness of the shear zone and the diffusion coefficients of tracers; see Table 7.2 in Chapter 7). Others parameters are determined using a calibration process; a combination of parameters is found that yields the best fit to experimental data. In practice, parameters that are thought to be tracer-independent are fitted first using data for a non-sorbing tracer. Then, keeping these data fixed, tracer-dependent parameters (governing sorption and diffusion) are fitted using data for sorbing tracers. In many cases, although these fitted parameters are not taken directly from observations and independent experiments, their consistency with such data can be tested.

Once the model has been calibrated, so that all parameters are either fixed by the calibration process or taken directly from observations and independent experiments, the model can be used to make quantitative predictions about the results of future experiments – i.e. experiments with new dipole configurations.

Thus two levels of model transport testing can be distinguished:

Level 1: The ability of a model to reproduce, or fit, experimental observations (to within the experimental errors), using a set of parameter values that is consistent with independently determined data.

Level 2: The ability of a model to predict the outcome of future experimental observations (to within the experimental errors), using a set of parameters that is derived from independently determined data (including calibrated parameters from level-1 testing).

The value of level-2, *predictive* (or 'blind') testing is that, in general, there are aspects of modelling procedures that are subjective (e.g. the relative weighting given to simulation of the break-through peak, relative to the tail) and, if the "answer" is known in advance, as in level-1 *inverse* testing, then simulations can be biased (see comments in PATE et al. 1994). Predictive modelling can build confidence in the methodology for deriving parameters from field observations and from independent field and laboratory data and can show that the parameter values obtained by these means are acceptable. To obtain maximum benefit from predictive testing, it is desirable to make and document predictions in a transparent manner before the tracer test is performed, with a clear methodology defined for the setting of parameter values. It is also desirable to establish "success criteria" for the predictions, taking full account of experimental errors.

Both types of testing can, by demonstration of "goodness of fit" (within the success criteria), build confidence that the relevant features and processes have been identified and incorporated in a model that is used either directly, or in simplified form, in performance assessment, i.e. confidence that no key processes have been overlooked. It is important to examine as many plausible alternative models as possible in order, by falsifying some of these alternatives by their failure to predict experimental results, to narrow down the range of conceptual model uncertainty and to identify the processes that are most important.

As described in Section 2.2.2, MI includes both levels of model testing. One of the successes of MI is that it has built a culture of rigorous model testing and, perhaps more importantly, experience in predictive modelling within Nagra, JNC and their various contractors (ALEXANDER et al. 1997a and 1997b).

2.2.2 Procedure for Model Development and Confidence Building

The procedure for the development of transport models, and for building confidence in the models, is illustrated in Figure 2.1. The figure illustrates the interaction between three broad activities:

(i) *Model Formulation*

As indicated in Figure 2.1, a model of geosphere transport, whether a research model or an assessment model, is, in general, derived from hypotheses concerning:

- The types of water-bearing structures present in the rock.

  This includes the identification, classification and geometrical description of structures (fault zones, fractures, channels, etc.). Hypotheses concerning structure typically involve extrapolation of direct observations in the field, in tunnel walls, cores, etc., possibly supported by other evidence (e.g. geophysical, hydrogeological and hydrochemical studies).

- The transport processes that convey migrating species within the relevant structures.

  This includes solute transport processes, such as advection and diffusion, but may, in general, also include a range of other processes including sorption, precipitation at reaction fronts, colloid-facilitated transport and gaseous-phase transport. These hypotheses are supported by current scientific understanding of geosphere transport.

- The rates and spatial extent over which these processes operate.

  This includes the parameters that quantify the transport processes, e.g. Darcy velocity, flow-wetted surface, diffusion coefficients and porosity distribution. The determination of parameter values is the second of the broad activities identified in Figure 2.1.

(ii) *Determination of Parameter Values*

The determination of parameter values describing rates and spatial extents involves an assessment of all the information available from the characterisation of the rock, from field and independent laboratory experiments (such as batch sorption and laboratory diffusion experiments) and from natural analogues. As described in Chapter 6, these data may need to be interpreted by means of supporting, interpretative models (e.g. a linear or non-linear model of sorption) in order to provide parameter values for a transport model.

If all parameters of a transport model can be determined in this way, then the model can be used directly in predictive testing (see (iii), below). There may be some parameters, however, that cannot be taken directly from field and laboratory measurements, although it is often possible to place bounds on these parameters by drawing on wider scientific understanding (e.g. from relevant literature). It is then necessary to resort to inverse modelling to "calibrate" the model, providing parameter values for subsequent application in predictive modelling.

Inverse modelling involves the following steps:

- all "free" parameters that are not fixed by means of independent field and laboratory measurements are adjusted simultaneously (constrained within certain bounds, if these are known) until a best fit to a tracer transport break-through curve is obtained,
- the best fit model curves are compared with experimental curves and assessed against success criteria,

- if the comparison is unsuccessful, then either the derivation of fixed parameter values or the model formulation itself must be re-assessed,
- if the comparison is successful, then the fitted parameters are tested for consistency with independent data, i.e. from the characterisation of the rock and from other field and laboratory experiments (successful comparison and consistency with independent data both contribute to "level-1" confidence building, as defined in Section 2.2.1),
- if there is inconsistency with independent data, then either the derivation of fixed parameter values or the model formulation itself must be re-assessed,
- if the fitted parameters are consistent with independent data, then they can be taken into account when assessing available information:
  - to reduce the number of free parameters in further inverse-modelling exercises (e.g. with more complex tracers)
  - to determine whether free parameters can be eliminated and predictive modelling (e.g. of new experimental set-ups, with different flow fields) is possible.

(iii) *Predictive Model Testing*

This type of model testing involves the prediction of experimental break-through curves (in advance of the experiments) for a range of tracer experiments carried out under different flow conditions (pumping rates, separation of injection and withdrawal points, etc.) and/or using different tracers.

For each predicted (model) break-through curve:

- comparison is made of the model and experimental curves, with assessment against success criteria (taking account of an evaluation of experimental errors),
- if the comparison is unsuccessful, then either the derivation of fixed parameter values and/or the model formulation itself is re-assessed,
- successful comparison contributes to "level-2" confidence building, as defined in Section 2.2.1,
- following successful comparison, selection of a new experimental set-up (with different flow conditions and/or tracers with different transport-relevant properties) for further predictions – the procedure is repeated until it is judged that "sufficient confidence" in the model has been attained.

"Sufficient confidence" is not precisely defined. The aim, however, is to model a large number of experimental set-ups, since, as discussed in Section 2.2.1, a "good model" should describe a large class of observations. The ability of the transport model to predict the behaviour of a variety of tracers in a range of different flow fields gives confidence that the model can be applied to the transport of radionuclides in a performance assessment, provided adequate characterisation of the repository system and suitable independent experimental data are available.

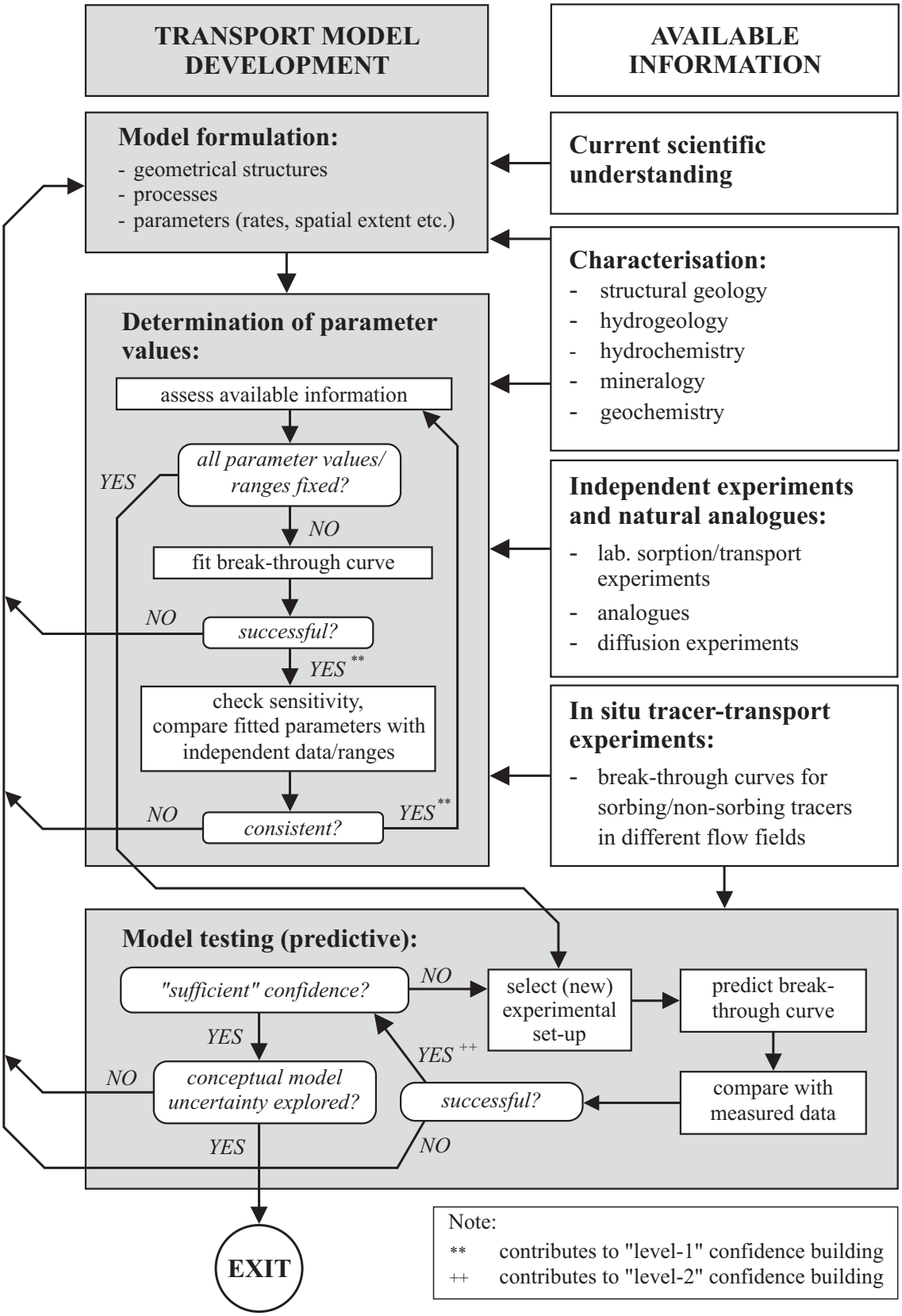

Fig. 2.1: The contributions of tracer experiments, laboratory and field data and current scientific understanding to the development and testing of transport models

In practice, assessment models are often (conservatively) simplified versions of the more detailed research models of the type applied to MI[6]. This is because, in spite of the large amount of information that is acquired in the course of characterising a potential repository site, the detailed characterisation that has been carried out in support of MI is not practicable for each individual fracture within the large-scale networks of fractures of relevance to performance assessment. Furthermore, the large number of calculations required in performance assessment (in order to explore parameter sensitivity and to evaluate the consequences of uncertainty) means that models are required that are relatively simple, avoiding excessive demands on computer time and memory (although this is now much less critical than in the past). Having achieved confidence in a research model through predictive model testing, an assessment-model developer is in a strong position to decide where simplifications can be justified in terms of either conservatism or insignificant effects.

[6] The same code (RANCHMDNL) has, in fact, been used both in the PSI modelling of the migration experiment and in recent Nagra performance assessments. In the case of the migration experiment, however, the code is applied in the framework of a relatively complex conceptualisation of transport pathways (multiple stream tubes with a range of properties, as described in Chapter 6), that aims at realism. In the case of recent Nagra performance assessments, a single transport pathway is, in general, modelled, with conservatively chosen properties.

3 OVERVIEW OF THE FIELD WORK

Th. Fierz

In this chapter, a brief overview of the field work carried out within MI is presented. The overview is based on a detailed experimental report (FIERZ 1998) listing field personnel, test objectives, form and quantities of tracers used, details of the test equipment set-up, borehole set-up, dipole set-up and all parameters measured, and commenting on the quality of the data produced. In the present overview, all tracer tests are described including preliminary tests carried out to develop a suitable experimental set-up and to refine equipment, as well as experiments for transport model testing. Further details of the preliminary tests can be found in FRICK et al. (1992a).

3.1 Aims of the Field Programme

Model testing that achieves the objectives outlined in Chapter 2 is only possible if field experiments are carefully planned and implemented, so that experimental artefacts are kept small and the conditions prevailing during the experiment are well understood. Rigorous standards were set for chemical and hydrogeological stability of the artificially induced dipole flow fields, as well as long-term stability and sensitivity of the equipment for tracer analysis. Any possibility of tracer sorption on the experimental equipment had to be ruled out and dispersion of the injected tracers within the experimental equipment had to be minimised and quantified.

Prior to the carrying out of tracer experiments for transport model testing, a number of preliminary tracer tests were carried out with for the following purposes:

- Determination of locations at which suitable dipole flow fields could be established.

  Suitable dipole fields are those produce break-through curves that can be measured accurately, not only around their peaks, but including their tails, since the tails are indicative of certain important transport processes (see Chapter 7). Transport models will give less information about these processes if the tails are truncated. For this reason, it is important that a high proportion of injected tracer is recovered in reasonably achievable times (at least for non-sorbing tracers). This is favoured by the use of narrow dipoles flow fields, in which the rate of water extraction greatly exceeds the rate of water injection. Such flow field are also much less sensitive to hetereogenieties in the hydrogeological properties (especially transmissivity) of the shear zone, and thus give rise to break-through curves that are more straightforward to interpret, allowing modelling to focus on transport process identification.

  In addition, for both modelling and radioprotection reasons, closed dipoles are desired – i.e. 100 % recovery of a non-reactive tracer.

- Optimisation and improvement of test equipment.

  Tracer injection and detection techniques were greatly improved, e.g. through the development of downhole fluorescent tracer detection equipment, packer systems with low interval volumes, packer systems with sorption-proof materials, helium tracer techniques and online radiotracer analysis.

3.2 Overview of Field Work from 1988 to 1996

Tracer tests were conducted between in 1988 and 1996. The programme of tests can be divided chronologically into the following phases (see also Table 3.1):

1988 – 1990 (Phases 1-4), preliminary tests and optimisation and improvement of test equipment:

Phase 1: Preliminary tests with non-sorbing tracers

Phase 2: Development of new methodologies, optimisation of test set-up

Phase 3: Preliminary tests with ^{24}Na

Phase 4: Implementation of improved techniques/equipment

1991 – 1996 (Phases 5-9), tracer experiments for transport model testing using conservative (non-sorbing) and sorbing tracers in various dipole flow fields:

Phase 5: Tracer experiments for transport model testing using Sr, Na, and I in a 4.9 m (injection to extraction) dipole flow field

Phase 6: Tracer experiments for transport model testing using Sr, Na, Rb in a 1.7 m flow field

Phase 7: Transport experiments for transport model testing using non sorbing tracers in a 14 m flow field

Phase 8: Tracer experiments for transport model testing using Cs, Sr, He in a 1.7 m flow field

Phase 9: Tracer experimemts for transport model testing using Cs, Sr, He in a 4.9 m flow field

Tab. 3.1: Simplified timetable of field tracer tests (Phases 1-9)

Phase	1988	1989	1990	1991	1992	1993	1994	1995	1996
1									
2									
3									
4									
5									
6									
7									
8									
9									

Table 3.2 gives a general overview of the scale of tracer tests (distance from water injection to water extraction location), the associated boreholes and the different tracers employed. In Table 3.3, details of each individual tracer test are listed.

The following sections give more details of the work conducted in each of the phases.

Tab. 3.2: Scale of most frequently used dipole flow fields (distance from injection to extraction location), associated injection and extraction boreholes, as well as the tracers used

Dipole Distance [m]	Input Borehole BOMI	Withdrawal Borehole BOMI	Investigation Phases	Non-reactive Tracers	Reactive Tracers
1.7	87.009	87.006	6 / 8	Uranine, He-3, He-4, I-123, Br-82	Na-24, Sr-85, Rb-86, Tc-99m, Cs-137
4.9	86.004	87.006	5 / 9	Uranine, He-3, He-4, I-123, H-3, Br-82	Na-24, Na-22, Sr-85, Cs-137
14	86.004	87.010	7	Uranine, He-3, I-123, Br-82	Tc-99m
Equipment Tests				Uranine, He-3, He-4, Br-82	Na-22, Sr-85, Co-58, Se-75, Cs-137, Cs-134

3.2.1 Phase 1: Preliminary Tests with Conservative Tracers

In this phase, potential dipole flow fields were evaluated in preliminary tests using the conservative tracers uranine (Na-fluorescene) and ^{82}Br, and the suitability of the test equipment was checked.

Potential dipole fields were generated using different pairs of boreholes from BOMI 86.004, BOMI 87.006 and BOMI 87.009, and different injection and extraction flow rates. The reasons for selecting this portion of the MI shear zone were the following:

(i) The need to avoid the unsaturated and partly saturated zone close to the laboratory tunnel.

(ii) The desire to minimise perturbation of the dipole flow field by any background flow of groundwater (the unperturbed pressure distribution in this part of the shear zone is relatively flat).

(iii) The need for a high hydraulic conductivity, that allows dipole flow fields giving high tracer recovery in reasonably achievable experimental times.

The preliminary tests indicated that this portion of the MI shear zone was indeed suitable for use in further test phases and the test equipment was shown to provide good reproducibility of the break-through curves. The minimisation of dispersion of the injected tracers within the experimental equipment by improvement of the experimental set-up was, however, identified as a major task for Phase 2.

Tab. 3.3: List of tracer tests (note: missing numbers denote equipment tests)

Run	Date of tracer injection	Phase	Flow field BOMI	Tracer used	Injection flow rate [ml/min]	Extraction flow rate [ml/min]
#1	12.07.88	1	86.004 → 87.009	Uranine, Br-82	259	618
#2	14.07.88	1	86.004 → 87.009	Uranine, Br-82	41	191
#3	20.07.88	1	86.004 → 87.006	Uranine, Br-82	77	219
#4	26.07.88	1	86.004 → 87.006	Uranine, Br-82	70	204
#5	06.09.88	1	86.004 → 87.006	Uranine, Br-82	78	195
#6	13.09.88	1	86.004 → 87.006	Uranine, Br-82	26	79
#7	20.09.88	1	87.006 → 86.004	Uranine	76	205
#8	04.10.88	1	87.006 → 86.004	Uranine, Br-82	24	82
#14	06.12.88	2	86.004 → 87.006	Uranine	73	221
#15	13.12.88	2	86.004 → 87.006	Uranine	63	219
#16	14.12.88	2	86.004 → 87.006	Uranine	68	250
#21	26.04.89	2	86.004 → 87.006	Uranine, Br-82, He-4	31	80
#22	11.05.89	2	86.004 → 87.006	He-4	30	76
#29	27.06.89	3	86.004 → 87.006	Uranine, Na-24, He-4	78	167
#30	04.07.89	3	86.004 → 87.006	Uranine, Na-24, He-4	21	70
#31	10.07.89	3	86.004 → 87.006	Uranine, Na-24, He-4, Br-82	5	80
#32	23.08.89	4	86.004 → 87.006	Uranine, He-4	80	160
#33	14.09.89	4	86.004 → 87.006	Uranine, He-4	78	155
#40	02.10.89	4	86.004 → 87.006	Uranine, He-4, Br-82	30	85
#41	07.03.90	4	86.004 → 87.006	Uranine, He-4	30	80
#42	14.03.90	4	86.004 → 87.006	Uranine, He-4, Br-82	50	150
#43	21.03.90	4	86.004 → 87.006	Uranine, Br-82	53	150
#44	11.06.90	4	86.004 → 87.006	Uranine	10	150
#45	26.06.90	4	86.004 → 87.006	Uranine, Br-82	10	150
#46	03.07.90	4	86.004 → 87.006	Uranine, Na-22, He-4	10	150
#47	05.02.91	5	86.004 → 87.006	Uranine, I-123	51	150
#48	07.02.91	5	86.004 → 87.006	Uranine, Na-24	51	150
#49	19.02.91	5	86.004 → 87.006	Uranine, I-123	10	150
#50	27.02.91	5	86.004 → 87.006	Uranine, Na-22, Sr-85	10	150
#51	26.11.91	5	86.004 → 87.006	Uranine	10	150
#52	22.01.92	6	87.009 → 87.006	Uranine	10	150
#53	28.01.92	6	87.009 → 87.006	Uranine	48	148
#54	29.01.92	6	87.009 → 87.006	Uranine	48	148
#55	04.02.92	6	87.009 → 87.006	Uranine, Br-82		147
#56	04.02.92	6	87.009 → 87.006	Uranine, Br-82		128
#57	07.02.92	6	87.009 → 87.006	Uranine, Br-82		45
#58	11.02.92	6	87.009 → Drift	Uranine, Br-82		
#59	24.02.92	6	87.009 → 87.006	Uranine	10	150
#60	26.02.92	6	87.009 → 87.006	Uranine	6.6	97
#61	09.02.92	6	87.009 → 87.006	Uranine, Na-24	10	148
#62	12.03.92	6	87.009 → 87.006	Uranine, Na-24	48	148
#63	20.03.92	6	87.009 → 87.006	Uranine, He-4	6.6	100
#64	26.03.92	6	87.009 → 87.006	Uranine, He-4	6.6	100
#65	31.03.92	6	87.009 → 87.006	Uranine, Na-24	8	120
#66	14.04.92	6	87.009 → 87.006	Uranine, Na-24, Sr-85	8	120
#67	21.05.92	6	87.009 → 87.006	Uranine, He-4	10	150
#68	04.06.92	6	86.004 → 87.009	He-4	10	150

Tab. 3.3: List of tracer tests (continuation)

Run	Date of tracer injection	Phase	Flow field BOMI	Tracer used	Injection flow rate [ml/min]	Extraction flow rate [ml/min]
#69	09.04.92	6	86.004 → 87.009	Uranine, He-4	10	150
#70	19.06.92	6	86.004 → 87.009	Uranine, He-4	15	225
#71	23.06.92	6	87.006 → 87.009	Uranine	22	330
#72	25.06.92	6	87.009 → 87.006	Uranine	4	60
#73	30.06.92	6	87.009 → 87.006	Uranine, Br-82	4	60
#74	18.08.92	6	87.009 → 87.006	Uranine, Na-24	5.6	120
#75	25.08.92	6	87.009 → 87.006	Uranine, Rb-86, Sr-85	8	120
#76	27.10.92	7	86.004 → 87.010	Uranine, He-4	51	150
#77	09.12.92	7	86.004 → 87.010	Uranine, He-3, I-123	51	150
#78	13.01.93	7	86.004 → 87.010	Uranine, He-3, I-123	10	150
#79	16.02.93	7	86.004 → 87.010	Uranine, Br-82, Tc-99m	10	150
#80	16.03.93 17.03.93 24.03.93 06.04.93 21.04.93	8	87.009 → 87.006	Uranine, Br-82 Uranine, Cs-137 Uranine Uranine, Br-82 Uranine, He-3	8	120
#81	18.05.93 19.05.93	8	87.009 → 87.006	Uranine Uranine	8	120
#82	25.05.93	8	87.009 → 87.006	Uranine, Tc-99m	8	120
#83	01.06.93	8	87.009 → 87.006	Uranine, Br-82	8	120
#84	02.06.93	8	87.009 → 87.006	Uranine, Br-82	8	120
#85	03.06.93 08.06.93	8	87.009 → 87.006	Uranine, Cs-137 Uranine, He-3	8	120
#86	24.08.93	8	87.009 → 87.006	Uranine, Cs-137	8	120
#86a	02.09.93	8	87.009 → 87.006	Uranine, He-3	8	120
#86b	02.11.93	8	87.009 → 87.006	Uranine, He-3	8	120
#86c	08.02.94	8	87.009 → 87.006	Uranine, He-3	8	120
#87	17.12.94	9	86.004 → 87.006	Uranine, He-3	10	150
#88	15.05.94	9	86.004 → 87.006	Uranine, He-3, Br-82, H-3	10	150
#89	21.06.94	9	87.006 → 86.004	Uranine	14	193
#90	18.07.94 13.09.94 28.09.94	9	87.009 → 87.006	Uranine, Cs-137 Uranine, Sr-85 Uranine, He-3	10	150

3.2.2 Phase 2: Development of Methodologies and Optimisation of Test Set-up

Minimisation of the dispersion of injected tracers:

Minimisation of dispersion of the injected tracers within the experimental equipment is desirable in order to avoid complex and poorly defined input functions for subsequent transport modelling exercises. The strategy to minimise such dispersion was:

- to reduce the "dead volume" of the equipment (the volume of tubing, etc. that tracers must pass through before reaching the MI shear zone),
- to reduce the volume of tracer solution that is passed to the equipment[7].

The impact of these changes on the break-through curves and tracer recovery is illustrated in Figure 3.1 which compares the last test using the original equipment with the first test using the new equipment. Such improvements continued over the duration of MI leading to tracer recovery values of 100 % (within analytical error).

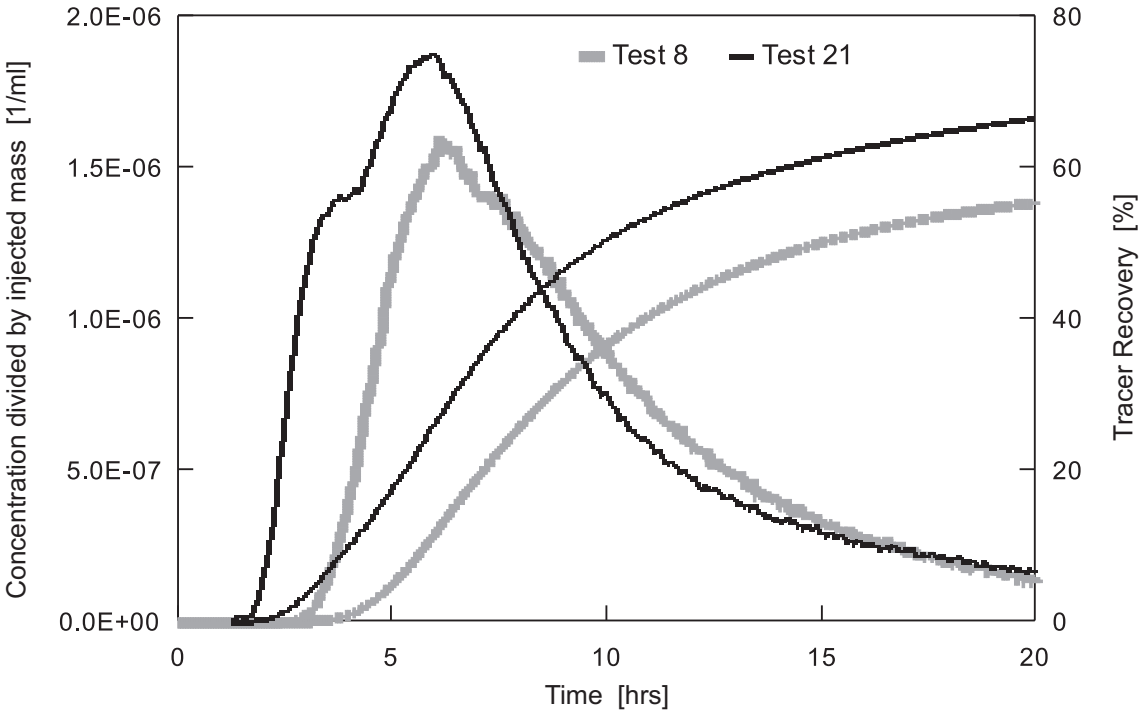

Fig. 3.1: Influence of test equipment volume on break-through curves; test 8 Phase 1, test 21 Phase 2 (with significantly reduced "dead volume")

Techniques for conservative tracers:

In collaboration with the University of Stuttgart (Institut für Wasserbau), several tracer experiments were carried out to test a newly developed fibre-optic fluorimeter. This system allows downhole measurement of fluorescent tracers (details in FRICK et al. 1992a). The prototype equipment proved unsuitable for application in the field and it was therefore decided to develop a more robust fluorimeter in order to make optimum use of the potential of the fibre-optic technology.

The He tracer technique (FRICK et al. 1992a, EIKENBERG et al. 1992) was first used in Phase 2 tests. This inert noble gas was foreseen as an additional (to uranine) conservative

[7] By injecting tracer through a rubber membrane directly into the dipole injection line using a syringe, input volumes of tracer solutions were reduced to by a factor of 40 to 80.

reference tracer used in conjunction with sorbing radionuclide tracers in the planned experiments for transport model testing[8].

Investigating the impact of injected water composition:

The water injected in order to create the dipole flow fields on Phases 1 and 2 differed slightly in its chemical composition from the undisturbed water in the MI shear zone[9]. A hydrogeochemical equilibrium test (EIKENBERG et al. 1991; see Chapter 5 for details) was carried out to investigate the impact of the injected water composition on the composition of water extracted from the dipole flow field. The concentrations of the most important anions and cations were measured in the extracted water as functions of time. This allowed the cation exchange capacity in the portion of the MI shear zone containing the dipole flow field to be estimated. It was also concluded that, due to potentially large changes in the *in situ* geochemical conditions, MI shear zone groundwater itself should be used in the planned experiments using sorbing tracers for transport model testing.

3.2.3 Phase 3: Preliminary Tests with weakly sorbing ^{24}Na

The first three preliminary tests with the weakly sorbing tracer sodium (in the form of ^{24}Na, with a 15 hour half life) were carried out using the same injection/extraction borehole combination, but with different injection and extraction flowrates (see Table 3.3 and FRICK et al. 1992a for further details).

The sodium break-through curve was less retarded with respect to that of the simultaneously injected uranine than had been expected on the basis of laboratory sorption experiments. Possible reasons are that:

(i) The *in situ* cation exchange capacity is significantly lower than in the laboratory experiments (as confirmed by the results of the hydrogeochemical equilibrium test performed in Phase 2).

(ii) The most effective exchange positions cannot be reached during the restricted residence time of the sodium tracer in the MI shear zone. Prolonged step (rather than pulse) tracer injection was therefore proposed (FRICK 1994), and implemented in Phase 4, which has the advantages of:

- prolonged tracer-rock interaction times
- less rapid changes of tracer concentration and smaller concentration gradients, which may improve equilibrium conditions and
- the basic assumption of fully reversible cation exchange reactions with rapid kinetics could be tested.

In spite of this rapid break-though, a number of problems arose with the experimental set-up, associated with the longer duration of Phase 3 tests compared to those in Phases 1 and 2. First, radioactive decay of ^{24}Na led to difficulties in measuring the tail of the break-through curve. Second, the flow rates in the dipole field varied by around 10 % during the experiments because the pumps used were insufficiently stable for long-term experiments. Third, the borehole used to

---

8 Also, as it has a much higher diffusivity than uranine, it proved to be an useful probe of accessible matrix porosity.

9 The injected water was taken from borehole BOEM 85.012, which is located at a distance of around 300 m from the MI shear zone.

extract water for injection into the dipole flow field (borehole BOMI 87.010) unsuitable for long-term experiments (although this fact only came to light in Phase 4).

These problems were addressed by the development and implementation of new techniques and equipment in Phase 4, as discussed below.

3.2.4 Phase 4: Development and Implementation of New Methods and Techniques

Dipole injection source

The location of the source of water for injection into the dipole flow field should be such that tracer cannot reach it in the course of an experiment; i.e. tracer should not be recirculated. In the first Phase 4 experiments (tests 32 and 40), however, tracer break-through was observed in borehole BOMI 87.010, which was used as such a source, indicating that small amounts of tracer were recirculated. A storage system for groundwater to be injected into the dipole was therefore installed.

Further reduction of "dead volume" and implementation of the fibre-optic fluorimeter

To further minimise "dead volume" and to implement the fibre-optic technique for *in situ* measurement of fluorescent tracers, a new packer system was developed, constructed and installed in the injection borehole. With the new interval design, it was possible to reduce the dead volume in the packer interval from approx. 1200 ml to 80 ml (FRICK et al. 1992a).

Modification of injection and extraction flow control

The two excentric-drive Moineau pumps were replaced by standard laboratory HPLC (high pressure liquid chromatography) pumps which provide extremely stable flow over a large pressure range. The first tests with the new HPLC pumps indicated highly stable flow rates. Prolonged use of these pumps, however, revealed some unexpected corrosion problems with the plungers (EIKENBERG & BÜHLER, 1990), even though these were made of a very stable sapphire (Al_2O_3) material. The sapphire plungers were therefore replaced by silica carbide, and no further leakage of the HPLC pumps was noted.

New tracer dosage for pulse and continuous injection (step input)

Tracer input by injection through a rubber membrane was noted to be somewhat inaccurate during Phase 3. The input volume of tracer solution (approx. 5 ml) could only be measured to around $\pm$ 10 %. A new tracer dosage system was developed in Phase 4; this involved introducing the tracer solution into the injection line using an HPLC dosing pump. The input volume was measured accurately using a Mettler electronic balance.

Na-22/uranine step input experiment (test 46)

This experiment is described in detail in FRICK et al. (1992a). The weak retardation of Na observed in Phase 3 was again observed; 1500 hours after tracer input, 90 % of the tracer had been recovered. Using the relatively long-lived sodium isotope ^{22}Na (with a half life of 2.6 years) allowed a large part of the tail of the sodium break-through curve to be measured.

3.2.5 Phase 5: Tracer Experiments for Transport Model Testing in a 4.9 m Flow Field

To prepare for the tracer experiments for transport model testing, which used more strongly sorbing radionuclide tracers, sorption tests were carried out on the experimental equipment (EIKENBERG et al. 1994). Various changes in the experimental set-up (and material used) were made based on the results of these tests (see Figure 3.2). Test equipment and performance are documented in detail in EIKENBERG et al. (1994).

The tracer experiments carried out in this phase used slightly and moderately sorbing, as well as conservative, tracers. The modelling work carried out in Phase 5 ("level-1" model testing and model calibration) is described in Chapter 7.

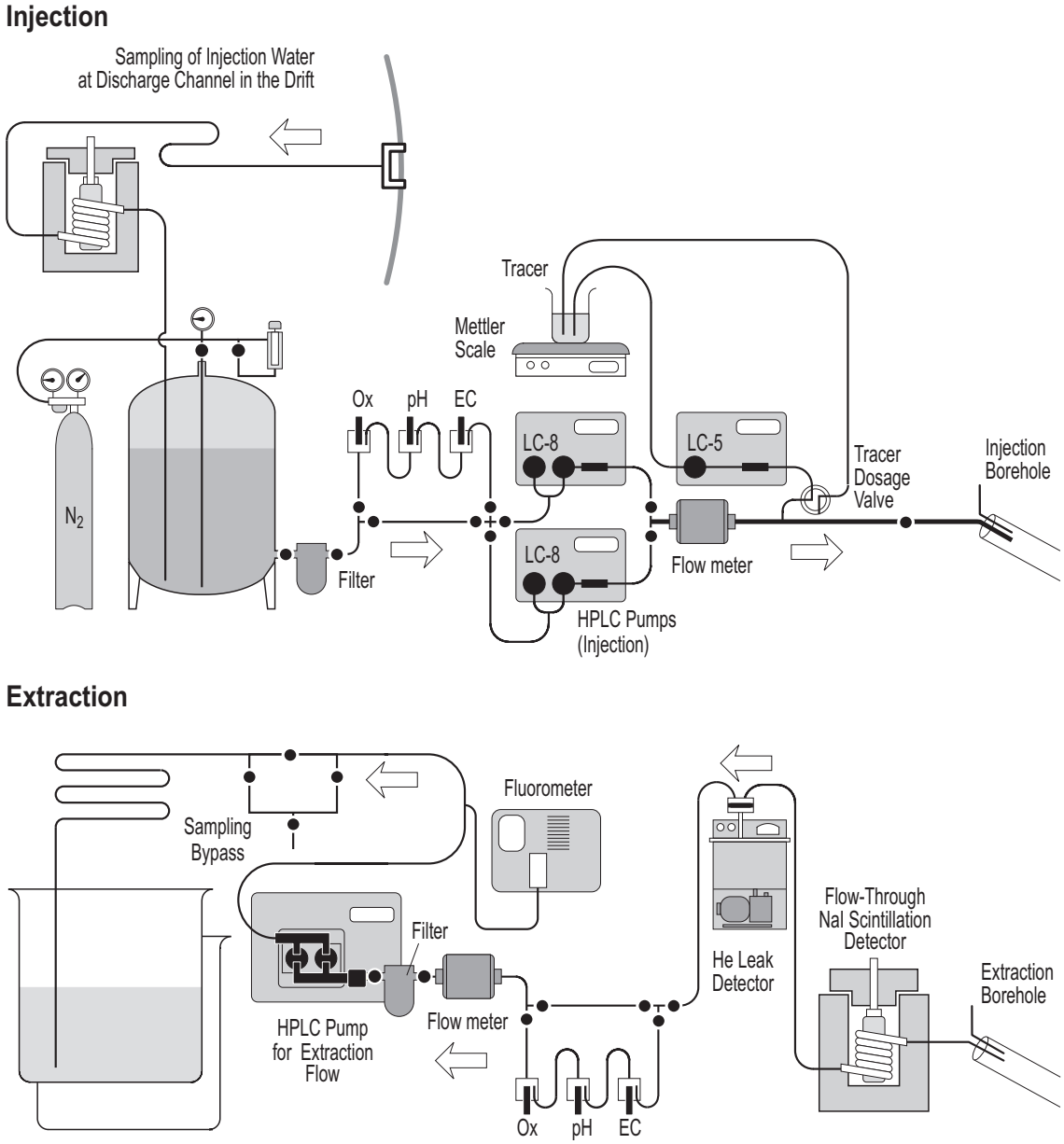

Fig. 3.2: Surface equipment set-up for the tracer experiments for transport model testing in Phases 5-9

During the sodium/strontium long-term experiment (test 50), which lasted more than 5000 hours, a continuous drop in pressure was observed in the extraction interval. This was interpreted as due to clogging, but the reason for the clogging was not discovered until the end of Phase 6. The gas-permeable teflon injection flow line allowed CO_2 and O_2 to diffuse into the injection water, leading to carbonate precipitation in the MI shear zone. The impact on the dipole field can be seen by comparing the results of tests 50 with those of test 51, carried out 9 months later (Figure 3.3), and also by observing the decrease of the pressure in the extraction interval during the course of test 50 (Figure 3.4).

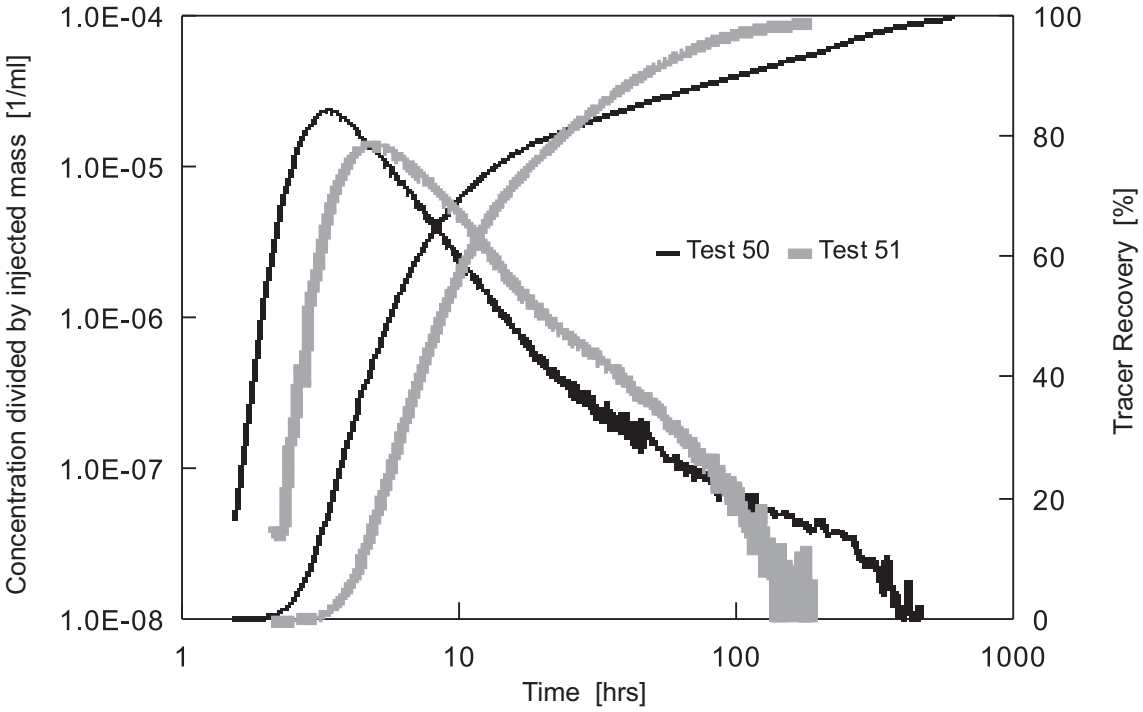

Fig. 3.3: Uranine break-through curves of test 50 and test 51, both tests using the 4.9 m flow field BOMI 86.004 → BOMI 87.006, injection flow rate of 10 ml/min and extraction flow rate of 150 ml/min

3.2.6 Phase 6: Tracer Experiments for Transport Model Testing with Na-24, Sr-85 and Rb-86 in a 1.7 m Flow Field

As in Phase 5, the tracer experiments carried out in Phase 6 used slightly and moderately sorbing, as well as conservative, tracers. These experiments were used for predictive ("level-2") model testing, as described in Chapter 7.

Also as in Phase 5, the long-term experiment using sodium/strontium as tracers (test 66) was affected by clogging around the extraction borehole. Once identified[10], the problem was solved by replacing the gas permeable teflon flow lines by nylon lines and the tests with sodium and strontium were repeated (tests 74 and 75). ^{86}Rb was also used as a shorter lived indicator of the

[10] O_2 diffusion tests showed that the O_2 concentration in groundwater from the MI shear zone rose from $< 3 \times 10^{-8}$ M to ~ 3×10^{-5} M after passing through 10 m of flow line (internal diameter of 4 mm or 6 mm), with a typical injection flow rate of 8 ml/min. This corresponds to around half the oxygen concentration in water that is saturated with respect to air.

possible behaviour of the longer-lived (and more strongly sorbing) ^{137}Cs, which was planned for use in later experiments (Figure 3.5).

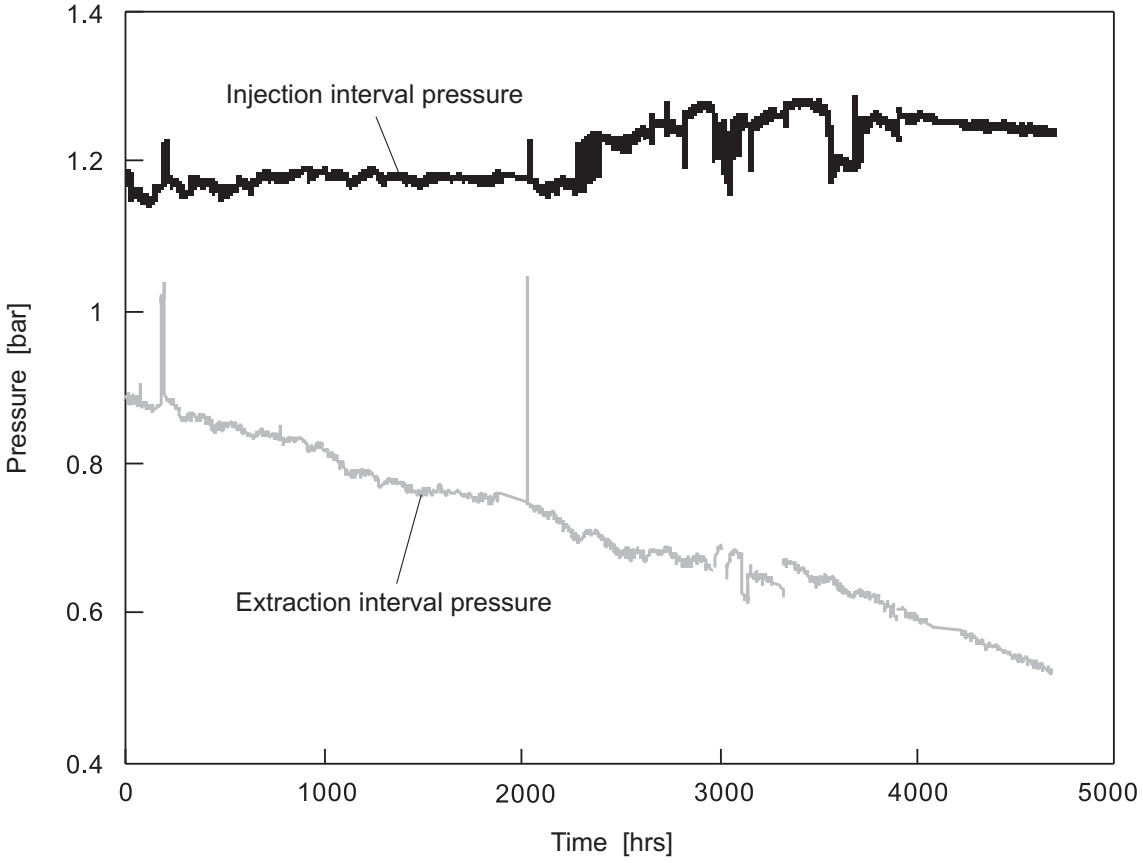

Fig. 3.4: Injection (BOMI 86.004) and extraction (BOMI 87.006) interval pressures required to maintain injection/extraction rates during test 50 illustrating the effect of clogging around the extraction interval

In order to quantify the change of hydrogeological properties of the migration fracture due to the presence of CO_2 and O_2 in the injection water, tracer tests using the GSF (Research Centre for Environmental Sciences, Munich) single-hole probe (SBP) (DROST 1984) were performed. Three experiments were carried out in monopole flow fields of varying strength (no injection flow, tracer input in BOMI 87.009, extraction from BOMI 87.006). An additional run was carried out in the undisturbed flow field between the MI shear zone and the laboratory tunnel. The tracer was injected into borehole BOMI 87.009 using the SBP and break-through was recorded in the laboratory tunnel.

3.2.7 Phase 7: Tracer Experiments for Transport Model Testing with I-123, He-3 and Tc-99m in a 14 m Flow Field

The experiments in the 14 m flow field were restricted to conservative tracers Br, uranine and helium, since the test duration for reacting tracers would have been too long. The aim of the experiments was to obtain information on matrix diffusion in the MI shear zone (matrix diffusion as a retardation process is discussed in Chapter 6). The diffusivities of the three tracers (FRICK 1992) are not the same, due to differences in their charge and mass, and this should lead to differences in retardation. Figure 3.6 shows that helium is somewhat retarded with

respect to uranine and the recovery of helium at the end of the experiment is less, with about 15 % still retained within the shear zone. These observations may be indicative of a greater retardation of helium by matrix diffusion, although a weaker flow field (and hence longer test duration) may be required in order to produce a more significant effect.

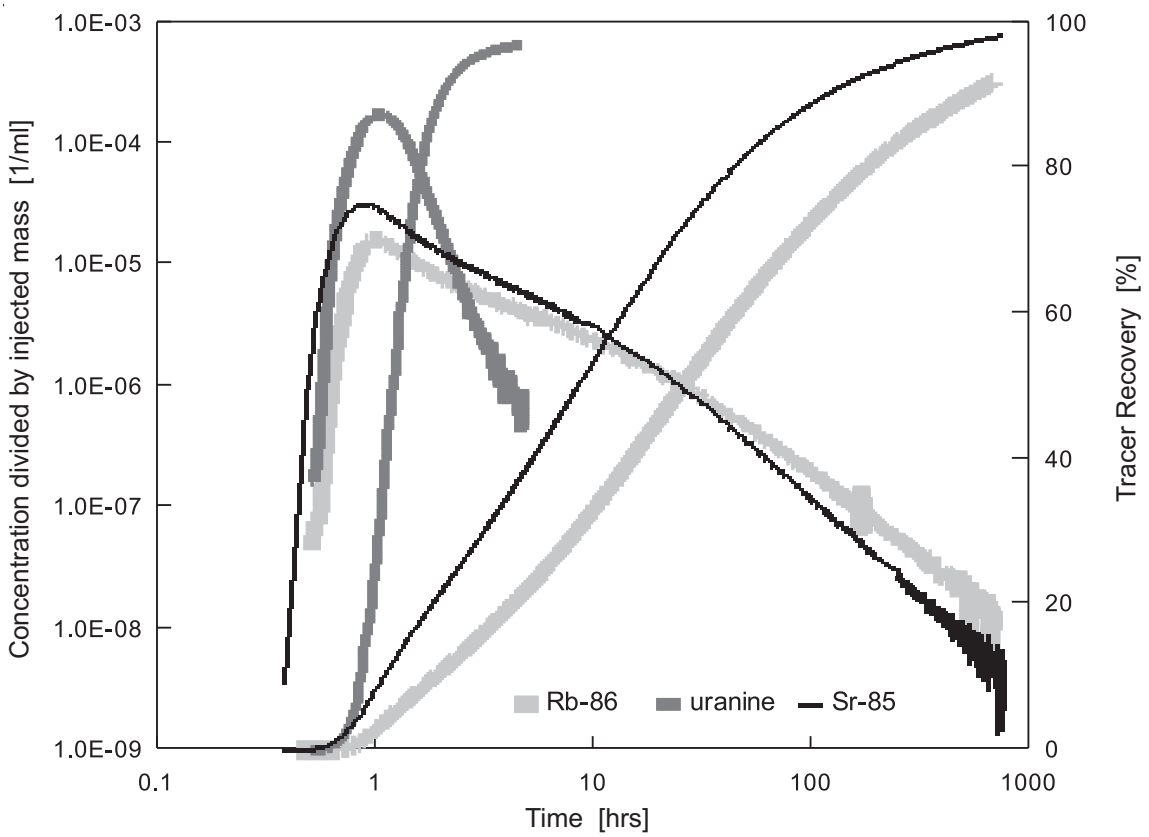

Fig. 3.5: Break-through and tracer recovery curves for test 75, 1.7 m flow field BOMI 87.009 → BOMI 87.006, injection flow rate of 8 ml/min and extraction flow rate of 120 ml/min

3.2.8 Phase 8: Tracer Experiments for Transport Model Testing with Cs-137, Tc-99m and He-3 in a 1.7 m Flow Field

The tracer experiments carried out in Phase 8 were focussed on the more strongly sorbing caesium tracer. The experiments were used mainly for predictive ("level-2") model testing, as described in Chapter 7.

Three long-term tracer experiments were carried out with caesium in Phase 8 (tests 80, 85 and 86; see Figure 3.7). The dipole flow field was the same for all three experiments. Carrier-free caesium (^{137}Cs), at low concentration with respect to the natural caesium background, was used in the first experiment (test 80) so as not to disturb the natural equilibrium between the groundwater and the rock. The sorption of caesium varies in a non-linear manner with the concentration of this element, as sorption sites become occupied (see Chapter 5).

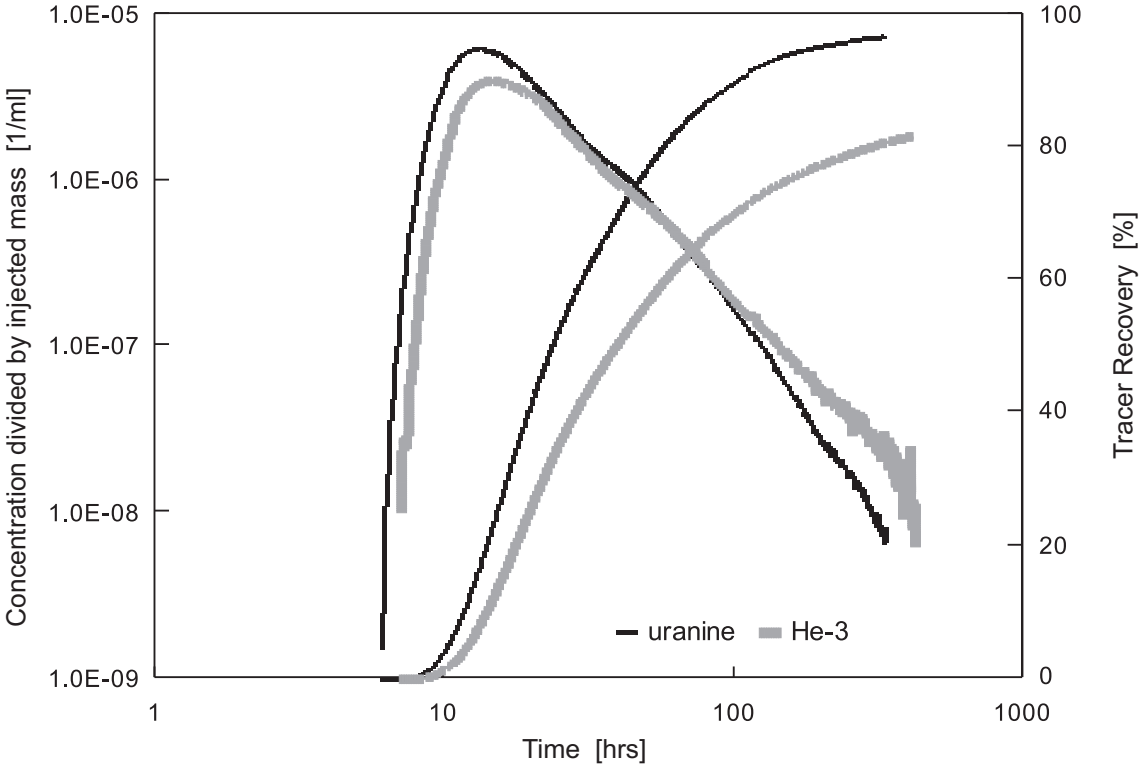

Fig. 3.6: Break-through and tracer recovery curves of uranine and He-3 in a 14 m flow field BOMI 86.004 → BOMI 87.010, injection flow rate of 8 ml/min, extraction flow rate of 120 ml/min (test 78)

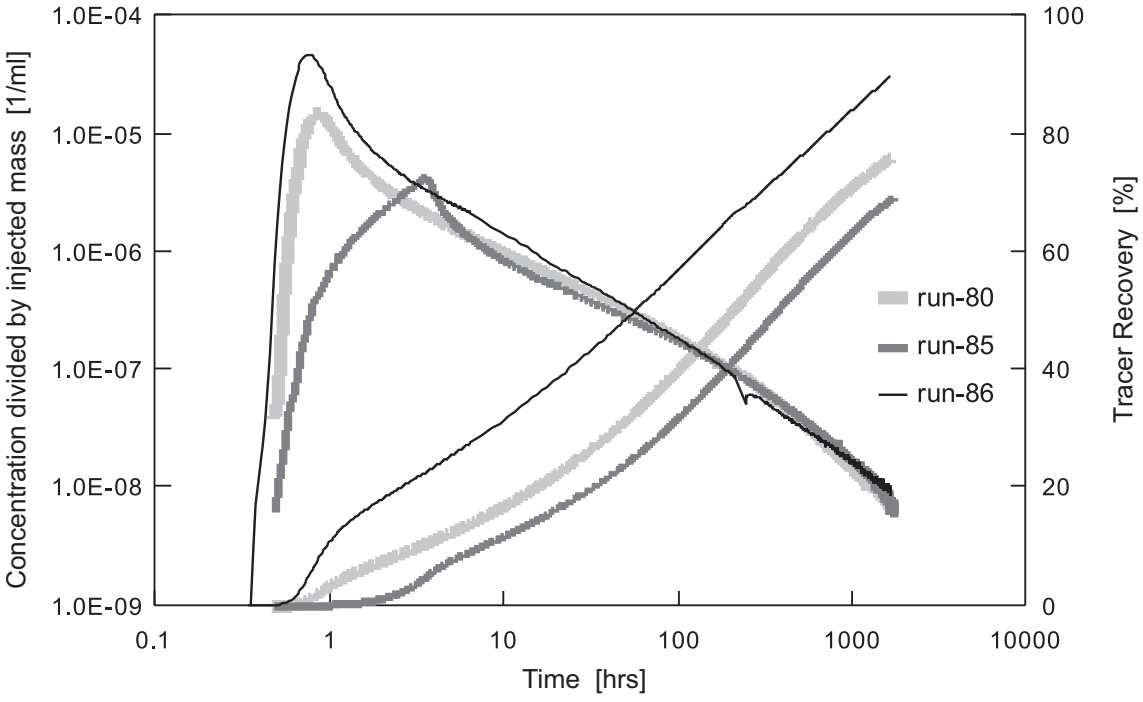

Fig. 3.7: Break-through and tracer recovery curves of Cs-137 in tests within a 1.7 m flow field BOMI 87.009 → BOMI 87.006, injection flow rate of 8 ml/min, extraction flow rate of 120 ml/min, test 80: pulse with carrier-free Cs-137; test 85: step (3 hrs) with carrier-free Cs-137; test 86: Cs-137 pulse with CsCl carrier

Higher concentrations of ^{137}Cs tracer, or of other caesium isotopes present in the carrier solution, could reduce the retardation of the tracer by sorption. To increase the time available for tracer-rock interaction in the flow field[11], it was proposed to use continuous tracer injection (step input) and lower dipole flow rates[12] (test 85). In test 86, CsCl was added as a carrier, to investigate its effect on caesium retardation. As expected, non-linear sorption behaviour resulted in a less retarded caesium break-through.

3.2.9 Phase 9: Tracer Experiments for Transport Model Testing with Cs-137, Sr-85, He-3 and H-3 in a 4.9 m Flow Field

Four conservative tracers, ^{3}He, ^{3}H, uranine and ^{82}Br, were used in test 88. The break-through curves of all the tracers were recorded as accurately as possible over at least three orders of magnitude in concentrations (see Figures 3.8 and 3.9). The break-through curves for all four tracers are very similar. There is some indication of a longer tail in the case of the uncharged tracers ^{3}He and ^{3}H compared to the negatively charged ^{82}Br and uranine, which might tentatively be attributed to differences in matrix diffusion due to anion exclusion and the higher diffusion coefficient of He.

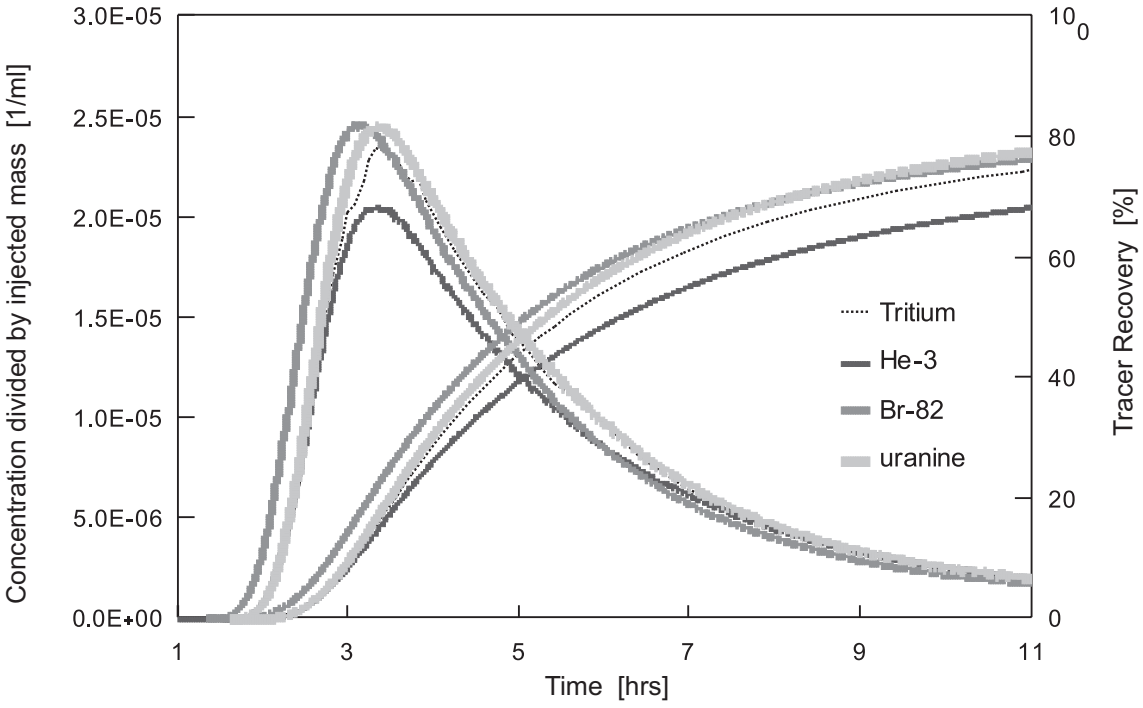

Fig. 3.8: Break-through and tracer recovery curves of uranine, Br-82, He-3 and H-3 (test 88); 4.9 m flow field BOMI 86.004 → BOMI 87.006, injection flow rate of 10 ml/min, extraction flow rate of 150 ml/min, linear scales

[11] Note that caesium also has relatively slow sorption kinetics.

[12] It became apparent that extraction rates less than 120 ml/min led to incomplete tracer recovery.

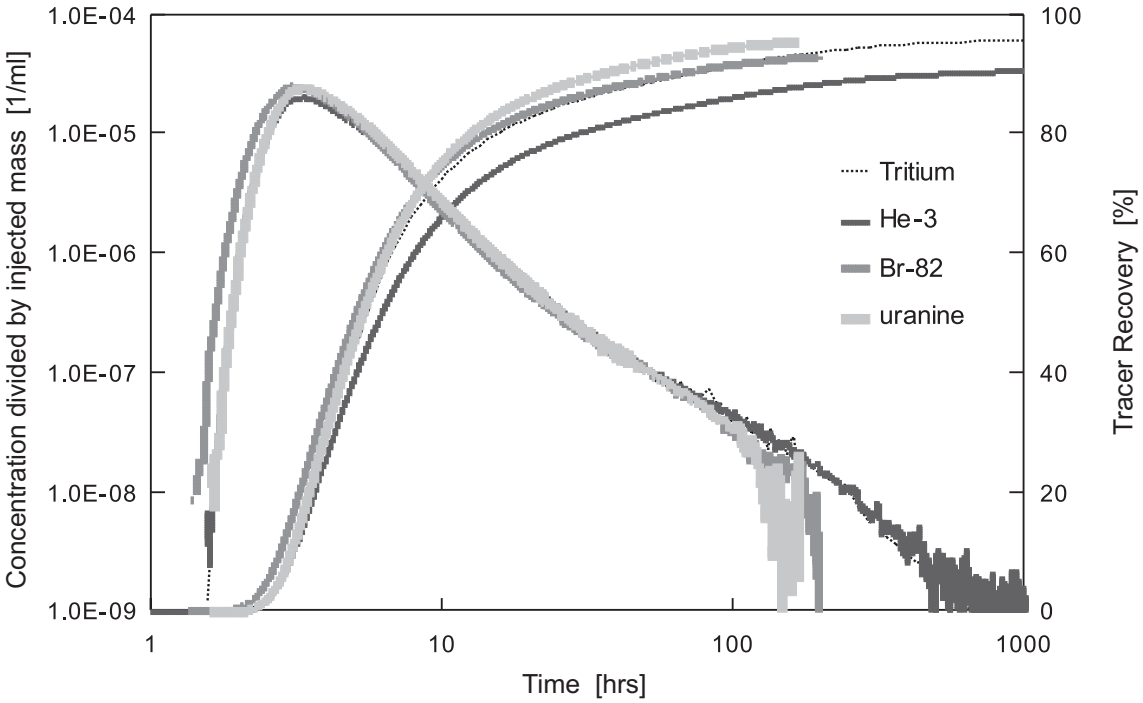

Fig. 3.9: Break-through and tracer recovery curves of uranine, Br-82, He-3 and H-3 (test 88); 4.9 m flow field BOMI 86.004 → BOMI 87.006, injection flow rate of 10 ml/min, extraction flow rate of 150 ml/min, log scales

One experiment (test 89) was carried out using the conservative tracer uranine in a dipole flow field directed counter to the background flow field. The aim was to acquire more information on the hydrogeological characteristics of the MI shear zone and, in particular, the background flow field directed towards the laboratory tunnel. No tracer was observed in the extraction borehole[13]. Break-through with 100 % recovery was, however, detected in the drainage water from the MI shear zone into the tunnel.

Given the success of the caesium experiments in Phase 8 in the shorter, 1.7 m dipole flow field, as well as promising model simulations (Chapter 7), a very long-term caesium run (test 90) was carried out in the 4.9 m flow field (Figure 3.10). The experiment continued over a period of 1.5 years following tracer input, and therefore highly stable conditions were required for the instruments driving the flow field and recording tracer break-through.

The measured caesium break-through matched well the break-through curve predicted by transport modelling. Even after 1.5 years, recovery was only 30 %, due to the strong sorption of the tracer.

[13] Compare this result with that for test 8. The difference in reaction of the shear zone to these largely similar tests is difficult to explain other than to invoke changes to the flow system over the lifetime of the MI experiment.

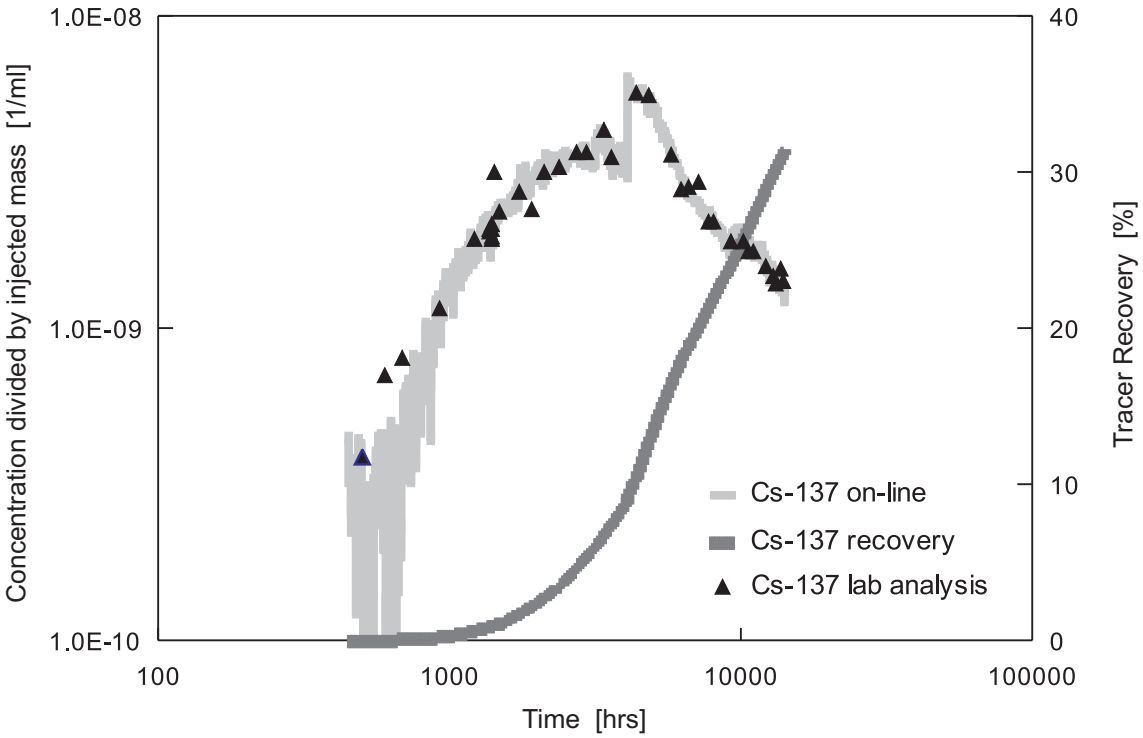

Fig. 3.10: Break-through and tracer recovery curves of Cs-137 (test 90); 4.9 m flow field BOMI 86.004 → BOMI 87.006, injection flow rate of 10 ml/min, extraction flow rate of 150 ml/min, log scales; note that the apparent jump in concentration at the break-through peak was due to a counter recalibration

3.3 Conclusions

Tracer experiments of sufficient quality for use in transport model testing were achieved because the following requirements were met:

Flow field:

- Minimal disturbance of chemical conditions within the fracture.
- Long-term stability of hydrogeological conditions (which places particularly high demands on the pumping equipment).
- Narrow unequal-strength dipole flow fields, that provide close to 100 % recovery (at least for non-sorbing tracers) and give break-through curves that are insensitive to heterogeneities in the hydrogeological properties of the MI shear zone, and are thus favourable to transport process identification.
- Sufficient distance from the laboratory tunnel to avoid the unsaturated or partly saturated zone in its vicinity.
- Minimal disturbance of the dipole flow field by background flow towards the tunnel.
- High hydraulic conductivity to keep the test duration within practical bounds.

Experimental equipment:

- Equipment that does not sorb the selected tracers, to avoid experimental artefacts.
- Maximal analytical range for on-line tracer analysis to minimise the tracer mass or activity required and to allow the resolution of the tails of break-through curves (important for transport process discrimination in subsequent modelling exercises).
- Tracer dosage equipment for pulse and continuous injection that precisely quantifies injected tracer mass or activity.
- Minimal "dead volume", to reduce spreading of injected tracer pulses in the equipment and downhole tracer detection to quantify this spreading.
- Pumps that provide long-term, constant flow rates.
- Pressure transducers that operate accurately over long periods.

Manpower:

- Fruitful interaction between field experimentalists, modellers and laboratory scientists.
- Continuity of personnel carrying out field work (minimal loss of technical knowledge and skills due to personnel changes during the eight-year field-testing programme).

Obtaining reliable experimental data for radionuclide transport process identification and model testing requires substantial time and resources (see Table 3.1). The practical experience built up during MI has greatly helped to speed up subsequent related studies both at the GTS (e.g. the RRP, CRR and HPF projects) and elsewhere (e.g. Kamaishi, Japan; Mt. Terri, Switzerland; Äspö, Sweden).

References

Detailed information about specific topics related to experimental set-up and the carrying out of field tracer tests is documented in various reports and publications. Table 3.4 contains a list of topics and associated reports that give technical details or summarise raw data. A more complete list of MI reports is given in the references chapter of the present report.

Tab. 3.4: Specific topics related to experimental set-up and the carrying out of field tracer tests, and associated reports giving technical details or summarising raw data

Topic	Associated report
• single borehole probe	DROST, W. (1984): Single Well techniques. In: Tracer methods in isotope hydrogeology 8, Vienna, Austria (IAEA).
• tracer analysis equipment • equipment sorption tests • evaluation of experimental errors • HPLC-pumping technique • tracer dosage techniques	EIKENBERG, J., HOEHN, E. & FIERZ, Th. (1994): Grimsel Test Site – Preparation and performance of migration experiments with radioisotopes of sodium, strontium and iodine. PSI Report 94-11, PSI, Würenlingen, Switzerland.
• helium tracer technique	EIKENBERG, J., BÜHLER, Ch. & FIERZ, Th. (1992): On-line detection of stable helium isotopes in migration experiments. Proc. of the 6th International Symposium on Water tracing, Sept. 21 – 26, Karlsruhe, Germany. FRICK, U. (1992): Beurteilung der Diffusion im Grundwasser von Kristallingesteinen – Ein Beitrag zur Kristallinstudie 1993. Unpubl. Nagra Internal Report, Nagra, Wettingen, Switzerland.
• hydrogeochemical equilibrium test	EIKENBERG, J., BAYENS, B. & BRADBURY, M.H. (1991): The Grimsel Migration Experiment: A Hydrogeochemical Equilibrium Test. Nagra Technical Report NTB 90-39, Nagra, Wettingen, Switzerland.
• raw data • test summaries	FIERZ, Th. (1998): The Nagra-PNC Grimsel Radionuclide Experiment, Documentation of Tracer Experiments 1988 – 1996. Unpubl. Nagra Internal Report, Nagra, Wettingen, Switzerland.
• test set-up • borehole instrumentation • low volume packer system • fibre optic fluorimeter (down hole uranine detection) • helium tracer technique • groundwater storage system	FRICK, U., ALEXANDER, W.R., BAYENS, B., BRADBURY, M.H., BOSSART, P., BÜHLER, Ch., EIKENBERG, J., FIERZ, Th., HEER, W., HOEHN, E., McKINLEY, I.G. & SMITH, P.A. (1992a): Grimsel Test Site: The radionuclide migration experiment – Overview of investigations 1985 – 1990. Nagra Technical Report NTB 91-04, Nagra, Wettingen, Switzerland.
• flow fields	FRICK, U. (1994): The Grimsel Radionuclide Migration Experiment – A Contribution to Raising Confidence in the Validity of Solute Transport Models Used in Performance Assessment. GEOVAL 94, Nagra, Wettingen, Switzerland.
• hydraulic characterisation • hydraulic test equipment	HOEHN, E., FIERZ, Th. & THORNE, P. (1990): Grimsel Test Site: Hydrogeological characterization of the migration experimental area. Nagra Technical Report NTB 89-15. Nagra, Wettingen, Switzerland.

4 GEOLOGICAL AND HYDROGEOLOGICAL CHARACTERISATION OF THE MIGRATION SHEAR ZONE

M. Mazurek, W.R. Alexander and P.M. Meier

4.1 Geological Characterisation

A detailed characterisation of the genesis, structure, mineralogy and pore-space distribution of the Migration Fracture is provided by BOSSART & MAZUREK (1991), and their report is the main basis for this summary, complemented by BRADBURY (1989) and MÖRI et al. (2001a and b).

4.1.1 Regional Setting

The Grimsel Test Site (GTS) is situated in the Aare Massif, a basement high in the Helvetic realm of the Alps. The Aare Massif consists of a metasedimentary envelope that was intruded by Hercynian (320 – 280 Ma B.P.) granitoids such as the Central Aare granite and the Grimsel granodiorite (the latter is the host rock of the MI shear zone). All rocks of the Aare Massif have been affected by Alpine greenschist metamorphism and deformation at about 25 Ma B.P. (DEMPSTER 1986). Peak Alpine metamorphic conditions in the vicinity of GTS are estimated at 400° C/2.5 – 3 kbars (CHOUKROUNE & GAPAIS 1983, MARQUER et al. 1985), and the rocks were subjected to ductile deformation, which is mainly characterised by a penetrative foliation and by discrete ductile (mylonitic[14]) shear zones, such as the MI shear zone.

The formation of brittle structures post-dates ductile deformation and can be attributed to the post-metamorphic regional uplift that is still currently operative, with rates (averaged at a regional scale) of 1 – 2 mm a^{-1}. In the case of the MI shear zone, the brittle structural elements include fault breccias and gouges created by cataclastic deformation[15] that occurred at significantly lower temperatures and pressures than was the case with the ductile deformation observed in the Aare Massif.

4.1.2 Genesis and Geometry of the MI Shear Zone

4.1.2.1 Structures related to Ductile Deformation

The MI shear zone is oriented parallel to the regional cleavage trend and dips subvertically (> 80°) towards the SE and, in places, also towards the NW. It is characterised by mica-rich mylonite bands with thicknesses of centimetres to decimetres, where the intensity of cleavage is high. At the northern boundary of the shear zone, the deformation gradient from the shear zone into the granodioritic gneiss is abrupt (Figure 4.1), while, on the south side, there is a more gradual transition to weakly deformed granodiorite. This pattern is observed in numerous boreholes penetrating the MI shear zone, and is also widely observed in other shear zones at the GTS. BOSSART & MAZUREK (1991) derive a shear strain along the ductile shear zone of at least several metres.

---

[14] A mylonite is a rock produced by ductile deformation. Macroscopically, mylonites are characterised by small-scale banding, and the cleavage intensity is often high. Microscopically, a considerable reduction of the grain sizes with respect to the undeformed source rock is typical; recrystallisation of deformed grains can be syn- or post-kinematic. Recrystallised grains of quartz often show a preferred orientation of the optical axes.

[15] Cataclasis is a process of brittle shear deformation, where shear stress is accommodated by frictional sliding and grain rotation. It can be localised to discrete horizons, where the rock may be ground to a very fine grained powder. Such focussed cataclasis, together with mechanical mixing of the particles, leads to the formation of fault breccias and gouges.

4.1.2.2 Structures related to Brittle Deformation

Brittle deformation is localised into very discrete horizons of fault breccia/gouge[16], with thicknesses typically in the range of millimetres. In a section across the shear zone, one or more such horizons are observed (Figure 4.1). Due to slight undulations in their orientation, the individual fault gouge horizons are interconnected on a scale of metres.

Fault gouges are formed at shallow crustal levels (generally less than 5 km overburden), where brittle rather than ductile deformation dominates. They are due to localised cataclastic shear movements along fault surfaces and are therefore cohesionless. Subsequent hydrothermal effects may cause mineralogical alterations and possibly increase the cohesion of the fault gouge by cementation. However, very little alteration is observed in the MI shear zone, so the gouge materials remain open and provide paths for water flow.

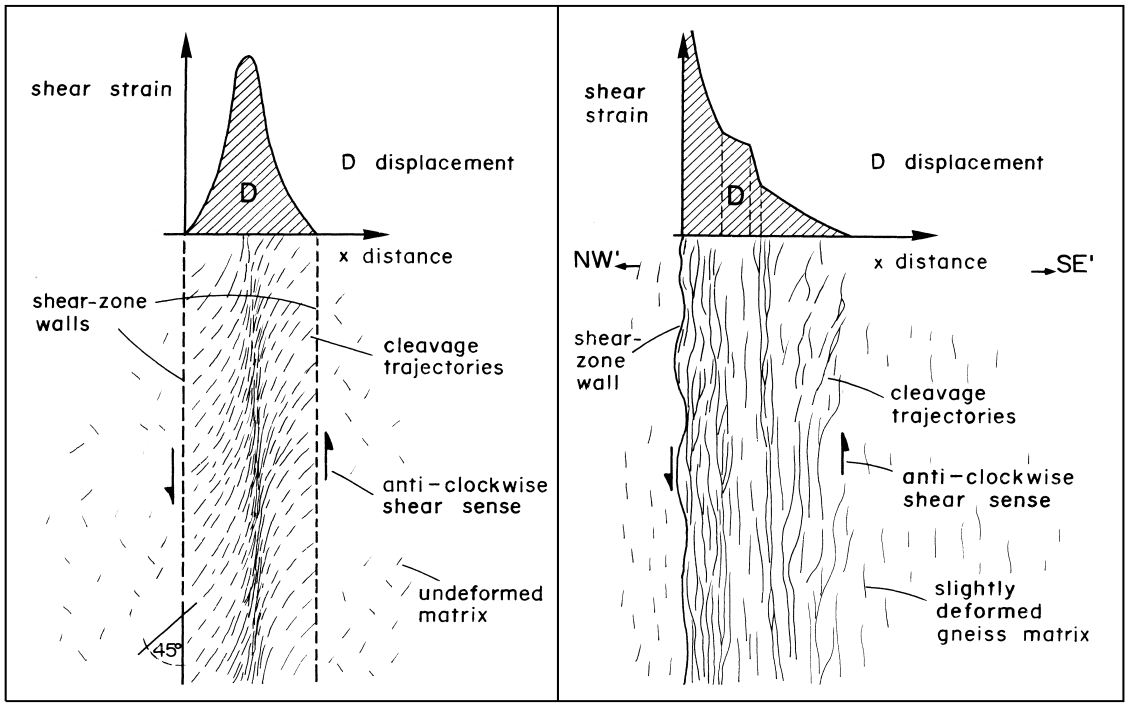

Fig. 4.1: Distribution of finite strain in an ideal ductile shear zone compared with structures of the MI shear zone at VT 420 (taken from BOSSART & MAZUREK 1991)

4.1.2.3 Interference of Ductile and Brittle Deformation Fabrics and Relation to Permeability

Ductile, mylonitic deformation occurred at elevated temperatures, such that deformation was plastic and recrystallization kept pace with shear strain. No discrete open fractures developed during this stage, and mylonitic shear zones *per se* are not preferential flowpaths (rather the contrary), due to their preferred orientation and low (~ 0.5 %) porosity.

[16] The distinction between fault breccias and gouges is determined by average particle size (> 1 mm for breccias, < 1 mm for gouges). Fault gouges are more frequent than breccias in the MI shear zone, and so, for simplicity, only the term "fault gouge" is used in the present report.

The transmissive portions of shear zones at the GTS are exclusively due to brittle deformation. The role of pre-existing ductile shear zones for present-day permeability is that they constitute mechanical weaknesses in the rock body and thus are preferentially reactivated by subsequent events of brittle deformation, such as the formation of fault gouges in the MI shear zone. Typically, fault gouges develop in the zones of highest ductile deformation (minimum grain size, maximum mechanical anisotropy [cleavage] and mica contents) or along sharp contacts between mylonite and granodiorite (lithologic boundary, e.g. NW wall of the MI shear zone). The resulting interference pattern of the two events of deformation gives rise to a flow porosity in fault gouges that are typically, but not exclusively, embedded in mylonite.

4.1.3 Mineralogy

The primary magmatic parent rock of the MI shear zone is a medium to coarse grained granodiorite, the major components of which are quartz, plagioclase, potassium feldspar and biotite, with accessory ilmenite, allanite (= orthite), apatite and zircon. As an effect of Alpine metamorphism, mineralogical transformations occurred throughout the rocks (but more extensively in mylonitic shear zones) and comprise mainly the growth of albite, biotite, chlorite, muscovite, epidote and titanite at the expense of the primary magmatic minerals. Typical mineralogical compositions are given in Table 4.1.

Tab. 4.1: Average mineralogical compositions of lithologies in, or close to, the MI shear zone; data (in vol.%) taken from MEYER et al. (1989), each group represents 2 – 5 analyses

Mineral	weakly foliated Granodiorite	Mylonite	Fault gouge
Quartz	23	17	15
Plagioclase/Albite	23	32	28
K-Feldspar	20	11	7
Biotite	14	30	41
Chlorite	3	< 1	< 1
Muscovite	8	5	4
Epidote	5	3	3
Titanite	2	2	2
Rutile	trace	trace	trace
Zircon	trace	trace	trace
Apatite	trace	< 1	trace
Ilmenite	1	trace	trace
Orthite	1	< 1	< 1
Clay Minerals	< 1	< 1	0 – 1

The mineralogy of fault gouges, i.e. the rock domains created by cataclastic deformation, is very similar to that of the adjacent wallrock. This is because brittle deformation was followed by only very limited hydrothermal fluid circulation, and so mineral alteration is of minor quantitative importance. The only hydrothermal product encountered in the fault gouges is a minor amount of smectite (max. 1 %)[17].

4.1.4 Porosity and Pore Space Distribution

4.1.4.1 Quantitative Porosimetry

The interconnected porosity of all lithological domains has been measured by the Hg-intrusion and water-saturation techniques (BOSSART & MAZUREK 1991) and *in situ* resin injection (MÖRI et al. 2001b). A dependence of porosity on rock type can be identified. Undeformed granodiorite has open porosities in the range of 0.8 – 1.5 vol.%[18], which decreases to 0.5 – 0.9 vol.% in mylonitic granodiorite. This result is consistent with microscopic observations, which show that recrystallised, fine grained mylonites have a denser structure than granodiorite. Wallrock porosities show a pronounced increase of porosity up to 2 vol.% close (a few cm) to the fault gouge horizons, presumably due to mechanical damage induced by the brittle deformation that reactivated and overprinted the dense mylonitic fabric. It is concluded that ductile (mylonitic) deformation reduces matrix porosity, in contrast to the enhancement of porosity due to brittle (cataclastic) deformation (see MÖRI et al. 2001a and b, for details).

4.1.4.2 Pore Space Distribution

The microscopic arrangement of pore spaces was studied in impregnated thin-sections (see BOSSART & MAZUREK 1991 and MÖRI et al. 2001a and b, for details).

The **fault gouges** show a very high, dispersed microporosity, roughly estimated at 10 – 40 vol.%. These pore spaces represent the microscopic voids between individual gouge particles and are more or less evenly distributed across the entire gouge volume. Due to the very small apertures of the individual pores, it appears unlikely that measured transmissivities in the migration fracture can be accounted for by flow through the gouge material. Two other types of pore spaces, namely planar microfractures along gouge/wallrock contacts and open channels within the gouges, are more likely candidates as the principal conduits for flow but *in situ* impregnation of parts of the MI experimental shear zone during the RRP experiment clearly shows flow (and radionuclide retardation) in the fault gouges. Channels within fault gouges are generated by the slow washing-out of the non-cohesive gouge material (internal erosion) by flowing groundwater[19].

---

[17] The smectite distribution in the fault gouge varies widely over distances of decimetres, indicating a channelised flow of the low-temperature hydrothermal fluid. This can have significant localised effects on the pattern of radionuclide retardation in the shear zone as the smectite has a relatively high cation exchange capacity (up to an order of magnitude greater than any other mineral phase present, see Chapter 5) which can easily swamp the effects of the other mineral phases present.

[18] These data (from BOSSART & MAZUREK 1991) are for samples Hg-intruded in the lab following recovery by core drilling. MÖRI et al. (2001b), however, report much lower values (around 0.4 – 0.6 vol.%) for a few representative samples resin impregnated *in situ* followed by coring. This suggests that all data obtained by laboratory based measurements may well overestimate the accessible porosity (see also discussion in OTA et al. 2001).

[19] In the shorter-term, washing out by the artificial flow fields imposed during MI (where pressures of over 10 bars were sometimes applied) has also occured (Chapter 3), but this mechanism still does not explain the existence of channels outside the experimental area.

The **wallrock matrix** contains a variety of different types of pore spaces:

- **Parallel channels (sheet-silicate porosity)** follow mica-rich bands, particularly in ultra-mylonitic areas of the shear zone, and are 0.001 – 0.05 mm wide. They are spatially highly anisotropic and allow water to flow mainly in a direction parallel to cleavage, although there is some restricted lateral branching. The parallel channels provide limited links between the fault gouges and the granodiorite gneisses outside the shear zone.
- **Grain boundary and transgranular porosity:** Planar pore spaces along grain boundaries (mainly of quartz and feldspars) have apertures of 0.001 – 0.02 mm and are present both in the mylonites and, to a greater extent, in less deformed granodiorite, where they constitute an interconnected network. Transgranular pores (i.e. microfractures cross-cutting mineral grains) are of secondary quantitative importance, and they do not occur in mylonites.
- **Solution porosity:** Diffuse pore space arrays can be observed to emanate from trans-granular pores in potassium-feldspar and plagioclase. They are interpreted as corrosion structures generated during Alpine greenschist metamorphism (sericitisation and albitisation of feldspars). Even though minor by volume, solution porosity can create large surfaces that are potentially important for matrix diffusion and sorption processes, especially where associated with the secondary sericite.

Different pore types predominate according to the degree of ductile deformation of the rock. Sheet-silicate pores dominate in zones of higher deformation (mylonites), while grain boundary pores are important in the granodiorite gneisses. All types of pore spaces appear to be inter-connected to some extent and represent an open (solute-accessible) porosity.

4.1.5 Flowpath Geometry

4.1.5.1 Flow Porosity

The MI shear zone is geometrically a relatively simple structure on a scale of metres. It basically consists of one single fracture (made up of 1 – 3 parallel fault gouge horizons when observed more closely[20]) that follows a pre-existing mylonitic shear zone. At other sites in crystalline basement rocks, such as in SKB's underground laboratory at Äspö, even the simplest brittle structures consist of a number of interconnected fractures with potentially contrasting flow properties (MAZUREK et al. 1996), and this complexity requires a detailed structural characterisation. During MI, however, neither branching of the structure nor associated joint systems (such as splay cracks) were identified and this apparent structural simplicity was reflected in the modelling (Chapter 6).

It is now known (see MÖRI et al. 2001a) that flow in the experimental shear zone is complex. It occurs in channels within the fault gouges (generated by internal erosion by flowing water), along microfractures along the gouge/wallrock contacts, within the highly porous fault gouge itself (see Figure 4.2) and in splays connecting the main fractures.

[20] Detailed examination of borehole BOMI 86-006 with a down-hole TV camera indicated the presence of several water-conducting features within the MI shear zone. This was verified following *in situ* resin injection and subsequent core recovery during the RRP project (see MÖRI et al. 2001a).

4.1.5.2 Wallrock Porosity

In most cases, flow porosity is restricted mainly to mylonitic wallrocks. These contain an interconnected network of microscopic pore spaces, even though it is substantially less well developed than that of the granodiorites. Pore spaces are mostly aligned parallel to cleavage (and to the fault gouges), such that the pore network is highly anisotropic. It follows that, while the whole wallrock volume is potentially accessible to diffusion and interconnected with flow porosity, the mylonites attenuate mass transfer in the direction perpendicular to flow (i.e. between fault gouge and granodiorite). In spite of this, clear evidence does exist of matrix diffusion across the shear zone and into the wallrock (see ALEXANDER et al. 1990a and b).

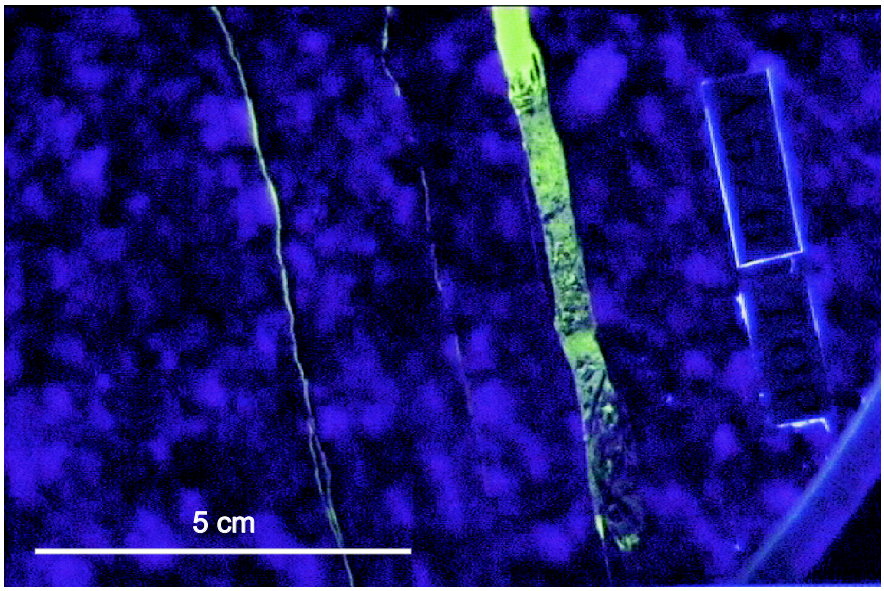

Fig. 4.2: *In situ* resin impregnated shear zone showing the complex structure of channels, fault gouge, breccia and splays in which flow occurs in the MI experimental shear zone (details in MÖRI et al. 2001a); UV light illuminated, scale in centimetres

4.2 Hydrochemical Characterisation

The hydrogeological characterisation of the site was mainly carried out between 1986 and 1990 with the hydrochemistry, colloidal and microbial populations of the groundwater studied in some detail. The main sources for the information presented here are BRADBURY (1989), DEGUELDRE et al. (1990 and 1996), EIKENBERG et al. (1991 and 1994), MILNER & CHRISTOFI (1985), CHRISTOFI & MILNER (1990) and FRICK et al. (1992a).

4.2.1 Hydrochemistry

The main groundwater flow in the GTS is concentrated in the numerous lamprophyre dykes which intrude the Grimsel granite and granodiorite with relatively minor flow in the shear zones. FRICK et al. (1992a; Table 2.2) provide data on the regional hydrochemistry, including major elements, gases and stable isotopes. The water is generally weakly mineralised and alkaline (pH 8.5 to 10.3).

The groundwater in the experimental shear zone is Na-Ca-HCO_3 type with a low ionic strength (0.0012 M) and is suboxic to anoxic (precise Eh is uncertain as the system is not at equilibrium; see Table 4.2 and comments in ALEXANDER 1991), alkaline (pH ~ 9.6) and the CO_2 content is less than 7×10^{-7} M. The rock-water system pH is reasonably well buffered (EIKENBERG 1989, EIKENBERG et al. 1994) but the Eh buffer capacity remains unknown (but is probably large – e.g. biotite – but kinetics may be slow).

Tab. 4.2: Chemical composition of discharging groundwater from the experimental shear zone (AU 96)

pH		9.6 ± 0 .2
Ionic strength [M]		0.0012
Temperature [°C]		12 ± 1
Electrical Conductivity [µS cm^{-1}]		103 ± 5
Cations:		
Na^+	[M]	6.0 - 6.9 × 10^{-4}
K^+	[M]	3.2 - 5.0 × 10^{-6}
Mg^{2+}	[M]	2.9 - 6.2 × 10^{-7}
Ca^{2+}	[M]	1.3 - 1.4 × 10^{-4}
Sr^{2+}	[M]	1.8 - 2.0 × 10^{-6}
Rb^+	[M]	1.9 - 2.5 × 10^{-8}
Cs^+	[M]	5.0 - 5.2 × 10^{-9}
[5] total cations	[eq L^{-1}]	9.5 - 9.9 × 10^{-4}
Anions:		
SO_4^{2-}	[M]	5.7 - 6.4 × 10^{-5}
SO_3^{2-}	[M]	5 × 10^{-7}
HS^-	[M]	1 × 10^{-6}
$H_2S_{(g)}$	[M]	1 × 10^{-6}
F^-	[M]	3.2 - 3.6 × 10^{-5}
Cl^-	[M]	1.5 - 1.8 × 10^{-4}
Br^-	[M]	2.7 - 4.2 × 10^{-7}
I^-	[M]	1.0 × 10^{-9}
[1] alk	[eq L^{-1}]	4.2 - 4.5 × 10^{-4}
[5] total anions	[eq L^{-1}]	10.2 - 10.4 × 10^{-4}
Other Species:		
Si	[M]	1.6 - 2.5 × 10^{-4}
Fe (total)	[M]	2.3 - 3 × 10^{-9}
Mn (total)	[M]	5 × 10^{-9}
Cu (total)	[M]	6 × 10^{-10}
U (total)	[M]	6 × 10^{-10}
CO_2	[M]	< 7 × 10^{-7}
[2] O_2	[M]	< 3 × 10^{-8}
N_2	[M]	7 - 8 × 10^{-4}
NH_4^+	[M]	5 × 10^{-10}
NO_2^-	[M]	not detected
NO_3^-	[M]	1 × 10^{-6}
TIC	[ppm]	2.6
TOC	[ppm]	0.5 - 0.9
[3] **Calculated:**		
[4] HCO_3^-	[M]	2.9 × 10^{-4}
[4] CO_3^-	[M]	4.2 × 10^{-5}
[4] OH^-	[M]	1.3 × 10^{-5}
[4] $H_3SiO_4^-$	[M]	4.2 × 10^{-5}
H_4SiO_4	[M]	2.1 × 10^{-4}

Legend:
[1] alk = alkalinity
[2] on site measurements at the Grimsel Test Site
[3] calculated for relevant pH and temperature
[4] major species contributing to alkalinity
[5] total anion concentrations are slightly smaller than the cation content; this might be caused by small systematic errors in the alkalinity, which is particularly sensitive to precise pH determination.

Data are compiled from BAJO et al. (1989), AKSOYOGLU et al. (1991), DEGUELDRE et al. (1990), EIKENBERG et al. (1991 and 1994), ALEXANDER (1991) and FRICK et al. (1992a).

4.2.2 Colloids

The colloid concentration in the groundwater in the exerimental shear zone has been determined several times (see DEGUELDRE et al. 1990 and 1996, for an overview). The colloid populations are approximately:

10^{14} colloids L^{-1} of > 10 nm diameter

10^{12} colloids L^{-1} of > 50 nm diameter

10^{7} colloids L^{-1} of > 450 nm diameter

The total mass of colloids is about 50 – 100 ppb for the size range 10 – 450 nm and 100 – 200 ppb for the 10 – 1000 nm size range. The colloids consist mainly of amorphous silica with small amounts of mica and calcium silicates.

4.2.3 Microbes

MILNER & CHRISTOFI (1985) and CHRISTOFI & MILNER (1990) reported maximum microbial populations of 5×10^{6} bacteria L^{-1}, consisting of aerobic and anaerobic heterotrophic spore-forming bacteria, heterotrophic iron precipitating bacteria, fungi, sulphate reducing bacteria, denitrifying bacteria and nitrifying bacteria. FRANCIS et al. (1999) reported mean populations of 3×10^{7} bacteria L^{-1}, consisting of heterotrophic and autotrophic bacteria including *Acetobacterium* sp. Some of the cells isolated from the groundwater by FRANCIS et al. (1999) were elongated and "...appear almost stalked (these cells may have been attached to the rock surfaces)" and they also note that the physical form of the cells suggests a lack of nutrients in the rock-water system.

4.3 Hydrogeological Characterisation

The original hydrogeological characterisation of the site was carried out in the mid- to late-eighties, and reported in detail in HOEHN et al. (1990) and FRICK et al. (1992a). More recently, during the RRP project, additional work was carried out to take account of advances in both measurement techniques and in hydrogeological modelling. This work is summarised briefly below and in more detail in Appendix 1. The source report is MEIER (2002), with additional information in MEIER (1997) and MEIER et al. (1997).

4.3.1 Work in Preparation for Tracer Experiments for Transport Model Testing

Field work on the hydrogeological characterisation and hydrogeological modelling of the MI shear zone in the mid- to late-eighties focussed primarily on the determination of suitable dipole flow fields for the planned tracer tests and on a general description of the hydrogeological conditions. The hydrogeological models were used to explore a range of views and concepts regarding the MI shear zone transmissivity distribution and flow field. Others were used to estimate the potential impact of boundary conditions (e.g. the impact of the laboratory tunnel on the background flow) and to check the validity of conventional hydrotest analyses.

As discussed in Chapter 3, a requirement of the tests was to find a portion of the shear zone where the unperturbed pressure distribution is relatively flat. Some understanding of the heterogeneity of the transmissivity distribution is also required for transport model testing (Chapter 6), although, as described in Chapter 3, narrow unequal-strength dipole flow fields were generally used and these give breakthrough curves that are insensitive to such heterogeneity.

4.3.2 Subsequent Work

Subsequent work on the hydrogeological characterisation of the MI shear zone has been performed that takes advantage of developments in experimental and hydrogeological modelling methods since the earlier studies. The results of this work have not, so far, been used in the context of transport model testing, except for a highly simplified model that excluded the retardation process of matrix diffusion, and are not therefore, reported in the main text (a description of the work is, however, given in Appendix 1).

The inability of the simplified model to predict adequately tracer break-through of a conservative tracer may itself be a significant finding. It indicates the importance of the process of matrix diffusion (which is incorporated in all of the more successful models described in Chapters 6 and 7), as well as possibly indicating that the transmissivity field is still not adequately characterised. As mentioned in Chapter 2, it is important to examine as many plausible alternative models as possible in order, by falsifying some of these alternatives by their failure to predict experimental results, to narrow down the range of conceptual model uncertainty and to identify the processes that are most important.

Interestingly, the model predictions of transmissivity heterogeneity (on the metre to decametre scale; see Appendix 1) in the experimental shear zone have been shown to be largely correct (see MÖRI et al. 2002, for details) following the recent drilling of a suite of new boreholes and associated hydrogeological testing campaign conducted in the GTS Phase V project CRR (Colloid and Radionuclide Retardation Experiment).

5 LABORATORY AND HYDROGEOCHEMICAL FIELD TESTS IN SUPPORT OF THE MIGRATION EXPERIMENT

M. Bradbury and B. Baeyens

The laboratory physical and chemical characterisation studies performed in the period 1985 to 1990 are reported in detail in FRICK et al. (1992a) and the references given therein; these reports provide a basis for the present summary of the main highlights and conclusions. The hydrogeochemical equilibration experiment, carried out in the MI shear zone, is also discussed, since the results from this test are strongly related to, and complementary to, the laboratory investigations (see EIKENBERG et al. 1991, FRICK et al. 1992a). The final part of this chapter is devoted to a description of the derivation of in situ retardation parameters from laboratory measurements and, in particular, the most recent work in developing a caesium sorption model (see BRADBURY & BAEYENS 1992).

5.1 Aims of Laboratory and Field Tests

The main aims of the laboratory and field investigations in support of MI were:

- to gain a sufficient understanding of the MI shear zone hydrogeochemical system to support the selection of suitable sorbing tracers (radionuclides) for tracer tests
- to determine the sorption properties of these tracers in laboratory experiments
- to predict the *in situ* sorption properties of the MI shear zone based on the laboratory data.

The laboratory experiments are discussed in Section 5.2. They centred on rock-water interaction tests and batch-sorption measurements on crushed mylonite (see Chapter 3 for a description of this material). In addition to these static tests, laboratory tracer-transport experiments were also performed on intact, small-diameter core samples containing a single, simple fracture.

The hydrogeochemical equilibration experiment is discussed in Section 5.3. This was carried out in the MI experimental shear zone, in a standard dipole flow field. Instead of break-through curves from injected radionuclides, however, the integral response to a step change in chemical composition of the injected water, achieved by mixing water from a hydrochemically distinct (but otherwise similar) shear zone, was analysed.

In Section 5.4, the estimation of *in situ* sorption properties from laboratory results is described. It is important to note that the material used in the laboratory experiments did not have precisely the same composition as the fault gouge in the shear zone seen by the MI tracers (see Table 3.1). It was therefore critical to characterise the system fully and to understand the sorption mechanisms so that models could be formulated which allowed the *in situ* sorption properties to be predicted. This is particularly true in the case of caesium, which is discussed in detail in the final part of this chapter.

As described in Chapter 7, *in situ* sorption properties were also obtained by fitting tracer-transport models to experimental break-through curves. A comparison of the sorption properties derived from independent laboratory and field tests with those derived from modelling tracer break-through curves provides a test of the concepts involved both in the interpretation of these independent tests and in the transport-modelling studies. This is an important test of the applicability of laboratory-produced retardation data for the prediction of *in situ* radionuclide retardation.

5.2 Laboratory Tests

5.2.1 Rock-Water Interaction Tests

These tests were designed to study the interaction of crushed mylonite with groundwater and, in particular, to examine the chemical stability of the system over experimentally long times. Chemical stability is a key concern in the interpretation of both batch-sorption measurements and tracer-transport experiments, in which it is assumed that the systems remain chemically stable over the time scale of the experiments (from several days to several hundred days, depending on the experiment).

The rock-water interaction tests consisted simply of contacting disaggregated shear zone material (particle size less than 2 mm) with groundwater in closed containers, which were shaken periodically. The water composition was monitored at regular intervals over periods of up to 200 days. Since suitable glove boxes were not available at the time that the tests were carried out, a cover gas of N_2 was used in an attempt to limit CO_2 contamination. The parameters investigated in the tests were (BAJO et al. 1989):

- the initial water composition (natural and artificial groundwater)
- temperature (laboratory, about 25° C, *in situ* 12.5° C)
- rock to water ratio (1 : 2 and 1 : 10).

The most important conclusion drawn from the observed evolution of water composition was that it was driven by cation exchange reactions occurring on the crushed mylonite. Cation exchange capacity (*CEC*) determinations, carried out subsequently on the crushed mylonite samples used in the rock-water interaction tests, showed clearly that the quantities of exchangeable cations on the mylonite were large enough to account for the observed changes in water composition in all of the rock-water interaction tests. Furthermore, the changes in cation concentrations in the aqueous phase were quantitatively consistent with the changes in the cation occupancies on the mylonite for each individual cation (when the quantities were expressed on an equivalent scale).

Water chemistry and cation exchange data were subsequently used to derive selectivity coefficients from which it was possible to predict values of the distribution coefficient, R_d[21], for the major cations in this system. This was achieved using the cation exchange model briefly described in Appendix 2. The application of the model resulted in the identification of three sorbing tracers for tracer-transport tests:

- weakly-sorbing sodium
- moderately-sorbing strontium

both of which were expected to sorb linearly, and

- more strongly-sorbing caesium

which was expected to display non-linear sorption[22].

---

[21] The distribution coefficient corresponds to the amount of a tracer sorbed (per unit mass of solid), divided by the amount in solution (per unit volume of solution). The coefficient is a directly measurable quantity and implies no assumptions regarding the kinetics, linearity and reversibility of sorption. In models that assume rapid, linear and reversible sorption (e.g. those described in Chapters 6 and 7), the distribution coefficient is equated to the sorption constant, K_d (see Section 6.3.3 for further discussion).

[22] In the tracer-transport tests, caesium was injected at a low tracer concentration with respect to the natural caesium background, so that linear sorption could be assumed in this particular case.

5.2.2 Batch-Sorption Tests

The purpose of the batch-sorption measurements, carried out at trace concentrations of $^{22}Na^{+}$, $^{85}Sr^{2+}$ and $^{137}Cs^{+}$, was to check experimentally the predictions of their sorption behaviour made on the basis of the cation exchange model (see Appendix 2). In addition, sorption tests using the conservative tracers $^{82}Br^{-}$ and $^{131}I^{-}$ were performed.

All experiments were carried out in controlled atmosphere glove boxes. Samples of shear zone material were repeatedly crushed, until all the material passed through, initially, a 250 μm sieve and, subsequently, a 63 μm sieve, in order to obtain < 250 and < 63 μm size fractions.

The main results of this series of laboratory investigations are documented in AKSOYOGLU et al. (1991) and are repeated briefly here:

Bromine and Iodine

Experiments with bromine and iodine revealed, as expected, no detectable sorption of these anions on shear zone material (within the "estimated total error" of 0.30 $m^3 kg^{-1}$).

Sodium and Strontium

Experiments on the coarse (< 250 μm) size fraction showed pronounced kinetic effects. Sodium distribution coefficients were still increasing at the termination of the experiment (49 days) and the strontium experiments required at least 30 days before reaching stable distribution coefficients.

For the < 250 μm mylonite size fraction, sodium exhibited linear sorption over the equilibrium concentration range (from ~ 10^{-10} M to ~ 2×10^{-8} M; NB: groundwater concentration of ~ 6×10^{-4} M), with an average distribution coefficient of 2.3 (± 0.1) × 10^{-3} $m^3 kg^{-1}$. This is a factor of ~ 3 greater than the value of 0.7 (± 0.1) × 10^{-3} $m^3 kg^{-1}$ calculated on the basis of the cation exchange model (i.e. based on the *CEC*, the fractional ion occupancy and the water-chemistry data). This difference was considered to be too great to be caused by experimental error alone. A hypothesis, postulating the existence of Na^{+} exchange sites within the < 250 μm particles, which could be reached by sodium, but not by the large AgTU complex used in the cation exchange measurements (see AKSOYOGLU et al. 1991), was put forward to explain this discrepancy.

The kinetics of sodium sorption carried out on crushed shear zone material with a particle size < 63 μm size, were rapid, with equilibrium reached within 24 hours. The measured distribution coefficient of 2.5 (± 0.2) × 10^{-3} $m^3 kg^{-1}$, corresponding to a calculated *CEC* of ~ 13 meq kg^{-1} (AKSOYOGLU & MANTOVANI 1989) which was in considerably better agreement with the directly determined *CEC* value of 2.3 (± 0.1) × 10^{-3} $m^3 kg^{-1}$ than in the case of the larger particle-size data. These results are consistent with what would be expected on basis of the explanation given above.

The sorption of strontium was also, as expected, linear and independent of solid-liquid ratio. Over the whole equilibrium concentration range (from ~ 2×10^{-11} M to ~ 10^{-8} M; NB: groundwater concentration of ~ 2×10^{-6} M), the distribution coefficient was found to be 67 (± 4) × 10^{-3} $m^3 kg^{-1}$ on the coarse mylonite material. The predicted value, based on the cation exchange model (i.e. based on the measured *CEC*, the fractional ion occupancy and the water-chemistry data), was 61 (± 10) ×10^{-3} $m^3 kg^{-1}$. Given the experimental uncertainties, this agree-

ment was considered to very good. Likewise, for the < 63 µm data, the measured and calculated distribution coefficients for strontium, 110 (± 10) × 10^{-3} m^3 kg^{-1} and 111 (± 7) × 10^{-3} m^3 kg^{-1}, respectively, were in excellent agreement.

Due to the uncertainties associated with the kinetic effects in the sorption tests carried out on the larger particle sized mylonite, and because the material in contact with flowing groundwater in the MI shear zone is presumed to be dominated by the fault gouge, the sodium and strontium sorption values for < 63 µm material are used for the estimation of *in situ* sorption properties (Section 5.4.1).

Caesium

Caesium sorption on crushed shear zone material (< 63 µm) was measured at a solid/liquid ratio of 1 : 10, at equilibrium caesium concentrations ranging from ~ 10^{-9} M to ~ 10^{-4} M (NB: groundwater concentration of ~ 5 × 10^{-9} M) and two different K^+ concentrations (7.7 × 10^{-5} M and 6.4 × 10^{-4} M). Sorption results are plotted in Figure 5.1 (from AKSOYOGLU et al. 1991). The sorption of caesium is non-linear and is clearly influenced by the competition with potassium. At caesium concentrations below 10^{-8} M to 10^{-9} M (corresponding to a caesium loading on the solid of about 5 × 10^{-6} mol g^{-1}) the sorption appears to tend towards a constant value of R_d (as it must, with ambient [Cs] ~ 5 × 10^{-9} M). These data are discussed in more detail in connection with the caesium sorption model (results also shown in Figure 5.1) described in Section 5.4.2.

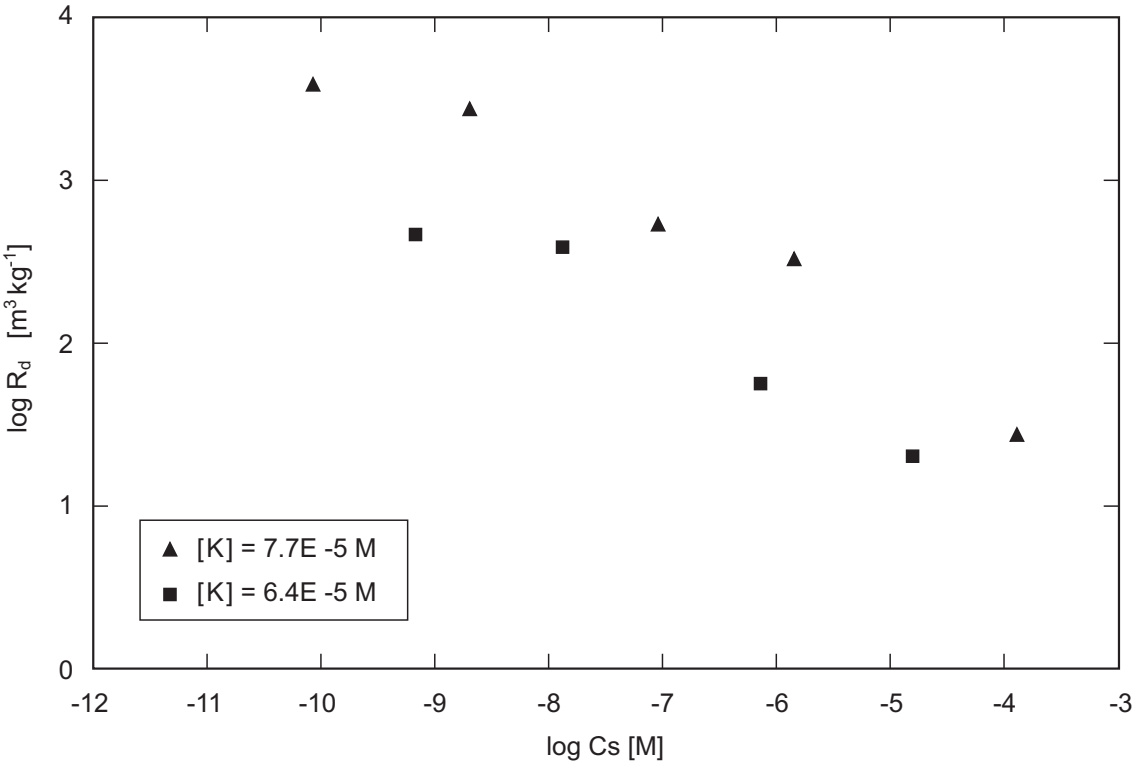

Fig. 5.1: Experimental data for caesium sorption on Grimsel shear zone material (mylonite; < 63 µm size fraction) in synthetic Grimsel groundwater at two artificially enhanced potassium concentrations (AKSOYOGLU et al. 1991)

5.2.3 The Dynamic Infiltration Experiment

The high-pressure infiltration experiment was designed to investigate the transport behaviour of radionuclides through simple fractures in small, cylindrical core samples, a few centimetres in length, under conditions simulating the lithostatic pressure found *in situ*. Several experimental investigations were carried out using this apparatus. Data from experiments on drill cores from the crystalline basement of Northern Switzerland, using a sorbing (^{233}U) tracer, were selected as test case 1b of the international INTRAVAL project (JAKOB & HADERMANN 1991). Furthermore, experiments were carried out using fractured granodiorite cores from the Grimsel Test Site, with simultaneous injection of pulses of non-sorbing ($^{82}Br^-$) and sorbing ($^{24}Na^+$) tracers (SMITH 1991). Taken together, the breakthrough-curves for non-sorbing and sorbing tracers should, in principle, allow the various parameters describing the retardation processes of sorption and matrix diffusion to be separately determined, in a procedure analogous to that described for the field tracer-transport experiments in Chapter 7.

In the course of the analysis of these two-tracer experiments, however, it became clear that dispersion of the non-sorbing tracer in the apparatus was similar in magnitude to the effects of dispersion and matrix diffusion in the sample itself. It was found to be impossible to separate the effects of these different processes, seriously limiting the usefulness of the results and invalidating the results of the INTRAVAL exercise.

The source of the problem lies in the design of the so-called "end-pieces", between which the rock core is retained (see SMITH 1991 for diagrams). In the original design, the end-pieces consist of a central bore, leading to a spiral groove formed in the face in contact with the sample. Infiltration fluid enters the sample continuously as it passed around the spiral. At the upstream end-piece, scoping calculations indicated that the non-sorbing tracer, which migrates without retardation through the sample, could travel a significant distance into the sample near the centre-axis (where it first comes into contact with the sample) before it reaches the outer part of the spiral, giving rise to a curved tracer front within the sample. The resultant artificial spreading of the break-through curves was reinforced by a similar process at the downstream end-piece. It was therefore decided to dispense with these tests in the MI project. The solution of the analogous problem of "dead volume" in the equipment for the field tracer tests is discussed in Chapter 3.

5.3 The Field Hydrogeochemical Equilibration Test

The hydrogeochemical equilibration test was conceived as a preparatory study for possible tracer-transport experiments, in which it might be necessary to inject water with a chemical composition different to that naturally occurring in the MI shear zone if a constant supply of water in the quantities required could not be guaranteed over the anticipated experimental time scales. The original aim was to observe how the chemistry of the MI shear zone water responded to the injection of a "foreign" water and to determine the time required to reach new steady-state conditions.

A step input of an imported water ("EM-water" from a genetically similar shear zone intersected by borehole BOEM 85.012), which is chemically slightly different from the water naturally flowing in the MI shear zone ("MI-water"), was injected into the MI shear zone (see EIKENBERG et al. 1991). A dipole flow field was established between borehole BOMI 86.004 (the injection well) and borehole BOMI 87.006 (the extraction well, see Figure 1.2) and a total of 22 water samples was taken from the extraction well for subsequent laboratory analyses.

The results of the hydrogeochemical equilibration test showed clearly that anions such as F^- and Cl^- reached steady-state concentrations in the extracted water within ~ 50 hours, whereas the major cations, Na^+ and Ca^{2+}, required ~ 150 hours. The three cations, Sr^{2+}, K^+ and Mg^{2+} showed evidence of being retarded more strongly. Sr^{2+} did not reach steady-state until after ~ 250 hours and K^+ and Mg^{2+} appeared to be still increasing slowly when the experiment was terminated after ~ 312 hours. The conclusion from the first part of the work was that EM-water should not be used as a source of injection water in any migration experiment with sorbing tracers (see Chapter 3).

The evolution of ionic concentrations was analysed and interpreted by EIKENBERG et al. (1991), on the assumption that the relevant processes operating during transport of ions in the dipole flow field were:

- "mixing" (dispersion and dilution), which is assumed to operate in the same way for all transported species
- sorption by weak cation exchange (Appendix 2) on the surfaces of shear zone material – although, during the test, multi-ionic cation exchange processes occurred simultaneously, the dominating mechanism was cation exchange between Na^+ (sorbed on shear zone minerals under equilibrium conditions with MI water) and dissolved Ca^{2+} in EM water.

Applying laboratory derived selectivities for the shear zone material (Appendix 2), these data provide a direct measurement of the flow field exchange capacity (the *CEC* integrated over the mass of interacting rock contacted by the dipole flow field), which was of the order of 300 – 400 meq. Finally, under simplifying assumptions concerning porosities and the geometry of the flow field (see EIKENBERG et al. 1991 for details), rough estimates of mass-related parameters can be deduced:

- the *in situ* cation exchange capacity (*CEC*) is in the order of 2.4 meq g^{-1}
- the *in situ* sorption coefficients for sodium and strontium are ~ 0.2×10^{-3} m^3 kg^{-1} and 8×10^{-3} m^3 kg^{-1}, respectively.

In the next section, these *in situ* values are compared with the estimates from the rock-water interaction and batch-sorption tests, corrected for the differences between the experimental systems in the laboratory and in the field.

5.4 Estimation of *In Situ* Sorption Properties

5.4.1 Sorption Properties of Sodium and Strontium

There are slight differences in the composition of the material used in the laboratory experiments and that seen by tracers used in transport experiments in the MI shear zone. In particular, whereas the minerals present in the crushed shear zone material (used in the laboratory experiments) and fault gouge (also seen by migrating tracers) are virtually the same (see Table 3.1), their modal compositions are different. This implies that:

- the selectivity coefficients are probably very similar in both cases (major sorbing phases are the mica-type minerals), but that
- there will be differences in sorption values in the two cases, since e.g. the cation exchange capacities will be different.

The absolute values of the *CEC* are dependent on the conditions under which measurements are made (e.g. particle size, pH and experimental method). Several *CEC* determinations for crushed shear zone material were carried out using the silver-thiourea method at pH ~ 7. The results ranged in values from ~ 3 meq kg^{-1} ("loosely" disaggregated material and very gentle shaking, as described in BAEYENS et al. 1989) to ~ 6 meq kg^{-1} (crushed and sieved material with a size fraction < 250 μm) to ~ 13 meq kg^{-1} (crushed and sieved material with a size fraction < 63 μm, as described in AKSOYOGLU et al. 1991) and up to 25 meq kg^{-1} (*W.R. ALEXANDER, unpublished data*). A further set of measurements, where the material was disaggregated by vigorous shaking during the *CEC* determinations, yielded values of ~ 9 meq kg^{-1} *(B. BAEYENS, unpublished data*). Thus, the laboratory *CEC* data depend strongly on the state of aggregation of the mylonite and size of the particles.

An important point to note concerning the above series of data was that measured and predicted sorption values for sodium and strontium were in generally good agreement whenever the selectivity coefficients (BAEYENS & BRADBURY 1989) were used in conjunction with the appropriate *CEC* to calculate the sorption values (see Section 5.2.2 and AKSOYOGLU et al. 1991). Scaling sorption values with *CEC* values is appropriate when the sorption mechanism is cation exchange and when the different rock samples have similar mineral compositions.

Probably the most reliable laboratory sorption data available for sodium and strontium sorption are those given in AKSOYOGLU et al. (1991) (see Section 5.2.2), where measurements were made on crushed mylonite samples (< 63 μm) having a *CEC* of ~ 13 meq kg^{-1} (AKSOYOGLU & MANTOVANI 1989). These data are reproduced in Table 5.1.

Tab. 5.1: *In situ* sodium and strontium sorption values, calculated from laboratory measurements; R_d(Na) and R_d(Sr) data, deduced from the field hydrogeochemical equilibrium test, are included for comparison

	CEC (meq kg^{-1})	Scaling factor [2]	R_d (Na) (m^3 kg^{-1})	R_d (Sr) (m^3 kg^{-1})
Crushed shear zone material (< 63 μm)	13 [1]	-	$(2.3 \pm 0.1) \times 10^{-3}$	$(110 \pm 10) \times 10^{-3}$
Calculated *in situ* values	-	~ 5	$(0.7 \pm 0.2) \times 10^{-3}$	$(20 \pm 2) \times 10^{-3}$
Hydrogeochemical equilibration test [3]	2.4	-	0.2×10^{-3}	8×10^{-3}

Notes:
(1) Using the data of AKSOYOGLU et al. (1991)
(2) Scaling factor = (*CEC* for mylonite (< 63 μm))/(*CEC* from hydrogechemical eq. test) = 13/2.4 = ~ 5
(3) No error bands have been given for the "best estimate" values deduced from the hydrogeochemical equilibrium experiment, but the uncertainty in the values given may be up to a factor of two

In order to estimate sorption values appropriate for *in situ* conditions in field migration tests from laboratory measurements on mylonite, the corresponding *in situ CEC* value for MI shear zone material is required. A value of ~ 2.4 meq kg^{-1} was deduced from the field hydrogeochemical equilibrium test and represents the average fault gouge *CEC* "seen" by the water in the

flow field of the test. Unfortunately, there is currently no way of judging how reliable this value may be. Recent *CEC* measurements, however, carried out in the laboratory on fault gouge material from the migration fracture, indicate values between 5 and 10 meq kg^{-1} (*B. BAEYENS & M.H. BRADBURY, unpublished data*). The lower *in situ* estimate of 2.4 meq kg^{-1} would therefore appear to be reasonable, since the whole of the flow field is not composed of fault gouge and all of the material therein is not neccessarily accesible to the flowing groundwater.

Finally, because the mineralogies of mylonite and fault gouge are similar (Table 3.1) and the major sorption mechanism for sodium and strontium is cation exchange, the criterion given above for scaling sorption values over corresponding *CEC* values is fulfilled. Hence, estimates for sodium and strontium *in situ* R_d values were obtained by reducing the laboratory sorption values given in Table 5.1 by 5.4; i.e. the ratio of the *in situ CEC* to the mylonite (< 63 μm) *CEC*. The sodium and strontium R_d values deduced from the field hydrogeochemical equilibrium test are also given for comparison in Table 5.1. The discrepancies between these two data sets (factor of about 2) give some indication of the uncertainties in the estimated values.

5.4.2 The Caesium Sorption Model

The results of batch-sorption tests for caesium on crushed mylonite were presented in Section 5.2.2. These results could not, however, be scaled to give values appropriate to fault gouge in the same way as was done for sodium and strontium because the sorption of caesium is significantly influenced by competition with any potassium in the experimental system. In the batch-sorption tests, it was not possible to obtain potassium concentrations in the conditioned water of less than 7.7×10^{-5} M, whereas, in natural Grimsel groundwater, the concentration is ~ 3.8×10^{-6} M; i.e. a factor of ~ 20 lower. Furthermore, because caesium is widely observed to sorb non-linearly, a mechanistic model is needed in order to predict the influence of potassium at the different caesium concentrations. The sorption model described in this section was developed to meet this requirement. The model is presented in more detail in BRADBURY & BAEYENS (1992).

For a constant water chemistry, non-linear sorption generally implies:

- that one aqueous species is sorbing on two or more sites with different binding characteristics, or
- that two or more different aqueous species are sorbing on one site type, or
- a combination of these.

Caesium has an extremely simple water chemistry and is present only as the hydrated monovalent cation, Cs^+. Non-linear sorption characteristics therefore imply that caesium is sorbing on at least two different types of site. Furthermore, it is well established and documented in the open literature that caesium sorbs by some kind of a cation exchange mechanism[23]. The present caesium sorption model thus considers cation exchange on two types of site with different sorption selectivities (affinities):

(i) High-selectivity (frayed-edge) sites:

The first set of cation exchange sites considered are the high-selectivity (or frayed-edge) sites (*FES*). These sites are responsible for the uptake of caesium on the solid phase at trace concentrations. Their sorption capacity is small in comparison with the total *CEC* of

[23] The partial irreversibility of Cs sorption is also well known, indicating that simple cation exchange is not the only mechanism involved.

the material, but they have a high selectivity for monovalent cations, particularly K^+, Rb^+ and Cs^+. The nature of these high-selectivity sites is such that, for steric reasons, they are only occupied by monovalent cations with low hydration energies. In most natural rock groundwater systems, this means that these sites are occupied by K^+. The sorption of Cs^+, at trace concentrations, then occurs via cation exchange with K^+, i.e.

$$K^+ - FES + Cs^+ \Leftrightarrow Cs^+ - FES + K^+$$

(ii) Low-selectivity (planar) sites:

The second set of sites considered are the normal "planar" cation exchange sites (*PS*). These sites have a considerably lower sorption selectivity for caesium than the frayed-edge sites, but a much higher sorption capacity, These sites cannot be treated in the same way with respect to caesium sorption as the frayed-edge sites, since they are available to all cations. Fractional ion occupancies on planar sites will be determined by the water composition and selectivity coefficients: i.e., competitive effects from monovalent and bivalent cations are important. Caesium can sorb on the planar sites by exchanging with monovalent (M^+) and bivalent (B^{2+}) cations:

$$M^+ - PS + Cs^+ \Leftrightarrow Cs^+ - PS + M^+$$

$$B^{2+} - PS + 2\ Cs^+ \Leftrightarrow 2\ Cs^+ - PS + B^{2+}$$

The bivalent cations Mg^{2+}, Ca^{2+} and Sr^{2+} are chemically very similar, and their selectivity coefficients with respect to other cations, in a wide variety of clay systems, have been shown to be approximately the same. On this basis it is assumed that the bivalent cations can be grouped together and their exchange behaviour with respect to caesium described with a single selectivity coefficient. Separate coefficients are used to describe the exchange of caesium with the monovalent Na^+ and K^+.

An analytical solution can be derived for the complete set of exchange reactions which – together with selectivity coefficients from the literature – yield a description of the non-linear sorption of caesium. A summary of the data used is given in Table 5.2 (the site concentrations are based on laboratory measurements), and the fit of the analytical solution to the laboratory data for caesium sorption is shown in Figure 5.2 at two different potassium concentrations.

Tab. 5.2: Site concentrations and selectivity coefficients for modelling caesium sorption on mylonite (BRADBURY & BAEYENS 1992)

Types of sites	Site concentration (eq. g^{-1})	Selectivity coefficients
frayed-edge sites	6.5×10^{-8}	3000 (Cs/K)
planar sites	1.3×10^{-5}	40 (Cs/Na) 500 (Cs/bivalent cations) 5 (K/Na)

The encouraging fit between experiment and model prediction supported the application of the analytical solution, together with the selectivity data presented in Table 5.2, to model *in situ* caesium sorption in the MI shear zone.

The additional data used to derive the Cs isotherm shown in Figure 5.2 are:

- a value for the "*in situ CEC*" of MI shear zone fault gouge of 2.4 meq kg^{-1}, based on the results of the hydrogeochemical equilibration experiment (Section 5.3 and Section 5.4)
- a frayed-edge site capacity of 0.012 meq kg^{-1} (i.e. 0.5 % of the *CEC*)
- a natural caesium background concentration in Grimsel groundwater of 5×10^{-9} M (AKSOYOGLU et al. 1991; EIKENBERG et al. 1994).

For active caesium concentration levels (i.e. tracer concentrations) below this value, the "sorption" occurs via isotope exchange and its magnitude is fixed at a value corresponding to the (inactive) caesium background concentration: i.e., the apparent sorption of radio-caesium at added concentrations below 5×10^{-9} M is constant. This result is used in the modelling of caesium tracer transport, as discussed briefly in Chapter 7.

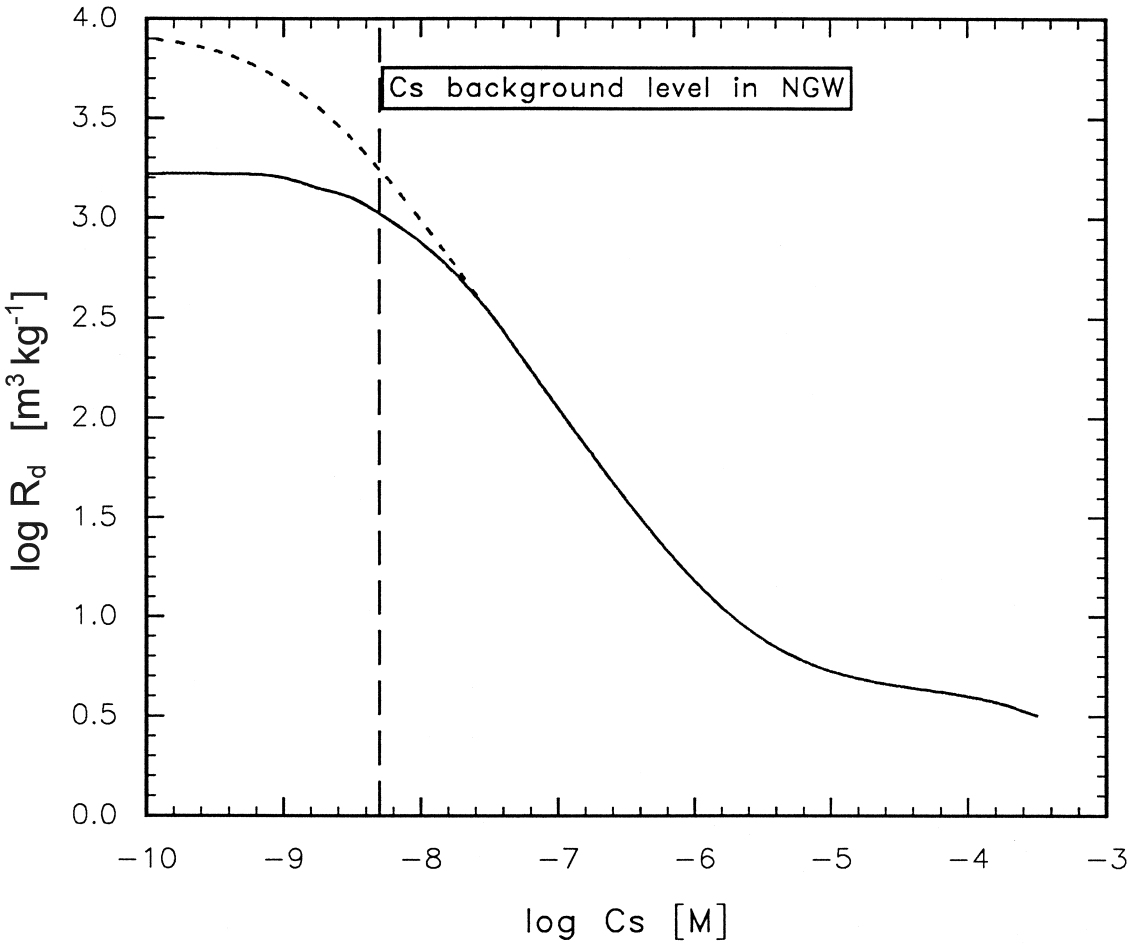

Fig. 5.2: Predicted *in situ* caesium sorption on MI shear zone fault gouge (cf. with Figure 5.1 for the laboratory experiments); as there is some variability in the measured K concentration in the groundwater (NGW) in the experimental shear zone (see Table 4.2), predictions were made for high K content (dashed line) and low K (solid line)

6 DESCRIPTION OF TRANSPORT MODELS FOR THE MIGRATION EXPERIMENT

P.A. Smith, I.G. McKinley and W.R. Alexander

A detailed description of the PSI model of tracer migration in the MI shear zone is given in JAKOB et al. (1989) and HEER & HADERMANN (1996). These reports are the main basis for this summary, complemented by a description of the JNC model in UMEKI et al. (1995), a description of the ETH model in KUNSTMANN et al. (1997) and personal communications from the staff of JNC and ETH. In addition, a brief overview is given on the treatment of sorption in transport codes.

6.1 Introduction

This chapter describes the solute-transport models that have been applied to the migration experiment. Different models developed by different research groups have been applied in order to examine a range of plausible alternative concepts and, by attempting to falsify some of these alternatives, to narrow down the range of conceptual model uncertainty and to identify the processes that are most important in describing solute transport. The transport models and the organisations responsible for their development are:

- the "PSI model" – developed by PSI, Switzerland
- the "JNC model" – developed by JNC, Japan
- the "ETH model" – developed by the Institute of Hydromechanics and Water Resources, Swiss Federal Institute of Technology (ETH), Switzerland.

All of these models are derived from hypotheses concerning:

- the transport processes that convey solutes through water-conducting features in a rock, based on the experience of the modelling teams
- the types of structures present in the MI shear zone, supported by direct observations available at the time from tunnel walls and cores[24]
- the rates and spatial extent[25] over which the processes operate, supported by hydrogeological testing conducted at that time in the field and by independent laboratory experiments such as batch sorption experiments.

The relationship between these hypotheses and the solute-transport models (and the codes that solve their governing equations) is illustrated in Fig. 6.1.

---

[24] The improved data now available (see MÖRI et al. 2001a, b) add significantly extra information on connectivity between fractures and the role of the fault gouge in radionuclide retardation and this would undoubtedly have changed some assumptions inherent in the models.

[25] The spatial extent of the overall dipole flow field is broadly determined by the experimental set-up. Hypotheses regarding spatial extent are, however, required in order to model matrix diffusion (i.e. the extent of connected porosity into which tracers can diffuse). Again, the new data noted in Chapters 4.1 and 4.3 would have had an impact on the assumptions made at the time.

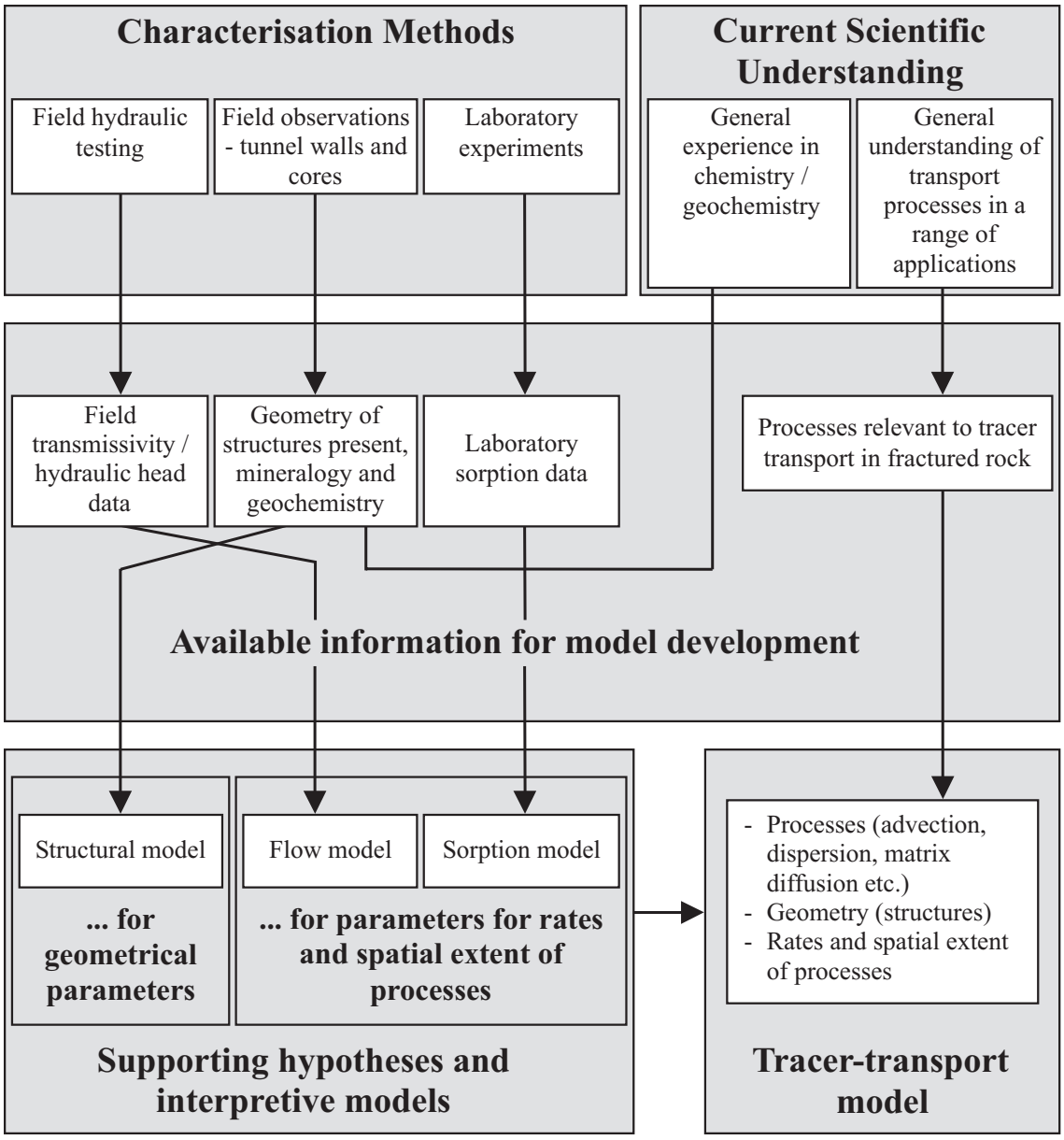

Fig. 6.1: The use of supporting hypotheses and interpretive models to interpret field and laboratory data in terms of input parameters of a transport code

The differences between models reflect, to some degree, uncertainty in the key transport processes that should be incorporated in the codes. More importantly, however, limitations in:

- the extent to which the natural complexity of the migration shear zone has been characterised (at least before the RRP project; see Chapters 1 and 4) and

- the degree to which it is possible to represent the natural complexity of both features and processes in available codes[26]

mean that this complexity must be reduced by averaging and geometrical simplification in order to derive parameter values for the transport codes. There are differences between the models in the degree to which averaging is performed and the choices made in simplifying the geometry of the shear zone.

The transport processes and the models/codes in which they are incorporated are discussed in Section 6.2. The derivation of (simple) parameter values for the transport codes from (complex) field and laboratory data is accomplished via "supporting models". The supporting models are discussed in Section 6.3 and describe:

- the large-scale distribution of flow within the plane of the shear zone – Section 6.3.1
- the small-scale structure of the shear zone – Section 6.3.2
- sorption processes – Section 6.3.3.

6.2 Transport Processes and Codes

6.2.1 Concepts and Processes Common to all Models

In accordance with current understanding of geosphere transport processes, in all of the transport models that have been applied to the migration experiment, the dominant mechanisms for solute transport are assumed to be:

- advection and dispersion within the shear zone and
- retardation due to matrix diffusion and sorption onto the mineral surfaces[27].

In order to describe advection within the shear zone, it is necessary first to describe the metre-scale pattern of water flow. Models to derive this pattern of flow are discussed in Section 6.3.1. The flow model may either be incorporated into the transport code (Section 6.2.2), or be a separate (analytical) solution of the flow pattern.

In order to describe both advection/dispersion within the shear zone and retardation due to matrix diffusion, it is further necessary to describe its internal structure. The observed structure of the shear zone is described in Section 4.1 and illustrated in Figure 6.2.

---

[26] The PSI research group, for example, opted to use an existing computer code (RANCHMDNL) that was not "purpose-built" for the migration experiment, but rather for a range of applications (principally Nagra performance assessments). Features of the model are, therefore, to some extent, dictated by features of the (pre-existing) code. Even a "purpose-built" code would be limited in the complexity that it could incorporate before difficulties associated with computer speed and storage are encountered. This is, however, becoming a less important constraint on model development than was the case during MI.

[27] The ETH model was initially formulated as a single-porosity model, without matrix diffusion, but with transverse, as well as longitudinal dispersion. Attempts to fit this model to experimental results were, however, unsuccessful – the travel-time differences along streamlines were found to be insufficient to explain the observed tailing. Matrix diffusion is implemented in the model described herein.

The shear zone is considered to comprise:

- "flow porosity" (Section 4.1.5.1), identified with channels within the fault gouges and micro-fractures along the gouge/wallrock contacts, where transport of solutes is by advection in flowing water
- diffusion-accessible porosity, connected to the flow porosity and identified with pore spaces within the fault gouge and within the mylonitic "wallrock porosity" (Section 3.5.2), where water is stagnant and transport of solutes is by molecular diffusion.

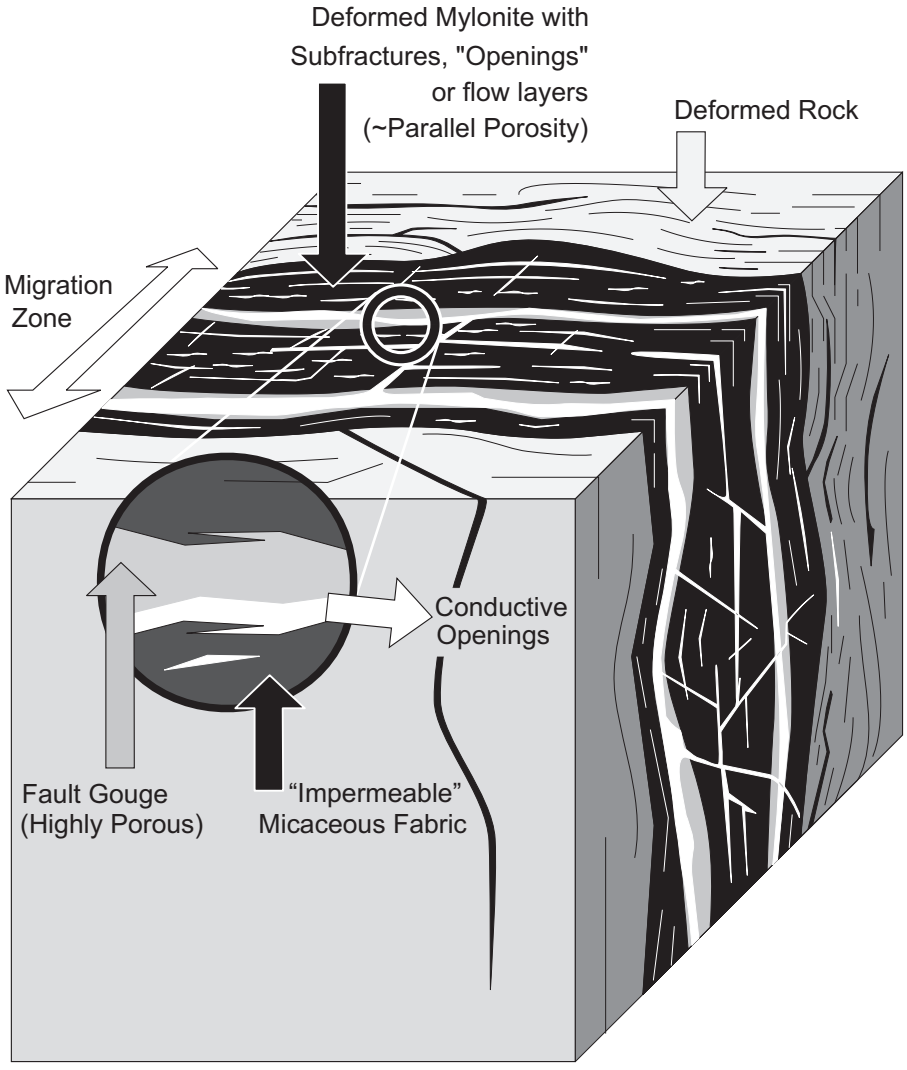

Fig. 6.2: Schematic representation of the internal structure of the MI shear zone

Diffusion into the stagnant pore water of the granodiorite surrounding the shear zone[28] is assumed to be irrelevant from the point of view of transport during the duration of these short experiments.

[28] This assumption is reasonable for the relatively short time scales of the migration experiment. Diffusion into the rock adjoining the shear zone would, however, provide significant retardation of solute transport over the time scales of repository performance assessment (see, e.g. NAGRA 1994 and ALEXANDER et al. 1990a and b).

The distribution of flow porosity and diffusion-accessible, matrix porosity within the shear zone must be simplified in order to apply the available computer codes (Section 6.2.2). The geometrical simplification of this small-scale[29] structure of the shear zone is discussed in Section 6.3.2.

The range of chemical processes that are together termed "sorption" is described by highly simplistic formulations within the transport models, as discussed in Section 6.3.3.

6.2.2 Capability of the Available Codes

All of the codes solve the governing equations for solute advection through a parallel-walled channel or fracture (representative of the channels within the fault gouges and of the micro-fractures along the gouge/wallrock contacts). The model channel may be infilled with a sorbing porous medium (representing all, or a part, of the fault gouges), that retards the advection process. The variability of fracture/channel properties within the shear zone, and inter-connections between fractures/channels, are not modelled explicitly by the transport codes, but rather the resulting mechanical dispersion is modelled as a Fickian diffusion process.

The model channel lies within a porous sorbing medium that forms two regions of uniform thickness, one adjacent to each of the parallel fracture walls, that are accessible to matrix diffusion, and represent all, or part of, the fault gouges, as well as the mylonitic wallrocks.

The features and processes incorporated within the different transport codes are described in Table 6.1. The following key differences are noted:

- The JNC code calculates realisations of the dipole flow field in a heterogeneous transmissivity field within the MI shear zone. The PSI and ETH models rely on separately calculated analytical solutions of the flow field, with a homogeneous (averaged) transmissivity field (see also Section 6.3.1).
- The PSI code calculates advection and dispersion along a one-dimensional pathway. The two-dimensional dipole flow field must thus be discretised into a set of one-dimensional pathways (stream tubes) in order to apply the code. The JNC and ETH codes calculate advection and dispersion in a two-dimensional flow field (see also Section 6.3.1). Longitudinal dispersion is modelled by all three codes. Only the ETH code, however, calculates transverse dispersion.
- All codes are able to model the effects of a fracture infill that is assumed to be instantaneously saturated by migrating solutes. This capability is, however, only applied in modelling the MI experiment in the case of the JNC model (see also Section 6.3.2).
- All three codes are able to calculate rapid, reversible, linear sorption on channel and matrix-pore surfaces. In addition, the PSI and JNC codes are able to simulate non-linear sorption and the JNC code is able to simulate first-order sorption kinetics and partially irreversible sorption (see also Section 6.3.3).

[29] The scale of the shear zone width – i.e. a few centimetres.

Tab. 6.1: Features and processes incorporated in the PSI, JNC and ETH transport codes

Feature / Process	PSI Transport Code (RANCHMDNL)	JNC Transport Code	ETH Transport Code (GTTS)
Pattern of water flow (see Table 6.2 for details)	Separately calculated analytical solution – 1-D, constant-velocity flow along a finite number of pathways, each representing a stream tube within the 2-D dipole flow field	Realisations of the dipole flow field in a 2-D zone of heterogeneous transmissivity, calculated numerically	Separately calculated analytical solution – 2-D flow in a dipole field, with the option of a constant, uniform background flow
Advection (see also Table 6.3)	1-D advection in parallel-walled fractures (with or without infill) that represent the flow porosity along a pathway	2-D advection in parallel-walled fractures (with or without infill) that represent the flow porosity along a pathway	
Dispersion	Longitudinal dispersion modelled as a diffusion-like process, transverse dispersion neglected		Longitudinal and transverse dispersion modelled
Retardation (of advection/dispersion) due to sorption on fracture surfaces/infill material	Rapid, reversible sorption (either linear or non-linear) modelled on fracture surfaces and/or infill material	Sorption (either linear or non-linear), with options for first-order kinetics and for partial sorption irreversibility, modelled on the surfaces of the fracture infill material	Rapid, linear, reversible sorption on fracture surfaces and/or infill material
Matrix diffusion	1-D diffusion modelled in a porous medium (matrix) surrounding the parallel-walled fractures, diffusion limited by the separation of the fractures		
Retardation (of matrix diffusion) due to sorption on matrix pore surfaces	Rapid, reversible sorption (either linear or non-linear) modelled on matrix pore surfaces	Sorption (either linear or non-linear), with options for first-order kinetics and for partial sorption irreversibility, modelled on matrix pore surfaces	Rapid, linear, reversible sorption modelled on matrix pore surfaces

6.3 Supporting Models

6.3.1 Large-Scale Distribution of Flow within the Shear Zone Plane

The distribution of flow within the plane of the shear zone is controlled by:

- the background flow of groundwater within the shear zone,
- the injection and withdrawal rates of the MI dipole,
- the heterogeneity of transmissivity within the shear zone plane.

The background flow in the region where the migration experiments were performed is small with respect to the imposed flow (see FRICK et al. 1992a and Chapter 3) and is neglected. The injection and withdrawal rates are accurately known for each test (Chapter 3) and provide input parameters for the models of water flow.

There are several common hypotheses adopted within the PSI, JNC and ETH models for the calculation of the distribution of flow in the plane of the shear zone:

- The migration zone, defined as that part of the experimental shear zone that is important for MI, can be represented by a confined, planar aquifer. This assumption is supported by geological investigations (see Section 4.1).
- The flow in the aquifer obeys Darcy's law.
- The dipole flow field is stable for the duration of an experiment. This has been tested by repeatedly injecting non-sorbing tracers and measuring break-through curves[30].

The heterogeneity of transmissivity within the migration zone may be complex and was only partially characterised at the time of the modelling exercises (transmissivity had been measured at seven locations, where boreholes intersect the shear zone). The transmissivity field must be simplified in any case in order to model flow. As shown in Table 6.2, differences between the models of flow distribution arise from differences in the way in which this simplification is performed. In the PSI and ETH models, it is assumed that the MI shear zone can be characterised by an average, homogeneous, isotropic transmissivity. This assumption was supported at the time by an evaluation of interference tests and hydrogeological modelling (HERZOG 1989, FRICK et al. 1992b, pp. 4-5). The JNC model is based on a heterogeneous, isotropic transmissivity field, obtained from an interpolation of the seven, measured transmissivity values and, with the hindsight afforded by the data in Section 4.3, now may be seen to be a more appropriate approach.

The assumption of a homogeneous, isotropic transmissivity allows the flow field to be calculated analytically in the PSI and ETH models and then input into the transport codes. The flow field for the heterogeneous transmissivity field of the JNC model is evaluated numerically, in a calculation that is integrated into the transport code.

Since the PSI code calculates advection and dispersion along one-dimensional pathways, the two-dimensional analytical solution of the flow field must be further simplified in order to calculate transport (HERZOG 1991). As illustrated in Figure 6.3, the flow field is divided into two parts:

- an inner region, defined by all flow lines originating at the injection hole (if the extraction pumping rate is larger than the injection rate these flow lines all terminate at the extraction hole)
- an outer region, that contributes to dilution in the withdrawal hole.

The inner flow field is divided into a number of stream tubes (typically ten). For each stream tube, an average[31] water velocity and a migration distance is calculated from the analytical

---

[30] Experimental runs which did not comply to this rule were not modelled.

[31] The "average water velocity" is here defined as the ratio of stream tube length to water transit time, rather than the arithmetic mean of the velocity itself, since the matrix-diffusion effect is related to the water transit time. Taking the arithmetic mean of the velocity would give undue weight to the high velocities near the injection and extraction points.

solution and input into the transport code. The calculated tracer break-through curve is a superposition of the contributions from individual stream tubes.

Tab. 6.2: The modelling of the large-scale distribution of flow within the shear zone plane in the PSI, JNC and ETH models

Feature	PSI Model	JNC Model	ETH Model
Background groundwater flow within the shear zone	Neglected (constant pressure head boundary condition at large distances from the injection and extraction points)		Neglected (but constant background flow with arbitrary direction and magnitude could be included if required)
Heterogeneity of the transmissivity field	Heterogeneity neglected – transmissivity modelled as uniform, absolute value of transmissivity not required	Interpolation of the seven measured transmissivity values accomplished using fractal theory	As in PSI model
Method of solution	Analytical solution for 2-D unequal dipole flow within a uniform transmissivity field	Finite-difference code modelling 2-D flow within a single fractal realisation of the heterogeneous transmissivity field	As in PSI model
Interface to transport code	Analytical 2-D flow field discretised into a finite number of stream tubes, each carrying an equal water flow, 1-D advection/dispersion modelled along each stream tube using code RANCHMDNL	Code for flow modelling incorporated within transport code (see Table 6.1), 2-D flow field provides input for modelling 2-D advection/dispersion	Analytical 2-D flow field is the basis of finite-element transport calculations, 2-D advection and dispersion modelled

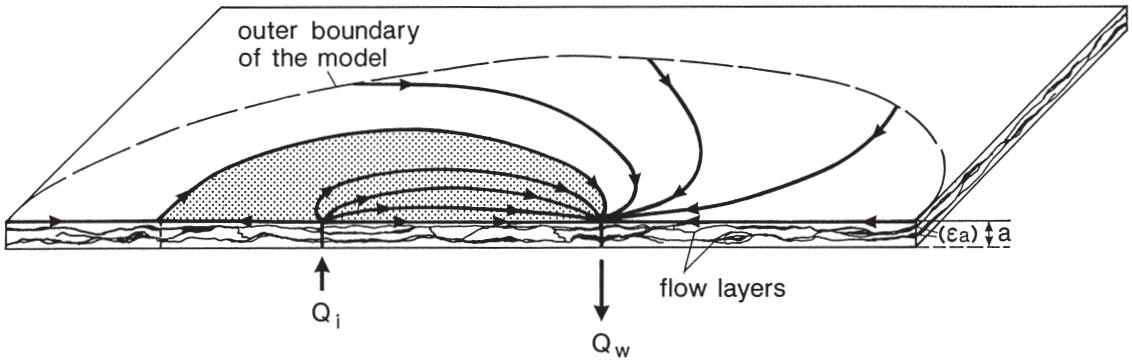

Fig. 6.3: Dipole flow field in the MI shear zone, indicating the inner and outer regions considered in the PSI model (based on Fig. 1 in HEER & HADERMANN 1996 and Fig. 3 in HADERMANN & HEER 1996)

For all of the models, in order to obtain a water velocity from the Darcy flux calculated by the groundwater flow models, a model is required for the distribution of flow porosity. In each case, the migration zone is assumed to be characterised by an average, homogeneous flow porosity. This assumption was supported by the then observed simplicity of the structure of the MI shear zone on a scale of metre (see Section 4.1.5.1). The division of the porosity, based on the observations available at the time, between flow porosity and diffusion-accessible porosity is discussed in the following section.

6.3.2 Small-Scale Structure of the Shear Zone

The observed structure of the MI shear zone, described in Section 4.1.5 and illustrated in Figure 6.2, must be simplified in order to define parameters that can be input into the transport codes.

In all three models, the "flow porosity" (i.e. channels within the fault gouges and micro-fractures along the gouge/wallrock contacts) is modelled as a number of equally-spaced, parallel-walled fractures. In the JNC model, only a single fracture is considered, but the fracture contains infill material. The PSI and ETH models consider several parallel fractures without infill (Figure 6.4). The flow porosity, that connects the Darcy velocity to the advection velocity required as input by the transport codes, is a function of the fracture aperture, the number of parallel fractures and the porosity of the infill (if any).

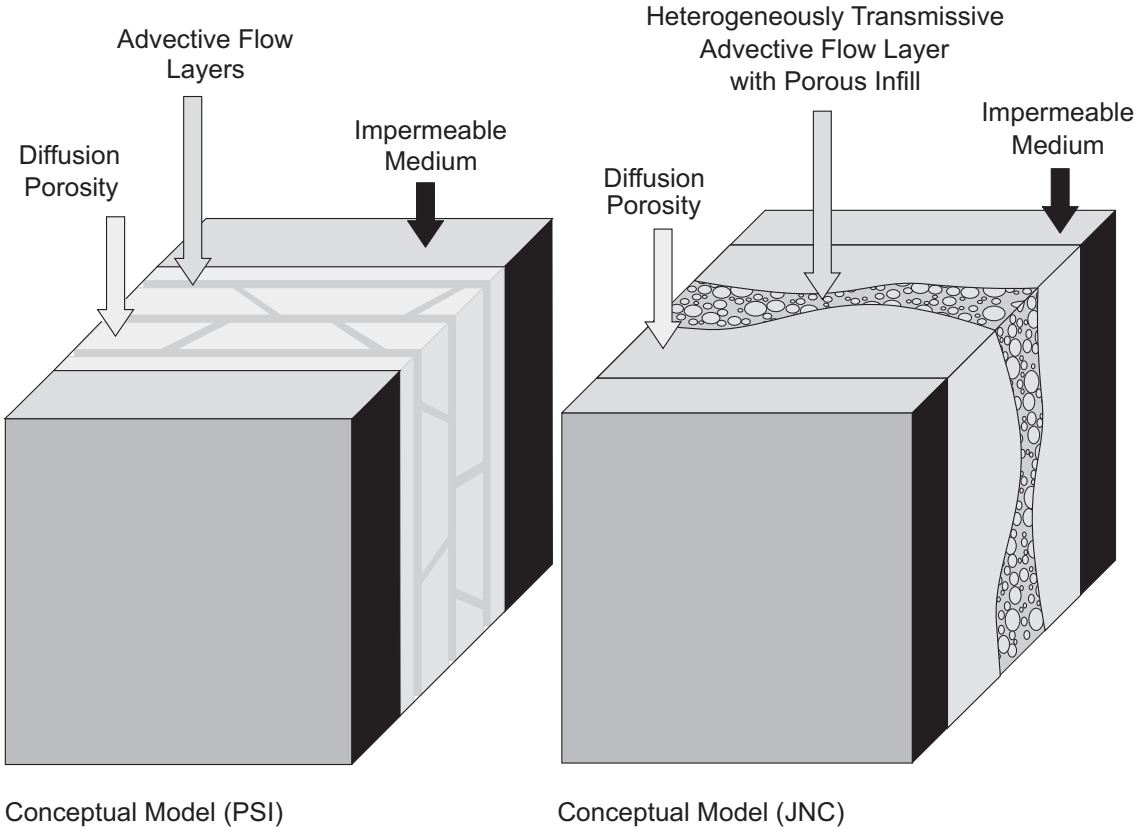

Fig. 6.4: PSI and JNC models of the small-scale structure of the MI shear zone; the ETH model is identical to the PSI model in this respect

The model assumptions regarding the diffusion-accessible porosity (i.e. pore spaces within the fault gouge and within the mylonitic "wallrock porosity") differ between the models. In the PSI and ETH models, this porosity is homogeneously distributed within the material adjacent to the model fractures. Diffusion is modelled explicitly within this material and the extent of diffusion-accessible rock is limited by the fracture spacing. In the JNC model, this porosity is divided between the model-fracture infill and the material adjacent to the model fracture. The conceptual basis of the JNC model is that "islands" of fault gouge/mylonite between the channels and micro-fractures that convey flowing water are divided into (i), smaller islands that are treated as infill grains and (ii), larger islands that are treated together as two homogeneous regions of porous matrix on either side of the model fracture. The infill grains (i.e. the smaller islands of fault gouge/mylonite) are considered to be sufficiently small that the part of the diffusion-accessible porosity they contain is effectively instantaneously saturated by migrating solutes. Diffusion is only modelled explicitly in the porous matrix on either side of the model fracture (i.e. the larger islands of fault gouge/mylonite).

6.3.3 Sorption Processes: A Brief Overview

6.3.3.1 Background

In its simplest form, sorption is used to describe the removal of an element or radionuclide from a liquid phase at the surface of a solid phase – the substrate. This basic description of an interaction between solid and liquid phase species encompasses several sorption mechanisms (NEA 1983). Sorption processes include a number of removal mechanisms as depicted in Figure 6.5.

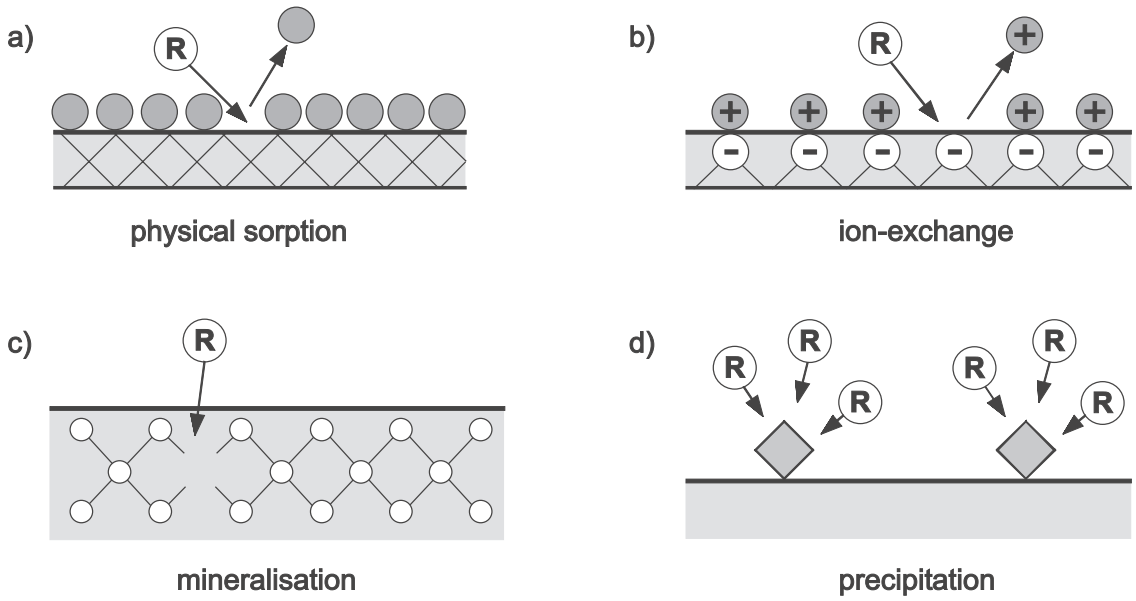

Fig. 6.5: Schematic representation of the main retardation processes of relevance to radionuclide transport in groundwater: physical sorption, ion exchange, mineralisation and precipitation (based on Fig. 5 from McKINLEY & HADERMANN 1985)

R = Radionuclide

The specific processes resulting in the loss of solute from the liquid (aqueous) phase are rarely identified individually or distinguished experimentally, particularly when these processes can occur simultaneously and many systems exhibit hybrid behaviour (SERNE 1992). Frequently, sorption may be distinguished only as a physical or chemical process, depending on the nature and strength of the attractive forces involved. The principal removal mechanisms, however, as they relate to radionuclides in groundwater, are recognised as listed below.

Physical adsorption involves non-specific, long-range attractive forces between solute species and substrate, the best examples of which are hydrogen-bonding and van der Waal's forces (dipole-dipole interactions). In such cases, physical adsorption is rapid and totally reversible. The sorption of trivalent and tetravalent actinide complexes on metal oxide substrates at neutral pH has been considered to occur mainly by physical adsorption (SERNE 1992).

Electrostatic adsorption is a general term describing short-range coulombic attraction between charged solute species and substrate. Ion exchange is a specific example of an electrostatic adsorption process, which is fast and generally reversible (see Appendix 2 for further details).

Specific sorption may be slow or rapid and corresponds to adsorption involving a particular radionuclide, irrespective of the net charge on the mineral (substrate). As an example, sorption of caesium by illite may be considered in this category (BROUWER et al. 1983).

The previous mechanisms are considered true sorption or surface-related processes and SERNE (1992) discusses the sensitivity of each of the above processes to environmental physico-chemical parameters. On the other hand, the processes discussed below constitute removal mechanisms but must not be confused with sorption as defined above.

Chemical substitution or mineralisation involves the diffusion and incorporation of an element or species into the solid matrix. This process is relatively slow and possibly irreversible but may include physical adsorption or ion exchange as an initial surface interaction process.

Precipitation is the formation and accumulation of a solid phase in a regular three-dimensional arrangement, and is a function of the solubility of the solid phase. Precipitation should not be regarded as sorption, since the formation of a precipitate is primarily a function of the aqueous phase (SPOSITO 1986) but may be facilitated by the presence of particular mineral surfaces ("surface precipitation").

Co-precipitation is also acknowledged as an important additional mechanism by which a radionuclide may be removed from solution, even when solubility constraints do not apply to the radionuclide being co-precipitated. Co-precipitation of radionuclides with calcite from groundwaters which are over-saturated with respect to this mineral can be a major removal mechanism (PINGITORE 1986 and BRUNO & SANDINO 1988).

6.3.3.2 The K_d Concept

As commented upon many times (e.g. McKINLEY & HADERMANN 1985 and McKINLEY & ALEXANDER 1992), use of K_d throughout the sorption literature is widespread but often causes confusion due to the different ways in which this parameter is perceived and interpreted. The following discussion indicates the thermodynamic basis for an idealised concept.

Application of the thermodynamic K_d concept is based on the distribution law originally formulated by Nernst (ANDERSON & CRERAR 1993) which may be expressed via the following equation:

$$\ln \frac{a_s}{a_L} = -(\mu_s - \mu_L)/RT \qquad (6.1)$$

where a_s = activity of the species on the solid phase
a_L = activity of the species in the liquid phase
μ_S = standard free energy of the species on the solid surface (J mol^{-1})
μ_L = standard free energy of the species in solution (J mol^{-1})
R = universal gas constant (= 8.314 J K^{-1} mol^{-1})
T = temperature (K)

K_d, the distribution coefficient, is then defined as follows:

$$Kd = \frac{a_S}{a_L} \qquad (6.2)$$

The above equations indicate the thermodynamic basis for K_d applicable to an ideal system at equilibrium, i.e. the sorption reaction is completely reversible. As stated above, K_d is independent of solute concentration, and is specified for a particular temperature, although the parameter should vary with temperature in a recognised manner, (K_d proportional to $e^{(-1/T)}$). Furthermore, the distribution law strictly applies only to one species distributed between two phases, one of which is, in this case, an ideal solution.

In practice (i.e. experimentally), equilibrium is assumed to have been reached for the sorption process and concentrations are used instead of activities (Figure 6.6), yielding the following general equation:

$$Kd = \frac{[X]_S}{[X]_L} \qquad (6.3)$$

The square brackets in the above equation denote molar concentration, and subscripts S and L refer to the solid and liquid phases respectively. The relationship between activity and concentration ($a = [X]\,\gamma$) incorporates a factor γ, the activity coefficient, which is a measure of the approach to ideality of each component in the system. Thus, use of concentrations rather than activities in the expression for K_d (equation 6.3) means that activity coefficient corrections (deviations from ideality) are ignored.

The Nernst relationship demonstrates a thermodynamic basis for K_d, but its application relies on ideal behaviour of radionuclides in solution. Interactions between minerals and groundwater which are not equilibrated can alter the chemistry of the overall system, which in turn affects the equilibrium distribution of a nuclide between the two phases. In addition, equation (6.1) strictly applies to the distribution of only one species between liquid and solid phases, whereas a nuclide often exists in solution as more than one species, the proportions of each being established via independent equilibria.

An alternative approach, therefore, involves treating K_d as an empirical parameter. The underlying assumptions which are inherent in defining a thermodynamic K_d, i.e. sorption being at equilibrium, reversible, and independent of concentration of the sorbing species, are generally not established or confirmed during experimental determinations. SPOSITO (1986) states that "for a K_d value to be meaningful, various geochemical parameters (e.g. pH, complexing agents, competing ions) must be specified. Thus, K_d can hardly be considered to be a thermodynamic constant. Rather, it is a comprehensive parameter, describing a particular set of experimental conditions."

In order to recommend K_ds representative of reference conditions – in terms of both mineralogy and groundwater – the sorption data which provide the basis for K_d value selection need then to be measured under experimental conditions which are as close as possible to these reference conditions. To avoid confusion, K_d is thus often replaced by a less rigorous parameter, the distribution ratio R_d.

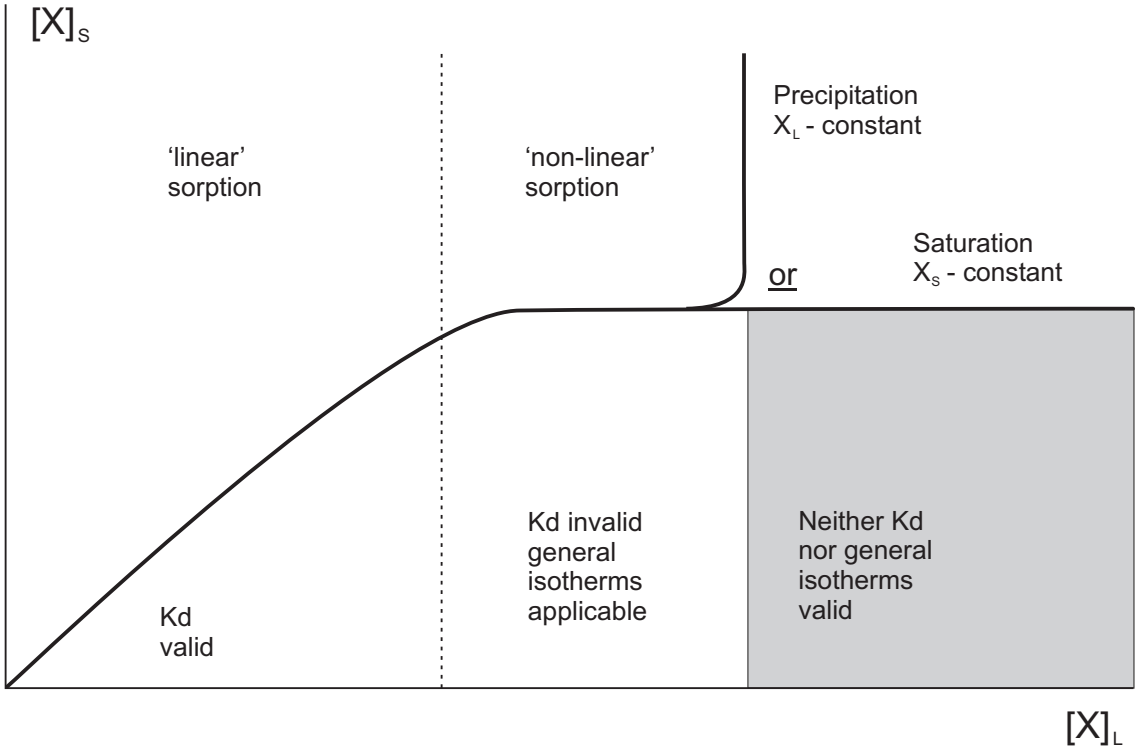

Fig. 6.6: Illustration of the relationships between radionuclide concentrations in aqueous X_L and solid X_S phases, including a comparison between the region where K_d values and isotherms are applicable (after McKINLEY & ALEXANDER 1992)

Such a purely empirical approach has been expanded to define R_d as a complex polynomial function of dependent geochemical parameters (e.g. VANDERGRAAF et al. 1992). All such approaches can, however, be used only to interpolate between experimental data points and cannot strictly be used to extrapolate sorption behaviour to other conditions.

6.3.3.3 Representation of Sorption in Transport Models

The complexity of solute transport in a geological formation has been discussed at some length in many reports (e.g. McKINLEY & HADERMANN 1985, FRICK et al. 1992a, McKINLEY & ALEXANDER 1992 and HEER & HADERMANN 1996). A flow system may be described mathematically in terms of a transport model which is generally applied to a small volume element – the representative elementary volume (REV). This REV is selected to be as small as possible, while being considered as representative of the overall rock-water system. In the

absence of sorption, the migration of a nuclide through a porous medium is represented by the following one-dimensional equation describing material transport into and out of the REV:

$$\frac{\partial [X]_L}{\partial t} = H \frac{\partial^2 [X]_L}{\partial x^2} + D \frac{\partial^2 [X]_L}{\partial x^2} - V_w \frac{\partial [X]_L}{\partial x} \qquad (6.4)$$

where $[X]_L$ = concentration of nuclide in solution (mol m^{-3})
H = hydrodynamic dispersive coefficient ($m^2 s^{-1}$)
D= diffusivity ($m^2 s^{-1}$)
x = length of flowpath (m)
V_w = velocity of transporting solution ($m s^{-1}$)
t = time (s)

The above equation contains, respectively, a dispersive term, a diffusive term, and an advective term. For simplicity, loss of material by radioactive decay is not included in the above equation, but this can be easily added. When sorption is incorporated in the mathematical modelling, the above equation becomes:

$$\frac{\partial}{\partial t}\left(\varepsilon [X]_L + \rho_b [X]_S\right) = H\varepsilon \frac{\partial^2 [X]_L}{\partial x^2} + D\varepsilon \frac{\partial^2 [X]_L}{\partial x^2} - \varepsilon V_w \frac{\partial [X]_L}{\partial x} \qquad (6.5)$$

where $[X]_S$ = concentration of nuclide in the solid phase (mol kg^{-1})
ρ_b = bulk density ($kg m^{-3}$)
ε = effective porosity

The model requires that initial and boundary conditions for the concentration of a radionuclide in the aqueous phase be defined. Subsequent solution of equation (6.5), however, relies on a simple relationship between the concentration of the nuclide in the aqueous phase and its concentration in the solid phase.

The simplest relationship is clearly a K_d (equation 6.3) and, in most transport codes, this is how sorption is represented. In principle, it is possible with modern numerical methods to incorporate more complex representations of sorption (e.g. as polynomial functions; VANDERGRAAF et al. 1992) or even via fully mechanistic models which are incorporated into coupled transport/ chemical reaction models (e.g. READ et al. 1987, READ 1992 and LIU & NERETNIEKS 1997).

The main fundamental constraint on the degree of complexity of the representation of sorption in transport models is usually set by the limited availability of data on sorption of radionuclides of interest in the rock/water system involved. A more practical constraint may be set by computational requirements, which require a balance between the degree of detail of the flow system representation and that of the sorption processes. Complex three-dimensional simulations of solute transport through dual porosity media (e.g. advective flow in a fractured rock with diffusion into connected matrix porosity) are almost exclusively restricted to simple K_d sorption models. On the other hand, fully coupled chemical/transport models greatly simplify flow (usually to a one-dimensional equivalent porous medium).

Computational constraints are also set by the timescales simulated by numerical models: rather detailed models can be used to simulate short-term laboratory or field migration experiments, but these need to be simplified considerably in order to simulate migration over kilometre distances and hundred thousand year timescales as may be needed for repository performance

assessment. More extensive discussion of solute transport models and their limitations can be found in the excellent reviews by YEH & TRIPATHI (1989) and MANGOLD & TSONG (1991).

In the PSI, JNC and ETH models, sorption on the surfaces of both the flow porosity and the diffusion-accessible porosity is calculated under the assumption that it is both, instantaneous and reversible. The JNC model also allows the option of including first-order sorption kinetics and an irreversible sorption component. In the ETH model, linear sorption is assumed; i.e. sorption is represented by a concentration-independent distribution coefficient (the sorption constant, K_d), equal to the equilibrium radionuclide concentration in the sorbed phase, divided by the concentration in the aqueous phase. The PSI and JNC models also allow non-linear sorption to be represented via a Freundlich isotherm[32], in place of K_d.

[32] ***Freundlich isotherm***: The Freundlich equation is: $[X]_S = K[X]_L^n$ with K and n normally assumed to be empirical constants. The linear form of the above equation is: $\log [X]_S = \log K + n \log [X]_L$ which allows experimental data to be fitted to obtain K and n. It should be stressed that the flexibility of log-log transforms allows relatively easy curve fitting but does not guarantee accuracy beyond the range of the experimental data.

7 APPLICATION OF TRANSPORT MODELS TO THE MIGRATION EXPERIMENT

W. Heer and P.A. Smith

The application of the PSI transport model is described in HEER & HADERMANN (1996), HADERMANN & HEER (1996) and HEER et al. (1994). The material in these reports is summarised in this chapter, and is complemented by the results of JNC and ETH modelling exercises, given in UMEKI et al. (1995), KUNSTMANN et al. (1997) and in personal communications from the staff of JNC and ETH, and by a new, generic description of the features of tracer break-through curves.

7.1 Introduction

This chapter presents a summary of the application to the migration experiment of the PSI, JNC and ETH solute-transport models, described in Chapter 6. The chapter focusses primarily on the PSI model, which has been developed and refined over a period of several years and has been applied to experiments using a wide range of sorbing and non-sorbing tracers in different flow fields. Development and application of the PSI model has followed the procedure outlined in Section 2.2.2, involving both *inverse* modelling, in order to "calibrate" the model and provide a limited form of model testing (as defined in Section 2.1), and *predictive* (or 'blind') modelling, which is considered to provide a more exacting test of the model and contributes strongly to the validation (confidence-building) process.

The application of the JNC and ETH models is discussed in less detail. Nevertheless, the examination of different model concepts is valuable in determining the significance of various sources of conceptual-model uncertainty, both on the scale of MI itself and (although beyond the scope of the present report) on the much larger scales of space and time that are of relevance to performance assessment.

As described in Chapter 6, differences between the models concern the (simplified) *model representation* of processes and structures, rather than the *identification* of these processes and structures, where there is a consensus between the models. In particular, all the models assume that the form of a tracer break-through curve is determined by:

- advection and dispersion within the shear zone and
- retardation due to matrix diffusion and sorption onto the mineral surfaces.

Section 7.2 outlines the general forms that tracer break-through curves can take and the way in which these forms are determined by the four characteristic time-scales that describe the processes. This section is generic, applying equally well to all three models. The differences between the models affect mainly the individual physical parameters that generate the characteristic time-scales and their relationship to empirical data and observations, such as the geometric form of structures within the shear zone.

Section 7.3 describes the application of the PSI transport model, with inverse modelling of experiments in a larger, 4.9 m dipole flow field and predictive modelling of experiments in a smaller, 1.7 m dipole flow field.

Section 7.4 describes the application of the JNC and ETH transport models to experiments in the 4.9 m dipole flow field.

Section 7.5 presents conclusions that are drawn from these various modelling exercises.

The notation used in this chapter is defined in Appendix 3.

7.2 The Form of Tracer Break-Through Curves

The typical form of a break-through curve for a sorbing tracer is shown in Figure 7.1. A typical break-through curve has the following general features as time increases:

- a delay between initial injection (time zero) and initial break-through
- a period of increasing tracer concentration, followed by a maximum (peak break-through)
- a period of decreasing tracer concentration that tends towards an asymptotic "tail", with a concentration that varies in proportion to $t^{-3/2}$
- a "tail-end perturbation" where concentration first rises above the asymptote, then eventually drops below it.

These features are assumed to reflect the underlying processes of advection and dispersion within the shear zone and retardation due to spatially-limited matrix diffusion and sorption onto the mineral surfaces. The physical parameters that describe these processes (which may differ between the various models applied to MI) can be combined to give four "characteristic times" that together determine the form of a break-through curve. The characteristic times are:

- t_A and t_D: an *advection time* and *dispersion time*, that also account for the effects of sorption on the surfaces of the "flow porosity" (see Sections 6.2.1 and 3.5.1)
- t_{MD} and t_{MP}: a *matrix-diffusion time* and *matrix-propagation time*, that also account for the effects of sorption on the surfaces of diffusion-accessible porosity (see Sections 6.2.1 and 3.5.2).

Analytical expressions for the characteristic times are given in Appendix 4 (Equations A4.1 to A4.4) and values are calculated for the specific case plotted in Figure 7.1. Although a description of a break-through curve based only on these characteristic times is necessarily approximate, it nevertheless provides some insight into the underlying processes and, in particular, into the possibility of differentiating between processes from the form of a break-through curve. The effects of each process (and corresponding characteristic times) on the form of tracer break-through curves are discussed in the following Sections (and the limitations of this approach are noted here and in Chapter 8).

7.2.1 The Effects of Advection on Break-Through

The advection time, t_A, is equivalent to the shortest transit time for a tracer through the "flow porosity" in the (hypothetical) absence of matrix diffusion. It can be regarded as a coupling parameter between the hydrological and tracer-transport models (Chapter 6), since it influences the predicted tracer break-through via the flow field. The advection time is proportional to the flow porosity, ε_f, (as defined in Table A3.2) and to the retardation factor, R_f, for sorption on flow-wetted surfaces (Table A3.3). Increasing either of these parameters increases the transport time along a stream line. For a narrow dipole flow field, where transport is concentrated around the shortest stream line linking the injection and extraction points of the dipole, and in the absence of matrix diffusion, the effect of increasing these parameters is to delay the break-through curve.

The dashed line in Figure 7.1 represents a break-through curve, calculated with the process of matrix diffusion (and also sorption) "switched off". In this particular example, the dipole flow

field is narrow (i.e. β, the ratio of extraction rate to injection rate, is high) and the peak of the break-through curve is closely approximated by the advection time[33]. The effect on break-through of increasing the width of the flow field is discussed in HEER & HADERMANN (1996, p. 31 and p. 131). Briefly, the width of the break-through curve is increased and a tail is generated.

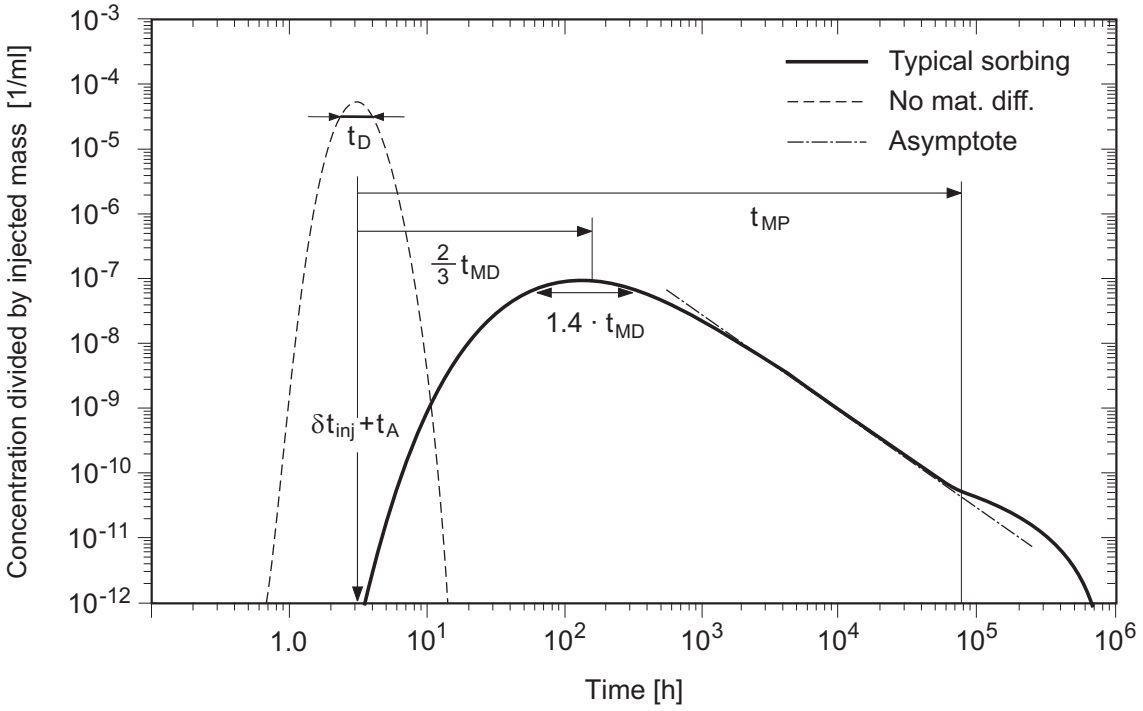

Fig. 7.1: The typical form of a break-through curve for a sorbing tracer (calculated using the PSI model for the case of Sr in the 4.9 m dipole flow field, with $\beta = 16$), with corresponding characteristic times, as defined in Appendix 4; the calculated break-through curve with matrix diffusion and sorption "switched off" is also shown by the dashed curve

7.2.2 The Effects of Dispersion on Break-Through

In the (hypothetical) absence of matrix diffusion, longitudinal dispersion is the predominant process determining the peak duration and height of a break-through curve (e.g. the dashed break-through curve in Figure 7.1), by smearing the injected tracer pulse over a characteristic spatial width (2σ). This width is dependent on the advection distance, but not on advection time, and therefore not on the retardation due to sorption on flow-wetted surfaces[34]. The smeared tracer pulse is advected to the extraction point with an average velocity $\approx L_0/t_A$[35]. The dispersion time, t_D, which characterises the duration of break-through in this hypothetical case (and also provides an indicator of the break-through height), is therefore defined as $2\sigma/(L_0/t_A)$.

---

33 A correction, δt_{inj}, to account for the delay in the injection tubing is also required (see Chapter 3 for details).

34 Heterogeneity in sorption may, however, contribute to dispersion, as discussed in GELHAR (1987). None of the models applied to MI considered such an effect.

35 To simplify the explanation, the main effects of dispersion are explained under the assumption of a constant average velocity.

The dispersion time is proportional to the advection time, and is therefore also proportional to the flow porosity, ε_f, and to the retardation factor, R_f, for sorption on flow-wetted surfaces. Decreasing either of these parameters would lead to a break-through of shorter duration (due to higher advection velocities) and greater maximum concentration, for unchanged pumping rates. The reason for the increased break-through concentrations is, in the case of a decreased flow porosity, the smaller total water-conducting cross section and, in the case of a decreased retardation factor, the larger fraction of the tracer in the water, while the spatial width of the smeared tracer pulse in the direction of flow remains unchanged.

7.2.3 The Effects of Matrix Diffusion on Break-Through

The combined effects of matrix diffusion and sorption on break-through are clearly shown by the differences between the dashed and solid curves in Figure 7.1, i.e. a delay, reduction and widening of the peak and the development of a pronounced tail. The influence of the characteristic times t_{MD} and t_{MP} is illustrated further by the parameter variations plotted in Figure 7.2.

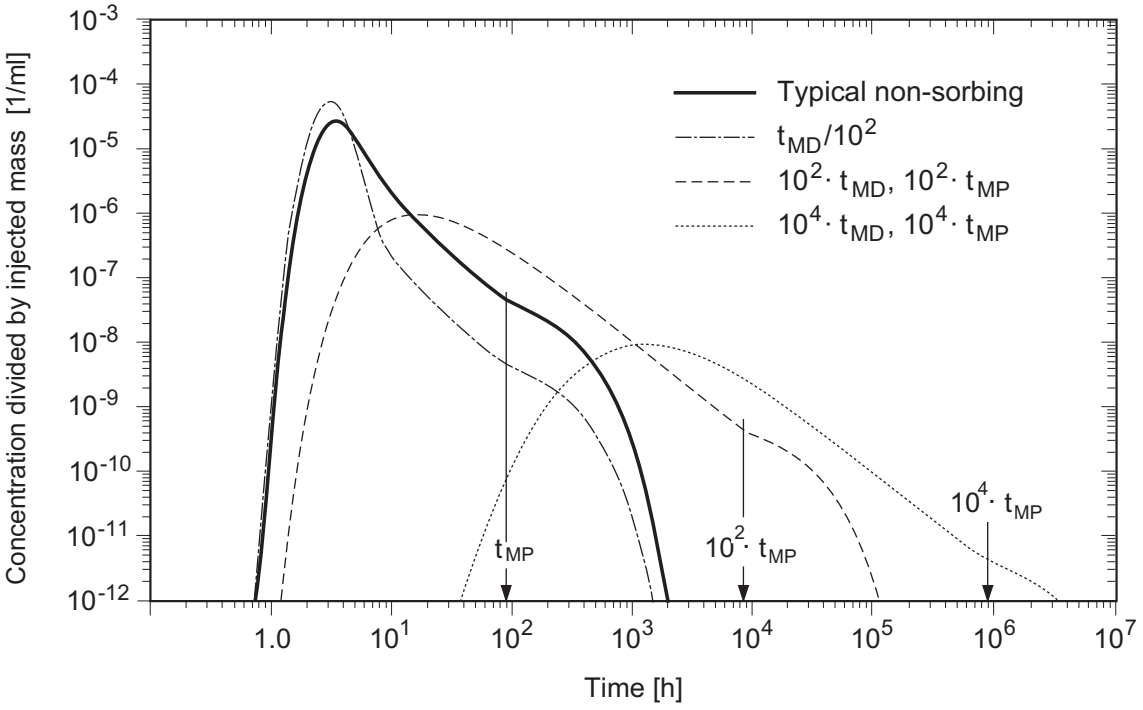

Fig. 7.2: Parameter variations, illustrating the effect of the characteristic times t_{MD} and t_{MP} on the shape of a break-through curve

The effect of matrix diffusion can, to a large extent, be described by the matrix-diffusion time, t_{MD}, which characterises both the delay of break-through peak with respect to the advection time t_A and, if the effect of matrix diffusion dominates over dispersion ($t_D << t_{MD}$), the duration of the break-through peak (with a corresponding reduction in break-through concentrations).

The delay and widening of the peak is essentially due to the loss of tracer from the migrating pulse to the diffusion-accessible porosity, driven by a concentration gradient (that is enhanced,

in the case of sorbing tracers, by sorption on pore surfaces). Once the pulse has passed, the concentration gradient is reversed and tracer diffuses back from the porous rock zone to the "flow porosity". After a sufficiently long time, this back-diffusion decreases according to $t^{-3/2}$, giving rise to the asymptotic behaviour depicted in Figure 7.1. The $t^{-3/2}$ asymptote provides an important "finger print" of matrix diffusion.

The $t^{-3/2}$ asymptote represents a (hypothetical) case in which there is no limit to the depth of diffusion-accessible porosity. In reality, this depth is limited[36] giving rise to the "tail-end perturbation", where concentration first rises above the asymptote (due to the restriction on outward diffusion), then eventually drops below it (due to the reduced total mass in the matrix). The time of occurrence of the "tail-end perturbation" is closely related to the matrix-propagation time, t_{MP}.

7.2.4 Determination of Physical Parameters from the Break-Through Curves

Each of the four characteristic times is defined in terms of certain physical parameters that describe the underlying processes (Equations A4.1 to A4.4). The determination of parameter values is discussed in Section 2.2.2. In principle, if all the physical parameters could be derived from independent experiments and observations, then the four characteristic times could be derived in advance of the tracer tests and the break-through curves predicted. This procedure would constitute "level-2", *predictive* confidence building in the transport models, as defined in Section 2.2.1.

In practice, not all of the physical parameters can be determined in this way and it is necessary to resort to inverse modelling to "calibrate" the models, providing parameter values for subsequent application in predictive modelling. The ability of the model to fit a break-through curve, with fitted parameters that are consistent with (if not predicted by) independent experiments and observations constitutes weaker, "level-1" confidence building.

The above discussion suggests that, in principle, it is possible (by inverse modelling), to determine the four characteristic times that determine the form of a tracer break-through curve, and thus obtain information regarding the underlying processes and the parameters that describe them. In practice, however, the amount of information that can be obtained in this way is sometimes limited. The following difficulties arise:

- *Resolution of the apparatus and duration of experimental runs*

  For example, only if a break-through curve for a non-sorbing tracer is measured down to the "tail-end perturbation" ($t > t_{MP}$) can the diffusion-accessible porosity ε_p and the corresponding pore diffusion constant D_p be determined separately ($t_{MD} \propto \varepsilon_p^2 D_p$ and $t_{MP} \propto 1/D_p$, cf. Eqs. A4.3a and A4.4a). Similarly, for sorbing tracers, resolution of the "tail-end perturbation" is necessary in order to discriminate between the retardation factor for matrix diffusion and the pore diffusion constant ($t_{MD} \propto \varepsilon_p^2 R_p D_p$ and $t_{MP} \propto R_p/D_p$). Care has been taken in MI to measure the break-through curve accurately up to times that are about three orders of magnitude greater than the time of peak break-through and down to concentrations that are about three orders of magnitude lower than the maximum. For the more strongly

[36] Although not available at the time of the modelling exercises, new data from the RRP project (MÖRI et al. 2001a and b) indicate that 1) there is limited diffusion in the mylonite, 2) transport of radionuclides into the fault gouge is rapid and may be considered more as flow in a permeable media than diffusion *per se*, 3) the porosity values available at the time of the modelling exercise were probably over-estimates for the mylonite and the rock matrix and under-estimates for the fault gouge.

sorbing tracers, however, the tail-end perturbation occurs so late that it is impossible to determine it experimentally.

- *Experimental conditions may be such that one process masks another*

  In general, the asymptotic tailing provides a means of discriminating between sorption on the surface of the diffusion-accessible porosity and sorption on the surface of the "flow porosity". If, however, the matrix-propagation time is small compared to the duration of a migrating tracer pulse, the whole thickness of the diffusion-accessible porosity reaches essentially the same concentration as the pulse. The time dependence of the diffusion process can no longer be observed in the asymptotic form of the break-through curve and matrix diffusion acts identically to additional (≈ instantaneous) sorption on the surface of the "flow porosity".

- *There exist more unknown physical parameters than free fit parameters*

  Considering equations A4.1 to A4.4, since the number of physical parameters exceeds the number of characteristic times, some of the physical parameters must be fixed using additional information (e.g. geological considerations and laboratory experiments), in order that the remaining physical parameters may be calibrated using the characteristic times.

7.3 Application of the PSI Transport Model

7.3.1 Methodology

The methodology adopted in applying the PSI transport model is:

STEP 1: For an initial experimental flow field:

- to fit, by inverse modelling, the experimental break-through curves for non-sorbing and sorbing tracers and derive a set of fit parameters (essentially the four characteristic times), as described in Section 7.3.2
- to derive, from the fit parameters, individual physical parameters and compare these with the results of independent experiments and observations, as described in Section 7.3.3.

  This tests whether the model concept is consistent with the available information ("level-1" confidence building) and provides an opportunity to adapt the concept if necessary (it was, in fact, unnecessary to adapt the PSI concept).

STEP 2: For a different experimental flow field in the same shear zone, where the different processes are weighted differently:

- to predict, using the calibrated model, the experimental break-through curves for the new flow field, as described in Section 7.3.4.

  This provides a sensitive test, not only for the model concept ("level-2" confidence building), but also for the numerical procedures.

7.3.2 Inverse Modelling

The transport behaviour of uranine, which is assumed to be non-sorbing[37], weakly sorbing sodium, moderately sorbing strontium and more strongly sorbing caesium has been investigated in a 4.9 m dipole flow field. The experimental conditions are summarised in Table 7.1.

Tab. 7.1: Conditions of experiments used for inverse modelling

Parameter	Test 50	Test 90
Dipole distance L_0 [m]	4.90	4.90
Tracers	Uranine Sodium Strontium	Caesium
Extraction rate Q_e [ml/min]	148.5	150
Extraction to injection rate ratio β	15.97	15.00
Characterisation of flow field $f(\beta)$	7.881×10^{-1}	7.804×10^{-1}

The experimental conditions, the resolution of the apparatus and the duration of experimental runs were such that, for uranine and sodium, four free fit parameters, related to the four characteristic times discussed in Section 7.2, could be determined from the break-through curves by inverse modelling (for strontium and caesium, the "tail-end perturbation" was not measured and only three fit parameters could be determined). The fit parameters actually selected can be interpreted as the variable part of t_A, $(t_D/t_A)^2$, t_{MD}, and t_{MP}[38]. These fit parameters have the advantage over many other possible combinations of physical parameters in that each affects a specific aspect of the break-through curves (e.g. t_{MP} essentially defines the position of the tail-end perturbation; see Figure 7.1) and therefore an adjustment to one of the fit parameters has an easily understood consequence in terms of the break-through curve shape.

Uranine

The fit of the PSI model to the experimental break-through curve for uranine is presented in Figure 7.3. Unlike the example in Figure 7.1, the position of the break-through peak calculated using the full model is fairly close to that calculated without matrix diffusion, showing that its position and shape are, to a large extent, governed by advection and dispersion. The lack of sorption in the case of uranine reduces the impact of matrix diffusion, although matrix diffusion nevertheless reduces the peak height by a factor of 2.5. The observation that the first part of the

---

[37] In reality, all tracers are affected by some form of interaction with the geosphere. In MI, a range of 'non-sorbing' tracers was employed and a range of behaviour was observed. Uranine, for example, is a relatively large molecule and will therefore be excluded from small pore spaces or may be retarded by filtration processes in the shear zone. Br^- and I^-, due to their charge, may also be similarly affected. $^{4,3}He$ displays a somewhat longer 'matrix diffusion tail' than the other non-sorbing tracers, presumably because the uncharged, small He is not affected by size or charge exclusion and has a higher molecular diffusion rate, leading to greater access of the diffusion accessible porosity. Referring to Figures 3.8 and 3.9, however, the effect on the break-through curves is generally small.

[38] The four fit parameters can be expressed as: $a\varepsilon_f R_f$, a_L, $n^2\varepsilon_p^2 D_p R_p$, and $d^2 Rp/D_p$.

tail closely follows the $t^{-3/2}$ asymptote is an experimental indication of the occurrence of matrix diffusion. The presence of a "tail-end perturbation" indicates that the depth of diffusion-accessible porosity is limited.

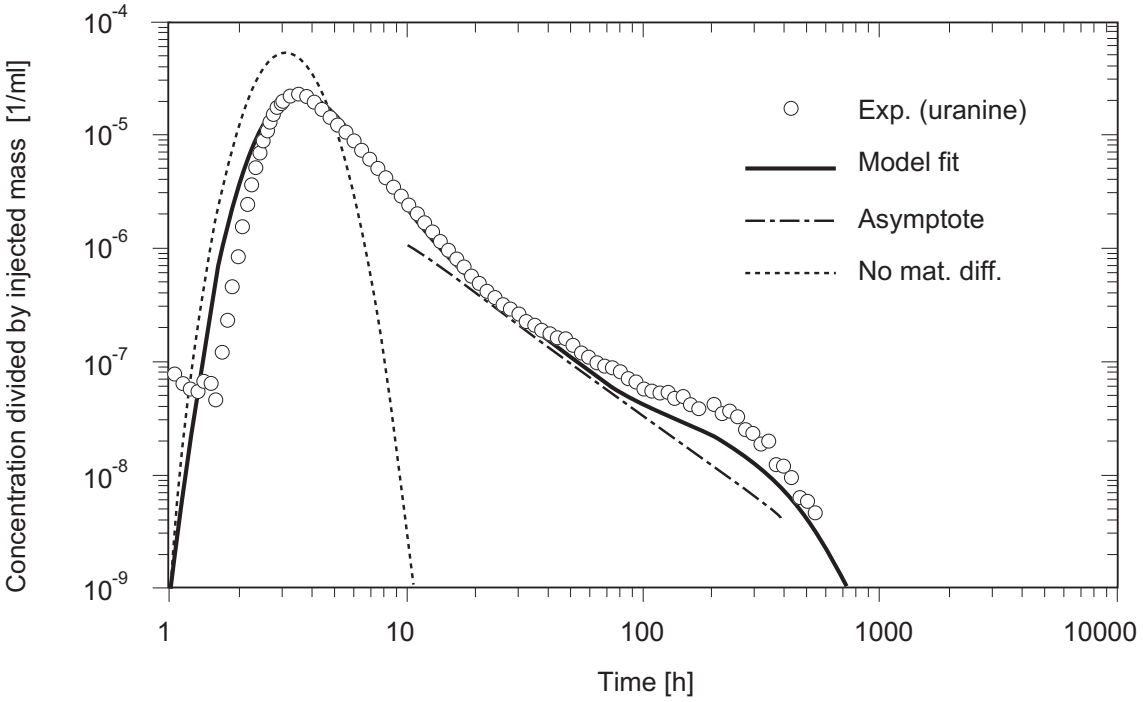

Fig. 7.3: The break-through curve of uranine, assumed to be non-sorbing, for the 4.9 m dipole flow field (Test 50)

Comparing the fitted model to the results of the experiment shows that it is possible to reproduce the different aspects of the experimental break-through curve rather well. The divergence of the model and the experimental results at the front edge of the break-through curve is a minor effect, considering the logarithmic time scale. The divergence around the "tail-end perturbation" (although the concentration is, at this stage, about three orders of magnitude lower than that at the peak) indicates that a more realistic modelling concept for the diffusion-accessible porosity might improve this part of the fit.

The characteristic times of the fit are given in Table 7.2. They confirm the dominance of dispersion over matrix diffusion in determining the width of the peak ($t_D >> t_{MD}$), define, via Equation A4.3e, the asymptote presented in Figure 7.3, and also give approximately the time that the "tail-end perturbation" starts (t_{MP} = 86 h).

Sodium

The fit of the PSI model to the experimental break-through curve for sodium is presented in Figure 7.4. The position and height of the peak are little changed with respect to the uranine results. Due to the (weak) sorption of sodium, however, the impact of matrix diffusion is increased, which is reflected, for example, in the increased concentrations at which the $t^{-3/2}$ asymptotic behaviour is observed. From Table 7.2, it is seen that only t_{MD} and t_{MP} have to be adapted to fit the experiment. Comparing the fitted model to the results of the experiment shows that it is again possible to reproduce the different aspects of the experimental break-through curve closely.

Tab. 7.2: Characteristic times derived by fitting the PSI model to the results of the 4.9 m dipole experiments (Test 50), the physical parameters derived from the characteristic times and, for comparison, independently determined physical parameters

Tracer	Characteristic times [1]	Physical parameters derived from the fit [1]	Physical parameters determined independently [1]
Fixed for all tracers [2]		$a = (5 \pm {}^{5.0}_{2.5}) \cdot 10^{-2}\ m$ $n = 4 \pm {}^{2}_{1}$ $\tilde{\rho}_p = (2.67 \pm 0.20) \cdot 10^{3}\ kg/m^3$	
Uranine (assumed to be non-sorbing)	$t_A = 2.47 \pm 0.12\ h$ $t_D = 1.58 \pm {}^{0.17}_{0.16}\ h$ $t_{MD} = (2.47 \pm {}^{0.25}_{0.23}) \cdot 10^{-1}\ h$ $t_{MP} = (8.55 \pm {}^{3.8}_{2.6}) \cdot 10^{1}\ h$	$\varepsilon_f = (7.4 \pm {}^{7.4}_{3.7}) \cdot 10^{-3}$ $2b = (9.3 \pm {}^{4.6}_{3.0}) \cdot 10^{-5}\ m$ $a_L = (2.5 \pm {}^{0.5}_{0.4}) \cdot 10^{-1}\ m$ $\varepsilon_p = (6.2 \pm {}^{6.8}_{3.2}) \cdot 10^{-2}$ $D_p = (2.5 \pm {}^{11}_{2}) \cdot 10^{-11}\ m^2/s$	$2b << 8.3 \cdot 10^{-4}\ m$ $\varepsilon_p = (1.2 \pm {}^{0.8}_{0.5}) \cdot 10^{-1}$ $D_p = (7.5 \pm {}^{8}_{4}) \cdot 10^{-11}\ m^2/s$
Sodium (weakly sorbing)	$t_A = 2.47\ h$ $t_D = 1.58\ h$ $t_{MD} = 2.15 \pm {}^{0.22}_{0.20}\ h$ $t_{MP} = (4.27 \pm {}^{5.3}_{2.4}) \cdot 10^{2}\ h$	$R_f = 1$ $a_L = 2.5 \cdot 10^{-1}\ m$ $R_p = 6.6 \pm {}^{4.0}_{2.5}$ $K_d = (1.3 \pm {}^{1.6}_{0.7}) \cdot 10^{-4}\ m^3/kg$ $D_p = (3.3 \pm {}^{14}_{2.7}) \cdot 10^{-11}\ m^2/s$	$K_d = (4.3 \pm {}^{6.0}_{0.2}) \cdot 10^{-4}\ m^3/kg$ $D_p = (2.3 \pm {}^{2.4}_{1.3}) \cdot 10^{-10}\ m^2/s$
Strontium (moderately sorbing)	$t_A = 2.47\ h$ $t_D = 1.58\ h$ $t_{MD} = (2.24 \pm {}^{0.47}_{0.39}) \cdot 10^{2}\ h$ $t_{MP} > 5 \cdot 10^{3}\ h$	$R_f = 1$ $a_L = 2.5 \cdot 10^{-1}\ m$ $R_p = (9.1 \pm {}^{10}_{5}) \cdot 10^{2}$ $K_d = (2.1 \pm {}^{3.8}_{1.4}) \cdot 10^{-2}\ m^3/kg$	$K_d = (1.3 \pm {}^{1.9}_{0.1}) \cdot 10^{-2}\ m^3/kg$
Caesium (more strongly sorbing)	$t_A = 2.42\ h$ $t_D = 1.55\ h$ $t_{MD} = 6.16 \cdot 10^{3}\ h$ [3] $t_{MP} > 1.3 \cdot 10^{4}\ h$	$R_f = 1$ $a_L = 2.5 \cdot 10^{-1}\ m$ $R_p = 1.3 \cdot 10^{4}$ [3] $K_d = 2.9 \cdot 10^{-1}\ m^3/kg$ [3]	$K_d = 1.6\ m^3/kg$ [3]

Note:

1) The presented parameter values correspond to the medians of log-normal distributions, with ranges corresponding to one geometric standard deviation. The ranges given for the physical parameters include the contributions of the fixed parameter uncertainties.

2) In addition, pore diffusion coefficients of 2.5×10^{-11} m^2 s^{-1} and 5.0×10^{-11} m^2 s^{-1} were fixed for strontium and caesium, respectively.

3) Preliminary value, error undefined.

Strontium

The fit of the PSI model to the experimental break-through curve for strontium is presented in Figure 7.5. The sorption of strontium, which is only moderate, nevertheless reduces the peak height by a factor of 250 and delays the time of the peak time by a factor of 45, with respect to the uranine results. The asymptotic tail is reached relatively late, due to the flat shape of the peak (which is a consequence of the dominance of matrix diffusion over dispersion ($t_{MD} >> t_D$)) and no "tail-end perturbation" is observed within the duration of the experiment. From Table 7.2, it is seen that only t_{MD} has to be adapted to fit the experiment (t_{MP} can only be

expressed as a lower bound, since the "tail-end perturbation" is not measured). The good fit between the fitted model and the results of the experiment gives some confidence in the sorption concept applied within the PSI transport model.

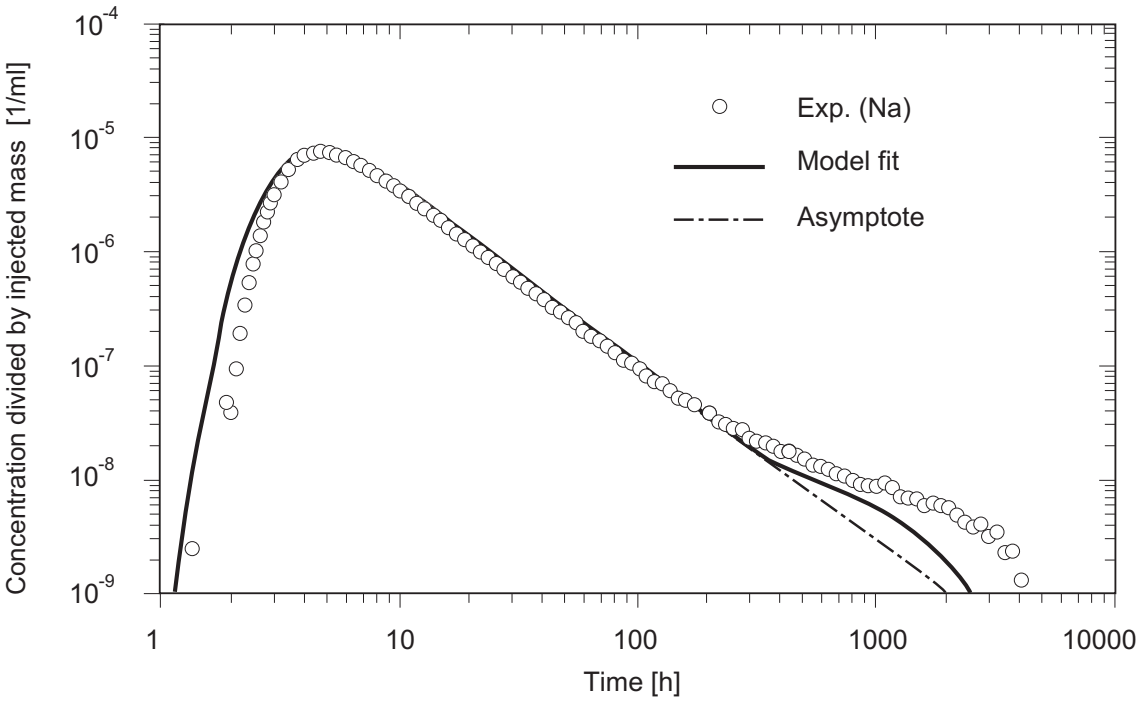

Fig. 7.4: The break-through curve of weakly-sorbing sodium for the 4.9 m dipole flow field (Test 50)

Caesium

The fit of the PSI model to the experimental break-through curve for caesium is presented in Figure 7.6. The sorption of caesium, which is relatively strong, reduces the peak height by a factor of about 7000 and delays the time of the peak time by a factor of about 1000, with respect to the uranine results. The break-through curve of caesium, though shifted due to the stronger sorption, has a similar shape to that of strontium and no new mechanism had to be invoked to explain its form. From Table 7.2, it is seen that, as in the case of strontium, only t_{MD} has to be adapted to fit the experiment. Caesium was injected at a low tracer concentration with respect to natural caesium background, so that linear sorption could be assumed (see Section 5.4.2). The good fit between the fitted model and the results of the experiment again gives confidence in the sorption concept applied within the PSI transport model.

7.3.3 Derivation of Physical Parameters and Comparison with Independently-Determined Values

The parameters deduced from the inverse modelling described in Section 7.3.2 are summarised in Table 7.2. To deduce physical parameters, from the four characteristic times that are adjusted to fit the PSI model, the following assumptions are made:

1. For all of the tracers, fixed values, based on structural and geological analysis, are assumed for (i), the width, a, of the width of the zone where flow occurs, (ii), the number, n, of parallel-walled model fractures and (iii), the bulk density, $\widetilde{\rho}_p$, of the diffusion-accessible porosity.
2. The values of the flow porosity, ε_f, and the diffusion accessible porosity, ε_p, deduced from inverse modelling of the break-through curve for uranine (assumed to be non-sorbing), are assumed also to be valid for the sorbing tracers.
3. Independently estimated pore diffusion coefficients are assumed for the moderately sorbing strontium and the more strongly sorbing caesium (the pore diffusion coefficients could not be derived from the characteristic times since, in the absence of a measured "tail-end perturbation", no matrix-propagation time was available).

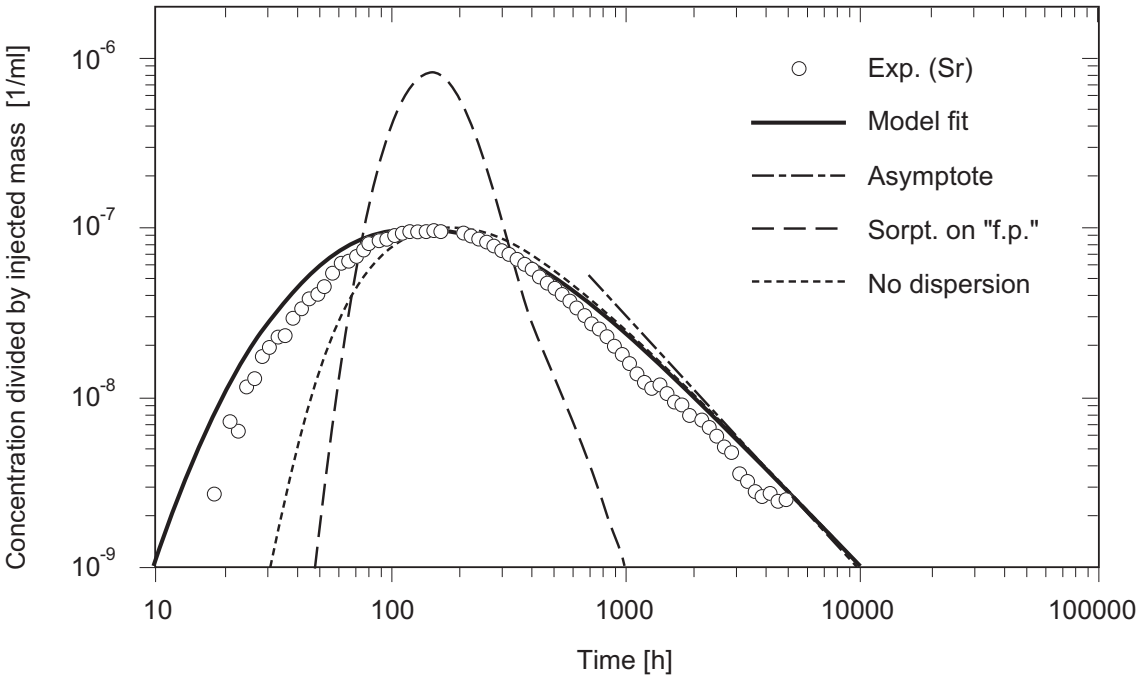

Fig. 7.5: The break-through curve of moderately-sorbing strontium for the 4.9 m dipole flow field (Test 50)

Notes:

1) The dashed line, sorpt. on "f.p.", shows the results of a calculation where sorption on the surfaces of the "flow porosity" is adjusted to give the correct peak time and sorption on matrix pore surfaces is set to zero. The match to the experimental results, and, in particular, the width of the peak, is poor.

2) The dotted line, "no dispersion", shows the results of a calculation where dispersion is not included. Effects on the break-through curve are confined to the leading edge, due to the dominance of matrix diffusion at later times.

Table 7.2 also shows a comparison of the parameter values deduced from the break-through curves with independent estimates. The following observations are made:

- For all tracers:
  - Although no independent estimate of the dispersion length, a_L, is available, the applicability of the PSI model is dependent on the process of advection being dominant over that of dispersion at the location where the break-through curve is measured. a_L (0.25 m), as derived from the characteristic time t_D, is found to be tracer-independent and to be a factor of 20 smaller than the dipole size (4.9 m), indicating the applicability of the PSI model concept.
- For uranine (assumed to be non-sorbing):
  - The observed average width of the fault gauge (0.83 mm) provides an upper bound for the aperture, *2b*, of a single, parallel-walled model fracture. *2b*, as derived from the characteristic time t_A, is a factor of nine less than this upper bound (0.093 mm), and is therefore consistent with the PSI model concept.
  - The independently estimated diffusion-accessible porosity (0.12) is consistent with ε_p derived from the characteristic times t_{MD} and t_{MP} (0.06), within the ranges of uncertainty.
  - The independently estimated pore diffusion constant (8×10^{-11} m^2 s^{-1}) is consistent with D_p derived from the characteristic times t_{MD} and t_{MP} (3×10^{-11} m^2 s^{-1}), within the ranges of uncertainty.
- For the sorbing tracers:
  - No retardation due to sorption on "flow porosity" surfaces was required to fit the break-through curves for any of the sorbing tracers ($R_f = 1$), supporting the PSI assumption of open model fractures, without infill.
  - The independently estimated pore diffusion constant (2×10^{-10} m^2 s^{-1}) is consistent with D_p derived from the characteristic times t_{MD} and t_{MP} (3×10^{-11} m^2 s^{-1}), within the (relatively large) ranges of uncertainty, although the expected tracer-dependence, due to the very different sizes of the sodium ion and the uranine molecule, is not observed.

Batch sorption constants for sodium and strontium, extrapolated to field conditions, agree, within a factor of three (six in the case of caesium) and within two standard deviations, with the sorption coefficients, K_d, derived from the characteristic times.

A comparison between K_ds derived from laboratory and field tests, as discussed in Chapter 5, and K_ds derived by inverse modelling of break-through curves, is given in Table 7.3. The (perhaps surprisingly) good agreement reflects the high quality of field and laboratory experiments, but also the similarity between the laboratory procedure used to prepare the rock samples and the geological processes that are responsible for generating the fault gouge. The main conclusion from this comparison is that, for tracers that sorb rapidly, linearly and that exhibit a reversible cation exchange, the results of laboratory experiments can be extrapolated reasonably well to field conditions, provided adequate care is taken in selecting and preparing the rock samples.

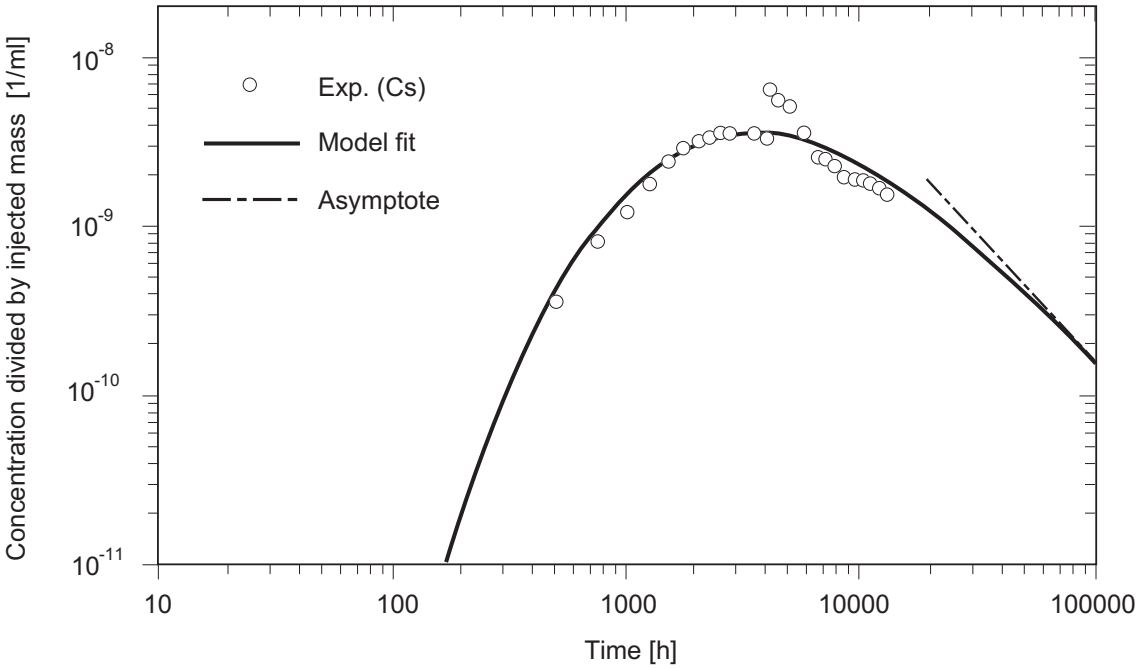

Fig. 7.6: The break-through curve of strongly-sorbing caesium for the 4.9 m dipole flow field (Test 50)

Note: The perturbation at 4000 h was caused by a pump failure.

Tab. 7.3: Sorption coefficients derived from the PSI analysis of the migration experiments and from complementary laboratory measurements (see Chapter 5)

Experiment		K_d [$m^3\,kg^{-1}$]		
		Na	Sr	Cs
Migration	Fitting PSI transport model	$\left(1.3 \pm {}^{1.6}_{0.7}\right) \cdot 10^{-4}$	$(2.1 \pm {}^{3.8}_{1.4}) \cdot 10^{-2}$	0.29
Supporting laboratory and field tests	See Section 5.4	$(7 \pm 2) \cdot 10^{-4}$	$(2 \pm 0.2) \cdot 10^{-4}$	1.6

7.3.4 Predictive Modelling

The transport behaviour of the same tracers has been investigated in a 1.7 m dipole flow field in the same part of the migration shear zone. The experimental conditions are summarised in Table 7.4 and the predicted characteristic times are given.

Differences in experimental conditions were hopefully minimised as the experiments above were selected because they took place around the same time as the experiments analysed by inverse modelling.

In reducing the size of the dipole flow field from 4.9 m to 1.7 m:

- The advection time, t_A, is reduced by a factor of between about 6 and 8, reflecting mainly the proportionality of t_A to the square of the dipole distance L_0 (Equation A4.1a).
- The matrix diffusion effect is substantially reduced – e.g. t_{MD} is reduced by a factor of between about 40 and 64 reflecting mainly the proportionality of t_{MD} to the fourth power of the dipole distance L_0 (Equation A4.3a).

Thus, these experiments provide a sensitive test of the PSI model and, in particular, the representation of the matrix-diffusion process.

Tab. 7.4: Conditions of experiments used for predictive modelling and predicted characteristic times

Parameter	Test 52	Test 61	Tests 66 (Sr) & 80 (Cs)
Dipole distance L_0 [m]	1.7		
Tracers	Uranine	Sodium	Strontium & Caesium
Extraction rate Q_e [ml/min]	150	148	120
Extraction to injection rate ratio β	14.80	15.00	15.00
Characterisation of flow field $f(\beta)$	7.893×10^{-1}	7.787×10^{-1}	7.804×10^{-1}
Characteristic times t_A, t_D, t_{MD}, t_{MP} [h]	0.309, 0.331, 0.00385, 85.5	0.309, 0.331, 0.0336, 428	For Sr: 0.381, 0.409, 5.34, 77'700 For Cs: 0.381, 0.409, 153, 556'000

Uranine and Sodium

Comparisons of prediction and experiment for uranine (assumed non-sorbing) and weakly-sorbing sodium are shown in Figures 7.7 and 7.8, respectively. For both tracers, excellent agreement is obtained.

Strontium

A comparison of prediction and experiment for moderately-sorbing strontium is shown in Figure 7.9. The overall agreement is reasonable. Particularly significant from the point of view of model testing is the strongly reduced break-through time, which supports the model of advection through narrow, open model fractures within the fault gouge. If advective transport occurred homogeneously throughout the fault gouge, a much more strongly retarded break-through curve would have been expected[39].

[39] As noted in Chapter 6, new data from the RRP project indicates that reality lies somewhere between these two extremes. This is discussed further in Chapter 8.

Caesium

A comparison of prediction and experiment for more-strongly sorbing caesium is shown in Figure 7.10. The PSI model successfully predicts the final tail, but fails to predict the fast break-through of this tracer. An additional calculation, with a lower value assigned to the sorption coefficient, also fails to predict the overall form of the break-through curve. These results indicate that either additional processes must be incorporated in the PSI model, or the representation of existing processes must be refined, in order for the model to describe caesium break-through in the 1.7 m dipole field adequately. Caesium sorption kinetics (irrelevant for the larger time scales characterising the 4.9 m dipole) and the new data on the flow field characteristics would be the most obvious candidates for incorporation in a refined model.

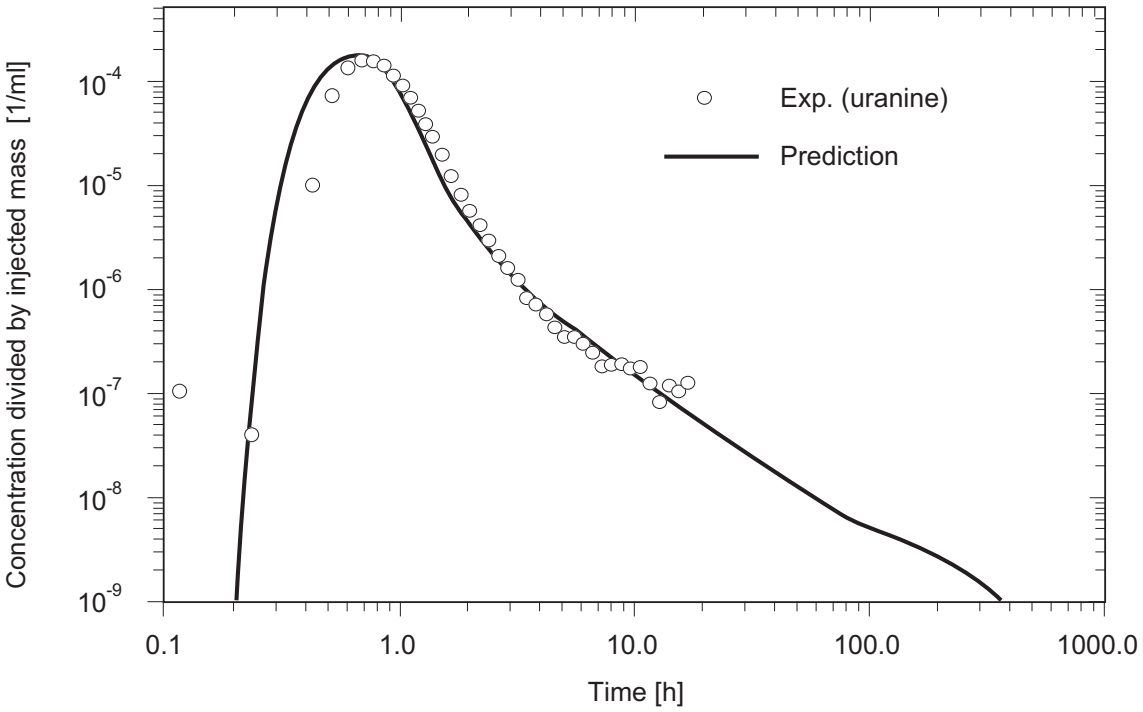

Fig. 7.7: Comparison of prediction and experiment for uranine break-through in the 1.7 m dipole flow field

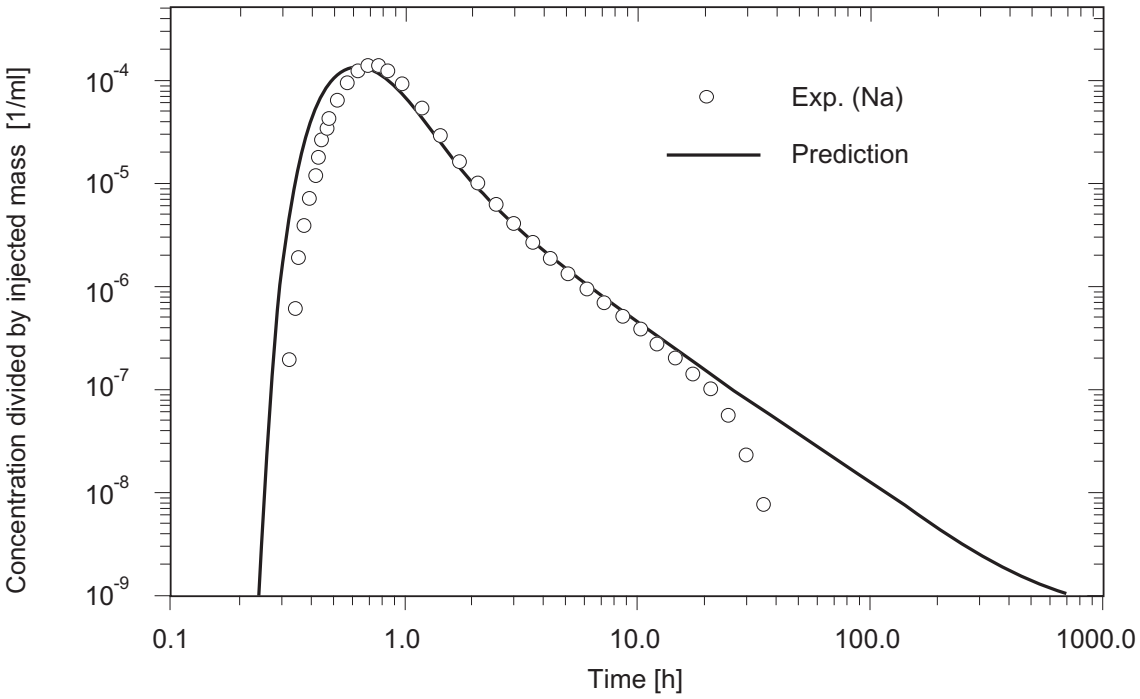

Fig. 7.8: Comparison of prediction and experiment for sodium break-through in the 1.7 m dipole flow field

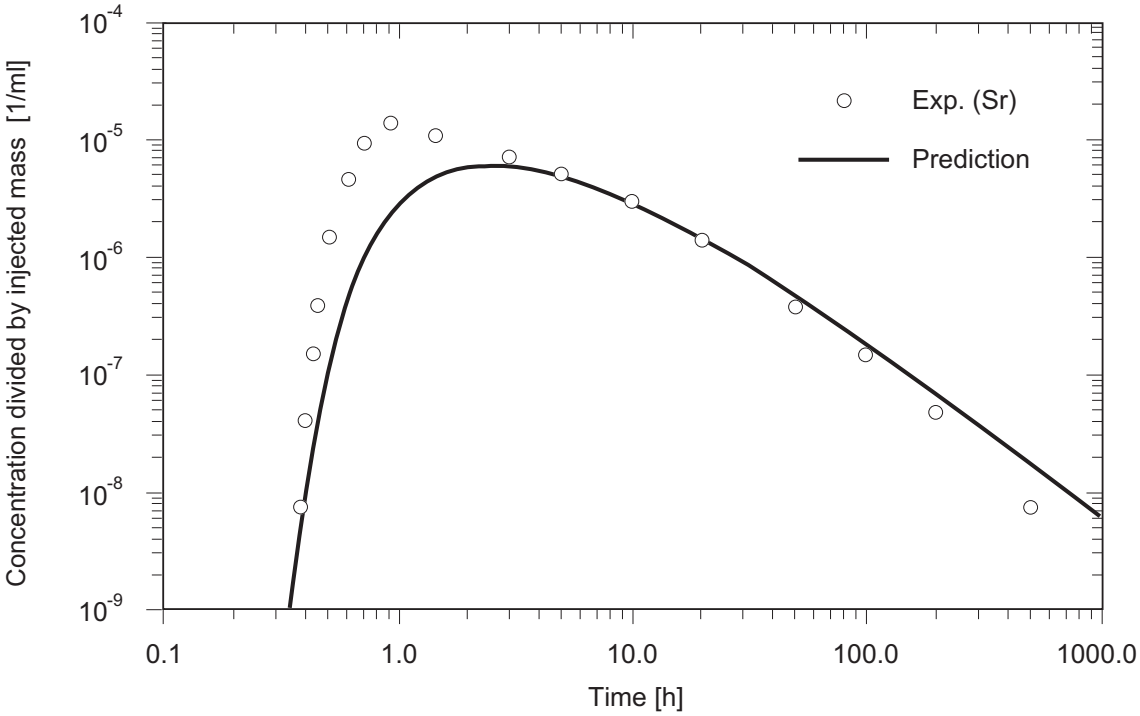

Fig. 7.9: Comparison of prediction and experiment for strontium break-through in the 1.7 m dipole flow field

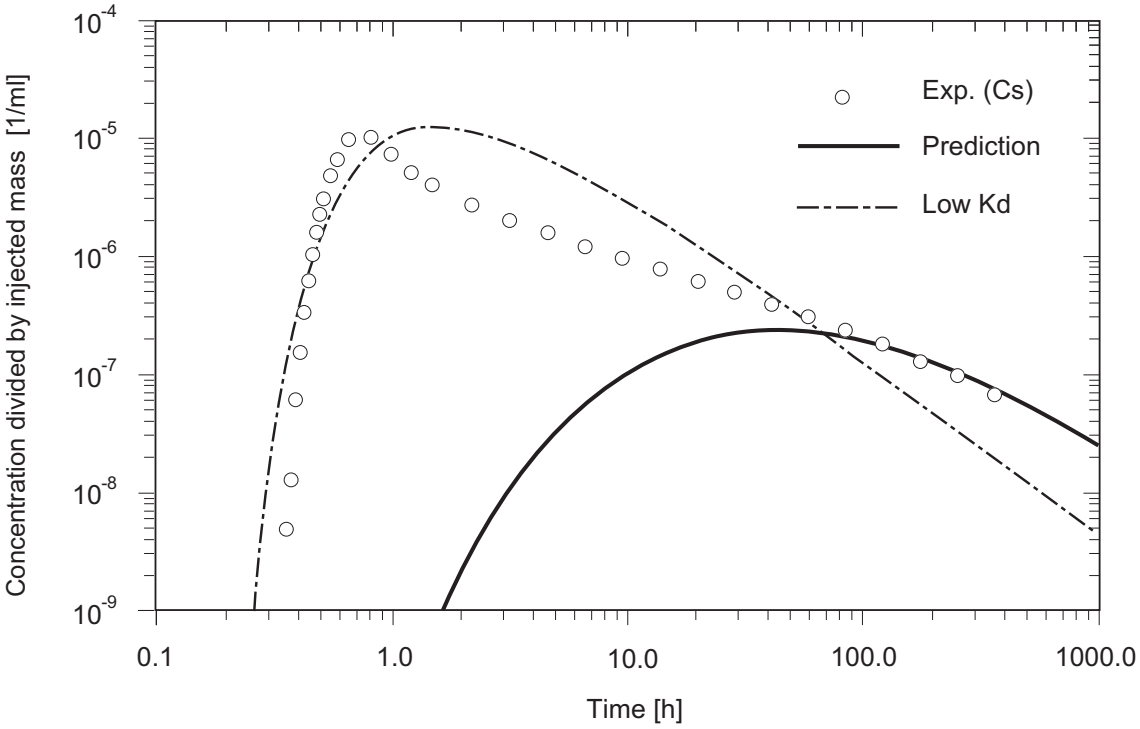

Fig. 7.10: Comparison of prediction and experiment for caesium break-through in the 1.7 m dipole flow field

7.4 Application of the JNC and ETH Transport Models

7.4.1 General Remarks

A number of cases have been analysed using the models of JNC and ETH. Currently, the availability of final results is somewhat limited. Nevertheless some additional insight can be gained from the analysis of these results, contributing to the basic understanding of transport mechanisms.

7.4.2 The JNC Model

JNC propose to apply their model to several tests, with a range of different tracers dipole flow fields. Documentation in UMEKI et al. (1995) and in the present report is currently, however, limited to Test 50 (see Table 7.1).

The methodology adopted in applying the JNC transport model is somewhat different to that described in Section 7.3.1 for the PSI model, and may be summarised as:

STEP 1: Fix geometrical parameters of the model from the results of geological and structural analysis.

STEP 2: For a non-sorbing tracer (uranine) fit, by inverse modelling, the experimental break-through curve and thereby derive the remaining model parameters, thus calibrating the model.

STEP 3: For different sorbing tracers (sodium and strontium), predict the experimental break-through using the calibrated model, in conjunction with sorption coefficients derived from laboratory batch experiments (with no attempt to extrapolate these measured data to *in situ* conditions).

Uranine (inverse modelling)

The fit of the JNC model to the experimental break-through curve for uranine is presented in Figure 7.11. As in the case of the PSI model, an excellent fit can be obtained with a suitable choice of parameters. The JNC model differs from that of PSI principally in (i) its inclusion of an infill within the model fractures and (ii), its inclusion of a heterogeneous transmissivity in the shear zone. The similarity in the fits of the two models indicates that, from the break-through of a non-sorbing tracer, it is not possible to judge which model is a better representation of reality[40], although the choice of model influences the parameters derived by inverse modelling.

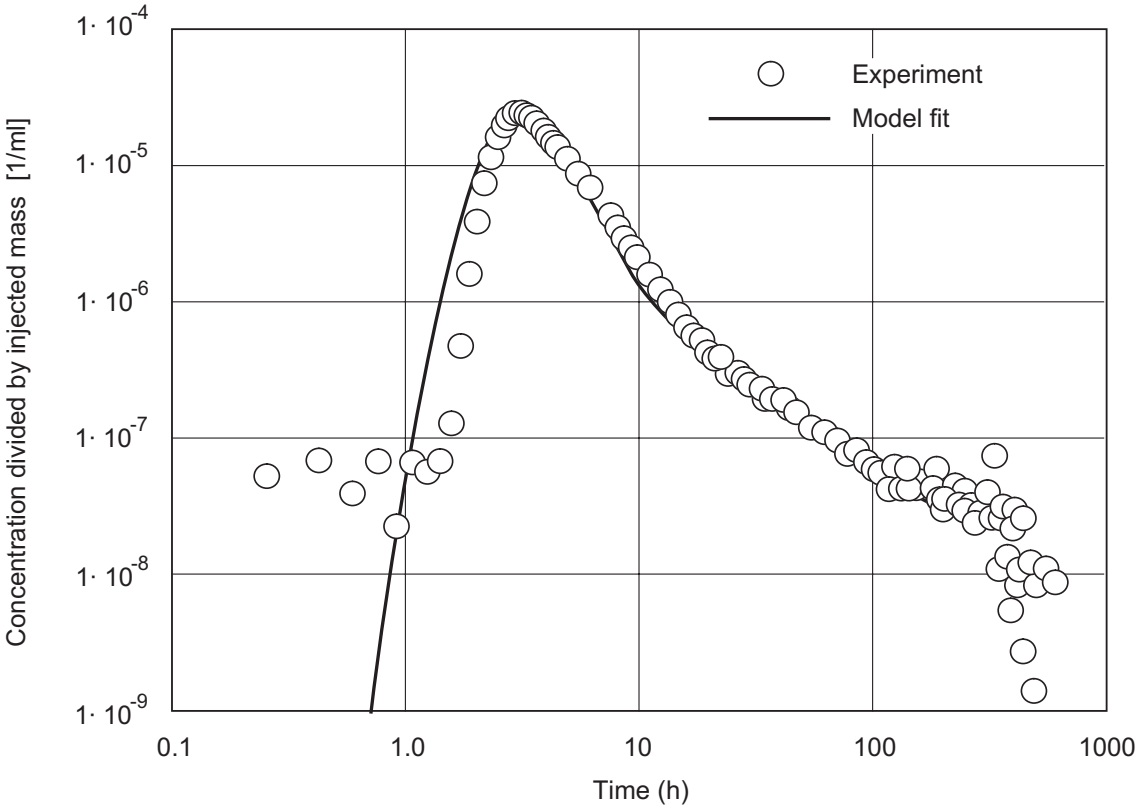

Fig. 7.11: The break-through curve for uranine, assumed to be non-sorbing, in the 4.9 m dipole flow field, fitted using the JNC model (taken from Fig. 3 of UMEKI et al. 1995)

[40] The new data produced in the RRP project (MÖRI et al. 2001a) and in the new hydrogeological analyses (MEIER 2002) clearly indicate that the JNC code was the more appropriate representation. Nevertheless, the results of the JNC model and the PSI model show very little difference indicating that both codes are relatively insensitive to differences in the geosphere representation (discussed further in Chapter 8).

The parameters used to fit the JNC model to this break-through curve are presented in Table 7.5. The following observations are made:

- As noted in Section 7.3.2, the position and shape of the break-through peak are, to a large extent, governed by advection and dispersion. A key parameter determining the characteristic times for these processes (Equations A4.1 and A4.2) is the flow width, $a \cdot \varepsilon_f$. The value derived from the JNC model is larger, by a factor of 3.5, than that derived from the PSI model, reflecting, possibly, a channelling effect caused by the heterogeneity of transmissivity.
- Three, rather than four, parameters are fitted using the JNC model, indicating that the "tail-end perturbation" is not considered explicitly. As discussed in Section 7.2.4, it is necessary to model the "tail-end perturbation" if the diffusion-accessible porosity ε_p and the corresponding pore diffusion constant D_p are to be determined separately.
- The value of $\varepsilon_p \cdot D_p$ derived from the JNC model is larger, by a factor of 32, than that derived from the PSI model, reflecting, possibly, the assumption of only a single model fracture and the numerically calculated, channelled flow field.

Tab. 7.5: Parameters of the JNC model fitted to the experimental break-through of uranine (assumed to be non-sorbing) in the 4.9 m dipole flow field and comparison with the parameters of the PSI model

Parameters	JNC		PSI	
	Basis	Value	Basis	Value
ε_i	Fit	1.3×10^{-1}	Assumption	1
a_L [m]	Fit	2.5×10^{-1}	Fit	2.5×10^{-1}
$\varepsilon_p \cdot D_p$ [m^2 s^{-1}]	Fit	5.00×10^{-11}	Derived from fit	1.55×10^{-12}
$2b$ [m]	Geology	1.00×10^{-2}	Derived from fit	9.3×10^{-5}
n	Assumption	1	Structure	4
$2b \cdot \varepsilon_i = a \cdot \varepsilon_f$ [m]	Derived from fit and from geology	1.3×10^{-3}	Fit	3.7×10^{-4}

Sorbing tracers (predictive modelling)

Break-through curves for sodium, calculated using different values of the sorption constant, K_d, are given in Figure 7.12. Referring to the sorption coefficients from complementary measurements, from which the values presented in Table 7.3 are derived, it can be seen that the predicted effect of sorption on the break-through peak is larger than that observed experimentally. Furthermore, the shape of the calculated break-through peak is typical of curves dominated by advection/dispersion/sorption on fracture infill. These observations indicate that the degree of sorption on fracture infill is over-estimated by the JNC model. On the other hand, for a K_d of 3.5×10^{-4} m^3 kg^{-1}, the tail of the break-through curve is reasonably well predicted, indicating that matrix diffusion and sorption on diffusion-accessible porosity are modelled appropriately. The predictions for strontium have the same break-through curve shape as the non-sorbing uranine, but shifted to later times and lower concentrations. They thus show neither the broad peak nor the tailing observed experimentally for strontium. This confirms that the degree of sorption on fracture infill is over-estimated by the JNC model.

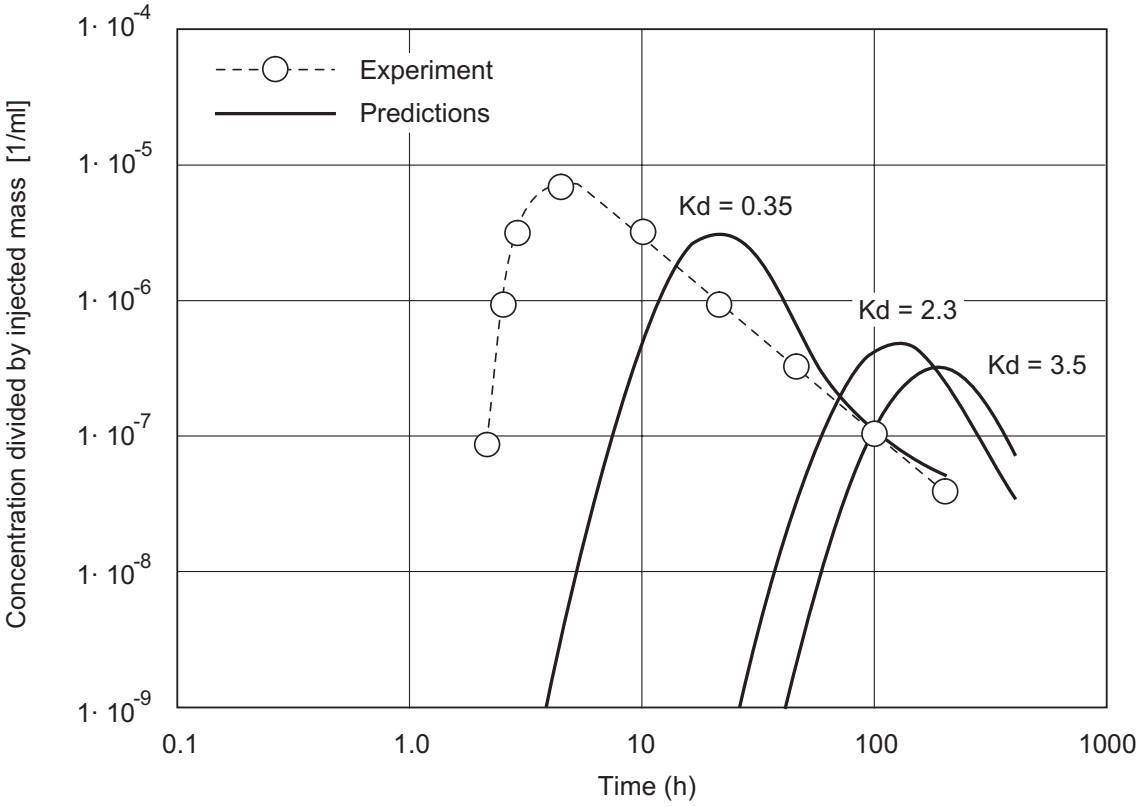

Fig. 7.12: Comparison of experiment and prediction of the JNC model for sodium break-through in the 4.9 m dipole flow field, using different sorption coefficients, given in units of 10^{-3} m^3 kg^{-1} (cf. Fig. 4 and 5 in UMEKI et al. 1995)

The sorption on fracture infill would be reduced, and the agreement between prediction and observation improved, if with model-fracture aperture, *2b*, were to be reduced, while simultaneously increasing the infill porosity, ε_i, such that a constant flow width, $a\varepsilon_f$, is maintained. The inverse modelling of the uranine break-through curve does not yield independent values for *2b* and ε_i and it was necessary to resort to geological observations to fix the aperture. The failure to predict the break-through peak indicates the need to re-visit the assumptions that underlie the interpretation of these observations in terms of an aperture.

7.4.3 The ETH Model

Discussion of the application of the ETH model is restricted to break-through curves for uranine, again assumed non-sorbing and moderately sorbing strontium in 4.9 m and 1.7 m dipole flow fields. The experimental conditions are summarised in Table 7.6.

The methodology adopted in applying the ETH transport model is similar to that described in Section 7.3.1 for inverse modelling using the PSI model, i.e. fitting, by inverse modelling, of the experimental break-through curves for non-sorbing and sorbing tracers and derivation of a set of lumped parameters. In the case of the PSI model, these lumped parameters are essentially the four characteristic times. In the case of the ETH model, the choice of lumped parameters is different and there is an additional, fifth lumped parameter, due to the consideration of the process of transverse dispersion in the ETH model. A further key difference between the models is that the flow field is more accurately represented in the ETH model (finite elements) than in

the PSI model (stream tubes with constant individual water velocities). The inverse modelling of MI tracer tests gives some insight into the relevance of these differences.

The physical parameters, and combinations of physical parameters, that can be deduced by re-arranging the lumped parameters, are indicated in the summary of inverse modelling results for the 4.9 m dipole flow field given in Table 7.7.

Tab. 7.6: Conditions of experiments to which the ETH model has been applied

Parameter	Test 50	Test 75	Test 80
Dipole distance L_0 [m]	4.90	1.74	
Tracers	Uranine, Na, Sr	Uranine, Sr, Rb	Uranine, Cs
Extraction rate Q_e [ml/min]	148.5	121	120
Extraction to injection rate ratio β	15.97	15.125	15.00
Characterisation of flow field $f(\beta)$	7.881×10^{-1}	7.814×10^{-1}	7.804×10^{-1}

Uranine

The fit of the ETH model to the experimental break-through curve for uranine in the 4.9 m dipole flow field is presented in Figure 7.13. As in the case of the PSI and JNC models, an excellent fit can be obtained with a suitable choice of parameters. The fit of the ETH model in the case of the faster, 1.7 m dipole flow field (not discussed in further detail in this text) also shows good agreement.

Tab. 7.7: Physical parameters and characteristic times derived by fitting the ETH model to the results of the 4.9 m dipole experiments (Test 50), and a comparison of the characteristic times with those deduced by fitting the PSI model to the same experiments

Tracer	Parameters deduced by fitting the ETH model	Characteristic times	
		ETH model	PSI model
Uranine (assumed to be non-sorbing)	$\varepsilon_f = 7.9\times10^{-3}$ $a_L = 1.54\times10^{-1}\ m$ $a_T = 7.75\times10^{-1}\ m$ $\varepsilon_p = 5.8\times10^{-2}$ $D_p = 2.96\times10^{-11}\ m^2/s$	$t_A = 2.64\ h$ $t_D = 1.32\ h$ $t_{MD} = 2.55\times10^{-1}\ h$ $t_{MP} = 7.20\times10^{1}\ h$	$t_A = 2.47\pm0.12\ h$ $t_D = 1.58\pm^{0.17}_{0.16}\ h$ $t_{MD} = (2.47\pm^{0.25}_{0.23})\times10^{-1}\ h$ $t_{MP} = (8.55\pm^{3.8}_{2.6})\times10^{1}\ h$
Strontium (moderately sorbing)	$\varepsilon_f R_f = 1.74\times10^{-1}$ $a_L = 3.13\times10^{-1}\ m$ $a_T = 2.00\times10^{-3}\ m$ $\varepsilon_p D_p = 2.69\times10^{-11}\ m^2/s$ $\varepsilon_p R_p = 2.32$	$t_A = 58.1\ h$ $t_D = 41.5\ h$ $t_{MD} = 1.60\times10^{2}\ h$ $t_{MP} = 1.84\times10^{2}\ h$	$t_A = 2.47\ h$ $t_D = 1.58\ h$ $t_{MD} = (2.24\pm^{0.47}_{0.39})\times10^{2}\ h$ $t_{MP} > 5\cdot10^{3}\ h$

From additional sensitivity analyses, it was concluded in KUNSTMANN et al. (1997) that:

- the model break-through curve is not sensitive to the value assigned to the transverse dispersion coefficient
- the influence of the natural background flow is negligible.

These results support the assumptions of the PSI model whereby both, transverse dispersion and the natural background flow, are neglected.

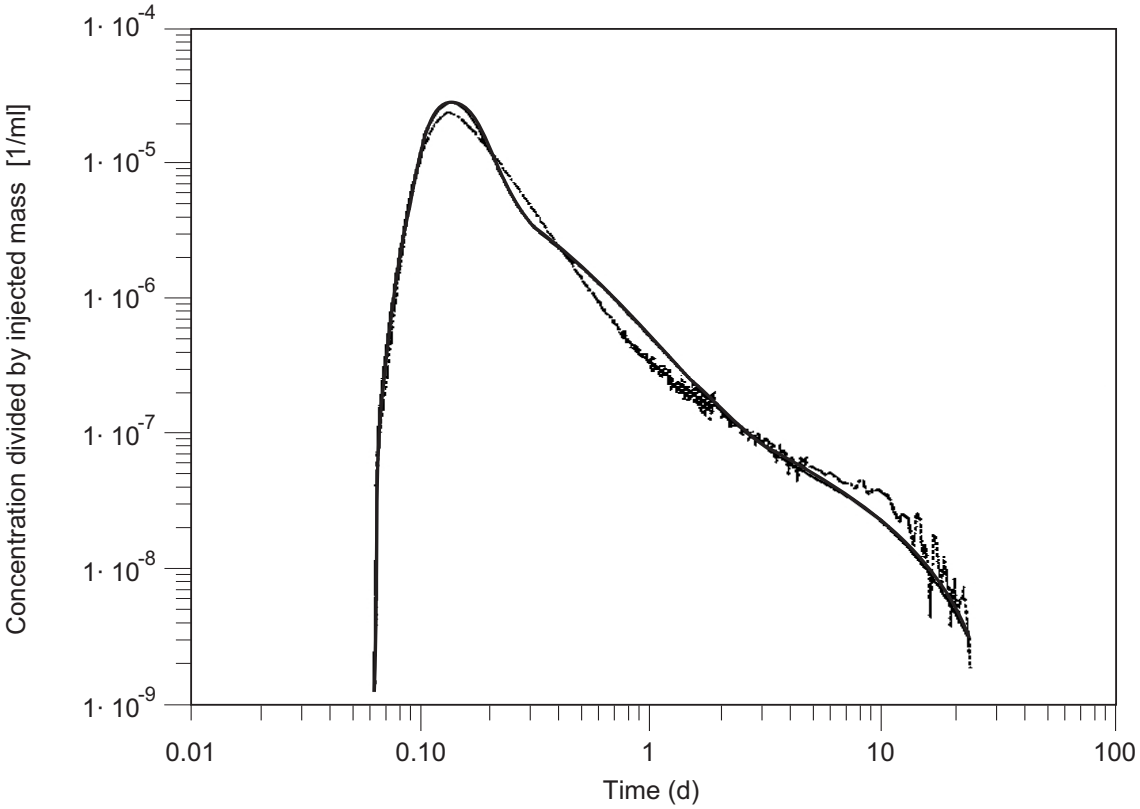

Fig. 7.13: The break-through curve for uranine, assumed to be non-sorbing, in the 4.9 m dipole flow field, fitted using the ETH model (taken from Fig. 5 of KUNSTMANN et al. 1997)

The characteristic times are close to the values deduced by fitting the PSI model, indicating that:

- The different parts of the fitted break-through curve are allocated, by the ETH model, to the same processes as by the PSI model. This is consistent with the result that the influence of transversal dispersion is small.
- The representation of the flow field by the PSI model, though less accurate than the representation by the ETH model, is, nevertheless, adequate for this application[41].

[41] Following discussions with ETH, PSI has also shown, by means of some supporting calculations, that the velocity peaks in the dipole flow field near the injection and extraction points have essentially no effect on the form of the fitted break-through curves, but lead to an over-estimate of longitudinal dispersion length by the PSI model, in the order of 10 % (cf. HEER 1997).

Strontium

The fit of the ETH model to the experimental break-through curve for strontium in the 4.9 m dipole flow field is presented in Figure 7.14, with the fitted parameters, and the characteristic times deduced from these, presented in Table 7.7.

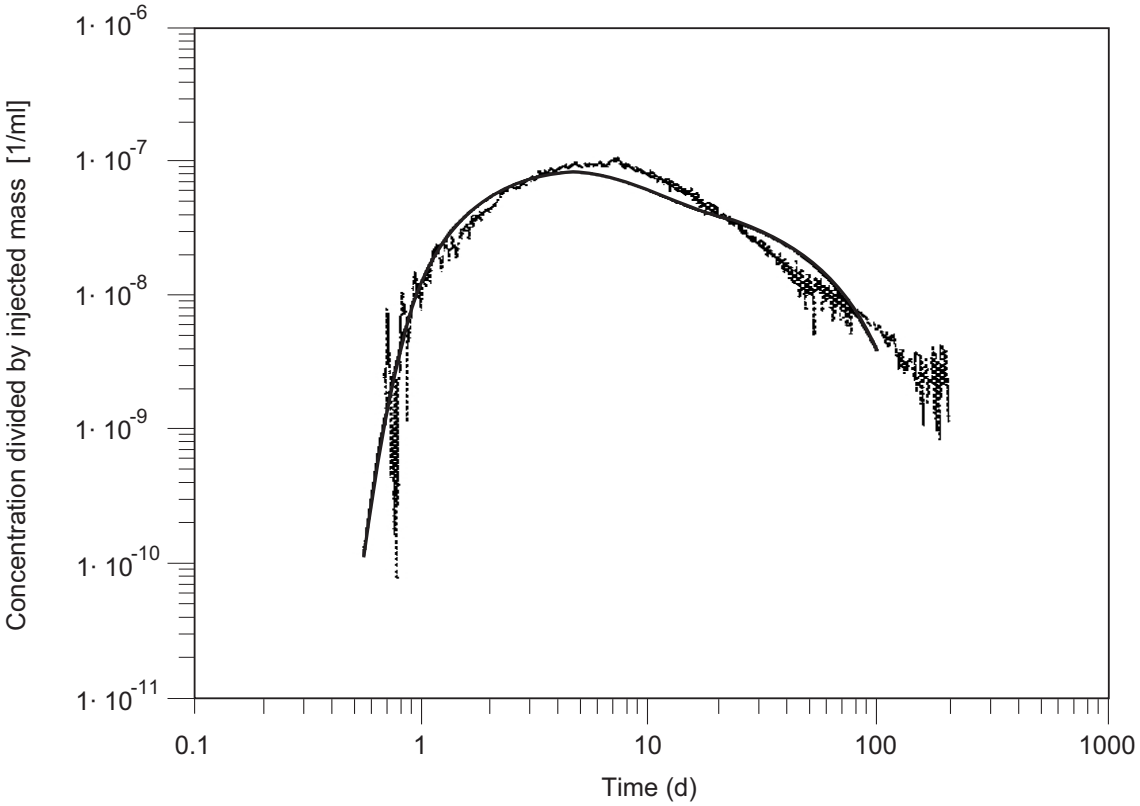

Fig. 7.14: The break-through curve for strontium, assumed to be non-sorbing, in the 4.9 m dipole flow field, fitted using the ETH model (taken from Fig. 9 of KUNSTMANN et al. 1997)

Although the ETH model fits the experimental curve reasonably well (a similarly reasonable fit is found for the 1.7 m dipole flow field), the characteristic times are significantly different to those deduced by fitting the PSI model. The following observations are made:

- Like the PSI model, the matrix-diffusion time, t_{MD}, for the ETH model of strontium break-through is increased substantially with respect to the model of uranine break-through, indicating the importance of matrix diffusion in the case of this moderately-sorbing tracer.
- Unlike the PSI model, the advection and dispersion times, t_A and t_D, for the ETH model of strontium break-through are also increased with respect to the model of uranine break-through, indicating that retardation within the "flow porosity" is also a feature of the ETH representation of strontium migration.
- Also unlike the PSI model, the matrix-propagation time, t_{MP}, for the ETH model of strontium break-through is increased relatively little with respect to the model of uranine break-through. From the value of t_{MP} deduced using the ETH model, the beginning of "tail-end perturbation" would be expected to occur at t_A+t_{MP} = 240 h (=10 d). Although the fitted break-through curve shows this "tail-end perturbation", it is not observed in the experimental results.

For the 1.7 m dipole flow field, the agreement between the ETH and PSI model values for t_{MD} and t_{MP} is reasonable. However, the ETH model values for the t_A and t_D of the strontium break-through curve are again (unlike the PSI model) increased with respect to that of the uranine break-through curve.

Additional calculations performed by PSI and ETH indicate that the discrepancies in the characteristic times are, to a large extent, explained by the coarse discretisation of the diffusion-accessible matrix used in the numerical solution of the governing equations of the ETH model. The solution technique did not, in its first implementation, adequately resolve the steep concentration gradients of sorbing tracers that can occur in the diffusion-accessible porosity.

7.5 Conclusions from the Application of Transport Models

From modelling studies of the GTS MI field experiments using tracers with a range of sorption behaviour and supported by the results of laboratory studies of rock-tracer interaction and by geological structural analysis, the following main conclusions can be drawn:

- The studies support the basic concepts, common to all three models, that tracer transport is determined by:
  - advection and dispersion within a few narrow, but transmissive, openings within the shear zone
  - retardation due to matrix diffusion into the stagnant water of the diffusion-accessible porosity, representing, to a large extent, the fault gouge, and sorption on mineral surfaces.
- Although this dual-porosity concept provides a highly simplified representation of a complex natural system, it is nevertheless able to describe, with reasonable accuracy, the experimental break-through curves for uranine, sodium, strontium and caesium in the 4.9 m dipole flow field.

In the case of the PSI model applied in both, inverse and predictive, modelling exercises:

- The physical parameters derived by inverse modelling are consistent with values from independent observations and measurements, supporting the underlying model concepts.
- Of special note is the agreement between values for the sorption constant, obtained by different laboratory and field techniques. In particular, for tracers that sorb rapidly and exhibit a reversible cation exchange, the results of laboratory experiments can be extrapolated reasonably well to field conditions, provided adequate care is taken in selecting and preparing the rock samples, so as to ensure that they properly reflect the geological character of the site.
- The success of the model in predicting the break-through for uranine, sodium, and strontium in the 1.7 m dipole flow field, where the different transport mechanisms are weighted differently, builds confidence in the underlying model concepts.
- The failure of the model to predict the break-through peak of caesium in the 1.7 m dipole flow field, while more successfully representing the last part of the tail, suggests that sorption kinetics, which has not, as yet, been included in the PSI model, may be a significant factor for this particular experiment (the effects of the sorption kinetics of caesium were not observed in the case of the 4.9 m dipole field and are not relevant in the long-term safety assessments of a repository for radioactive waste).

A number of more specific, but nevertheless informative, findings have also been made:

- The models predict that the process of matrix diffusion should manifest itself in the asymptotic form of the tails of the break-through curves, that decreases with time as $t^{-3/2}$. This asymptotic form is observed in the experiments. The observed "tail-end perturbation" is also consistent with the matrix-diffusion concept.
- The pore diffusion constant can only be deduced by inverse modelling if the break-through curve is measured down to the "tail-end perturbation". This requires a major experimental effort in order to measure the break-through curve for a time period that is several orders of magnitude longer, and for concentrations that are orders of magnitude lower, than the break-through peak.
- The process of transverse dispersion is not important in the narrow dipole flow field of the MI tracer tests.
- In calculating sorbing tracer migration using the dual-porosity concept, it is important to adopt a numerical procedure that adequately resolves the steep concentration gradients that occur in the diffusion-accessible porosity.

In summary, the field tracer tests performed within MI, which have been performed with an exceptional degree of precision, have provided a good basis for building confidence in radionuclide transport models. The application of models to these tests supports the current understanding of tracer transport mechanisms in crystalline rock and thus lends support to the inclusion of these same processes in models for repository safety assessment. However, the fact that all three codes are insensitive to the finer details of the real flow system means that care must be taken when transferring these results to performance assessment codes.

8 DISCUSSION AND CONCLUSIONS

I.G. McKinley, P.A. Smith and W.R. Alexander

8.1 Achievements of the Grimsel Migration Experiment

The Grimsel Migration Experiment was, from its first outline specifications (see Chapter 1 and McKINLEY & GROGAN 1984), foreseen as an integrated study of geochemistry and radionuclide migration in fractured rock. The key component of this study was identified as *in situ* tracer tests utilising radionuclides, but it was recognised that an extensive range of supporting laboratory, field and modelling studies was required in order to ensure that such tracer tests can be adequately interpreted and thus contribute to the goals of providing data and testing models for repository performance assessment (cf. ALEXANDER et al. 1998). It was further noted that an evolutionary development approach should be adopted, with the field studies proceeding sequentially, testing methodology and equipment and determining the technical feasibility of increasingly difficult phases of work.

A further period of planning work and a decade of experimental studies have confirmed the value of this broad-based approach. Although the time, manpower and budget requirements were greater than originally envisaged, co-sponsorship by JNC and technical support by the University of Berne, PSI and Solexperts has resulted in an unique database that has significantly enhanced the understanding of solute behaviour in fracture-flow systems.

Referring to the original aims of MI (Section 1.3), some highlights of the project have been in:

1. **The development of methodologies for site characterisation**

   The need to perform accurate *in situ* migration tests has led to the development and refinement of special equipment and to the evolution of an effective testing methodology. A spin-off of this work has been the identification of important artefacts (e.g. sorption on equipment, the role of "dead-space" in lines and packed-off intervals) that call into question many of the results of similar studies carried out elsewhere. Extensive experience has been gained in the handling of radionuclides under *in situ* conditions. Following the evolutionary development approach, initial tests with chemically simple, short-lived radionuclides stimulated the development of technology that later allowed the use of longer-lived and chemically more complex radionuclides, culminating in the use of α-emitting actinides in a tracer-cocktail injection at the end of MI. The experience gained has since been further utilised in the EP, CRR and HPF projects in the GTS and in other URLs including Mont Terri and Äspö.

2. **The study of the hydrology and geochemistry of a fractured rock**

   A database has been assembled in the course of MI that contains a substantial amount of information on:

   - regional- and local-scale geology, hydrogeology and isotope hydrology;
   - hydrochemistry of flowing groundwater, evaluated over many years and including special determinations of colloidal, dissolved-organic and microbial populations.

3. **The focussing of laboratory, field and modelling studies on the detailed characterisation of a single water-conducting feature**

   The MI database also includes small- to micro-scale structural analysis of the MI shear zone, as well as characterisation of mineralogy and porosity. Natural decay-series isotope profiles perpendicular to the plane of the MI shear zone provide unambiguous evidence of connected matrix porosity extending for some centimetres from the regions of groundwater

flow and advective tracer transport. In addition, laboratory work in support of the MI project has involved studies of rock-water interaction and radionuclide sorption. The latter has included the evaluation of sorption kinetics, reversibility and concentration-dependence. Many of these observations and data have provided input to the predictive modelling of tracer transport.

4. **The testing of models of radionuclide transport**

   The emphasis in the MI project has been, where possible, on the assessment of the *predictive* capability of transport models (as opposed to the *fitting* of models to experimental results, which provides a weaker test of the models). Within the limitations noted below, the modelling exercises have been a success and given confidence that relevant processes are understood and adequately represented in the models, that no relevant processes have been overlooked and that, with appropriate consideration of the differences in conditions, laboratory data (e.g. on sorption and diffusion) can be applied to field-scale experiments, giving some support to their application in performance assessment.

   Perhaps more important has been the development of a culture of rigorous model testing and, arguably more importantly, of predictive model testing in the organisations involved.

8.2 Limitations

The successful modelling of the MI tracer tests gives support to the model representation of structures and processes that exist in, or operate on, spatial and temporal scales that are similar to, or smaller than, the tests themselves. A major difficulty with such tests lies in the extrapolation of this conclusion to the larger scales that are relevant to performance assessment: no information is provided on processes that, though irrelevant on the spatial and temporal scales of field tracer tests, may be important over scales relevant to performance assessment.

It is possible that different model representations of the structures and processes relevant to the MI tracer tests would be similarly successful *fitting* the results of (at least some) tests and, for this reason, alternative models were developed by three independent research groups. The aim was, by attempting to falsify some of these alternatives, and, in particular, by making independent *predictions* of the results of tests in advance of the tests being performed, to narrow down the range of conceptual model uncertainty and to identify the processes that are most important in describing solute transport. This aim was only partially fulfilled, since:

- The differences between the models were rather minor and thus the range of conceptual-model uncertainty was small. All models were built upon the dual-porosity concept, and no attempt was reported, for example, to understand the test results without invoking matrix diffusion.
- Due to limitations in the available manpower, *predictive* model testing was confined mainly to the PSI group. The alternative models of JNC and ETH were generally able to *fit* the results of the tests to which they were applied, but, to a large extent, their predictive power remains to be demonstrated.
- As the new data provided by the EP and CP projects show, all three models are insensititve to the finer details of the *in situ* flow system. None of the three models considered the effects of chanelling, multiple flowpaths or unlimited matrix diffusion but, despite this, successfully predicted (PSI) or fitted (JNC, ETH) the experimental data.
- As such, these results clearly show the limitations of the approach of using simple breakthrough curves to differentiate between processes and structures in flow system.

In spite of these limitations, the applicability of the dual-porosity concept in general to the MI tracer tests has been convincingly demonstrated and confidence in its applicability to performance assessment has been enhanced.

8.3 Conclusions

Overall, the Grimsel Migration Experiment has demonstrated that the methodology adopted for:

- geological and hydrological characterisation of water-conducting features
- simplification of this characterisation for modelling purposes
- the adaptation of laboratory data (particularly sorption data) to field conditions
- numerical solution of the governing equations for solute transport in dual-porosity media,

is indeed applicable to the modelling of solute transport through a fractured crystalline rock. Nevertheless the fact that all three codes examined appear to be insensitive to features of the flow system, which could play a role in radionuclide retardation in a repository host rock, requires further consideration. These results also indicate the limitations of the approach of process identification by examination only of the form of break-through curves especially when tails are not examined in detail.

Apart from the technical achievements (and limitations) noted above, the experience of working in a multi-disciplinary team on a long-term, challenging project has been considered to be of value to all participants, establishing successful communications between geologists, laboratory and field experimenters and modellers.

9 ACKNOWLEDGEMENTS

In a project as large and as long running as the Migration Experiment many people from a wide range of organisations are involved and we would like to thank all of them. In particular, thanks go to U. Frick (Nagra), E. Hoehn (EAWAG, formerly PSI), S. Aksoyoglu, M. Mantovani, C. Bajo, J. Hadermann and K. Bischoff (all PSI) and H. Umeki (NUMO, formerly JNC). Special thanks also to the staff of the GTS for their support over the years, to our colleagues at HSK for helping us to find practical solutions to the difficulties of working with radionuclides in the environment and to Dr J. Eikenberg, PSI, for a thorough review of this report. Finally, thanks to Nagra and JNC for funding this work as part of the Nagra-JNC jointly funded GTS radionuclide migration programme (RMP) and for agreeing to provide the MI raw data free-of-charge to interested organisations (details on www.grimsel.com).

10 REFERENCES

AKSOYOGLU, S. & MANTOVANI, M. (1989): GTS Laboratory Programme Progress Report: Cation Exchange Capacity Measurements on Grimsel Mylonite; Unpubl. PSI Internal Report. Paul Scherrer Institute, Würenlingen and Villigen, Switzerland.

AKSOYOGLU, S., BAJO, C. & MANTOVANI, M. (1991): Grimsel Test Site – Batch Sorption Experiments with Iodine, Bromine, Strontium, Sodium and Caesium on Grimsel Mylonite. Nagra Technical Report NTB 91-06, Nagra, Wettingen, Switzerland; PSI Report 83, Paul Scherrer Institute, Würenlingen and Villigen, Switzerland.

ALBERT, W., BÜHNEMANN, J., HOLLIGER, K., MAURER, H.R., PRATT, G. & STEKL, I. (1999): Grimsel Test Site – Further Development of Seismic Tomography. Nagra Technical Report NTB 97-05. Nagra, Wettingen, Switzerland.

ALEXANDER, W.R. (1991): Redox state of the Grimsel Test Site (GTS) radionuclide Migration Experiment (MI) groundwater/rock system Unpubl. Nagra Internal Report. Nagra, Wettingen, Switzerland.

ALEXANDER, W.R., MACKENZIE, A.B., SCOTT, R.D. & McKINLEY, I.G. (1990a): Natural analogue studies in crystalline rock: The influence of water-bearing fractures on radionuclide immobilisation in a granitic rock repository. Nagra Technical Report NTB 87-08. Nagra, Wettingen, Switzerland.

ALEXANDER, W.R., McKINLEY, I.G., MACKENZIE, A.B. & SCOTT, R.D. (1990b): Verification of matrix diffusion in granite by means of natural decay series disequilibria. Sci. Basis Nucl. Waste Manag. XIII, 567-576.

ALEXANDER, W.R., BRADBURY, M.H., McKINLEY, I.G., HEER, W., EIKENBERG, J. & FRICK, U. (1992): The Current Status of the Radionuclide Migration Experiment at the Grimsel Underground Rock Laboratory. Sci. Basis Nucl. Waste Manag. XV, 721-728.

ALEXANDER, W.R., HATANAKA, K., UMEKI, H. & FRICK, U. (1994): The Nagra/PNC Radionuclide Migration Experiment: First Phase of the Rigorous Testing of a PNC Transport Model. Proc. Inter. Conf. Geological Disposal Rad. Waste, Tokai, November 1993. PNC Report. PNC, Tokyo, Japan.

ALEXANDER, W.R., FRIEG, B., OTA, K. & BOSSART, P. (1996): The RRP Project – Investigating Radionuclide Retardation in the Host Rock. Nagra Bulletin 27 (June, 1996), 43-55. Nagra, Wettingen, Switzerland.

ALEXANDER, W.R., FRIEG, B., OTA, K. & BOSSART, P. (1997a): The assessment of radionuclide entrapment in repository host rocks. OECD Proceedings: Workshop on Field Tracer Experiments (Role in the Prediction of Radionuclide Migration), Cologne, Germany, 28-30 August, 1996. NEA/OECD, Paris, France.

ALEXANDER, W.R., McKINLEY, I.G., FRICK, U. & OTA, K. (1997b): The Grimsel Field Tracer Migration Experiment – What have we achieved after a Decade of Intensive Work? Proc. of the First GEOTRAP Workshop: Field Tracer Experiments, Role in the Prediction of Radionuclide Migration, Cologne, Germany 28th – 30th August 1996.

ALEXANDER, W.R., GAUTSCHI, A. & ZUIDEMA, P. (1998): Thorough testing of performance assessment models: the necessary integration of in situ experiments, natural analogues and laboratory work. Abstract in: Sci. Basis Nucl. Waste Manag. XXI, 1013-1014.

ALEXANDER, W.R., FRIEG, B. & OTA, K (eds.) (2001a): Grimsel Test Site – Investigation Phase IV (1994-1996): The Nagra-JNC *in situ* study of safety relevant radionuclide retardation in fractured crystalline rock II: the RRP project methodology development, field and laboratory tests. Nagra Technical Report NTB 00-06. Nagra, Wettingen, Switzerland.

ALEXANDER, W.R., SMITH, P.A. & McKINLEY, I.G. (2001b): Radioactivity in the geological environment. Ch. 5 in: SCOTT, E.M. (ed.): Modelling Radioactivity in the Environment. Elsevier, Amsterdam (*in press*).

ALEXANDER, W.R., OTA, K., MÖRI, R. & McKINLEY, I.G. (2002): Synthesis of the results of the 15 year Nagra-JNC Radionuclide Migration Programme. Geochem. Trans. (*in prep).*

ANDERSON, G.M. & CRERAR, D.A. (1993): Thermodynamics in geochemistry – the equilibrium model. Oxford University Press, Oxford, England.

BACHU, S. & UNDERSCHULZ, J.R. (1992): Regional scale porosity and permeability variations, Peace River Arch area, Alberta, Canada. AAPG Bull. 76/4, 547-562.

BAERTSCHI, P., ALEXANDER, W.R. & DOLLINGER, H. (1991): Grimsel Test Site – Uranium migration in crystalline rock: Capillary solution transport in the granite of the Grimsel Test Site. Nagra Technical Report NTB 90-15. Nagra, Wettingen, Switzerland.

BAEYENS, B. & BRADBURY, M.H. (1989): Selectivity Coefficients and Estimates of In-situ Sorption Values for Mylonite. In: BRADBURY, M.H. (ed.) (1989): Grimsel Test Site – Structural Geology and Water Flow Paths in the Migration Shear Zone. Nagra Technical Report NTB 88-23, Nagra, Wettingen, Switzerland; PSI Report 28, Paul Scherrer Institute, Würenlingen and Villigen, Switzerland.

BAEYENS, B., AKSOYOGLU, S. & BRADBURY, M.H. (1989): Cation Exchange Characteristics of Mylonite. In: BRADBURY, M.H. (ed.) (1989): Grimsel Test Site – Structural Geology and Water Flow Paths in the Migration Shear Zone. Nagra Technical Report NTB 88-23, Nagra, Wettingen, Switzerland; PSI Report 28, Paul Scherrer Institute, Würenlingen and Villigen, Switzerland.

BAJO, C., AKSOYOGLU, S. & MANTOVANI, M. (1989): Groundwater Stability and Rock-water Interaction Experiments. In: BRADBURY, M.H. (ed.) (1989): Grimsel Test Site – Structural Geology and Water Flow Paths in the Migration Shear Zone. Nagra Technical Report NTB 88-23, Nagra, Wettingen, Switzerland; PSI Report 28, Paul Scherrer Institute, Würenlingen and Villigen, Switzerland.

BARKER, J.A. (1988): A generalized radial flow model for hydraulic tests in fractured rock. Water Resour. Res. 24/10, 1796-1804.

BARTEN, W. (1996): Linear Response Concept Combining Advection and Limited Rock Matrix Diffusion in a Fracture Network Transport Model. Water Resour. Res. 32/11, p. 3292, Eqs. 69-71.

BLÜMLING, P. & SATTEL, G. (1988): Tomographic Investigations. Nagra Bulletin Special Edition 1988, 35-40. Nagra, Wettingen, Switzerland.

BOSSART, P. & MARTEL, S.J. (1990): Hydrogeological implications of ductile and brittle deformations in the Grimsel Crystalline, upper Aare valley, Switzerland. Unpubl. Nagra Internal Report. Nagra, Wettingen, Switzerland.

BOSSART, P. & MAZUREK, M. (1991): Grimsel Test Site – Structural geology and water flowpaths in the migration shear zone. Nagra Technical Report NTB 91-12. Nagra, Wettingen, Switzerland.

BRADBURY, M.H. (ed.) (1989): Grimsel Test Site – Laboratory investigations in support of the Migration Experiments. Nagra Technical Report NTB 88-23, Nagra, Wettingen, Switzerland; PSI Report 28, Paul Scherrer Institute, Würenlingen and Villigen, Switzerland.

BRADBURY, M.H. & BAEYENS, B. (1992): Modelling the Sorption of Cs: Application to the Grimsel Migration Experiment. PSI Annual Report 1992, Annex IV, 59-64. Paul Scherrer Institute, Würenlingen and Villigen, Switzerland.

BRÄUER, V., KILGER, B. & PAHL, A. (1989): Grimsel Test Site – Engineering geological investigations for the interpretation of rock stress measurements and fracture flow tests. Nagra Technical Report NTB 88-37E. Nagra, Wettingen, Switzerland.

BREDEHOEFT, J.D. & PAPADOPULOS, S.S. (1980): A Method for Determining the Hydraulic Properties of Tight Formations. Water Resour. Res. 16/1, 233-238.

BREWITZ, W., BRASSER, Th., KULL, H. & HUFSCHMIED, P. (1988): Ventilation Test. Nagra Bulletin Special Edition 1988, 46-49. Nagra, Wettingen, Switzerland.

BROUWER, E., BAEYENS, B., MAES, A. & CREMERS, A. (1983): Caesium and rubidium ion equilibria in illite clay. J. Phys. Chem. 87, 1213-1219.

BRUNO, J. & SANDINO, A. (1988): The thermodynamics and kinetics of coprecipitation and its effect on radionuclide solubility. Radiochim. Acta, 44/45, 17-22.

BUTLER Jr., J.J. (1988): Pumping tests in nonuniform aquifers: The radially symmetric case. J. Hydrol. 101(1/4), 15-30.

BUTLER Jr., J.J. (1990): The role of pumping tests in site characterization: Some theoretical considerations. Ground Water, 28/3, 394-402.

BUTLER Jr., J.J. (1991): A stochastic analysis of pumping test in laterally non-uniform media. Water Resour. Res. 27, 2401-2414.

BUTLER Jr., J.J. & LIU, W.Z. (1991): Pumping tests in non-uniform aquifers – The linear strip case. J. Hydrol. 128, 69-99.

BUTLER Jr., J.J. & LIU, W.Z. (1993): Pumping tests in nonuniform aquifers: The radially asymmetric case. Water Resour. Res. 29/2, 259-269.

CARBONELL, J.A. & CARRERA, J. (1992): MARIAJ Code for the automatic interpretation of pumping tests. Unpubl. Users manual, Universidad Politecnica de Catalunya. Barcelona, Spain.

CARRERA, J. & NEUMAN, S.P. (1986): Estimation of aquifer parameters under steady-state and transient conditions: I. Background and Statistical framework. Water Resour. Res. 22/2, 199-210.

CARRERA, J., MEDINA, A., AXNESS, C. & ZIMMERMAN, T. (1995): Formulations and Computational Issues of the Inversion of Random Fields. Kovacs Colloquium, December 1995. UNESCO, Paris, France.

CHOUKROUNE, P. & GAPAIS, D. (1983): Strain pattern in the Aar granite (Central Alps): Orthogneiss developed by bulk inhomogeneous flattening. J. Struct. Geol. 5, 411-418.

CHRISTOFI, N. & MILNER, C.R. (1990): Microbial examination of groundwater from the Grimsel Test Site: The results of two studies carried out by the Napier Polytechnic of Edinburgh. Unpubl. Nagra Internal Report. Nagra, Wettingen, Switzerland.

COOPER Jr., H.H. & JACOB, C.E. (1946): A generalized graphical method for evaluating formation constants and summarizing well-field history. Eos Trans. AGU 27/4, 526-534.

CORREA, N.R. (ed.) (1994): Modeling of groundwater flow at the subregional scale – Boundary conditions, transient and thermal effects, inverse modeling: Grimsel Test Site. Nagra Technical Report NTB 94-07. Nagra, Wettingen, Switzerland.

DAVEY, A., KARASAKI, K., LONG, J.C.S., LANDSFELD, M., MENSCH, A. & MARTEL, S.J. (1990): Analysis of hydraulic data from the MI fracture zone at the Grimsel Rock Laboratory, Switzerland. NDC-15, LBL-27864, Lawrence Berkeley Laboratory, Berkeley, California.

DEGUELDRE, C., BAEYENS, B., GOERLICH, W., RIGA, J., VERBIST, J. & STADELMANN, P. (1989): Colloids in water from a subsurface fracture in granitic rock, Grimsel Test Site, Switzerland. Geochim. Cosmochim. Acta 53, 603-610.

DEGUELDRE, C., LONGWORTH, G., MOULIN, V., VILKS, P., ROSS, C., BIDOGLIO, G., CREMERS, A., KIM, J., PIERI, J., RAMSAY, J., SALBU, B. & VUORINEN, U. (1990): Grimsel Test Site – Grimsel colloid exercises: An international intercomparison exercise on the sampling and characterisation of groundwater colloids. Nagra Technical Report NTB 90-01. Nagra, Wettingen, Switzerland.

DEGUELDRE, C., PFEIFFER, H.-R., ALEXANDER, W.R. WERNLI, B. & BRUETSCH, R. (1996): Colloid properties in granitic groundwater systems. I: sampling and characterisation. Appl. Geochem. 11, 677-695.

DEMPSTER, T.J. (1986): Isotope systematics in minerals: biotite rejuvenation and exchange during Alpine metamorphism. Earth Planet. Sci. Lett. 78, 355-367.

DROST, W. (1984): Single Well techniques. In: Tracer methods in isotope hydrogeology 8. IAEA, Vienna, Austria.

EARLOUGHER Jr., R.C. (1977): Advances in Well Test Analysis. Soc. of Petroleum Engineers, Monograph Volume 5 of the Henry L. Doherty Series, 264 pp.

EGGER, P. (1986): Grimsel Test Site – Tests for excavation effects (machine excavated tunnel): A preliminary summary. Unpubl. Nagra Internal Report. Nagra, Wettingen, Switzerland.

EIKENBERG, J. (1989): Abschätzung von geochemischen Veränderungen bei Stollenluft-infiltrationen in die Grimsel Migrationskluft. Unpubl. PSI Internal Report. Paul Scherrer Institute, Würenlingen and Villigen, Switzerland.

EIKENBERG, J. & BÜHLER, Ch. (1990): Thermodynamische Speziationsberechnungen zum Versagen von HPLC-Pumpen im Felslabor Grimsel. Unpubl. PSI Internal Report. Paul Scherrer Institute, Würenlingen and Villigen, Switzerland.

EIKENBERG, J., BAEYENS, B. & BRADBURY, M.H. (1991): Grimsel Test Site – The Grimsel Migration Experiment: A Hydrogeochemical Equilibration Test. Nagra Technical Report NTB 90-39, Nagra, Wettingen, Switzerland; PSI Report 100, Paul Scherrer Institute, Würenlingen and Villigen, Switzerland.

EIKENBERG, J., BÜHLER, Ch. & FIERZ, Th. (1992): On-line detection of stable helium isotopes in migration experiments. Proc. of the 6th International Symposium on Water Tracing, Sept. 21 – 26, Karlsruhe, Germany.

EIKENBERG, J., HOEHN, E. & FIERZ, Th. (1994): Grimsel Test Site: Preparation and Performance of Migration Experiments with Radioisotopes of Sodium, Strontium and Iodine test. PSI Report 94-11. Paul Scherrer Institute, Würenlingen and Villigen, Switzerland.

EIKENBERG, J., RÜTHI, M., ALEXANDER, W.R., FRIEG, B. & FIERZ, Th. (1998): The excavation project in the Grimsel Test Site – in situ high resolution gamma and alpha spectrometry of ^{60}Co, ^{75}Se, ^{113}Sn, ^{152}Eu, ^{235}U and $^{237}Np/^{233}$. Pa. Sci. Basis Nucl. Waste Manag. XXI, 655-662.

FALK, L., MAGNUSSON, K.-Å, OLSSON, O., AMMANN, M., KEUSEN, H.R. & SATTEL, G. (1988): Grimsel Test Site – Analysis of radar measurements performed at the Grimsel Rock Laboratory in October 1985. Nagra Technical Report NTB 87-13. Nagra, Wettingen, Switzerland.

FIERZ, Th. (1998): The Nagra-PNC Grimsel Radionuclide Experiment – Documentation of Tracer Experiments 1988 – 1996. Unpubl. Nagra Internal Report. Nagra, Wettingen, Switzerland.

FINSTERLE, S., SCHLUETER, E. & PREUSS, K. (1990): Exploratory simulations of multiphase effects in gas injection and ventilations tests in an underground laboratory. NDC-13, LBL-28810, Lawrence Berkeley Laboratory, Berkeley, California.

FLACH, D. & NOELL, U. (1989): Felslabor Grimsel – Neigungsmessungen zur Ermittlung neotektonischer Vorgänge. Nagra Technical Report NTB 89-11. Nagra, Wettingen, Switzerland.

FRANCIS, A.J., GILLOW, J.B., DUNN, M., LUCERO, D. & PAPENGUTH, H. (1999): Microbial studies in support of the Grimsel Colloid- and Radionuclide-Retardation (CRR) Experiment. Unpubl. Nagra Internal Report. Nagra, Wettingen, Switzerland.

FRICK, U. (1988): Hydrochemische Analysen durch das Mineralwasserlabor (Dr. Senften, Probenahmen vom 8.4.1988 und 11.5.1988) – Überraschende Resultate nach Injektionsversuch vom 11. März 1988. Unpubl. Nagra Internal Memorandum. Nagra, Wettingen, Switzerland.

FRICK, U. (1992): Beurteilung der Diffusion im Grundwasser von Kristallingesteinen – Ein Beitrag zur Kristallinstudie 1993. Unpubl. Nagra Internal Report. Nagra, Wettingen, Switzerland.

FRICK, U. (1994): The Grimsel Radionuclide Migration Experiment – A Contribution to Raising Confidence in the Validity of Solute Transport Models Used in Performance Assessment. GEOVAL 94, NEA/OECD, Paris, France.

FRICK, U., BAERTSCHI, P. & HOEHN, E. (1988): Migration investigations. Nagra Bulletin, Special edition 1988, 23-34. Nagra, Wettingen, Switzerland.

FRICK, U., ALEXANDER, W.R., BAEYENS, B., BOSSART, P., BRADBURY, M.H., BÜHLER, Ch., EIKENBERG, J., FIERZ, Th., HEER, W., HOEHN, E., McKINLEY, I.G. & SMITH, P.A. (1992a): Grimsel Test Site – The Radionuclide Migration Experiment: Overview of Investigations 1985 – 1990. Nagra Tech. Report NTB 91-04, Nagra, Wettingen, Switzerland; PSI Report 120, Paul Scherrer Institute, Würenlingen and Villigen, Switzerland.

FRICK, U., ALEXANDER, W.R. & DROST, W. (1992b): The Radionuclide Migration Experiment at Nagra's Grimsel Underground Test Site – A Comprehensive Programme Including Field, Laboratory and Modelling Studies. IAEA Paper IAEA-SM-319/27 in: Isotope Techniques in Water Resources Development 1991, IAEA, Vienna, Austria.

FRIEG, B., ALEXANDER, W.R., DOLLINGER, H., BÜHLER, Ch., HAAG, P., MÖRI, A. & OTA, K. (1998): In situ impregnation for investigating radionuclide retardation in fractured repository host rocks. J. Contam. Hydrol. 35, 115-130.

GELHAR, L. (1987): Applications of Stochastic models to Solute Transport in Fractured Rocks. SKB Technical Report 87-05. SKB, Stockholm, Sweden.

GEMPERLE, R. (1989): Migration Grimsel Field Laboratory – Long Term (35 day) Constant Q Test in BOMI 87.009, Test Description and Analysis. Unpubl. Solexperts Field Report. Solexperts, Schwerzenbach, Switzerland.

GEOTEST AG (1987): Grimsel Test Site: Fracture zone investigation (FRI) – Geological documentation of the test field. Unpubl. Geotest AG Report for Nagra. Nagra, Wettingen, Switzerland.

GEOTEST AG & INGENIEURUNTERNEHMUNG AG BERN (1981): Sondierbohrungen Juchlistock-Grimsel. Nagra Tech. Report NTB 81-07. Nagra, Wettingen, Switzerland.

GÓMEZ-HERNÁNDEZ, J.J., SOVERO, H. & SAHUQUILLO, A. (1995): Some issues on the analysis of pumping tests in heterogeneous aquifers. Hydrogeology 3, 13-18.

GRIM, R.E. (1953): Clay Mineralogy. McGraw-Hill. Inc., New York.

GUIMERÁ, J. & CARRERA, J. (1997): On the interdependence of transport and hydraulic parameters in low permeability fractured media. Hard Rock Hydrosystems. Proceedings of Rabat Symposium S2, May 1997. IAHS Publ. No. 241.

HADERMANN, J. & HEER, W. (1996): The Grimsel Migration Experiment: Integrating Field Experiments, Laboratory Investigations and Modelling. J. Cont. Hydr. 21, 87-100, Proc. of the Fourth International Conference on Chemistry and Migration Behaviour of Actinides and Fission Products in the Geosphere, Charleston, SC USA, December 12th – 17th, 1993, 765-771.

HEER, W. (1997): Grimsel Migration Experiments: Test Calculations. Unpubl. PSI Internal Report. Paul Scherrer Institute, Villigen PSI, Switzerland.

HEER, W. & HADERMANN, J. (1996): Grimsel Test Site – Modelling Radionuclide Migration Field Experiments. Nagra Technical Report NTB 94-18, Nagra, Wettingen, Switzerland; PSI Report 94-13, Paul Scherrer Institute, Würenlingen and Villigen, Switzerland.

HEER, W., HADERMANN, J. & JAKOB, A. (1994): Modelling the Radionuclide Migration Experiments at the Grimsel Test Site. Proc. IAHR Symposium on Transport and Reactive Processes in Aquifers, Zurich, April 11 – 15, A.A. Balkema, Rotterdam, Netherlands, 297-302.

HERZOG, F. (1989): Hydrologic Modelling of the Migration Site in the Grimsel Rock Laboratory – the Steady State. Nagra Technical Report NTB 89-16, Nagra, Wettingen, Switzerland; PSI Report 35, Paul Scherrer Institute, Würenlingen and Villigen, Switzerland.

HERZOG, F. (1991): Grimsel Test Site – A Simple Transport Model for the Grimsel Migration Experiments. Nagra Technical Report NTB 91-31, Nagra, Wettingen, Switzerland; PSI Report 106, Paul Scherrer Institute, Würenlingen and Villigen, Switzerland.

HOEHN, E., FIERZ, Th. & THORNE, P. (1990): Grimsel Test Site – Hydrogeological Characterisation of the Migration Experimental Area. Nagra Technical Report NTB 89-15, Nagra, Wettingen, Switzerland; PSI Report 60, Paul Scherrer Institute, Würenlingen and Villigen, Switzerland.

HSK & KSA (1993): Guideline of Swiss Nuclear Installations: Protection Objectives for the Disposal of Radioactive Wastes. Swiss Federal Nuclear Safety Inspectorate (HSK) and Federal Commission for the Safety of Nuclear Installations (KSA) HSK-R-21/e. HSK, Villigen, Switzerland.

HUFSCHMIED, P. & ADANK, P. (1988): Modelling groundwater flow in the rock body surrounding the Grimsel Test Site. Nagra Bulletin Special Edition 1988, 50-52. Nagra, Wettingen, Switzerland.

JAKOB, A. & HADERMANN, J. (1991): INTRAVAL Test Case 1B – Modelling Results. Nagra Technical Report NTB 91-27, Nagra, Wettingen, Switzerland; PSI Report 105, Paul Scherrer Institute, Würenlingen and Villigen, Switzerland.

JAKOB, A., HADERMANN, J. & ROESEL, F. (1989): Radionuclide Chain Transport with Matrix Diffusion and Non-Linear Sorption. Nagra Technical Report NTB 90-13, Nagra, Wettingen, Switzerland; PSI Report 54, Paul Scherrer Institute, Würenlingen and Villigen, Switzerland.

KELLEY, V.A. & FRIEG, B. (1990): Grimsel Test Site – Field investigations (Interference Tests, Fluid Logging and Constant-Rate Withdrawal Test) in the BK area, December 1989 – March 21, 1990. Unpubl. Nagra Internal Report. Nagra, Wettingen, Switzerland.

KEUSEN, H.R., GANGUIN, J., SCHULER, P. & BULETTI, M. (1989): Grimsel Test Site – Geology. Nagra Technical Report NTB 87-14E. Nagra, Wettingen, Switzerland.

KICKMAIER, W. & McKINLEY, I. (1996): Investigations in Phases I to III (1983 – 1993) at the Grimsel Test Site – a Retrospective. Nagra Bulletin 27, 5-14. Nagra, Wettingen, Switzerland.

KICKMAIER, W., VOMVORIS, S., ALEXANDER, W.R., MARSCHALL, P., FRIEG, B., WANNER, W. & HUERTAS, F. (2001): Grimsel Test Site – Nagra's underground research laboratory in crystalline rock: status of the scientific programme 1997 – 2002. Hydrogeology (*in press*).

KUHLMANN, U. (1989): Applications of NAMMU: Results of four test examples. Unpubl. Nagra Internal Report. Nagra, Wettingen, Switzerland.

KULL, H. & MIEHE, R. (1995): Felslabor Grimsel – Der Einfluss der Stollen-Ventilation auf die hydraulischen Fliessverhältnisse im ausbruchsnahen Gebirgsbereich (Kristallin). Nagra Technical Report NTB 94-04. Nagra, Wettingen, Switzerland.

KULL, H., BREWITZ, W. & KLARR, K. (1993): Grimsel Test Site – Ventilation Test: In-situ experiment for determination of permeability in crystalline rock. Nagra Technical Report NTB 91-02E. Nagra, Wettingen, Switzerland.

KUNSTMANN, H., KINZELBACH, W. & MASTHOFF, R. (1997): Modelling Radionuclide Field Migration Experiments of the Grimsel Test Site. Unpubl. Nagra Internal Report. Nagra, Wettingen, Switzerland.

LABHART, T.P. (1966): Mehrphasige alpine Tektonik am Nordrand des Aarmassivs. Beobachtungen im Druckstollen Trift-Speicherberg (Gadmental) der Kraftwerke Oberhasli AG. Eclogae geol. Helv. 59/2, 803-830.

LACHASSAGNE, P., LEDOUX, E. & DE MARSILY, G. (1989): Evaluation of hydrogeological parameters in heterogeneous porous media. In: Groundwater Management: Quantity and Quality. Proceedings of the Benidorm Symposium, October 1989. IAHS Publ. 188, 3-18.

LIEDTKE, L. & ZUIDEMA, P. (1988): The Fracture System Flow Test. Nagra Bulletin Special Edition 1988, 41-45. Nagra, Wettingen, Switzerland.

LIEDTKE, L., GÖTSCHENBERG, A., JOBMANN, M. & SIEMERING, W. (1994): Fracture System Flow Test – Experimental and numerical investigations of mass transport in fractured rock: Grimsel Test Site. Nagra Technical Report NTB 94-02E. Nagra, Wettingen, Switzerland.

LIU, J. & NERETNIEKS, I. (1997): Coupled transport / reaction modelling with ion-exchange – Study of the long-term properties of bentonite buffer in a final repository. SKI Report 97-23. SKI, Stockholm, Sweden.

LONG, J.C.S., MAJER, E.L., KARASAKI, K., PETERSON Jr., J.E., DAVEY, A. & HESTIR, K. (1990): Hydrologic characterisation of fractured rocks – An interdisciplinary methodology. NDC-12, LBL-27863, Lawrence Berkeley Laboratory, Berkeley, California.

McKINLEY, I.G. & ALEXANDER, W.R. (1992): Constraints on the applicability of "in-situ" *Kd* values. J. Environ. Radioactivity 15, 19-34.

McKINLEY, I.G. & GROGAN, H. (1984): Specification of an Experimental Study of Geochemistry and Elemental Migration at the Grimsel Rock Laboratory. EIR Internal Technical Report TM-45-84-37. Paul Scherrer Institute, Würenlingen and Villigen, Switzerland.

McKINLEY, I.G. & HADERMANN, J. (1985): Radionuclide sorption data base for Swiss safety assessment. Nagra Technical Report NTB 84-40. Nagra, Wettingen, Switzerland.

McKINLEY, I.G., ALEXANDER, W.R., BAJO, C., FRICK, U., HADERMANN, J., HERZOG, F.A. & HOEHN, E. (1988): The Radionuclide Migration Experiment at the Grimsel Rock Laboratory, Switzerland. Sci. Basis Nucl. Waste Manag. XI, 179-187.

MAJER, E.L., PETERSON Jr., J.E., BLÜMLING, P. & SATTEL, G. (1990a): P-Wave imaging of the FRI and BK Zones at the Grimsel Rock Laboratory. Nagra-DOE Cooperative Project Report NDC-4/LBL-28807, August 1990.

MAJER, E.L., PETERSON Jr., J.E., BLÜMLING, P. & SATTEL, G. (1990b): Shear Wave Experiments at the US Site at the Grimsel Rock Laboratory. Nagra-DOE Cooperative Project Report NDC-7/LBL-28808, July 1990.

MAJER, E.L., MYER, L.R., PETERSON Jr., J.E., KARASAKI, K., LONG, J.C.S., MARTEL, S.J., BLÜMLING, P. & VOMVORIS, S. (1990c): Joint seismic, hydrogeological and geomechanical investigations of a fracture zone in the Grimsel Rock Laboratory, Switzerland. Nagra Tech. Ber. NTB 90-49. Nagra, Wettingen, Switzerland.

MANGOLD, D.C. & TSONG, C.F. (1991): A summary of subsurface hydrological and hydrochemical models. Reviews of Geophysics 29, 51-79.

MARQUER, D. & GAPAIS, D. (1985): Les massifs cristallins externes sur une transversale Guttannen – Val Bedretto (Alpes Centrales): structures et histoire cinématique. C. R. Acad. Sc. Paris 301/II, 543-546.

MARSCHALL, P. & VOMVORIS, S. (eds.) (1995): Grimsel Test Site – Developments in Hydrotesting, Fluid Logging and combined Salt/Heat Tracer Experiments in the BK Site (Phase III). Nagra Technical Report NTB 93-47. Nagra, Wettingen, Switzerland.

MARSCHALL, P., FEIN, E., KULL, H., LANYON, W., LIEDTKE, L., MÜLLER-LYDA, I. & SHAO, H. (1999): Grimsel Test Site – Investigation Phase V (1997-2002): Conclusions of the Tunnel Near-Field Programme (CTN). Nagra Technical Report NTB 99-07. Nagra, Wettingen, Switzerland.

MARTEL, S.J. & PETERSON Jr., J.E. (1990): Use of integrated geologic and geophysical information for characterizing the structure of fracture systems at the US/BK site, Grimsel Laboratory, Switzerland. NDC-12, LBL-27863, Lawrence Berkeley Laboratory, Berkeley, California.

MARTEL, S.J. & PETERSON Jr., J.E. (1991): Interdisciplinary characterization of fracture systems at the US/BK site, Grimsel Laboratory, Switzerland. Int. J. Rock Mech. Min. Sci. & Geomech. Abstr. 28/4, 295-323.

MAZUREK, M., BOSSART, P. & ELIASSON, T. (1996): Classification and characterization of water-conducting features at Äspö: Results of investigations on the outcrop scale. SKB/Nagra International Cooperation Report 97-01. Swedish Nuclear Fuel and Waste Management, Stockholm.

MEDINA, A., GALARZA, G. & CARRERA, J. (1995): TRANSIN-II, FORTRAN Code for Solving the Coupled Flow and Transport Inverse Problem. User's Guide, E.T.S.I. Caminos, Universidad Politecnica de Catalunya, Barcelona, Spain.

MEIER, P.M. (1997): Migration Experiment (MI) and Radionuclide Retardation Project (RRP) – Results of additional hydraulic testing in the Migration shear zone. Unpubl. Nagra Internal Report. Nagra, Wettingen, Switzerland.

MEIER, P.M. (2002): Migration Experiment (MI) and Radionuclide Retardation Project (RRP) – Modelling hydraulic- and tracer tests using a geostatistical inverse approach to characterise heterogeneity. Nagra Technical Report (*in prep.*). Nagra, Wettingen, Switzerland.

MEIER, P.M., FERNÁNDEZ, P., CARRERA, J. & GUIMERÁ, J. (1995): Results of hydraulic testing in boreholes FBX 95.001, FBX 95.002, BOUS 85.001, BOUS 85.002, FEBEX – PHASE 1. Unpubl. Internal Report E.T.S.I. Caminos, Universidad Politecnica de Catalunya, Barcelona, Spain.

MEIER, P.M., SÁNCHEZ-VILA, X. & CARRERA, J. (1997): Study of Transient Constant Rate Pumping Tests in Heterogeneous Media. Hard Rock Hydrosystems. Proceedings of Rabat Symposium S2, May 1997. IAHS Publ. No. 241.

MEIER, P.M., CARRERA, J. & SÁNCHEZ-VILA, X. (1999): An evaluation of Jacob's method for the interpretation of pumping tests in heterogeneous formations. Water Resour. Res. 34/5, 1011-1025.

MEYER, J., MAZUREK, M. & ALEXANDER, W.H. (1989): Petrographic and mineralogical characterisation of fault zones AU96 and AU126. Chap. 2 in: BRADBURY, M.H. (ed.): Grimsel Test Site – Laboratory investigations in support of the migration experiments. Nagra Technical Report NTB 88-23, Nagra, Wettingen, Switzerland.

MILLER, W., ALEXANDER, W.R., CHAPMAN, N.A., McKINLEY, I.G. & SMELLIE, J.A.T. (1994): Natural Analogue Studies in the Geological Disposal of Radioactive Waste. Nagra Technical Report NTB 93-03. Nagra, Wettingen, Switzerland.

MILLER, W.M., CHAPMAN, N.A., McKINLEY, I.G., SMELLIE, J.A.T. & ALEXANDER, W.R. (2000): Geological disposal of radioactive wastes and natural analogues. Pergamon, Amsterdam, The Netherlands.

MILNER, C.R. & CHRISTOFI, N. (1985): A microbial examination of groundwater from the Grimsel Test Site (Appendix). In: WEST, J.M. & GROGAN, H. (eds.): Microbiological research relevant to the Swiss Radioactive Waste Disposal Programme – A Review performed by potential contractors. Unpubl. Nagra Internal Report. Nagra, Wettingen, Switzerland.

MÖRI, A., FRIEG, B., OTA, K. & ALEXANDER, W.R. (eds.) (2001a): Grimsel Test Site – Investigation Phase IV (1994-1996): The Nagra-JNC in situ study of safety relevant radionuclide retardation in fractured crystalline rock III: the RRP project final report. Nagra Technical Report NTB 00-07. Nagra, Wettingen, Switzerland (*in press*).

MÖRI, A., SCHILD, M., SIEGESMUND, S., VOLLBRECHT, A., ADLER, M., MAZUREK, M., OTA, K., HAAG, P., ANDO, T. & ALEXANDER, W.R. (2001b): Grimsel Test Site – Investigation Phase IV (1994-1996): The Nagra-JNC in situ study of safety relevant radionuclide retardation in fractured crystalline rock IV: The in situ study of matrix porosity in the vicinity of a water-conducting fracture. Nagra Technical Report NTB 00-08. Nagra, Wettingen, Switzerland (*in press*).

MÖRI, A., GECKEIS, H., MISSANA, T., DURO, L., GUIMERÁ, J., OTA, K., SCHÜSSLER, W. & FIERZ, TH. (eds.) (2002): CRR Experiment Phase 1: Status Report. Unpubl. Nagra Internal Report. Nagra, Wettingen, Switzerland (*in press*).

MÜLLER, W.H. (1988): The Grimsel Test Site: Geological background of the area and special aspects of water flow. Nagra Bulletin Special Edition 1988, 13-20. Nagra, Wettingen, Switzerland.

NAGRA (1985): Grimsel Test Site – Overview and Test Programs. Nagra Technical Report NTB 85-46. Nagra, Wettingen, Switzerland.

NAGRA (1994): Kristallin-I Safety Assessment Report. Nagra Technical Report NTB 93-22. Nagra, Wettingen, Switzerland.

NEA (1983): Proc. NEA Workshop Sorption Modelling and Measurement for Nuclear Waste Disposal Studies. OECD/NEA, Paris, France.

NEUZIL, C.E. (1994): How permeable are clays and shales? Water Resour. Res. 30/2, 145-150.

NIVA, B., OLSSON, O. & BLÜMLING, P. (1988): Grimsel Test Site – Radar crosshole tomography with application to migration of saline tracer through fracture zones. Nagra Technical Report NTB 88-31. Nagra, Wettingen, Switzerland.

NOELL, U. & ZÜRN, W. (1991): Detaillierte Interpretation der Neigungsmessungen im Felslabor Grimsel. Unpubl. Nagra Internal Report. Nagra, Wettingen, Switzerland.

OHSE, W. (1983): Lösungs- und Fällungserscheinungen im System oberflächennahes unterirdisches Wasser / gesteinsbildende Minerale – Eine Untersuchung auf Grundlage der chemischen Gleichgewichts-Thermodynamik. Ph.D. Thesis, Christian Albrecht University, Kiel, Germany.

OTA, K., ALEXANDER, W.R., SMITH, P.A., MÖRI, A., FRIEG, B., FRICK, U., UMEKI, H., AMANO, K., COWPER, M.M. & BERRY, J.A. (2001): Building confidence in radionuclide transport models for fractured rock: The Nagra/JNC radionuclide retardation programme. Sci. Basis Nucl. Waste Manag. (*in press*).

PAHL, A., BRÄUER, V., HEUSERMANN, St., KILGER, B. & LIEDTKE, L. (1986): Results of Engineering Geological Research in Granite. Bull. Int. Assoc. Eng. Geol. 34, 59-65.

PAHL, A., HEUSERMANN, St., BRÄUER, V. & GLÖGGLER, W. (1989): Grimsel Test Site – Rock stress investigations. Nagra Technical Report NTB 88-39E. Nagra, Wettingen, Switzerland.

PAHL, A., LIEDTKE, L., NAUJOKS, A. & BRÄUER, V. (1992): Grimsel Test Site – Fracture System Flow Test. Nagra Technical Report NTB 91-01E. Nagra, Wettingen, Switzerland.

PATE, S.M., McKINLEY, I.G. & ALEXANDER, W.R. (1994): Use of Natural Analogue Test Cases to evaluate a new Performance Assessment TDB. CEC Report EUR 15176EN, Brussels, Belgium.

PINGITORE, N.E. (1986): Modes of coprecipitation of Ba^{2+} and Sr^{2+} with calcite. In: DAVIS, J.A. & HAYES, K.F. (eds.): Geochemical Processes at Mineral Surfaces. Am. Chem. Soc. Symposium Series 323, 574-586. ACS, Washington, D.C.

PTAK, T. & TEUTSCH, G. (1994): A comparison of investigation methods for the prediction of flow and transport in highly heterogeneous formations. In: DRACOS & STAUFFER (eds.): Transport and Reactive Processes in Aquifers, 1994 Balkema, Rotterdam.

READ, D. (1992): Geochemical modelling of uranium redistribution in the Osamu Utsumi mine, Poços de Caldas. J. Geochemical Exploration 45, 503-520.

READ, D., WILLIAMS, D.R. & LIEW, S.K. (1987): A coupled approach to radioelement migration modelling in the United Kingdom. In: TSANG, C.F.: Coupled Processes Associated with Nuclear Waste Repositories, 304-324. Academic Press, San Diego.

SÁNCHEZ-VILA, X. & CARRERA, J. (1995): Una ecuación alternativa para el transporte de solutos en medio heterogéneo. In: Proc. VI Simposio de Hidrogeología. Hidrogeología y Recursos Hidraulicos XIX, 829-843. AEHS, 23-27 octubre, Sevilla.

SÁNCHEZ-VILA, X., MEIER, P.M. & CARRERA, J. (1999): Pumping tests in heterogeneous aquifers: An analytical study of what can be obtained from their interpretation using Jacob's method. Water Resour. Res. 35/4, 943-952.

SCHNEEFUSS, J., GLÄSS, F., GOMMLICH, G. & SCHMIDT, M. (1989): Grimsel Tests Site – Heater Test / Final Report. Nagra Technical Report NTB 88-40E. Nagra, Wettingen, Switzerland.

SELROOS, J.O. (1996): Mass transfer effects on tracer tests conducted in a heterogeneous rock fracture. Nordic Hydrology 27/4, 215-230.

SERNE, R.J. (1992): Conceptual adsorption models and open issues pertaining to performance assessment. In: Radionuclide sorption from the safety evaluation perspective: Disposal of radioactive waste. Proc. of a NEA Workshop, Interlaken, Switzerland, 16 – 18 October 1991, 237-282. OECD/NEA, Paris, France.

SMITH, P.A. (1991): Modelling of Laboratory High-Pressure Infiltration Experiments. Nagra Tech. Report NTB 91-33, Nagra, Wettingen, Switzerland; PSI Report 116, Paul Scherrer Institute, Würenlingen and Villigen, Switzerland.

SMITH, P.A., ALEXANDER, W.R., KICKMAIER, W., OTA, K., FRIEG, B. & McKINLEY, I.G. (2001): Development and testing of radionuclide transport models for fractured rock: Examples from the Nagra/JNC Radionuclide Migration Programme in the Grimsel Test Site, Switzerland. J. Contam. Hydrol. 47, 335-348.

SPOSITO, G. (1986): Distinguishing adsorption from surface precipitation. In: DAVIS, A. & HAYES, K.F. (eds.): Geochemical Processes at Mineral Surfaces. Am. Chem. Soc. Symposium Series 323, 217-229. ACS, Washington, D.C., USA.

STALDER, H.A. (1981): Sondierbohrungen Juchlistock-Grimsel: Mineralogisch-petrographische Untersuchungen. Unpubl. Nagra Internal Report. Nagra, Wettingen, Switzerland.

STECK, A. (1968): Die alpidischen Strukturen in den zentralen Aaregraniten des westlichen Aaremassivs. Eclogae geol. Helv. 61, 19-48.

STIESS, H. (1990): Berechnungen zum Wärme-, Stoff-, und Nuklidtransport in einer Einzelkluft mit Hilfe von NAMMU: Theoretische Grundlagen, Verifikation und Berechnung der Wärmeausbreitung in einem zweidimensionalen Kluft-Matrix-System. Unpubl. Nagra Internal Report. Nagra, Wettingen, Switzerland.

STRELTSOVA, T.D. (1988): Well Testing in Heterogeneous Formations. John Wiley, New York, USA. 413 pp.

THEIS, C.V. (1935): The relation between the lowering of the piezometric surface and the rate and duration of discharge of a well using groundwater storage. Eos Trans. AGU 16, 519-524.

UMEKI, H., HATANAKA, K., ALEXANDER, W.R., McKINLEY, I.G. & FRICK, U. (1995): The Nagra/PNC Grimsel Test Site Radionuclide Migration Experiment: Rigorous Field Testing of Transport Models. Sci. Basis Nucl. Waste Manag. XVIII, 427-434.

VANDERGRAAF, T., TICKNOR, K.V. & MELNYK, T.W. (1992): The selection and use of a sorption database for the geosphere model in the Canadian nuclear fuel waste management program. In: Radionuclide sorption from the safety evaluation perspective: Disposal of radioactive waste. Proc. of a NEA Workshop, Interlaken, Switzerland, 16 – 18 October 1991, 81-120. OECD/NEA, Paris, France.

VOBORNY, O., ADANK, P., HÜRLIMANN, W., VOMVORIS, S. & MISHRA, S. (1991): Grimsel Test Site – Modelling of groundwater flow in the rock body surrounding the underground laboratory. Nagra Technical Report NTB 91-02. Nagra, Wettingen, Switzerland.

WARREN, J.E. & PRICE, H.S. (1961): Flow in heterogeneous media. Soc. Pet. Eng. J. I, 153-169.

WATANABE, K. (1991): Evaporation Measurements in the Grimsel Test Site. Unpubl. Nagra Internal Report. Nagra, Wettingen, Switzerland.

WBK Westfälische Berggewerkschaftskasse (1988): Felslabor Grimsel – Seismische Durchschallungstomographie. Nagra Technical Report NTB 88-06. Nagra, Wettingen, Switzerland.

WERNLI, B., BAJO, C. & BISCHOFF, K. (1984): Bestimmung der Sorptionskoeffizienten von Uran(VI) an Grimsel- und Böttsteingranit. Unpubl. PSI Internal Report, Paul Scherrer Institute, Würenlingen and Villigen, Switzerland.

WYSS, E. (1989): Felslabor Grimsel – Hydrogeologische Untersuchungen zur Bestimmung hydraulischer Potentiale. Nagra Technical Report NTB 89-01. Nagra, Wettingen, Switzerland.

WYSS, E. (1990): FLG Migrationstest: Drei Beispiele für das weitere Verständnis des hydraulischen Verhaltens. Unpubl. Nagra Internal Report. Nagra, Wettingen, Switzerland.

YEH, G.T. & TRIPATHI, V.S. (1989): A critical evaluation of recent developments in hydrochemical transport models of reactive chemical components. Water Resour. Res. 25, 93-108.

APPENDIX 1: CHARACTERISATION OF HETEROGENEITY IN THE MI EXPERIMENTAL SHEAR ZONE USING HYDROGEOLOGICAL TEST DATA

P.M. Meier

A1.1 Introduction

The original hydrogeological characterisation of the site was carried out in the mid- to late-eighties and so, during the RRP project, it was decided to carry out additional work that would take into account the advances in both measurement techniques and hydrogeological modelling. This section summarises the main report on this work (MEIER 2002) along with additional information from MEIER (1997) and MEIER et al. (1997).

The purpose of the work was to characterise the heterogeneous transmissivity and background flow field of the MI shear zone, both of which must be taken into account in the tracer test analysis (or at least, the decision to neglect them must be justified). SELROOS (1996) indicates that, given only a single experimental breakthrough curve, it may be impossible to discriminate between the effects of heterogeneity and matrix diffusion on the tailing. In fact, SÁNCHEZ-VILA & CARRERA (1995) use a matrix diffusion term to simulate the effect of heterogeneity.

The work reported here uses a geostatistical inverse technique to model hydrogeological steady-state and transient data and to derive a transmissivity distribution, which is consistent with qualitative information. This model may, in the future, serve as a basis for modelling tracer tests. The data sets used for hydrogeological model calibration stem from an additional hydrogeological testing campaign performed in May 1996 to obtain high quality early time data (documented in detail by MEIER 1997).

The following sections consist of qualitative and quantitative information on the hydrogeological conditions within the experimental shear zone, an overview of the geostatistical inverse modelling approach, the conceptual model, the model structure, the calibration process and a discussion of the results.

A1.2 Qualitative and Quantitative Information

This section summarises qualitative and quantitative information pertinent to the development of the conceptual model and to the validation of the transmissivity distribution obtained from the geostatistical inverse model (see Section A1.3).

A1.2.1 Qualitative information

The MI shear zone can be described as an almost vertical two-dimensional feature on the scale of at least 100 m. Three tunnels intersect the shear zone almost perpendicularly, at the same level and at distances of 33 and 40 m from each other. The inflow to the experimental tunnel in the centre (the site of the MI) has slowly decreased during the past 10 years and was, in May 1996, approximately 400 ml/min, whereas the inflow to the other two tunnels is smaller than 1 ml/min.

BOSSART & MAZUREK (1991) investigated the microscopic arrangement of the flowpaths within the shear zone and found that water flow takes place preferentially within some few millimetre wide arrays of channels (partially filled with fault gouge) in an otherwise relatively impermeable mylonitic fabric. The fault gouge consists of highly porous, unconsolidated

micaceous material. They also found a high degree of pore connectivity parallel to the shear zone and that the three most important pore spaces (fault gouge, sheet silicate porosity, grain boundary porosity) are interconnected and basically represent an open porosity. Furthermore, the pore connectivity appears to be higher in the horizontal direction than in the vertical direction. However, the investigations were performed only on a small rock sample and it is not known whether this anisotropy is typical for the whole experimental shear zone or is only a local effect. The aperture distribution of the three most important pore types is assumed to be close to log normal, based on analyses of cores from boreholes VE88.001 – VE88.004, that penetrate a shear zone with similar pore types.

The extension of the above observations to larger scales is difficult from the limited observations at the GTS, so BOSSART & MAZUREK (1991) investigated another shear zone at the surface, which is genetically similar to the MI shear zone. They found that fault gouges can extend to several meters and are often interrupted. They are therefore not interconnected two-dimensionally. However, in three dimensions, interconnection of fault gouges seems to be likely. In any case, fault gouges are interconnected by grain boundary and sheet silicate pores. They also found that fault gouges are linked to zones of highly ductile shear deformation, consistent with findings at the GTS.

Hydrogeological evidence that connected highly transmissive zones ("channels") can extend horizontally over more than 20 m was obtained from the hydrogeological investigations for the FEBEX project. The nearly horizontal boreholes FBX 95.001 and FBX 95.002 intersect, at 10 and at 20 m respectively, a shear zone similar to the experimental shear zone. Pressure responses in one of these boreholes due to hydrogeological testing in the other were immediate and of the same magnitude as in the tested borehole (MEIER et al. 1995).

Based on the above observations, it is thought that channels are preferentially oriented (sub)parallel to the horizontal as a consequence of vertical displacements of the shear zone walls. It is noteworthy that BOSSART & MAZUREK (1991) estimated a minimum displacement of 2.9 m in the vertical direction during ductile deformation.

The MI shear zone was explored by eight boreholes, which were instrumented with packer systems to measure static pressures and to conduct hydrogeological and tracer tests. Figure A1.1 shows the shear zone plane with the borehole locations, the experimental tunnel (diameter 3.5 m) and the locations of the inflow measurements performed in May 1996 (T. FIERZ, pers. comm. 1996). Note that the inflow rates of more than 100 ml/min are measured with high precision, whereas the other flow rates are considered relatively rough estimates due to the practical difficulties involved with such measurements. Inflow rates at points other than those indicated in Figure A1.1 are considered to be lower than 0.05 ml/min/m tunnel wall.

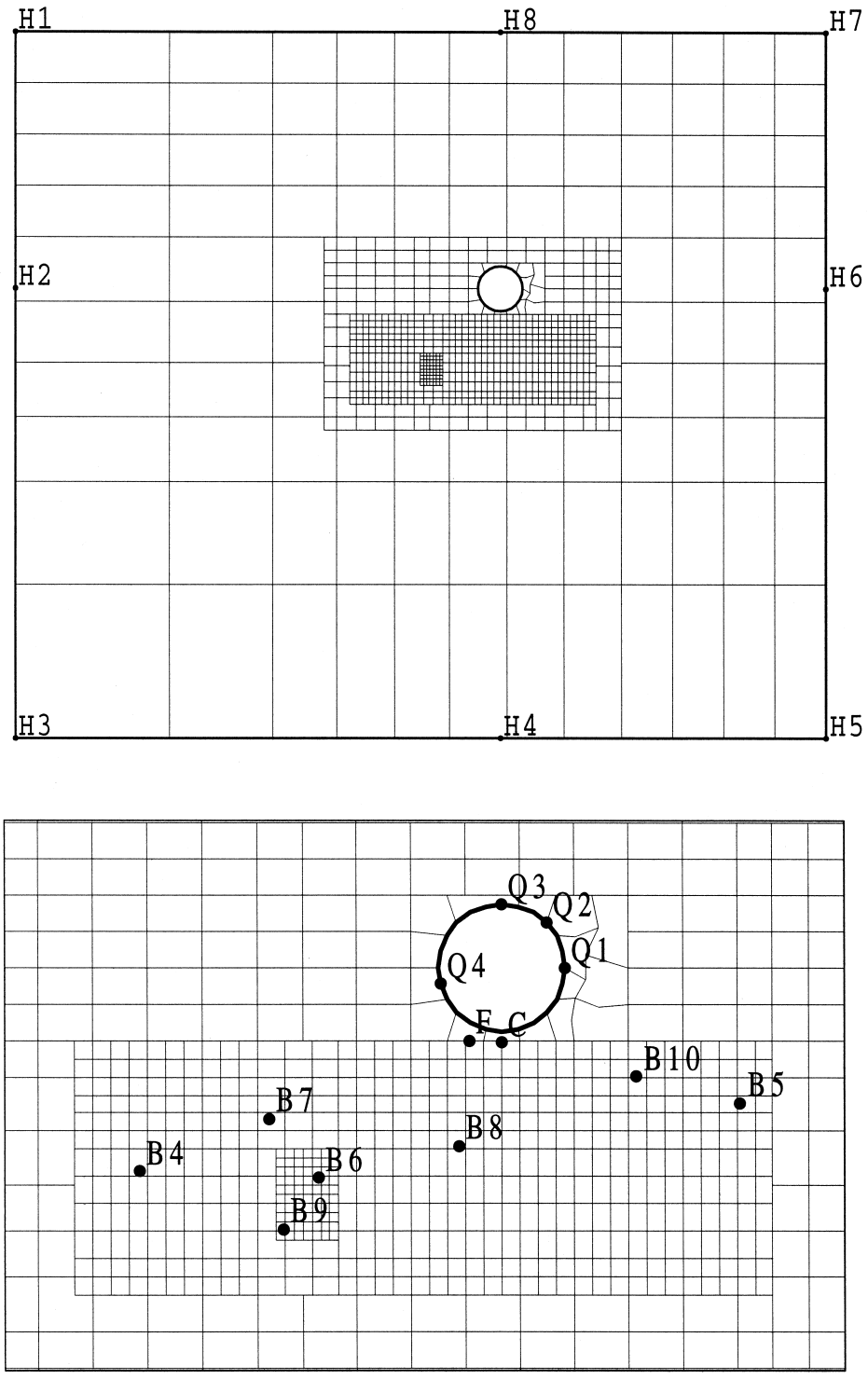

Fig. A1.1: The MI shear zone plane; upper part: full model domain with laboratory tunnel, transmissivity-(T-)zones and points of head (H) estimation (H1 – H8) in geo-statistical modelling (see Section A1.3), lower part: zone of tracer tests with T-zones, boreholes with T- and H-data (B4 – B10)

Note that "B" stands for "BOMI", C, F correspond to short boreholes with only H-data and Q1 to Q4 designate inflow points with significant flow rates (Q1 = 150 ml/min, Q2 = 200 ml/min, Q3 = 30 ml/min, Q4 = 20 ml/min)

C and F are short (30 cm) boreholes drilled within the shear zone plane and discharge 600 ml/min each when opened separately (HOEHN et al. 1990). C and F had to be packed-off to prevent lowering of the hydraulic head in the experimental shear zone. This fact may indicate that C and F are connected with the parts of the shear zone contributing most to total inflow to the experimental tunnel. It is noteworthy that pressures in C and F were temporally higher than pressures in BOMI 87.008 and BOMI 87.010 and that pressures in C and F are varying with time and were strongly affected by drilling activities (HOEHN et al. 1990). The relatively high static pressure heads in C and F (varying between about 3.2 and 7.0 m) reveal a high head gradient next to the lower part of the experimental tunnel. This and the low inflow rates (not measured, but considered to be smaller than 1 ml/min) at the floor of the experimental tunnel indicate a low transmissivity zone between boreholes C and F and the experimental tunnel (although it should be noted that the existence of an unsaturated or partly saturated zone around the experimental tunnel is indicated by partially degassed water, see FRICK et al. 1992a). In summary, the hydrogeological conditions within the shear zone are rather complex and vary with time particularly in the vicinity of the experimental tunnel.

Dipole tracer tests with the conservative tracer uranine were successfully conducted (tracer recovery of more than 95 %, depending on β, the ratio of extracted to injected water flow rate) with the configurations BOMI 86.004 – BOMI 87.006, BOMI 86.004 – BOMI 87.009, BOMI 87.009 – BOMI 87.006, and BOMI 86.004 – BOMI 87.010 indicating relatively good connections between these boreholes (see Chapter 3). Monomodal or bimodal break-through curves were observed in the dipole flow field BOMI 86.004 – BOMI 87.006 depending on β. High β (narrow dipole flow field) resulted in monomodal break-through curves and small β in bimodal break-through curves. These differences have been postulated to be a result of transmissivity heterogeneity or channelled flow within the experimental shear zone (FRICK et al. 1992a).

Uranine concentration was measured downhole in BOMI 87.009 during the dipole tracer tests with the configuration BOMI 86.004 – BOMI 87.006. The peak arrival time at BOMI 87.009 is smaller than at BOMI 87.006. This fact might indicate a "banana" shaped dipole flow field BOMI 86.004 – BOMI 87.006 (FRICK et al. 1992a; cf. Figure 1.1).

A connection between BOMI 86.004/BOMI 87.009 and BOMI 86.005 was accidentally discovered during a dipole pre-test (FRICK 1988). Water (water *A*) with a different chemical composition from the shear zone water (water *B*) was injected with a flow rate of 0.5 l/min in BOMI 86.004 while BOMI 87.009 was allowed to flow freely with a decreasing flow rate from 2 to 1.7 l/min. One month later, almost undiluted water *A* was detected in BOMI 86.005, (whereas pure water *B* was found in BOMI 87.009) indicating that flow had been from BOMI 86.004 to BOMI 86.005 and not, as expected from BOMI 86.004 to BOMI 87.009.

A1.2.2 Quantitative Information from Additional Hydrogeological Testing

A campaign of additional hydrogeological testing was performed in May 1996 to obtain high quality early time data, which allow the characterisation of the heterogeneity of the flow field in the MI shear zone. This work is documented in detail by MEIER (1997).

Test strategy

A sequence of withdrawal tests with differing flow period durations (5 s, 100 s, 10 min, 120 min) and with subsequent pressure recoveries was performed in all of the boreholes (with exception of BOMI 87.007). The first flow period of 5 s is treated as a pulse withdrawal test.

The objective of the increasing flow periods and subsequent recovery periods (RW/RWS test sequences) is to increase gradually the radius of investigation of the tests. Each RW/RWS test sequence characterises, therefore, a certain area of the shear zone around the well. The heterogeneity of the shear zone can then be deduced from the differences of the hydrogeological parameter estimations obtained from each RW/RWS test sequence.

Another possible test strategy would have been to conduct only one "long-term" (pump duration 120 min) RW/RWS test sequence and to analyse different time periods of the pump test. This test strategy leads only to a minor saving in test time and has the disadvantage that the recovery periods (RWS) following the short pump tests are not obtained. Practice and theory show that precisely these recovery data are very sensitive to changes in the interpretation of flow models. The RWS periods of the short pump periods are considered important for the calibration of flow models of heterogeneous media.

Interpretation approach

Most analytical solutions for pumping test interpretation assume that the aquifer can be subdivided into, at most, two or three regions with uniform parameters (e.g. STRELTSOVA 1988, BUTLER 1988 and 1990, BUTLER & LIU 1991 and 1993). Although such configurations imply severe simplifications of the complex structure of real heterogeneous formations, they can nevertheless provide insights into the behaviour of the system as revealed in the drawdown curves. Research on transient radial flow in heterogeneous systems resembling real formations has been concerned with estimates of transmissivity from pumping tests and their relationship to statistical parameters of the heterogeneous transmissivity field using a numerical approach (WARREN & PRICE 1961, LACHASSAGNE et al. 1989, BUTLER 1991). These authors conclude that transmissivity values obtained from late time data, using standard analysis techniques and especially Jacob's method, are close to the geometric mean of the transmissivity fields and are a reasonable representation of transmissivity on the regional scale (assumed boundary effects are negligible). GÓMEZ-HERNÁNDEZ et al. (1995) simulate pumping tests in non-stationary anisotropic T fields and conclude that the simulated drawdown curves can be misinterpreted as typical responses from a variety of homogeneous aquifer conceptual models (e.g. leaky aquifers, double porosity systems etc). These findings have important implications for the log-log diagnostic analysis commonly used to identify flow regimes and conceptual models.

The interpretation approach for the additional hydrogeological test data analysis consisted of applying well known analytical solutions (COOPER & JACOB 1946, THEIS 1935, BREDEHOEFT & PAPADOPULOS 1980, BARKER 1988) developed for homogeneous media to the data from the highly heterogeneous experimental shear zone. Some of the tests were analysed with the code MARIAJ (CARBONELL & CARRERA 1992) using an automatic optimisation procedure (maximum likelihood theory) for data fitting and parameter estimation based on analytical solutions. MARIAJ allows for linear boundaries, anisotropy, skin and wellbore storage effects to be taken into account. The resulting estimates for transmissivity and storativity are then interpreted within the context of heterogeneity. MEIER et al. (1997 and 1999) investigate the definition of transmissivity and storativity estimates obtained from conventional Jacob's analysis in different types of heterogeneous media using a numerical approach and the most important findings of these studies are summarised in the following.

MEIER et al. (1999) show that applying Jacob's method to late time drawdown data at observation points results in a strong spatial variability of storativity estimates (S_{est}) and in an almost homogeneous spatial distribution of transmissivity estimates (T_{est}). This is in agreement with field observations at several field sites, including the experimental GTS shear zone. Their

numerical simulations indicate that S_{est} depends mainly on the connectivity between the well and the observation points but also on the transmissivities within a certain catchment area surrounding both, the well and the observation points. Non-uniformities near the well have no effect on T_{est}. However, S_{est} values vary strongly in the near well region. A well location within a zone of T greater than T_{est} results in S_{est} values considerably greater than formation S and vice versa. Test values obtained from Jacob's method under radial flow conditions are close to the effective transmissivity for uniform flow conditions for the area of influence of the pumping test in multi-lognormal and non-multilognormal T fields. MEIER et al. (1999) consider non-multiGaussian T fields, with well connected highly permeable zones, to be realistic conceptual models for most heterogeneous formations. Therefore, the above conclusion has two significant implications. First, Jacob's method does indeed work very well in most heterogeneous formations. Second, the concept of effective T can be applied beyond the uniform flow framework in which it is usually derived.

As an example, the first test case of MEIER et al. (1999) is examined allowing a visual interpretation of the pressure responses during a pumping test in heterogeneous media. Figure A1.2 shows a sub domain (100 by 100 units of lengths) of a larger heterogeneous input T-field, which is characterized by its geometric mean Tg = 1.0, ln(T)-variance σ^2_Y = 4.0, and correlation structure, which is chosen as spherical isotropic with an integral scale of 10 unit lengths. The "W" denotes the well, the black triangles and the numbers refer to the observation points at radial distances of 10 and 30 unit lengths, respectively. A pumping test was simulated with a finite element code. The simulated drawdown curves at these points and the corresponding drawdown curves for a homogeneous medium (T = 1.0, S = 1.0) are shown in Figure A1.3.

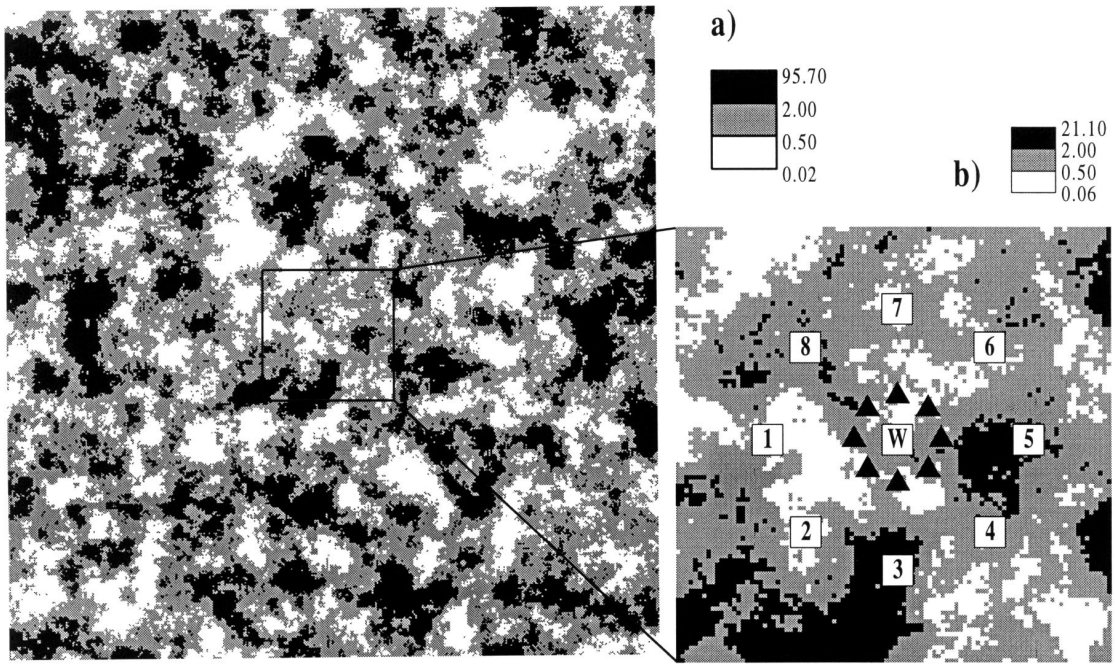

Fig. A1.2: Synthetic heterogeneous T-field

White represents low and black high T values, "W" denotes the pumping well, black triangles and the numbered squares indicate observation points at radial distances of 10 and 30 length units, respectively

All drawdown curves in Figure A1.3 exhibit late time slopes which are similar to the slope of the homogeneous case. The drawdown curves at the observation points 2 and 5 at radial distances of 30 unit lengths from the well illustrate the variability in early time pressure response in heterogeneous media. Observation point 2 and the well are connected through a zone of low T (white represents low T and black high T), which can easily be recognized in Figure A1.2. The drawdown response is therefore delayed with respect to the homogeneous case. Jacob's method yields S_{est} greater than real formation S because t_0, the intercept with the time axis of the straight line fitted through the late time data, is greater than for the homogeneous case. Observation point 5 and the well, however, are connected through a zone of high T. The drawdown response is therefore advanced with respect to the homogeneous case resulting in S_{est} smaller than real formation S.

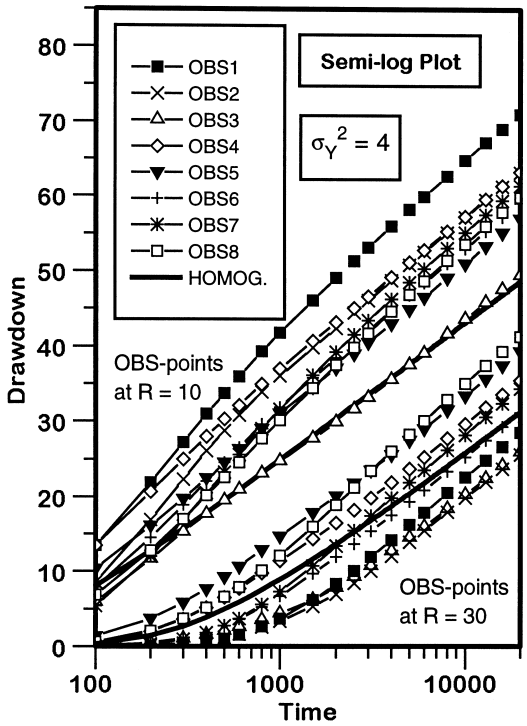

Fig. A1.3: Semi-log plot of the simulated drawdown at the observation points shown in Figure A1.2 for $\sigma^2_Y = 4.0$

Notice that late time slopes are approximately equal for all curves

Transmissivity distribution at the MI site

Transmissivity estimates are displayed in the upper part of Figure A1.4 for the single-hole tests and the cross-hole test performed by pumping in borehole BOMI 87.009. Transmissivity estimates derived from the short-term tests (pulse tests) range between 10^{-8} and 5×10^{-6} m^2/s revealing strong local heterogeneity. Cross-hole constant rate pumping tests of about two hours were performed in boreholes BOMI 86.004, 86.005, 87.006, 87.008 and 87.010 with pumping rates of 200 ml/min. Analysis of the late time data at pumping and at observation wells with Jacob's method resulted in a virtually constant T_{est} value for all tests of about 10^{-6} m^2/s, which is considered an effective transmissivity for the MI shear zone, and in a broad range of S_{est} from 4×10^{-7} to 5×10^{-2} (see lower part of Figure A1.4), consistent with the results from MEIER et al. (1999). A semi-log plot of the drawdown curves for the cross-hole pumping test in borehole

BOMI 87.009 is shown in Figure A1.5, as an example for the drawdown behaviour, which is similar to the other cross-hole tests. Straight lines with similar slopes start developing after about 3500 seconds for all drawdown curves. Boundary effects due to the influence of the experimental tunnel are surprisingly not observed before 25 hours of a long term pumping test (GEMPERLE 1989). This is possibly due to the presence of a zone of very low transmissivity between the boreholes and the experimental tunnel which is revealed by the inverse geostatistical modelling of the hydrogeological steady-state and transient data, presented below.

Note that the test strategy was changed for BOMI 87.007 and BOMI 87.011. Only very weak and noisy pressure responses were observed in BOMI 87.007 during the cross-hole tests. A qualitative pulse test analysis in BOMI 87.007 yielded a transmissivity smaller than 10^{-10} m^2/s. No pressure responses were observed in BOMI 87.011 during cross-hole testing. The static pressure head in BOMI 87.011 of 3.65 m is very low. A constant rate injection test was conducted in BOMI 87.011 with a flow rate of 200 ml/min for 10 minutes. Analysis of this test yielded a transmissivity of 2×10^{-6} m^2/s, a storativity of 1.5×10^{-1} and a wellbore storage constant of 1.5×10^{-7} m^3/Pa. Both the high wellbore storage constant and the high storativity may indicate the presence of entrapped air in the test interval, which is upwards inclined. Therefore the parameter estimates obtained for BOMI 87.011 are considered to be not reliable and data from BOMI 87.011 were not used for model calibration.

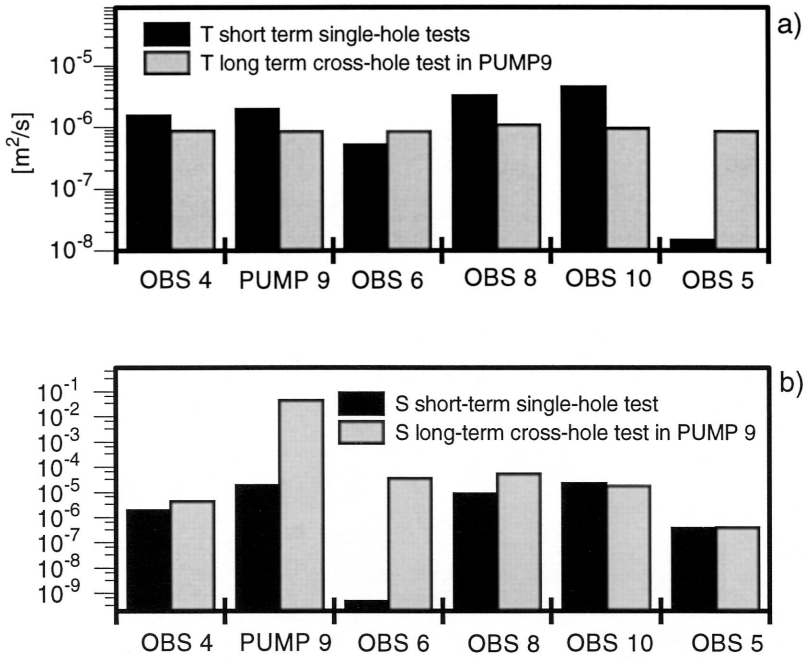

Fig. A1.4: Results from single-hole and cross-hole tests conducted in the experimental shear zone; upper part: transmissivity estimates, lower part: storativity estimates

Notice that transmissivities derived from short-term single-hole tests display a large variability in contrast to transmissivities from cross-hole tests, which remain virtually constant; however, storativities derived from single-hole and cross-hole tests span a wide range of values regardless of test duration

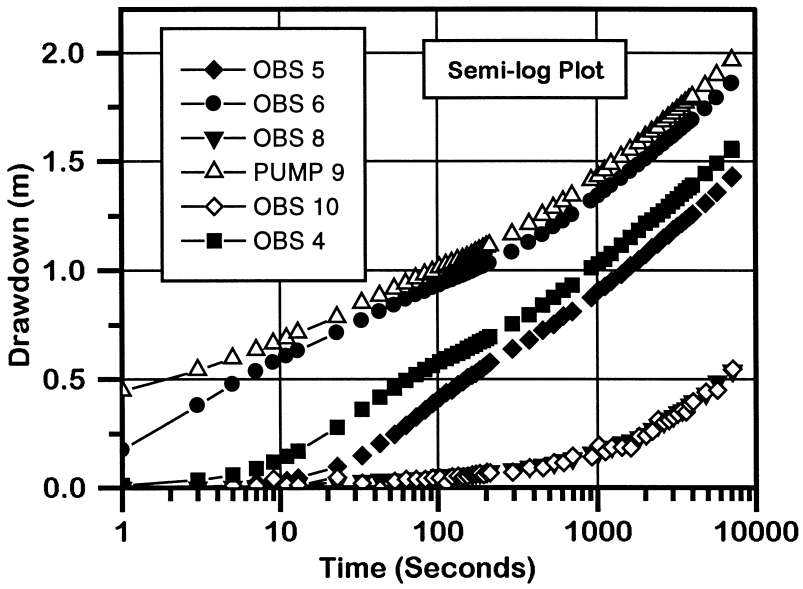

Fig. A1.5: Semi-log plot of the drawdown observed at the well and the observation points during the cross-hole test in BOMI 87.009

Storativity distribution at the MI site

Storativity estimates are displayed in the lower part of Figure A1.4 for the single-hole tests and the cross-hole test performed by pumping in borehole BOMI 87.009. The storativity estimates range from 5×10^{-10} to 10^{-5} for the short-term tests (pulse tests) and from 4×10^{-7} to 5×10^{-2} for the late-time data analysis using Jacob's method at pumping and observation wells. The strong variation of the S estimates derived from pulse tests is believed to reflect the uncertainties in estimating S from pulse tests, but may also reflect the interpretation problem inherent to using analysis methods that involve applying analytical solutions for homogeneous aquifers to field data from heterogeneous formations.

MEIER et al. (1999) and SÁNCHEZ-VILA et al. (1999) show that the storativity estimates obtained from Jacob's method at the well and at observation points depend on the heterogeneity of the transmissivity field. Storativity estimates obtained at a well located within a zone of high transmissivity are increased with respect to real aquifer storativity and vice versa. A good hydraulic connection between the well and an observation point results generally in a lower storativity estimate at the observation point and vice versa. This fact, together with the point transmissivity values, enables a qualitative description of the transmissivity distribution within the experimental shear zone to be made, since a relatively large number of cross-hole tests was conducted. Figure A1.6 shows the storativity estimates obtained at an observation point when pumping at the other wells and from single-hole tests.

The storativity estimates obtained from single-hole tests indicate that boreholes BOMI 87.008, 87.009 and 87.010 are located within zones of high transmissivity, whereas BOMI 86.004 and 87.006 lie within zones of intermediate transmissivity and BOMI 86.005 lies within a zone of low transmissivity. These conclusions are supported by the point transmissivity values obtained from pulse tests.

The storativity estimates obtained at BOMI 86.004, 87.006, 87.008, 87.009 and 87.010 when pumping in other wells (excluding pumping in BOMI 86.005, 87.007 and 87.011, for which no

pressure responses were observed in the observation wells) are within a relatively narrow range from 3×10^{-6} to 1×10^{-4}. A ranking of the hydraulic connectivity between these wells becomes therefore speculative. However, some speculative conclusions are provided in the following which may be used for comparison purposes with the results of the comprehensive flow model presented below.

Figure A1.6 may indicate that BOMI 87.009 is hydrogeologicalally better connected with BOMI 87.004 than with BOMI 87.006, that BOMI 87.004 is hydrogeologicalally slightly better connected with BOMI 87.009 than with BOMI 87.006 and that BOMI 87.006 is better connected with BOMI 86.004 than with BOMI 87.009. Such a connectivity pattern could explain the bimodal break-through curves observed during tracer tests between BOMI 86.004 and BOMI 87.006 with small β-values (ratio between extraction and injection rates). The observed "banana" shaped flow field (FRICK et al. 1992a) could possibly also be explained by this connectivity pattern considering also the influence of the natural flow field (stationary flow towards the experimental tunnel; all wells closed). The storativity estimates obtained for BOMI 86.005 may indicate a relatively low hydraulic connectivity with BOMI 87.010. In contrast BOMI 87.004 and 87.009 seem to be well connected with BOMI 86.005.

Note that storativity estimates obtained at observation points are practically identical to the storativity estimates obtained when interchanging well and observation well. For example, the storativity estimate obtained at BOMI 87.008 for pumping in BOMI 87.009 corresponds to the estimate obtained at BOMI 87.009 when pumping in BOMI 87.008. This is due to the principle of reciprocity which states that drawdown curves at observation points are identical when pumping well and observation well are interchanged (EARLOUGHER 1977). The small deviations from this principle in Figure A1.6 are due to the limited accuracy of the straight-line fitting procedure (Jacob's method) when determining the intercept with the time axis.

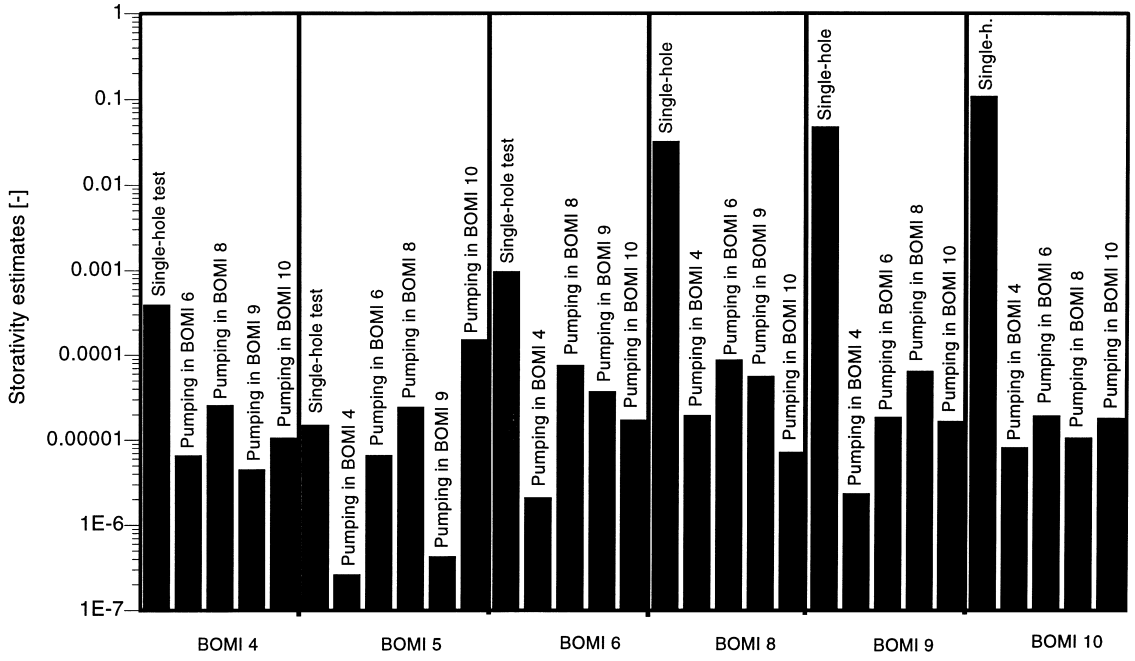

Fig. A1.6: Storativity estimates obtained from single-hole tests and at an observation point when pumping at the other wells

A1.3 Geostatistical Inverse Modelling

A1.3.1 Modelling Approach

Geostatistical inverse model is based on the maximum likelihood method (CARRERA & NEUMAN 1986), which can handle steady-state and transient information and allows the estimation of flow and transport parameters, all conditioned on transmissivity, head and concentration data. The formulations and the computational issues of the geostatistical approach (non-linear estimation) are explained in detail in CARRERA et al. (1995). Here, only the major practical steps are briefly described:

- the model domain is divided in a large number of T-zones
- prior information on the transmissivities of these zones and their covariance is obtained using block kriging
- non-linear estimation using the maximum likelihood method is performed with the finite element code TRANSIN-II (MEDINA et al. 1995)
- the calibration involves a trial-and-error procedure to select the best spatial correlation structure among a set of alternatives.

A1.3.2 Conceptual Model

The qualitative and quantitative information pertinent to the development of the conceptual model was described in Section A1.2. The model domain (Figure A1.1) is placed around the laboratory tunnel and extends in the vertical and the horizontal directions between 20 and 26 m towards the outer boundaries. The model domain consists of 769 T-zones, which are smaller in the region of the boreholes to resolve the heterogeneity in the region of the dipole tracer tests. Prior information on the transmissivities of the zones was obtained with block kriging using point T-values obtained from pulse tests in the boreholes shown in Figure A1.1 (MEIER 1997).

The two neighbouring tunnels are not included in the model domain to keep the computational effort as small as possible. Furthermore, no head or T- data are available next to these tunnels. However, their draining effect was considered by using eight initial head values at the corners and the mid-points of the sides (points H1 – H8 in Figure A1.1) from a sub-regional model (WYSS 1990) as prior information. The heads at these points were then estimated during steady-state model calibration. Heads in between were interpolated, which required defining 1-D elements of very large conductivity between each pair of boundary nodes.

The prescribed flow boundary conditions shown in Figure A1.1 (points Q1 – Q4) were used at the tunnel wall for steady-state model calibration. Zero drawdown conditions were imposed on all boundaries for transient model calibration.

The storativity was assumed to be homogeneous within the model domain, because it is virtually impossible to obtain storativity estimates from conventional hydrotest analysis and because porosity and compressibility, both controlling storativity, are not believed to vary within several orders of magnitude, as does transmissivity. A large variation in hydraulic conductivity and a comparatively small variation in porosity have been observed, for example, by GUIMERÁ & CARRERA (1997) for fractured rocks, PTAK & TEUTSCH (1994) for a porous alluvial aquifer, BACHU & UNDERSCHULZ (1992) for sandstone cores and NEUZIL (1994) for clays and shales.

A1.3.3 Calibration

The objective of the calibration was to obtain T-distributions that are consistent with head measurements obtained during different hydraulic conditions and that can be used as a possible basis for future tracer-test modelling.

The steps of the calibration process are:

(i) Assumption of a correlation structure for transmissivity in terms of a variogram model, a range and a sill; note that it was not possible to estimate a variogram because of the scarcity of the data (only seven point T-values were available).

(ii) Block kriging to obtain prior T-estimates for the T-zones shown in Figure A1.1 and their covariance matrix.

(iii) Non-linear estimation with code TRANSIN II using the prior T-estimates and their covariance matrix. Different hydraulic data sets corresponding to different hydraulic conditions and assumed boundary conditions were used. The first was a steady-state data set, consisting of the static heads (all boreholes closed) and inflow rates at the experimental tunnel. The remaining two were transient drawdown and recovery data sets from pumping tests with a flow period of 120 seconds at boreholes BOMI 87.009 and BOMI 87.006, respectively. The short flow period was chosen to avoid boundary effects, which can become significant for small storativity values. Estimation was carried out using only steady-state data, only transient data from the pumping test in BOMI 87.009 and all three data sets (steady-state and pumping tests in BOMI 87.009 and BOMI 87.006) simultaneously. The approach of CARRERA et al. (1995) was used to deal with multiple independent data sets. It consists of repeating the domain for each data set and calibrating the model with all of them simultaneously. In this manner, each point in reality is represented by up to three points in the model, one for steady state and one for each test.

(iv) Evaluation of the resulting T-distributions by (1), comparing them with the qualitative information discussed in Section A1.2.1 and (2), assessing their potential usefulness for future tracer test modelling.

The above steps were repeated for several correlation functions.

A1.4 Inverse Modelling Results

Several transmissivity distributions were obtained using different assumed correlation functions for transmissivity and boundary conditions (heads at the outer boundaries and inflow rates at the experimental tunnel). Preliminary attempts were made to model tracer break-through curves based on these distributions. It was found that boundary can have an important impact on the shape of the break-through curves. This introduces uncertainty into the interpretation of tracer tests, since no inflow measurements at the tunnel wall were made during the tracer tests, and thus the precise impact of the boundary condition is unknown.

Results of two representative cases with different correlation functions are presented below. A constant head (atmospheric pressure) boundary condition was imposed at the tunnel wall for tracer test modelling.

A1.4.1 Isotropic Correlation Function for Transmissivity

An isotropic correlation structure was assumed for block kriging using a spherical variogram with a range of 4 m and a sill (σ^2_{lnT}) of 36. Furthermore, low inflow rates at the experimental

tunnel, which was not measured, are assumed to be 0.05 ml/min/m tunnel wall. The prior estimates of the head values for the outer boundaries were taken from a sub-regional model (WYSS 1990).

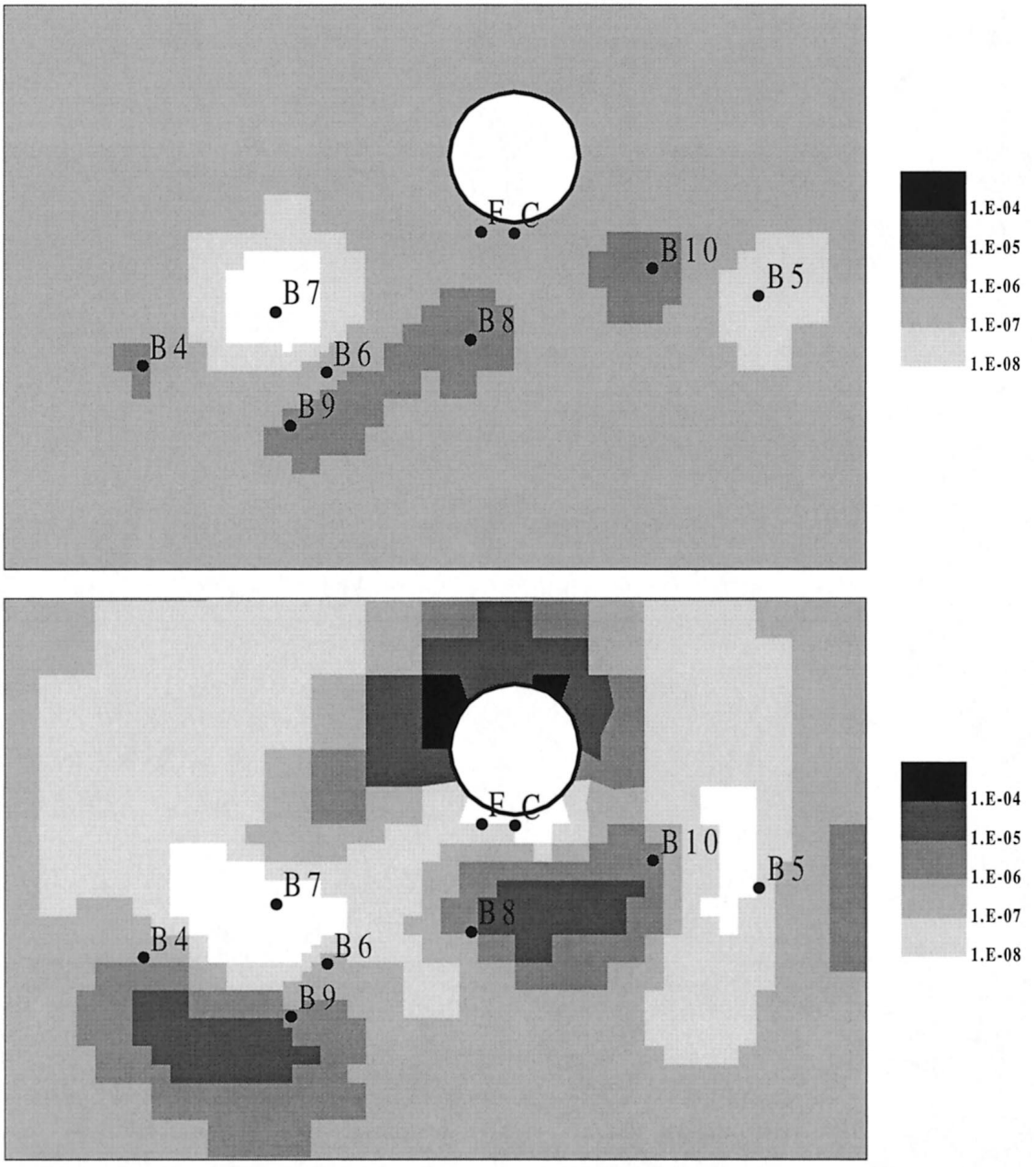

Fig. A1.7: Isotropic case, transmissivity distributions; upper part: block kriging, lower part: results from steady-state calibration

Results are summarised in terms of transmissivity maps for block kriging and the three calibration cases shown in Figures A1.7 and A1.8. Only the domain of interest is shown, which corresponds to the area shown in the lower part of Figure A1.1. The drawdown data fit obtained from simultaneous steady-state and transient calibration are shown in Figure A1.9. The data fits are considered excellent. Table A1.1 provides calculated and measured steady-state heads

obtained from the simultaneous calibration. The residuals h_c - h_m are small, with the exceptions of BOMI 87.010, C and F. It should be noted that measurements at C and F have a larger measurement error than the other measurements, as discussed in Section A1.2 of this Appendix. A storativity of 5×10^{-7} was obtained from model calibration.

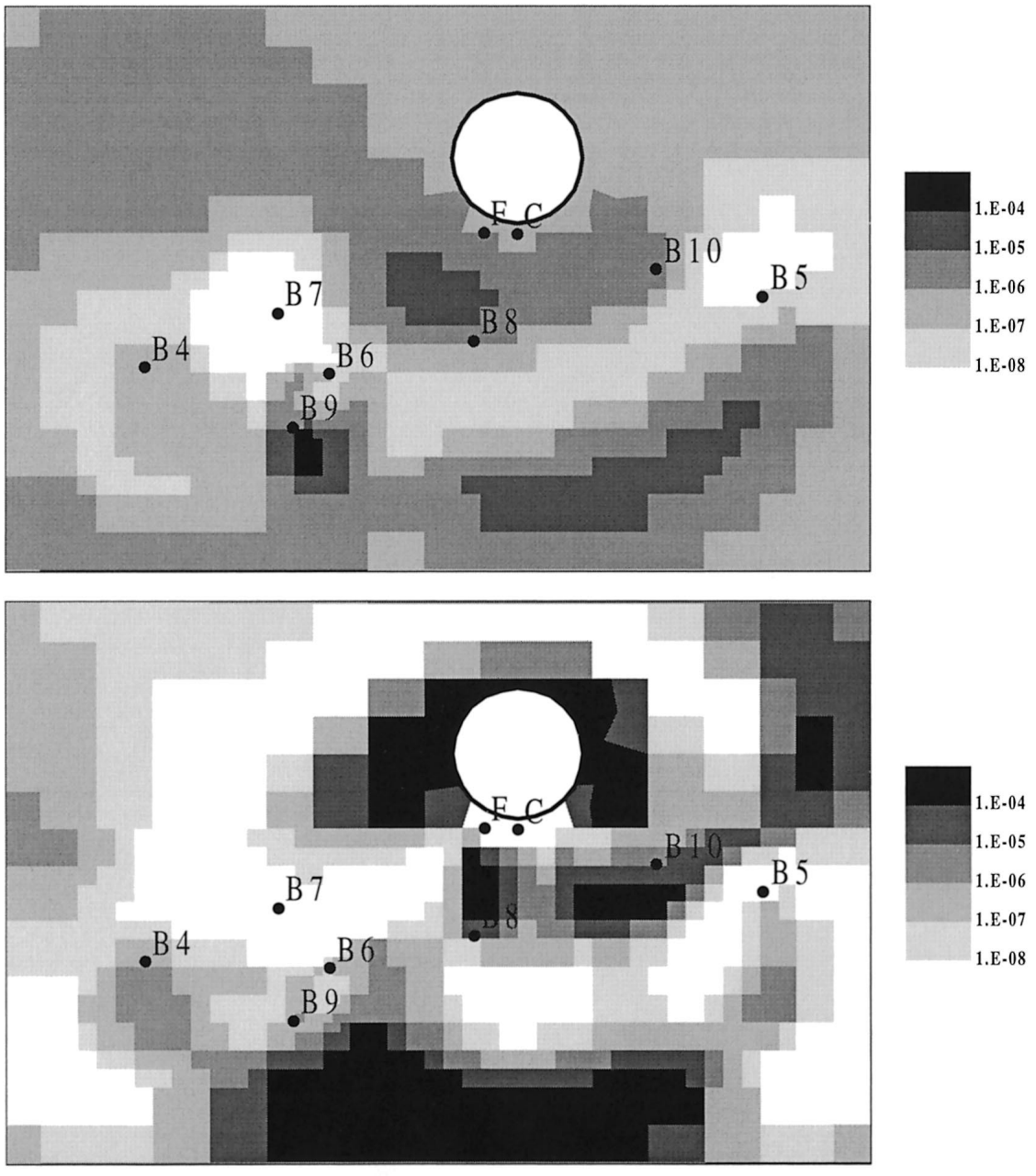

Fig. A1.8: Isotropic case, transmissivity distributions; upper part: results from transient calibration using drawdown data from the cross-hole pumping test in B9, lower part: results from simultaneous calibration using steady-state head data and transient drawdown data from cross-hole pumping tests in B6 and B9

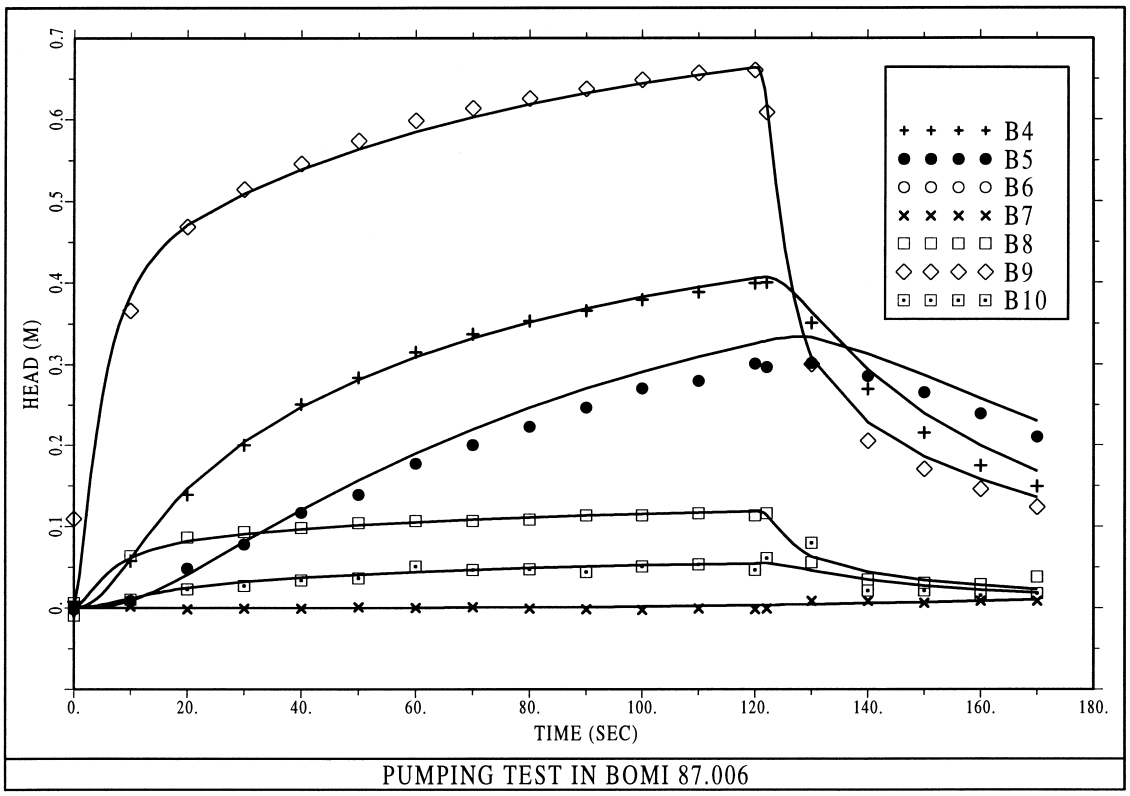

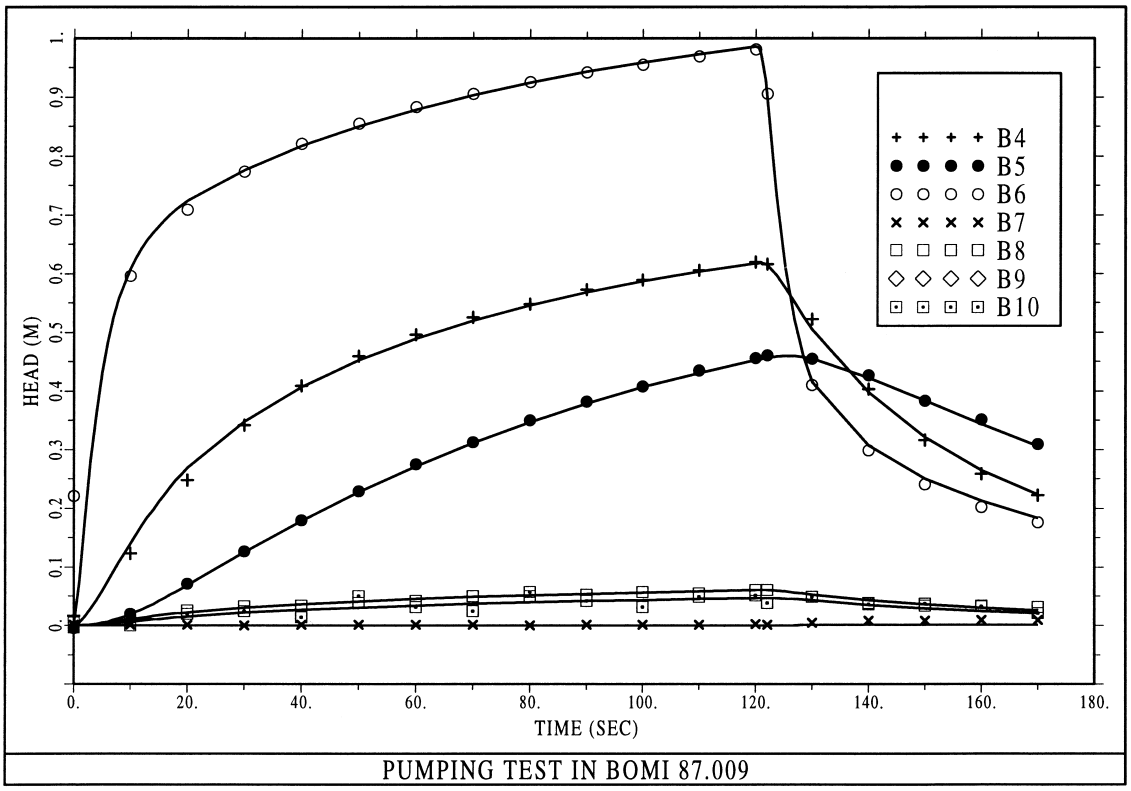

Fig. A1.9: Isotropic case, measured (symbols) and calculated (lines) drawdown data from simultaneous steady-state and transient calibration; upper part: cross-hole pumping test in B9, lower part: cross-hole pumping test in B6

Tab. A1.1: Calculated (h_c) and measured (h_m) steady-state heads (isotropic case)

Head [m]	BOMI 86.004	BOMI 86.005	BOMI 87.006	BOMI 87.007	BOMI 87.008	BOMI 87.009	BOMI 87.010	C	F
h_c	13.41	12.73	12.90	2.93	6.72	13.17	6.58	6.42	5.20
h_m	13.41	12.65	12.77	2.79	6.45	13.32	6.18	6.00	6.00
$h_c - h_m$	0.00	0.08	0.13	0.14	0.27	-0.15	0.40	0.42	-0.80

The lower part of Figure A1.7 and the upper part of Figure A1.8 indicate clearly that the steady-state and the transient data sets provide significantly different results. For example, the high head values at points C and F can only be explained by a zone of low transmissivity between them and the experimental tunnel. Such a zone is evident from the steady-state calibrations, but is not revealed by the calibration using only the transient data set. Instead, the upper part of Figure A1.8 indicates a relatively good hydraulic connection between borehole group BOMI 86.004 – BOMI 87.009 – BOMI 87.006 and the experimental tunnel which would cause an immediate and significant reduction of the inflow into the experimental tunnel after starting to pump in BOMI 87.009. However, only a small inflow reduction of about 2 % was observed within 10 minutes when pumping in BOMI 87.009 (GEMPERLE 1989). Furthermore, a quasi-steady-state regime is observed in BOMI 86.004, BOMI 87.009, BOMI 87.006 and BOMI 86.005 only after several weeks of pumping in BOMI 87.009, whereas steady-state conditions are reached within 3 days at BOMI 87.008 and BOMI 87.010 (GEMPERLE 1989). Another example is the high transmissive channel between borehole group BOMI 86.004 – BOMI 87.009 – BOMI 87.006 and borehole BOMI 86.005 shown in Figure A1.8. This channel is evident from the rapid pressure response in BOMI 86.005 when pumping in BOMI 87.009, BOMI 86.004 or BOMI 87.006 and its existence is corroborated by the accidental tracer dipole pre-test mentioned in Section A1.2 of this Appendix. However, such a channel is not revealed by the steady-state calibration results.

In summary, neither the calibration with only steady-state data nor the calibration with only transient data provide results which are consistent with all qualitative information. However, the results obtained from the simultaneous steady-state and transient calibration process are in good agreement with all available qualitative information and especially with the tentative description of the transmissivity distribution derived from the interpretation of the storativity estimates obtained from applying Jacob's method to late-time drawdown data (e.g. the discussion of storativity in Section A1.2.2). This indicates that an interpretation of storativity estimates obtained from Jacob's method can yield valuable qualitative information about heterogeneity.

The steady-state head field superimposed on the T-field obtained from simultaneous steady-state and transient calibration is shown in the upper part of Figure A1.10. The lower part of Figure A1.10 shows the tracer plume obtained from the simplifed[42] transport modelling of the dipole tracer test between BOMI 86.004 and BOMI 87.010. The tracer moves directly to the experimental tunnel without arriving at the extraction borehole BOMI 87.010, demonstrating a strong effect of the natural background flow and of the T-distribution in the vicinity of the experimental tunnel, and contrary to experimental observations (Chapter 3). This indicates that

[42] For this illustrative calculation, a highly simplified modelling approach was employed, that does not include matrix diffusion (unlike the models discussed in Chapters 6 and 7).

the T-field obtained assuming an isotropic correlation structure with an integral scale of 4 m can not be used as a basis for tracer test modelling.

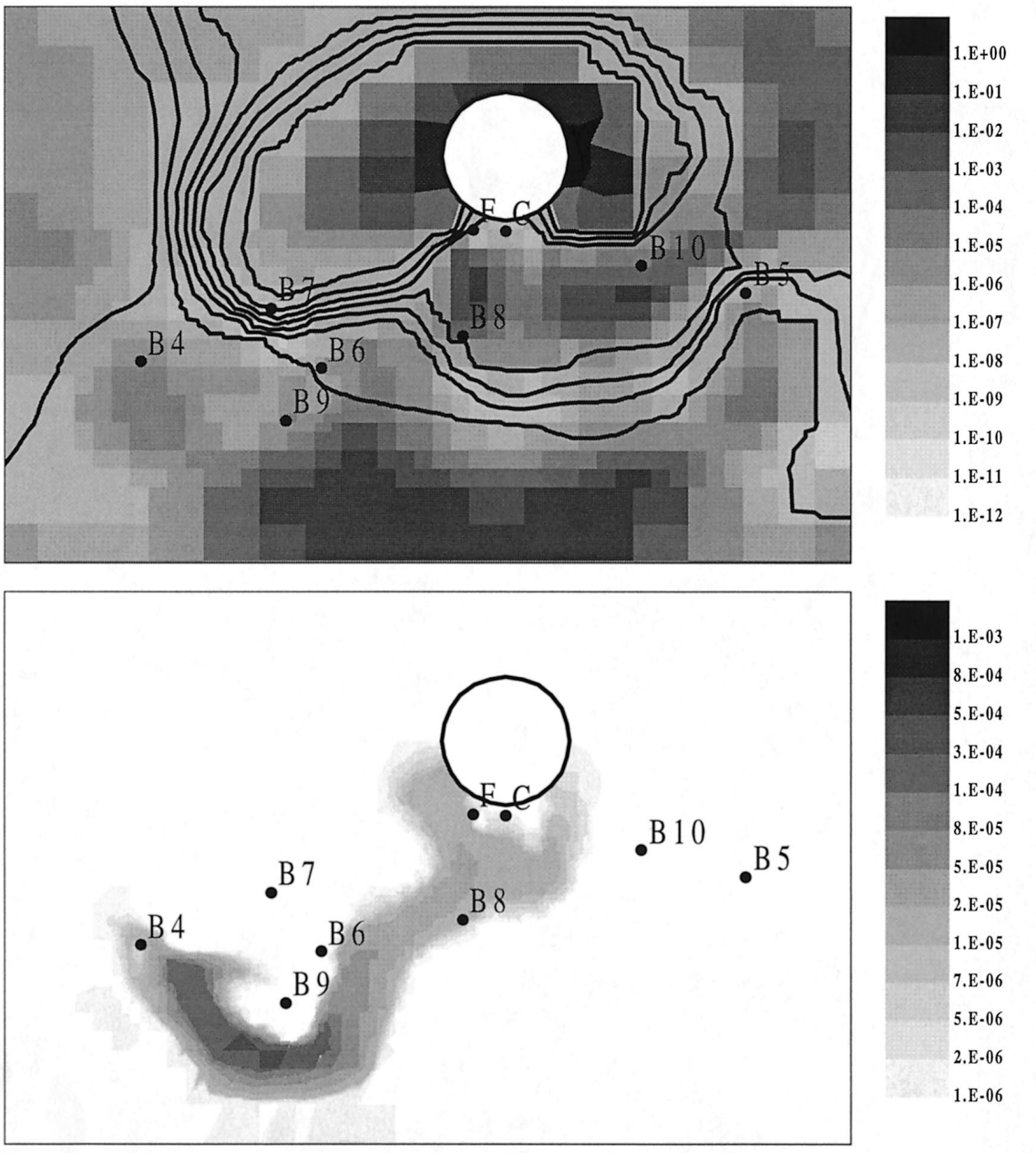

Fig. A1.10: Isotropic case; upper part: steady-state head field superimposed on T-field obtained from simultaneous steady-state and transient calibration, the head contour line next to the experimental tunnel indicates a head of 1 m and subsequent lines heads of 3, 5, 7, 9, 11, 13 and 15 m, lower part: tracer plume obtained for a tentative modelling of the dipole tracer test between B4 and B10

Other calibration cases with isotropic correlation structures but with different integral scales ranging from 2 to 12 m resulted in similar problems for modelling the tracer test between BOMI 86.004 and BOMI 87.010. It is intuitively evident that a zone of low transmissivity between

BOMI 87.007 and C is necessary to prevent a direct advective tracer flow into the experimental tunnel. Such a low transmissive zone can be produced using an anisotropic correlation structure and prior information on the T-distribution at the experimental tunnel, which is discussed in the next section.

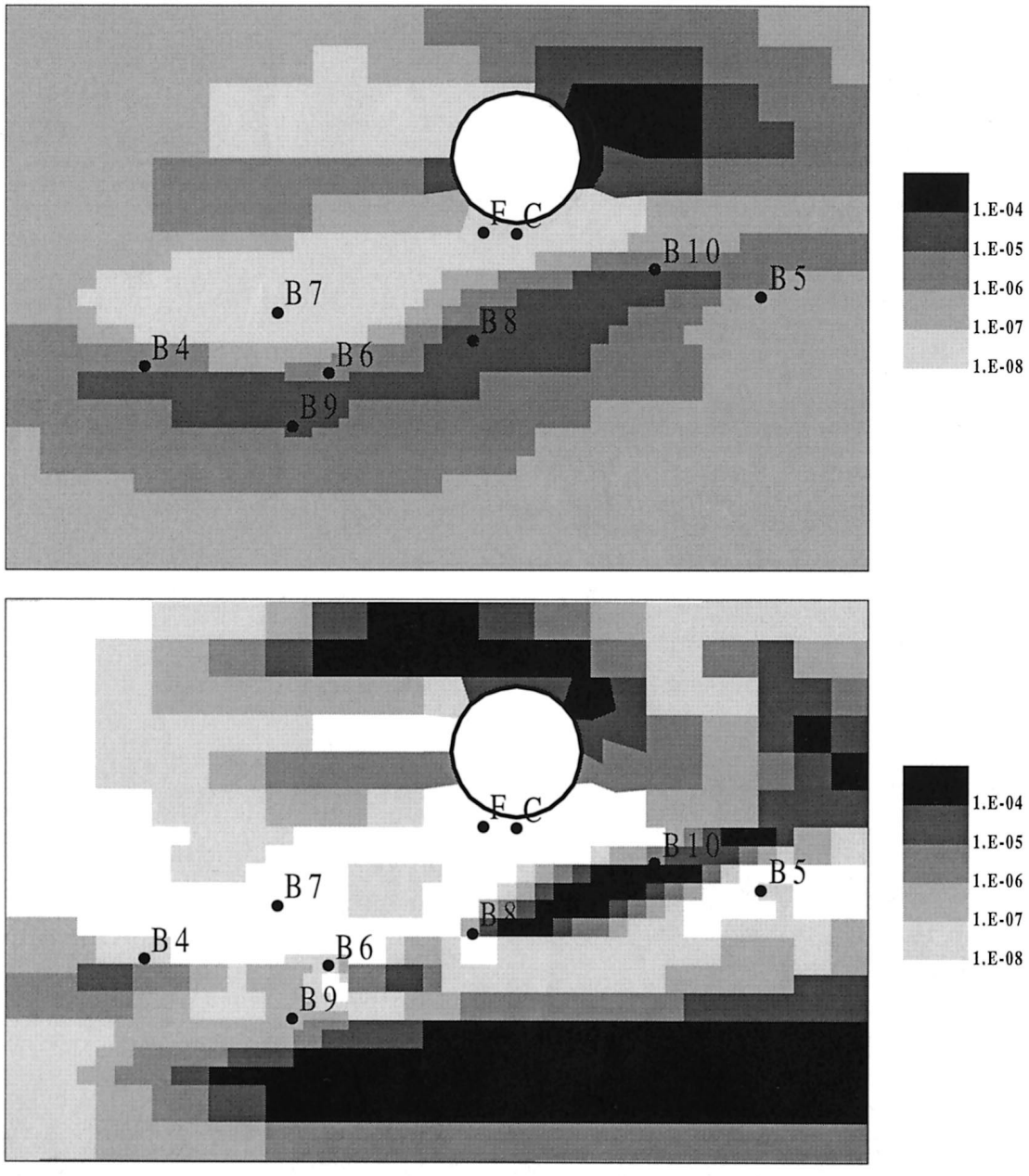

Fig. A1.11: Anisotropic case, transmissivity distributions; upper part: results from block kriging, lower part: results from simultaneous calibration using steady-state head data and transient drawdown data from cross-hole pumping tests in B6 and B9

A1.4.2 Anisotropic Correlation Function for Transmissivity

An assumed anisotropic correlation function can be based on the qualitative information on the preferred orientation of connected high transmissive zones (see Section A1.2.1). A spherical variogram with a sill (σ^2_{lnT}) of 100 and with ranges of 9.0 m in the horizontal and 2.5 m in the vertical direction was assumed. The estimated T-distribution obtained by block kriging is shown in the upper part of Figure A1.11. Note that, in this case, point T-values are also assumed for block kriging at the experimental tunnel corresponding to the inflow rates (high T-values at points with high inflow rates and vice versa) to stress the assumed correlation structure near the experimental tunnel. The differences of the assumptions between this case and the isotropic case can be clearly seen by comparing the T-fields obtained from block kriging (upper part of Figure A1.7 and upper part of Figure A1.11).

The T-distribution resulting from simultaneous steady-state and transient calibration is shown in the lower part of Figure A1.11. This T-distribution resembles the one obtained for the isotropic correlation function (lower part of Figure A1.8) and is also in agreement with all qualitative information already mentioned for the isotropic correlation function. The drawdown data fit obtained from simultaneous steady-state and transient calibration are shown in Figure A1.12. The quality of the data fits is excellent and is similar to that for the case of the isotropic correlation function. Table A1.2 provides calculated and measured steady-state heads which agree well with each other. Note that, in this case, it was assumed that head values at C and F are considerably lower than at BOMI 87.008 and BOMI 87.010 (see Section A1.2 for a discussion of the reliability of the head measurements at these locations). A storativity of 2.8×10^{-7} was obtained from model calibration, which is in good agreement with the isotropic case.

Tab. A1.2: Calculated (h_c) and measured (h_m) steady-state heads (anisotropic case)

Head [m]	BOMI 86.004	BOMI 86.005	BOMI 87.006	BOMI 87.007	BOMI 87.008	BOMI 87.009	BOMI 87.010	C	F
h_c	13.45	12.70	12.95	2.79	6.39	13.05	6.22	3.06	3.28
h_m	13.41	12.65	12.77	2.79	6.45	13.32	6.18	3.20	3.20
$h_c - h_m$	0.04	0.05	0.18	0.00	-0.06	-0.27	0.04	-0.14	0.08

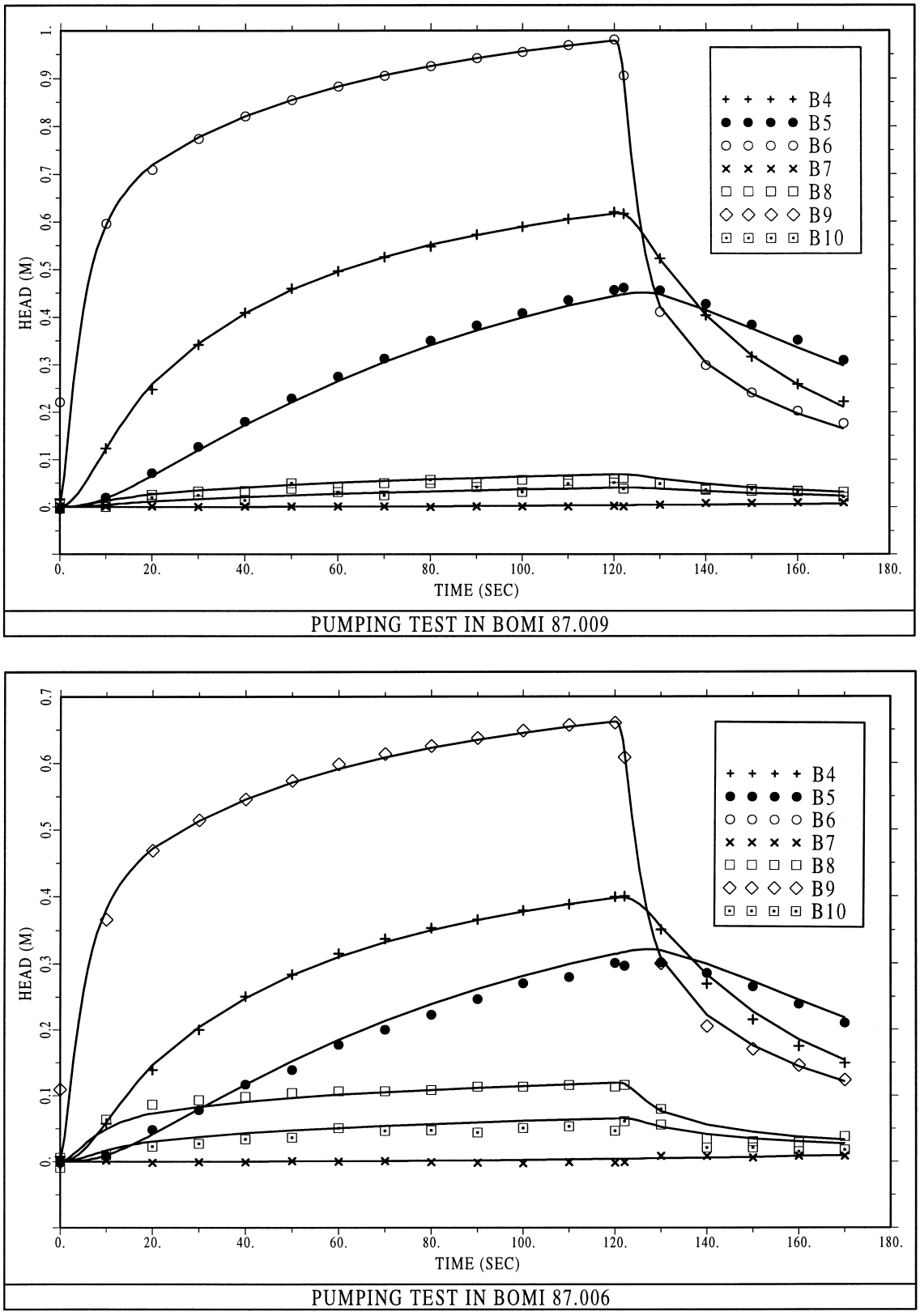

Fig. A1.12: Anisotropic case, measured (symbols) and calculated (lines) drawdown data from simultaneous steady-state and transient calibration; upper part: cross-hole pumping test in B9, lower part: cross-hole pumping test in B6

The steady-state head field superimposed on the T-field obtained from simultaneous steady-state and transient calibration is shown in the upper part of Figure A1.13.

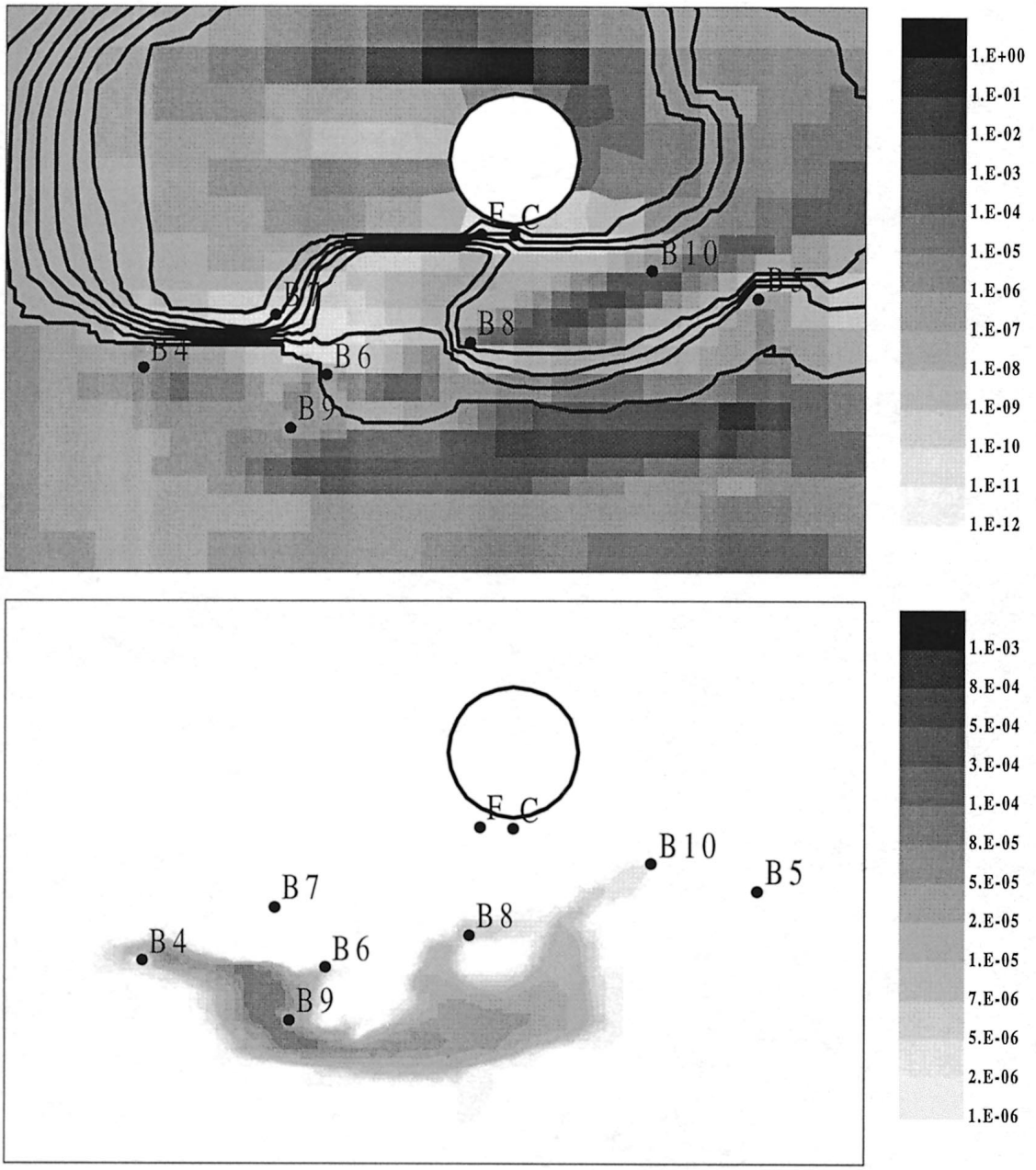

Fig. A1.13: Anisotropic case; upper part: steady-state head field superimposed on T-field obtained from simultaneous steady-state and transient calibration, the head contour line next to the experimental tunnel indicates a head of 1 m and subsequent lines heads of 3, 5 , 7, 9, 11, 13 and 15 m, lower part: tracer plume at an elapsed time of 6 hours obtained from modelling of the dipole tracer test between B4 and B10

The break-through curve for uranine in tracer test 78 between BOMI 86.004 and BOMI 87.010, was fitted using the same simplified transport model as for the isotropic case. The tracer plume and fitted break-through curve are shown in the lower part of Figure A1.13 and in Figure A1.14,

respectively. The quality of the fit is good and Figure A1.13 shows (in agreement with the observed good recovery of tracer) that the plume does not approach the tunnel wall. A longitudinal dispersivity of 0.27 m, a transversal dispersivity of 7.5×10^{-2} m and a porosity-thickness product of 8.6×10^{-4} m were obtained from the fit.

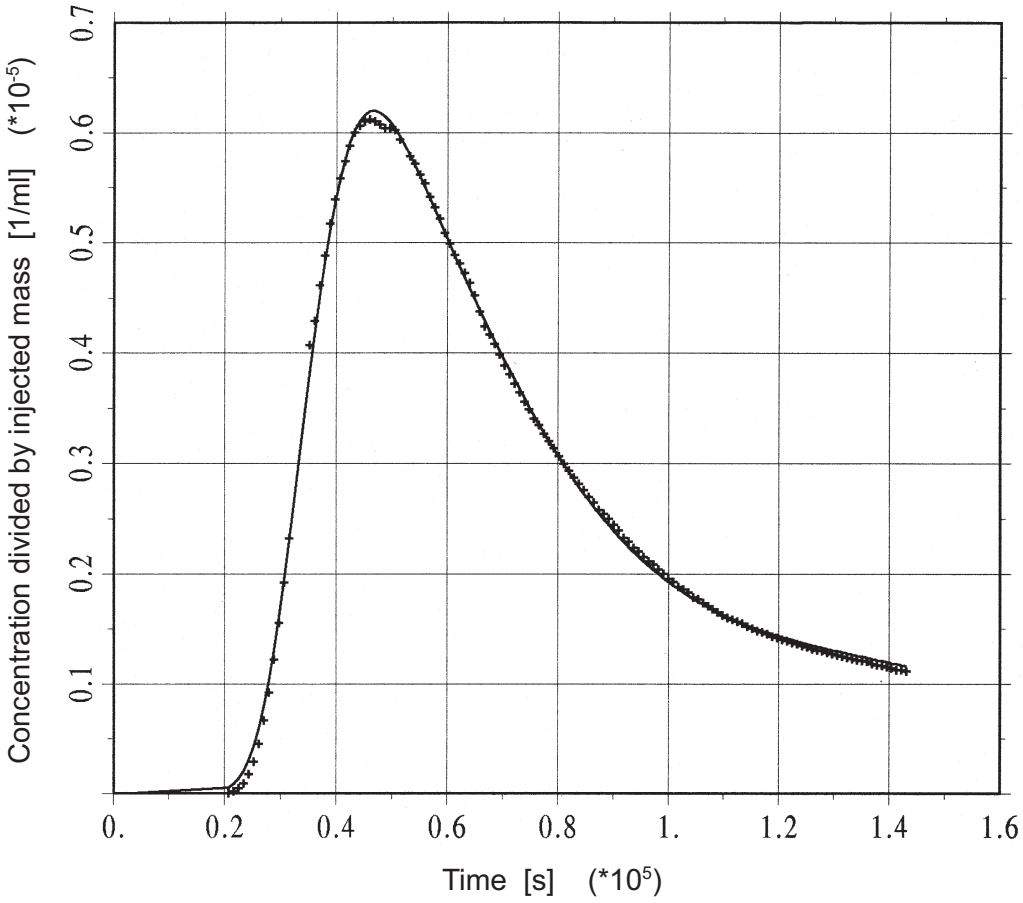

Fig. A1.14: Anisotropic case, measured (crosses) and calculated (line) break-through of uranine at the pumping well for the 14 m dipole flow field between BOMI 86.004 and BOMI 87.010

Table A1.3 indicates relatively large differences between calculated and measured steady-state heads at the boreholes for the dipole flow conditions. The estimated head values at the outer boundary are presented in Table A1.4, together with the initially assumed head values taken from WYSS (1990) and the values obtained from the simultaneous steady-state and transient calibration. The good agreement between the values of WYSS (1990) and the values obtained from the simultaneous steady-state and transient calibration, can be attributed to the fact that the model of WYSS (1990) was calibrated with steady-state head data during natural flow conditions. The relatively large differences between calculated and measured steady-state heads at the boreholes (Table A1.3) and the differences between heads at the boundaries during tracer test dipole steady-state conditions and the values obtained from the simultaneous steady-state and transient calibration (Table A1.4) could be due the fact that the outer boundary heads have

to change considerably for an adequate modelling of the dipole steady-state conditions. Note that the calculated inflow at the experimental tunnel during steady-state conditions is about 380 ml/min, whereas the natural (all boreholes closed) inflow at the experimental tunnel was about 450 ml/min at the time of tracer test run 78. The calculated inflow during dipole steady-state conditions is in agreement with the qualitative observations (Th. FIERZ, pers. comm. 1997) that no marked inflow rate changes took place when establishing the dipole tracer test fields.

Tab. A1.3: Calculated (h_c) and measured (h_m) steady-state heads during tracer test dipole steady-state flow conditions

Head [m]	BOMI 86.004	BOMI 86.005	BOMI 86.006	BOMI 87.007	BOMI 87.008	BOMI 87.009	BOMI 87.010	C	F
h_c	13.98	12.81	13.04	3.12	5.28	13.14	5.05	-	-
h_m	13.41	13.42	12.77	2.79	5.46	12.80	3.85	-	-
$h_c - h_m$	0.57	-0.61	0.27	0.33	-0.18	0.34	1.20	-	-

Tab. A1.4: Estimated steady-state heads at the points of the outer boundary shown in Figure A1.1 for different models and calibration cases

Head [m]	H1	H2	H3	H4	H5	H6	H7	H8
WYSS (1990)	20.00	17.00	19.50	15.00	15.00	15.00	18.00	17.00
St. & trans. calibration	20.20	17.07	19.30	14.89	14.86	14.94	17.93	17.05
Tracer calibration	20.16	16.85	19.05	14.75	14.36	12.42	17.82	16.99

An ultimate test of the anisotropic T-field shown in the upper part of Figure A1.15 is whether it can predict the break-though curve from a dipole flow field different to that used to derive transport parameters. For this exercise, a prediction was made of the break-through curve of tracer test 90 in the 4.9 m dipole flow field between BOMI 86.004 and BOMI 87.006.

Figure A1.15 shows that the predicted tracer break-through is retarded with respect to the measured tracer break-through. Some effects of heterogeneity in the transmissivity, not represented in the anisotropic T-field, cannot, however, be excluded. These aspects are further discussed in MEIER (2002).

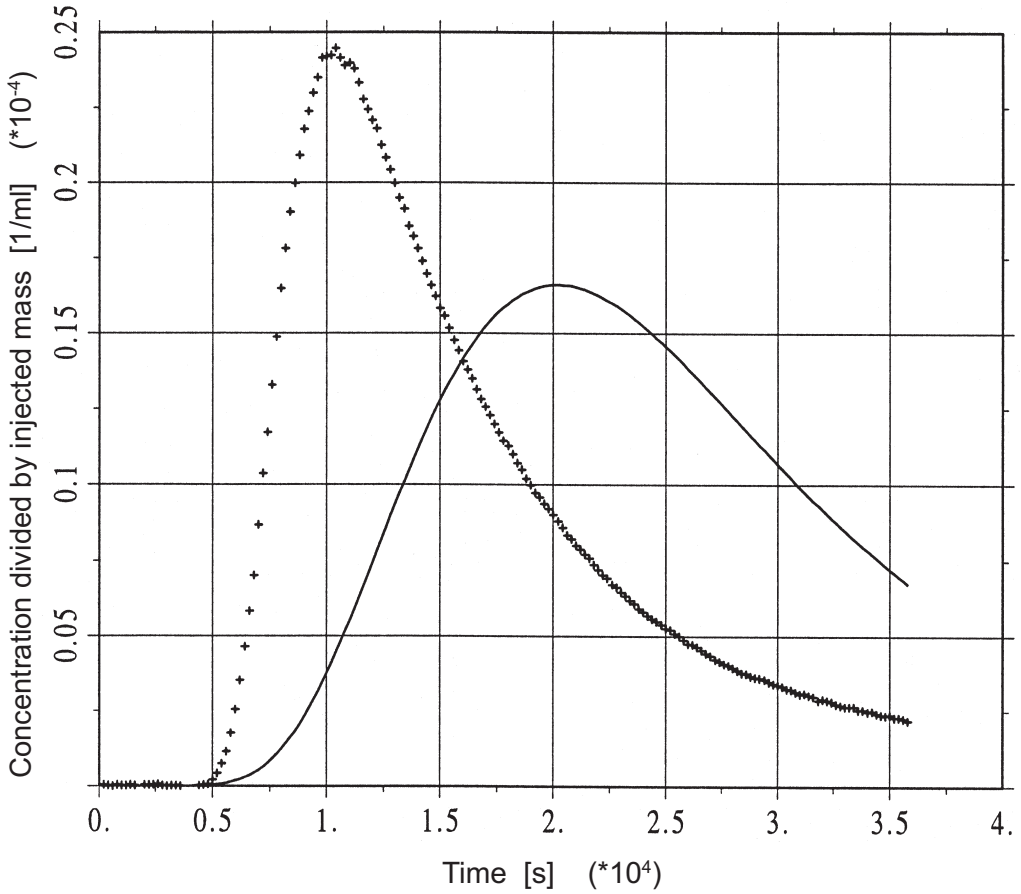

Fig. A1.15: Anisotropic case, measured (crosses) and predicted (line) break-through of uranine for the 4.9 m dipole field between BOMI 86.004 and BOMI 87.006 using the transport parameters obtained from the 14 m dipole tracer test

A1.5 Conclusions

The geostatistical inverse modelling of transient pumping tests and static pressure heads during "natural" flow conditions (all boreholes closed) yields T-distributions that are in good agreement with all qualitative information[43]. The T-distributions reveal the existence of channels within the experimental shear zone that are preferentially connected horizontally. This is in conceptual agreement with the findings from the microscopic investigations of BOSSART & MAZUREK (1991) and with hydraulic observations at another genetically similar shear zone at the GTS (MEIER et al. 1995). Further efforts should be made to characterise the shear zone at scales of tens of metres to reduce the uncertainty associated with the assumptions of correlation functions for transmissivity.

[43] Conventional hydrogeological tests provide valuable information on the transmissivity distribution within the experimental shear zone. The conventional Jacob's method applied to intermediate time (two hours) cross-hole pumping tests provides a robust estimation for the effective transmissivity of the experimental shear zone. In contrast, storativity estimates obtained from Jacob's method are strongly affected by the heterogeneity in transmissivity. However, storativity estimates provide valuable qualitative information on the connectivity between a pumping well and observation wells. Pulse tests provide point T-values, which are important input parameters for the geostatistical inverse model.

Only one T-field obtained with an anisotropic correlation function for transmissivity was suitable for modelling the dipole tracer test between BOMI 86.004 and BOMI 87.010 (14 m flow field). The breakthrough curve of uranine could be fitted with reasonable transport parameters. However, an attempt to predict the breakthrough curve for the smaller dipole flow field between BOMI 86.004 and BOMI 87.006 (4.9 m flow field) indicated that the simple model employed was inadequate, either because one or more relevant processes were omitted (matrix diffusion, see Chapters 6 and 7), or because of some remaining inaccuracy in the assumed anisotropic T-field.

APPENDIX 2: THE CATION-EXCHANGE MODEL

M.H. Bradbury and B. Baeyens

The surfaces of aluminosilicate minerals carry a permanent negative charge arising from isomorphic substitution of lattice cations by cations of a lower valence. Charge neutrality is maintained by the presence of an excess of cations in solution in close proximity to the surface. These cations, held around the outside of the aluminosilicate mineral structural units, "belong" to the surface and cannot be separated from it. They are, however, exchangeable and can undergo exchange reactions with ions in the aqueous phase. The cation exchange capacity[44] (*CEC*) of a solid is defined as the total quantity of cations sorbed exchangeably per unit mass. The *CEC* is usually expressed on an equivalent scale: for example, milliequivalents per gramme (meq g^{-1}). The *CEC* of a material is not a unique value, but varies, to a greater or lesser extent, with pH, particle size and the method of measurement (GRIM 1953).

Considering the general case of a cation B, valence Z_B, in the aqueous phase exchanging with cation A, valence Z_A, bound to the aluminosilicate mineral surface, the exchange reaction can be written as follows:

$$Z_B . A - Clay + z_A . B \Leftrightarrow Z_A . B - Clay + z_B . A \qquad \text{(A2.1)}$$

Cation exchange reactions are reversible, fast and stoichiometric. In the case of heterovalent exchange, the latter characteristic arises from the electroneutrality condition. A mass-action relation is normally used to describe the reaction in terms of a so-called selectivity coefficient, K_C, which is given by:

$${}^{B}_{A}K_C = \frac{N_B^{Z_A}}{N_A^{Z_B}} \cdot \frac{\alpha_A^{Z_B}}{\alpha_B^{Z_A}} \qquad \text{(A2.2)}$$

a_A and a_B are the solution activities of cations A and B, respectively. N_A and N_B are equivalent fractional occupancies, defined as the equivalents of A (or B) sorbed, per unit mass, divided by the cation-exchange capacity (*CEC*), in equivalents per unit mass:

$$N_B = \frac{\text{Quantity of cation B on permanent charge sites of clay minerals (meq kg}^{-1})}{\text{CEC (meq kg}^{-1})} \qquad \text{(A2.3)}$$

In a multi-ionic system, selectivity coefficients are defined with respect to a reference cation. The sum of the fractional cation occupancies (N_B values for the various cations) is equal to unity.

One method of determining K_C values is via sorption measurements. If a distribution coefficient, ${}^{B}R_d$ is defined for the sorption (by cation exchange) of cation B as:

$${}^{B}R_d = \frac{\text{Moles of B sorbed by cation exchange per unit mass}}{\text{Moles of B in aqueous solution per unit volume}} \qquad \text{(A2.4)}$$

[44] Note that cation exchange is only one of a spectrum of potential sorption mechanisms which can occur (cf. Section 6.3.3.1)

or,

$$ {}^{B}R_d = N_B . \frac{CEC}{Z_B} . (B)^{-1} \qquad \text{(A2.5)} $$

where (B) is the concentration of B in moles per unit volume. Hence,

$$ N_B = {}^{B}R_d . \frac{Z_B}{CEC} . (B) . \qquad \text{(A2.6)} $$

Substituting the expression for N_B from Eq. A2.6 into Eq. A2.2 yields a general expression relating the selectivity coefficient to the sorption of cation B:

$$ {}^{B}_{A}K_C = Z_B^{Z_A} . \left({}^{B}R_d \right)^{Z_A} . \frac{1}{\left(N_A\right)^{Z_B}} . \frac{1}{(CEC)^{Z_A}} . \frac{\left(\gamma_A\right)^{Z_B}}{\left(\gamma_B\right)^{Z_A}} . (A)^{Z_B} \qquad \text{(A2.7)} $$

where γ_A and γ_B are the solution activity coefficients of A and B, respectively[45].

Once the values of all parameters on the right-hand side of Eq. A2.7 have been determined, then the selectivity coefficient can be readily calculated. In particular:

(i) the *cation exchange capacity* of crushed shear zone material can be determined by the silver-thiourea method, as reported in AKSOYOGLU et al. (1991);

(ii) the *fractional cation occupancies* can be deduced from silver-thiourea extraction experiments carried out at different solid to liquid ratios, as described in BAEYENS & BRADBURY (1989).

Key results, taken from BAEYENS & BRADBURY (1989), are given in Table A2.1. Selectivity coefficients were calculated from Eq. A2.7 using major cation concentration data from the rock water interaction tests.

The selectivity coefficients calculated for Ca-Na, Ca-Mg and Ca-Sr were found to be reasonably independent of the rock-water ratio, particularly in view of the uncertainties in the experimental data. The mean values for these exchange reactions are also given in Table A2.1, together with their respective standard deviations. A selectivity coefficient that is independent of concentration (and of fractional occupancy), in a solution of otherwise constant composition, is an indication of linear sorption, i.e. sorbed quantities are directly proportional to concentration).

---

[45] If experiments are carried out with tracer concentrations below groundwater concentrations, sorption will be linear (isotope exchange dominant process). In the case where experiments have tracer concentrations above those of major ions in solution, the active exchange system is altered. In this case, equation A2.7 should be formulated so:

$$ \left({}^{B}R_d \right)^{Z_A} = \frac{{}^{B}_{A}K_C}{Z_B^{Z_A}} \cdot \frac{\left(N_A\right)^{Z_B}}{\left(A\right)^{Z_B}} \cdot (CEC)^{Z_A} \cdot \frac{\left(\gamma_B\right)^{Z_A}}{\left(\gamma_A\right)^{Z_B}} $$

which indicates that ${}^{B}R_d$ is independent of *(B)*, i.e. is not applicable to any solute showing non-linear sorption.

Tab. A2.1: Selectivity coefficients, K_C, and fractional cation occupancies, N_B, for ion-exchange reactions on crushed shear zone material

Crushed shear	Cation-exchange reaction							
zone material	$Ca_x + 2Na = 2Na_x + Ca$		$Ca_x + 2K = 2K_x + Ca$		$Ca_x + Mg = Mg_x + Ca$		$Ca_x + Sr = Sr_x + Ca$	
	N_{Na}	K_C	N_K	K_C	N_{Mg}	K_C	N_{Sr}	K_C
rock:water 2:1	0.06	1.02	0.18	38.2	0.08	0.57	0.013	0.87
rock:water 1:2	0.07	1.51	0.13	153	0.06	0.87	0.013	1.33
rock:water 1:10	0.06 0.06	0.82 1.01	0.08 0.08	361 280	0.04 0.04	0.95 0.91	0.015 0.014	1.26 1.41
mean K_C stand. dev.		1.1 ± 0.3				0.8 ± 0.2		1.2 ± 0.2

In the case of potassium, the exchange behaviour is non-linear. The inference is, therefore, that potassium sorption will also be non-linear. Since the chemistry of potassium is similar to that of caesium, and caesium has been used in the MI experiment (Chapter 7), the indication from laboratory experiments is that caesium will sorb non-linearly in this system.

On the basis of the calculated selectivity coefficients and of the water composition, sorption coefficients can be calculated using Eq. A2.7. The predicted R_d values depend directly on the magnitude of the *CEC*. The *in situ* sorption in the migration fracture will thus depend on the *in situ CEC*. This is discussed further in Section 5.4.1 for sodium and strontium, and Section 5.4.2 for caesium.

APPENDIX 3: NOTATION

P.A. Smith and W. Heer

The following tables present the notation used in Chapter 7 and Appendix 4.

Tab. A3.1: Parameters defining the imposed dipole flow field

$L_0\ [m]$	:	Distance between injection and extraction boreholes in the dipole flow field
$Q_i\ [ml/min]$	:	Injection rate for the dipole flow field
$Q_e\ [ml/min]$	:	Extraction rate for the dipole flow field
$\beta\ [-]$	:	Ratio of extraction to injection rate

Tab. A3.2: Parameters defining the parts of the MI experimental shear zone of high flow porosity

$a\ [m]$	:	Width of zone where flow occurs
$\varepsilon_f\ [-]$	:	Flow porosity (with respect to a)
$\varepsilon_f\, a\ [m]$	:	Flow width
$n\ [-]$	:	Number of parallel-walled model fractures (with or without fault gouge) that represent the flow within the width a

Tab. A3.3: Parameters defining tracer transport properties in the parallel-walled model fractures that represent the parts of the MI shear zone of high flow porosity

$b\ [m]$	:	Half aperture
$a_L\ [m]$	:	Longitudinal dispersion length
$K_{a,f}\ [m]$	:	Area-specific sorption coeff. for sorption on model-fracture surfaces (excluding possible fault gouge)
$\varepsilon_i\ [-]$	:	Porosity of possible fault gouge (accessible by flowing water)
$\tilde{\rho}_i\ [kg/m^3]$	:	Bulk density of possible fault gouge
$K_{d,i}\ [m^3/kg]$	:	Mass-specific sorption coefficient for sorption on model-fracture surfaces of possible fault gouge
$R_f\ [-]$	:	Retardation factor for sorption on model-fracture surfaces (including possible fault gouge)

Tab. A3.4: Parameters defining tracer transport properties in the diffusion-accessible porous zone

$d\ [m]$	:	Depth
$\varepsilon_p\ [-]$	:	Diffusion-accessible porosity
$\tilde{\rho}_p\ [kg/m^3]$	:	Bulk density
$D_p\ [m^2/s]$	:	Pore diffusion constant
$K_{d,p}\ [m^3/kg]$	:	Sorption coefficient
$R_p\ [-]$	:	Retardation factor

Tab. A3.5: Characteristic break-through times

$t_A\ [h]$	:	Advection time for the flowpath along the dipole axis (representing time of break-through peak maximum, taking into account advection and dispersion only)
$t_D\ [h]$	:	Dispersion time (representing the (1/√e)-width of break-through peak due to dispersion)
$t_{MD}\ [h]$	:	Matrix diffusion time (representing delay and tailing of break-through due to matrix diffusion)
$t_{MP}\ [h]$	:	Matrix propagation time (representing beginning of break-through "tail-end perturbation" due the effects of the outer boundary of diffusion-accessibile porous zone)

Tab. A3.6: Parameters defining the tracer injection and extraction

$M_0\ [mol]$	:	Total mass of injected tracer
$C_{inj}(t)\ [mol/m^3]$	:	Concentration of the tracer pulse, measured down hole at the tracer injection point
$\Delta t_{inj}\ [h]$	:	Down-hole (1/√e)-duration of the injected tracer pulse
$\delta t_{inj}\ [h]$	:	Down-hole delay of break-through maximum, due to the mechanisms operating in the injection apparatus (principally advection and asymmetric dispersion in the injection tubing)
σ	:	Spatial (1/√e)-half width of tracer peak at migration distance L_0
$C_f(t)\ [mol/m^3]$	:	Break-through concentration
$C_{f,m}\ [mol/m^3]$	:	Concentration maximum of the break-through curve
$t_m\ [h]$	:	Time of break-through curve maximum
$s\ [h]$	:	(1/√e)-width of break-through curve
$C_{f,a}(t)\ [mol/m^3]$	:	Asymptote characterising break-through tail (for $t >> t_m$ and $t < t_{MP}$)

APPENDIX 4: DEFINITION OF THE CHARACTERISTIC TIMES FOR BREAK-THROUGH CURVES

P.A. Smith and W. Heer

This appendix gives analytical expressions for the four characteristic times that define the form of break-through curves presented in Chapter 7. Similar expressions for three of these characteristic times are given in BARTEN (1996). The characteristic times are:

- t_A and t_D: an *advection time* and *dispersion time*, that also account for the effects of sorption on the surfaces of the "flow porosity"
- t_{MD} and t_{MP}: a *matrix-diffusion time* and *matrix-propagation time*, that also account for the effects of sorption on the surfaces of diffusion-accessible porosity.

Characterisation break-through curves using these four parameters is justified if it can be assumed that:

1. *Sorption is fast compared to other, time-dependent processes and can be represented by a linear isotherm (and therefore by concentration-independent retardation factors R_f and R_p).*

   For all of the experiments presented in Chapter 7, the injection concentrations were deliberately chosen well below the natural background concentration, in which case sorption is linear. No major effects of sorption kinetics were observed, with the exception of the Cs tracer in the fast, 1.7 m dipole flow field, the break-through of which cannot be characterised using the four-parameter concept.

2. *Transverse dispersion has only a minor influence on break-through.*

   According to the ETH analysis (KUNSTMANN et al. 1997), the effect of transverse dispersion on break-through is indeed very small in the investigated experiments.

3. *The natural background flow can be neglected with respect to the artificial flow of the experiments.*

   The experiments were conducted in a region of flat hydraulic potential and the artifical flow was induced using relatively high pumping rates (c.f. HEER & HADERMANN 1996, p. 17, hypothesis 6). The assumption of a background flow that is negligible with respect to the artificial flow was confirmed by the site hydrogeology analyses (see, for example, HOEHN et al. 1990).

The analytical expressions employ the system of notation given in Appendix 3. The analytical expressions have been applied to the data used to generate Figure 7.1. The characteristic times are indicated on the figure, showing their relationship to the form of a break-through curve. The data and corresponding characteristic times are presented in Table A4.1.

Advection time

The advection time, t_A, is a tracer transit time in the (hypothetical) absence of matrix diffusion. It is calculated along the dipole flow field axis (neglecting the natural, background flow), and therefore represents the *shortest* advection time through the "flow porosity". The advection time is most useful as a concept for narrow dipole flow fields (such as that corresponding to Figure 7.1), of the type that arise where the ratio, β, of extraction rate to injection rate is high.

The following expression for the advection time is based on Eq. 15 in HEER & HADERMANN (1996), p. 33[46]:

$$t_A = \left(\frac{\pi L_0^2 f(\beta)}{Q_e} \right) a \varepsilon_f R_f \qquad \text{(A4.1a)}$$

where:

$$f(\beta) = \frac{\beta}{(\beta-1)^2} \left[(\beta+1) - \frac{2\beta}{(\beta-1)} \ln \beta \right] \qquad \text{(A4.1b)}$$

and

$$R_f = 1 + \frac{1}{b} (1-\varepsilon_p) K_{a,f} + \frac{\tilde{\rho}_i}{\varepsilon_i} K_{d,i} \,. \qquad \text{(A4.1c)}$$

The function $f(\beta)$ is related to the shape of the dipole flow field. In the equation for the retardation factor R_f, the second and third terms on the right-hand side represent, respectively, the influence of sorption on (i), the solid interface between the "flow porosity" and the diffusion-accessible porous zone and on (ii), flow-wetted fault gouge material.

Dispersion time

The dispersion time, t_D, characterises the duration of tracer break-through in the (hypothetical) absence of matrix diffusion and largely determines the peak height of the break-through curve peak. It is based on the spatial width, 2σ, of a pulse that has been smeared by dispersion along a path that has an average advection velocity $\approx L_0/t_A$.

The following expression for the dispersion time is based on Eqs. A3.5 in HEER & HADERMANN (1996), p. 113[47]:

$$t_D = \frac{2\sigma}{L_0 / t_A} = 2\sqrt{2} \frac{t_A}{\sqrt{Pe}} \qquad \text{(A4.2a)}$$

where:

$$\sigma = \sqrt{2 a_L L_0} \qquad \text{(A4.2b)}$$

and

---

[46] The following changes in notation are employed: $\bar{t}_0 \rightarrow t_A / R_f$; $W_0(\beta) \rightarrow f(\beta)$; $Q_W \rightarrow Q_e$

[47] The following changes in notation are employed: $\sigma(z = L_0) \rightarrow \sigma$; $\bar{v} / R_f \rightarrow L_0 / t_A$; $(\varepsilon a) B \rightarrow Q_i / \bar{v}$; $(Q_i/Q_e) C_{f,m}$ (not diluted) $\rightarrow C_{f,m}$ (diluted); $t_m + \delta t_{inj} \rightarrow t_m$

$$Pe = \frac{L_0}{a_L}. \qquad \text{(A.4.2c)}$$

Taking into account the dilution of break-through concentration by external shear zone groundwater[48], the peak height of the break-though curve can be approximated by:

$$\frac{C_{f,m}}{M_0} \approx \sqrt{\frac{2}{\pi}} \cdot \frac{1}{Q_e} \cdot \frac{1}{t_D} \quad \text{for } Pe >> 1 \qquad \text{(A4.2d)}$$

The spatial variation of velocity along the stream lines that convey the tracer is not represented in these expressions. The dipole flow fields that are discussed in Chapter 7 are fairly uniform, but have large peaks near the injection and, especially, near the extraction borehole. The region of high velocity along a stream line near the extraction borehole covers only about 3 % of its total length. The increased velocity in this region widens the in-coming tracer pulse, but, since the pulse is also advected more rapidly, the break-through curve is essentially not altered.

Matrix diffusion time

The matrix diffusion time, t_{MD}, characterises, to a large extent, both the delay of break-through peak with respect to the advection time t_A and, if the effect of matrix diffusion dominates over dispersion ($t_D << t_{MD}$), the duration of the break-through peak (with a corresponding reduction in break-through concentrations).

The following expression for the matrix-diffusion time is based on Eqs. 27f, 28 and 29 in HEER & HADERMANN (1996), p. 52[49], also taking account of Eq. A4.1a:

$$t_{MD} = \left(\frac{\pi L_0^2 f(\beta)}{Q_e} \right)^2 . n^2 . \left(\varepsilon_p \sqrt{D_p R_p} \right)^2 \qquad \text{(A4.3a)}$$

where:

$$R_p = 1 + \frac{\tilde{\rho}_p}{\varepsilon_p} K_{d,p} \qquad \text{(A4.3b)}$$

Note that t_{MD} is independent of the flow width, $a\varepsilon_f$, since the change in the interface area, per unit volume of flowing water, is compensated for by the change in water velocity. In addition, t_{MD} is independent of the porosity, ε_i, of the fault gouge postulated in the JNC model (it is assumed, in applying the JNC model, that the presence of fault gouge does not block any of the diffusion-accessible pores). In the PSI and ETH models, $\varepsilon_i = 1$.

---

[48] Clearly this occurs at any time when the extraction rate is higher than the injection rate, the difference being supplied by groundwater in the shear zone.

[49] The following changes in notation are employed: $\left(1/\varepsilon_i\right)^2 \tau_0 \left(z = L_0\right) \rightarrow t_{MD}$;

$(Q_i/Q_e)C_{f,m}$ (not diluted) $\rightarrow C_{f,m}$ (diluted).

Assuming that the effect of matrix diffusion dominates over dispersion ($t_D << t_{MD}$), and taking into account the dilution of break-through concentration by external fracture water, break-through peak time, t_m, duration, s, and height, $C_{f,m}/M_0$, can be approximated by:

$$t_m \approx \delta t_{inj} + t_A + \frac{2}{3} t_{MD} \qquad \text{(A4.3c)}$$

$$s \approx 1.4 \cdot t_{MD} \qquad \text{(A4.3d)}$$

$$\frac{C_{f,m}}{M_0} \approx \frac{0.23}{Q_e} \cdot \frac{1}{t_{MD}} \qquad \text{(A4.3e)}$$

The asymptote, approximating the break-through tail generated by back-diffusion from the porous rock zone, is given by:

$$\frac{C_{f,a}(t)}{M_0} = \frac{1}{\sqrt{\pi} Q_e} \cdot \sqrt{t_{MD}} \cdot t^{-\frac{3}{2}} \quad \text{for } t >> t_m \text{ and } t < t_{MP} \qquad \text{(A4.3f)}$$

It can be interpreted as the total tracer flow from back-diffusion over one interface area divided by the total water flow of the corresponding part of the water conducting zone.

Matrix propagation time

The matrix propagation time, t_{MP}, provides an indication of the delay, following the advection time, t_A, of the beginning of the "tail-end perturbation". It can be interpreted as the time required for a short tracer pulse, diffusing from the outer boundary of the porous-rock zone back towards the interface between the "flow porosity" and the porous-rock zone, to generate a significant signal at the interface[50].

The following expression for the matrix propagation time is based on Eqs. A4.3d and A3.4 in HEER & HADERMANN (1996), pp. 114-115[51]:

$$t_{MP} = 0.20 \cdot \frac{d^2 R_p}{D_p} \qquad \text{(A4.4a)}$$

[50] A consequence of the assumed limited depth of matrix diffusion.

[51] The factor of 0.2 does not appear in the expression for the position of the "tail-end perturbation" in HEER & HADERMANN (1996). In the present report, the position calculated corresponds to the beginning of the "tail-end perturbation" whereas in HEER & HADERMANN (1996), however, an average position for the "tail-end perturbation" as a whole is calculated.

where:

$$d = \frac{a - a\varepsilon_f / \varepsilon_i}{2n} \approx \frac{a}{2n}. \qquad \text{(A4.4b)}$$

Tab. A4.1: The parameter values used to generate the break-through curves presented in Figure 7.1, and characteristic times calculated using the equations in this appendix

Parameter values			
L_0	=	4.9 m	
Q_e	=	8.910×10^{-3} m^3/h	(148.5 ml/min)
β	=	15.97	(Q_i = 9.3 ml/min)
Δt_{inj}	≈	0.4 h	
δt_{inj}	≈	0.6 h	
$a\varepsilon_f$	=	3.7×10^{-4} m	
a_L	=	2.5×10^{-1} m	
R_f	=	1	
d	=	6.20×10^{-3} m	($a = 5 \times 10^{-2}$ m, n = 4)
ε_p	=	6.2×10^{-2}	
D_p	=	9.00×10^{-8} m^2/h	(2.5×10^{-11} m^2 s^{-1})
R_p	=	908	
Characteristic times			
t_A	=	2.47 h	($f(\beta)$ = 0.7881)
t_D	=	1.58 h	
t_{MD}	=	224 h	
t_{MP}	=	7.76×10^4 h	